DEVELOPMENT OF TRANSPARENT PROTECTIVE SELF-HEALING COATINGS

by
Adam W Grzelak

A thesis submitted to the Department of Pure and Applied Chemistry, University of Strathclyde, in accordance with the requirements for the degree of Doctor of Philosophy

The University of Strathclyde
Pure and Applied Chemistry
January 2019

DEVELOPMENT OF TRANSPARENT PROTECTIVE SELF-HEALING COATINGS

by
Adam W Grzelak

This PhD thesis is the result of the author's original research. It has been composed by the author and has not been previously submitted for examination which has led to the award of a degree.

Signed: Date:

ACKNOWLEDGEMENTS

Firstly, I would like to express my deep gratitude to Dr J. J. Liggat, my research supervisor, for his patient guidance, enthusiastic encouragement and useful critique of this research work. I would also like to thank Dr P. Boinard and Dr E. Boinard, my industrial supervisors from Polaroid® Eyewear, for establishing the contact with the University of Strathclyde. Their advice, assistance and support during my project allowed me to keep my progress on schedule. I would also like to thank them for giving me access to their facilities at the Vale of Leven industrial estate, and help received during my research from all the Polaroid® Eyewear staff members.

My grateful thanks are also extended to Dr S. McCreath for his patience, guidance and support during my research. I would like to thank Dr P. L. Tang for his help in using infrared spectrometers and assistance with experimental design, preparation and interpretation of spectroscopic data. I would also like to thank Dr J. Lewicki for allowing me to carry out work at Lawrence Livermore National Laboratory and making my time there very enjoyable.

I would also like to extend my thanks to all the technical staff in the Pure and Applied Chemistry and Chemical Engineering departments of the University, including Mrs P. Keating, Mrs F. Sillars, Mr L. McCulloch, Mr C. Irving and Mr A. Clunie, for their help in offering me the resources, running various analytical instruments and sharing their knowledge and experience.

Finally, I wish to thank everyone in the Polymer Degradation Group, as well as my family and friends for their support and encouragement throughout my study.

ABSTRACT

Functional self-repair systems found in living organisms have inspired scientists to design artificial materials able to recover from wear and damage. One of the current goals in the field of self-healing materials includes creation of such materials for optical purposes.

The work presented in this thesis was focused on the development of novel, thermally-triggered, self-healing polyurethane coatings to be used as protective layers. Such materials must fulfil certain requirements: (i) the coating must be clear, transparent and exhibit haze below 2%, (ii) the coating must have a hardness of B or above, determined by the pencil hardness test, (iii) the glass transition temperature of the coating must be above room temperature and below 80 °C in order to enable a convenient, thermally-triggered healing, and (iv) the healing must be rapid, taking less than 10 minutes, and efficient, resulting in damage recovery of above 90%.

To achieve the requirements a series of waterborne aliphatic polyurethanes based on polyols of various lengths and structures were synthesised. Followed the choice of the most suitable polyol, different isocyanates were examined, including hexamethylene diisocyanate and isophorone diisocyanate. Subsequently, several chain extenders, including diol, alkoxyamine and diamine of various lengths and structures, were tested. Finally, various crosslinkers and internal emulsifiers were studied. The self-healing process was examined in detail and relationship between the self-healing process and the morphology of the materials was established.

Optimally designed coatings obtained up to 100% recovery within 10 minutes at 60 ˚C. The self-healing properties were found to be linked to phase-mixing of polyurethane matrix, creating an amorphous, homogenous and non-ordered polymer matrix with low haze values and high glass transition temperatures. At elevated temperatures a rearrangement of polymer was obtained, leading to the healing of scratches and disappearance of damage.

ABBREVIATIONS

AFM	atomic force microscopy
ASW	automated steel wool
ATR	attenuated total reflectance
BA	*n*-butyl acetate
BD	1,4-butanediol
BMI	bismaleimide
bPEI	branched poly(ethylenimine)
CE	chain extender
D1700	Desmophen 1700, polydiethylene adipate glycol
D670	Desmophen 670, branched hydroxyl bearing polyester
DA	Diels-Alder
DAT	dry abrasion test
DBP	dibutylphthalate
DBTDL	dibutyltin dilaurate
DCOMTS	1,7-dichlorooctamethyltetrasiloxane
DCPD	*N,N*-dicyclopentadiene
DEG	*N,N*-diethylene glycol
DGEBA	diglycidyl ether of bisphenol A
DMAC	dimethylacetamide
DMF	dimethylformamide
DMPA	dimethylolpropionic acid
DSC	differential scanning calorimetry
EA	ethanolamine
EG	ethylene glycol
ENB	5-ethylidene-2-norbornene
FT-IR	Fourier transform infrared
GMA	glycidyl methacrylate
H12MDI	fully hydrogenated diphenylmethane diisocyanate
HBPSi	hyperbranched polysiloxane
HDA	hexamethylene diamine
HDI	hexamethylene diisocyanate
HGF	hollow glass fibre
HPP	hard elastic polypropylene
HS	hard segments
IPDI	isophorone diisocyanate
l-PCL	linear poly(ε-caprolactone)
LSCM	laser scanning confocal microscopy
MBB	manual brass brush
MDI	methylene diphenyl diisocyanate
MIBK	methyl isobutyl ketone

MW	molecular weight
MWNTs	multiwalled carbon nanotubes
NHC	*N*-heterocyclic carbene
NMP	N-methyl pyrrolidine
n-PCL	branched poly(*ε*-caprolactone)
PA	primary electrons
PAA	poly(acrylic acid)
PBA	poly(1,4-butylene adipate glycol)
PCL	polycaprolactone
PDES	polydiethylsiloxane
PeD	1,5-pentanediol
PEG	polyethylene glycol
PH50	polycarbonate of pentanediol and hexanediol
PMF	poly(melamine formaldehyde)
PMMA	poly(methyl methacrylate)
PPG	poly(propylene glycol)
PrD	1,3-propanediol
PU	polyurethane
PUD	polyurethane dispersion
PUU	poly(urethane-urea)
RAFT	reversible addition-fragmentation chain-transfer
rDA	retro-Diels-Alder
RT	room temperature
SAN	styrene-acrylonitrile
SD	1,7-octamethyltetrasiloxanediol
SE	secondary electrons
SEM	scanning electron microscopy
SH	self-healing
SMASH	shape memory assisted self-healing
SS	soft segments
TAc	cellulose triacetate
TCE	1,1,1-tris(cynnamoyloxymethyl)ethane
TDI	toluene diisocyanate
TEA	triethylamine
T_g	glass transition temperature
THF	tetrahydrofuran
T_m	melting temperature
TMP	trimethylolpropane
TTC	trithiocarbonate
VOC	volatile organic compound
WAT	wet abrasion test

LIST OF FIGURES

Figure 1-1. The healing mechanisms of smart materials 5
Figure 1-2. Properties of self-healing systems 6
Figure 1-3. Stages of capsule-based healing 7
Figure 1-4. Stages of creation of multidimensional microchannel network using direct-write assembly 12
Figure 1-5. The multistep mechanism of self-healing *via* molecular diffusion 14
Figure 1-6. The summary of self-healing techniques based on reversible chemical reactions between the chains 16
Figure 1-7. Theoretical mechanism of self-healing of ionomers 19
Figure 1-8. Shape-memory assisted self-healing concept 22
Figure 1-9. Roller knife coating application system. 29
Figure 1-10. Wire-wound Mayer rod. 30
Figure 1-11. Mayer rod roller coating application system. 31
Figure 1-12. Reverse roll coating system. 32
Figure 1-13. Dip-coating system. 33
Figure 1-14. The acetylation of cellulose to cellulose triacetate. 34
Figure 1-15. Schematic representation of chain structure of PU and formed block copolymer. 37
Figure 1-16. Morphology of polyurethane matrix. 38
Figure 1-17. Reaction scheme of diol and diisocyanate forming polyurethane. 41
Figure 1-18. The pre-polymer method of polyurethane synthesis 42
Figure 1-19. The pre-polymer method of waterborne polyurethane dispersion. 45
Figure 1-20. The self-healing mechanism of PU coating. 47
Figure 1-21. The scheme of DA and rDA reactions in PU-DA. 51
Figure 1-22. Reversible photodimerization and photocleavage reactions of coumarin moieties upon irradiation with UV light. 52
Figure 1-23. An example of a micro-abrasion instrument - an automatic scratch tester BGD 520. 53
Figure 1-21. Model of polyurethane microphase morphology and visualisation of composition of various blocks discussed in Chapters 3 to 8. 60
Figure 2-1. Scheme of the synthesis of the solvent-borne polyurethane 70
Figure 2-2. Dual cartridge on-demand mixing and dispersing system with static mixer 70
Figure 2-3. Simplified scheme of the synthesis of diamine chain-extended polyurethane dispersions 71
Figure 2-4. Vector representation of a contact angle 74
Figure 2-5. A graph of a multi-reflection ATR instrument 77
Figure 2-6. A graph representing a DSC measuring cell 80
Figure 2-7. DSC heat-cool thermogram of a typical, semi-crystalline PU 80

Figure 2-8. Schematic representation of the change in specific volume of a polymer with temperature for a completely amorphous sample, a semi-crystalline sample and a completely crystalline sample. 81
Figure 2-9. A typical heat – cool – reheat DSC thermogram. 83
Figure 2-10. Pencil hardness tester set – Elcometer 501 85
Figure 2-11. Elcometer 107 cross-hatch cutter. 87
Figure 2-12. A graph representing a typical set-up of a haze meter 88
Figure 3-1. Structure of polyols 97
Figure 3-2. Synthesis of 1,7-SD from 1,7-DCOMTS. 98
Figure 3-3. Changes in the size of NCO peak during the reaction, ATR FT-IR 99
Figure 3-4. ATR FT-IR spectra of polyols D1700, D670 and coatings B1,B2 101
Figure 3-5. DSC heat-cool-reheat cycles of polyol D1700 and formulation B1. 103
Figure 3-6. DSC heat-cool-reheat cycles of polyol D670 and formulation B2. 106
Figure 3-7. ATR FT-IR spectra of polyol PCL2000 and coatings B3. 107
Figure 3-8. DSC heat-cool-heat cycle of polyol PCL2000 and formulation B3. 109
Figure 3-9. ATR FT-IR spectra of polyol PCL1000 and coatings B4, B5 and B6. 110
Figure 3-10. DSC heat-cool-heat cycle of polyol PCL1000, and B4, B5 and B6 112
Figure 3-11. ATR FT-IR spectra of polyol PH50 and coatings B7 and B8 113
Figure 3-12. DSC heat-cool-heat cycle of polycarbonate polyol PH50. 114
Figure 3-13. DSC heat-cool-heat cycle of formulations B7 and B8 115
Figure 3-14. ATR FT-IR spectra of polyol PH50 and coatings B7 and B8 116
Figure 3-15. DSC heat-cool-heat cycle of polyol PH200 and formulation B9. 117
Figure 3-16. DSC heat-cool-heat cycle of polyol PH300 and formulation B10. 118
Figure 3-17. Graphs of haze values of samples tested for SH properties 120
Figure 3-18. Percentage RT recovery of coatings prepared with various polyols. 121
Figure 4-1. Structure of HDI and IPDI. 127
Figure 4-2. FT-IR spectra of the coatings prepared with blends of isocyanates. 129
Figure 4-3. The interactions between N-H and C=O within polyurethanes 130
Figure 4-4. ATR FT-IR spectra of the samples: the NH and the carbonyl region. 131
Figure 4-5. Studies of temperature dependant phase-mixing of sample prepared with HDI/IPDI (50:50). 132
Figure 4-6. DSC curves of formulations: the first and the second heat cycle 134
Figure 4-7. Height, 2 µm AFM images of coatings 136
Figure 4-8. Phase contrast, 1 µm AFM images of coatings 136
Figure 4-9. Percentage recovery of the samples healing at RT and 60 ˚C 137
Figure 4-10. Stick models of HDI- and IPDI-based fragments of HS. 139
Figure 5-1. Structures of the CE used. 143
Figure 5-2. SEM images of coatings prepared with HDI. 145
Figure 5-3. SEM images of coatings prepared with IPDI. 146
Figure 5-4. ATR FT-IR spectra of HDI based coatings and IPDI based coatings. 147
Figure 5-5. NH region of FT-IR spectra of samples prepared with HDI and IPDI. 148
Figure 5-6. Carbonyl region of FT-IR spectra of s HDI and IPDI based samples 149

Figure 5-7. DSC curves of coatings prepared with HDI: first and second heat. 150
Figure 5-8. DSC curves of coatings prepared with IPDI: first and second heat. 151
Figure 5-9. Percentage recovery of samples prepared with HDI at RT and 60 ˚C... 153
Figure 5-10. Percentage recovery of samples prepared with IPDI at RT and 60 ˚C. 155
Figure 5-11. ATR FT-IR NH region of original and aged HDI-based coatings. 157
Figure 5-12. ATR FT-IR carbonyl region of original and aged HDI-based coatings.. 157
Figure 5-13. ATR FT-IR spectra of original and aged IPDI-based coatings: amine stretch and carbonyl stretch region. 158
Figure 5-14. DSC curves of HDI-based coatings after 12 weeks, first heat cycle..... 158
Figure 5-15. DSC curves of HDI-based coatings after 12 weeks, first heat cycle..... 159
Figure 5-16. Percentage recovery of HDI-based samples at RT and 60 ˚C. 160
Figure 5-17. Percentage recovery of IPDI-based samples at RT and 60 ˚C..... 161
Figure 5-18. ATR FT-IR spectra of aged of HDI-based coatings..... 162
Figure 5-19. Molecular level chain scission of PU exposed to UV/H_2O. 162
Figure 5-20. FT-IR spectra of IPDI-based coatings before and after weathering. ... 163
Figure 5-21. The increase of the length of CE and the size of hard blocks..... 165
Figure 5-22. Three structures of the HS, with the CE having reacted with two isocyanato groups, two isocyanatomethyl groups and isocyanato and isocyanatomethyl groups. 166
Figure 6-1. Structure of CE used. 169
Figure 6-2. ATR FT-IR spectra of the coatings. 171
Figure 6-3. ATR FT-IR spectra of samples: NH region and carbonyl region. 172
Figure 6-4. DSC curves of coatings: first and second heating cycle. 173
Figure 6-5. Percentage recovery of samples prepared at RT and 60 ˚C. 175
Figure 6-6. Hydrogen bonding between urethane groups, urethane and urea groups and urea groups – monodentate and bidentate. 178
Figure 7-1. Structure of trimers used: TMP and t-IPDI. 181
Figure 7-2. The smallest possible HS of samples prepared with TMP and t-IPDI. .. 183
Figure 7-3. ATR FT-IR spectra of the coatings prepared with t-IPDI and TMP. 184
Figure 7-4. NH region of ATR FT-IR spectra of the coatings prepared with t-IPDI and TMP. 185
Figure 7-5. Carbonyl region of ATR FT-IR spectra of the coatings prepared with t-IPDI and TMP. 186
Figure 7-6. DSC curves of coatings prepared with t-IPDI: first and second heat..... 187
Figure 7-7. DSC curves of coatings prepared with TMP: first and second heat. 188
Figure 7-8. Percentage recovery of samples prepared with t-IPDI at RT and 60 °C. 189
Figure 7-9. Percentage recovery of samples prepared with TMP, at RT and 60 °C. 191
Figure 7-10. The morphology of samples prepared with TMP and t-IPDI. 192
Figure 8-1. The structure of DMPA and neutralised DMPA within PU. 196
Figure 8-2. ATR FT-IR spectra of coatings prepared with EG and DEG. 200
Figure 8-3. NH region of FT-IR spectra of coatings prepared with EG and DEG. 201
Figure 8-4. Carbonyl region of FT-IR of coatings prepared with EG and DEG. 202

Figure 8-5. DSC curves of coatings prepared with EG and DEG..... 202
Figure 8-6. Percentage recovery of samples prepared with EG at RT and 60 ˚C..... 205
Figure 8-7. Percentage recovery of samples prepared with DEG at RT and 60 ˚C.. 206
Figure 8-8. The structures of HS prepared with EG and DMPA. 208
Figure 9-1. The first heat DSC cycle of samples PH50-IPDI-BD, PH50-IPDI-EG and PH50-IPDI-DEG. 211
Figure 9-2. Percentage recovery of the three coatings at RT and 60 ˚C..... 212
Figure 9-3. Visual representation of haze obtained during the first SH tests. 213
Figure 9-4. Visual representation of haze obtained during the second SH tests. ... 214
Figure 9-5. Visual representation of haze obtained during the third SH tests. 215
Figure 10-1. Recovery of sample PH50/IPDI/1,2-EG at elevated temperature 226

LIST OF TABLES

Table 1-1. A conversion table of the rod size and coating thickness..... 30
Table 1-2. Relative reaction rates of isocyanate with various chemical groups 43
Table 3-1. List of polyols used..... 97
Table 3-2. Structure and details of formulations prepared. 98
Table 3-3. Characterisation of coatings B1-B10..... 100
Table 3-4. The ATR FT-IR absorption regions..... 102
Table 3-5. Summary of DSC data of formulations prepared with various long chain polyols. 119
Table 3-6. Haze values of samples tested for SH properties. 120
Table 4-1. Composition and solid content of the dispersions. 127
Table 4-2. Characterisation of coatings. 128
Table 4-3. Characteristic IR bands for phase-mixed and -separated systems..... 131
Table 4-4. The DSC data obtained from histograms. 135
Table 4-5. Haze values of samples tested for SH properties at RT. 137
Table 4-6. Haze values of samples tested for SH properties at 60 °C..... 137
Table 5-1. Composition and solid content of the dispersions. 144
Table 5-2. Characterisation of coatings. 144
Table 5-3. Characteristic IR bands for phase-mixed and -separated systems..... 148
Table 5-4. The DSC data obtained from histograms. 152
Table 5-5. Haze values of HDI-based coatings healed at room temperature. 153
Table 5-6. Haze values of HDI-based coatings healed at 60 °C..... 153
Table 5-7. Haze values of IPDI-based coatings healed at room temperature. 155
Table 5-8. Haze values of IPDI-based coatings healed at 60 °C..... 155
Table 5-9. Change in haze of samples over 12 weeks 156
Table 5-10. DSC characterisation data of HDI-based samples..... 159
Table 5-11. DSC characterisation data of IPDI-based samples. 159
Table 5-12. Haze values of HDI-based coatings healed at RT after 12 weeks. 160
Table 5-13. Haze values of HDI-based coatings healed at 60 ℃ after 12 weeks..... 160
Table 5-14. Haze values of IPDI-based coatings healed at RT after 12 weeks. 161
Table 5-15. Haze values of IPDI-based coatings healed at 60 °C after 12 weeks. ... 161
Table 6-1. Composition and solid content of the dispersions. 169
Table 6-2. Characterisation of coatings. 170
Table 6-3. Characteristic IR bands for phase-mixed and -separated systems..... 172
Table 6-4. DSC characterisation data of samples prepared with various amounts of urea groups. 174
Table 6-5. Haze values of the coatings healed at room temperature. 175
Table 6-6. Haze values of the coatings healed at 60 °C..... 175
Table 7-1. Characterisation of polyurethane coatings prepared. 181
Table 7-2. Characterisation of polyurethane coatings prepared. 182

Table 7-3. The results of solvent resistance tests of the coatings..... 184
Table 7-4. Characteristic IR bands for phase-mixed and -separated systems..... 185
Table 7-5. DSC characterisation data of materials prepared with trimers..... 188
Table 7-6. Haze values of coatings prepared with t-IPDI healed at RT..... 190
Table 7-7. Haze values of coatings prepared with t-IPDI healed at 60 °C..... 190
Table 7-8. Haze values of coatings prepared with t-IPDI healed at RT..... 191
Table 7-9. Haze values of coatings prepared with t-IPDI healed at 60 °C..... 191
Table 8-1. List of formulations and their composition. 196
Table 8-2. Characterisation data of the polyurethane dispersions. 197
Table 8-3. Characterisation data of the polyurethane coatings. 198
Table 8-4. The results of solvent resistance tests of the coatings..... 199
Table 8-5. Characteristic IR bands for phase-mixed and -separated systems..... 201
Table 8-6. DSC characterisation data of HDI-based samples..... 204
Table 8-7. Haze values of coatings prepared with EG healed at RT..... 205
Table 8-8. Haze values of coatings prepared with EG healed at 60 °C..... 205
Table 8-9. Haze values of coatings prepared with DEG healed at RT..... 206
Table 8-10. Haze values of coatings prepared with DEG healed at 60 °C..... 207
Table 9-1. The summary of DSC data of samples PH50-IPDI-BD, PH50-IPDI-EG and PH50-IPDI-DEG. 211
Table 9-2. Haze values of the three coatings healed at room temperature. 212
Table 9-3. Haze values of the three coatings healed at 60 °C..... 212
Table 9-4. The haze values measured during the first SH test. 213
Table 9-5. The percentage recovery of haze obtained during the first SH test..... 214
Table 9-6. The haze values measured during the second SH test. 214
Table 9-7. The percentage recovery of haze obtained during the second SH test. 215
Table 9-8. The haze values measured during the third SH test. 215
Table 9-9. The percentage recovery of haze obtained during the third SH test. 216
Table 10-1. The summary of the findings of modifications of HS within PH50-IPDI formulations 225

CONTENT

Acknowledgements ii
Abstract iii
Abbreviations iv
List of Figures vi
List of Tables x
Content xii

1. Introduction 1
   1.1. Self-healing materials 1
      1.1.1. History and background 3
      1.1.2. Review of self-healing approaches 7
      1.1.3. Self-healing of optical materials 20
   1.2. Protective coatings 28
      1.2.1. Coating systems 28
      1.2.2. Cellulose triacetate 34
   1.3. Polyurethane coatings 35
      1.3.1. Structure, properties and applications of polyurethanes 35
      1.3.2. Synthesis and synthetic challenges 41
      1.3.3. Self-healing properties of polyurethanes 46
      1.3.4. Evaluation of self-healing properties 52
      1.3.5. Patents 55
   1.4. Summary and aim of research 58
   1.5. References 61
2. Experimental and instrumentation 68
   2.1. Synthesis and preparation of materials 68
      2.1.1. Materials 68
      2.1.2. Synthesis of solvent-borne formulations 68
      2.1.3. Preparation of formulations using dual cartridge 70
      2.1.4. Synthesis of waterborne formulations 70
      2.1.5. Preparation of solid samples 72
      2.1.6. Preparation of coatings 72
   2.2. Characterisation of dispersions 72
      2.2.1. Determination of solid content 72
      2.2.2. Determination of hard segment content 73
      2.2.3. Determination of contact angle 74
   2.3. Characterisation of coatings 76

2.3.1. Attenuated total reflectance fourier transform infrared spectroscopy (ATR FT-IR) 76
2.3.2. Differential scanning calorimetry (DSC) 79
2.3.3. Scanning electron microscopy (SEM) 84
2.3.4. Pencil hardness 85
2.3.5. Cross-cut adhesion 86
2.3.6. Haze 87
2.3.7. Solvent resistance 89
2.3.8. Contact angle 90
2.3.9. Weathering of the coatings 90
2.3.10. Damage of coatings 92
2.3.11. Self-healing evaluation 93
2.4. References 95
3. The influence of polyol on morphology and self-healing properties 96
3.1. Synthesis information 97
3.2. Characterisation of coatings 100
3.3. Characterisation of coatings' morphologies 101
3.4. Evaluation of self-healing properties 120
3.5. Summary and discussion 122
3.6. References 125
4. The influence of isocyanate on morphology and self-healing properties 126
4.1. Synthesis information 127
4.2. Characterisation of dispersions 127
4.3. Characterisation of coatings 128
4.4. Characterisation of coatings' morphologies 129
4.5. Evaluation of self-healing properties 137
4.6. Summary and discussion 139
4.7. References 141
5. The influence of diol chain extender on morphology and self-healing properties 142
5.1. Synthesis Information 143
5.2. Characterisation of dispersions 143
5.3. Characterisation of coatings 144
5.4. Characterisation of coatings' morphologies 146
5.5. Evaluation of self-healing properties 153
5.6. Ageing and weathering of polymers 156
5.7. Summary and discussion 163
5.8. References 167
6. The influence of amine chain extender on morphology and self-healing properties 168

6.1. Synthesis information 169
6.2. Characterisation of dispersions 169
6.3. Characterisation of coatings 170
6.4. Characterisation of coatings' morphologies 170
6.5. Evaluation of self-healing properties 175
6.6. Summary and discussion 177
6.7. References 179
7. The influence of crosslinking on morphology and self-healing properties 180
7.1. Synthesis Information 181
7.2. Characterisation of coatings 182
7.3. Characterisation of coatings' morphologies 184
7.4. Evaluation of self-healing properties 189
7.5. Summary and discussion 191
7.6. References 194
8. The influence of ionic content on morphology and self-healing properties 195
8.1. Synthesis Information 196
8.2. Characterisation of dispersions 197
8.3. Characterisation of coatings 198
8.4. Characterisation of coatings' morphologies 199
8.5. Evaluation of self-healing properties 204
8.6. Summary and discussion 207
8.7. References 209
9. Various modes of evaluation of self-healing properties 210
9.1. Morphology of the coatings used in the various SH tests 210
9.2. Multiple damage-heal cycles 213
9.3. Delayed healing of the coatings 214
9.4. Healing of the coatings without thermal trigger 215
9.5. Summary and discussion 216
10. Conclusions and further work 217
10.1 Recap of the project aims 217
10.2. The influence of the chemistry of soft segments 217
10.3. The influence of the chemistry of hard segments 219
10.4. Self-healing of the coatings 222
10.5. Final remarks and further work 229
10.6. References 232

1. INTRODUCTION

1.1. SELF-HEALING MATERIALS

Healing is a natural process that occurs in all living organisms.[1] The process involves regeneration or repair of damaged tissues, organs or biological systems and restoration of their health and normal functioning. The healing process of living organisms is entirely self-contained and consists of several steps. Initially, the damage of a tissue is sensed biochemically, and an inflammatory response is activated. Subsequently, cell proliferation occurs during which appropriate substances able to regenerate the tissue are transported to the damaged site. Finally, through a complex process involving a series of chemical reactions the damaged site can get repaired to fully fulfil its purpose.[2]

Wear, damage and failure of all materials are natural results of their use. A conventional approach to minimise these effects includes development of hard and robust materials exhibiting mechanical strength to resist damage and withstand high forces. The smart and functional self-repair systems found in living organisms inspired scientists to design artificial materials displaying similar properties, offering an alternative approach to withstanding damage. Ideally, these novel self-healing materials would extend the life-time of many devices, improve their resistance to accidental damage or mechanical wear, reduce replacement costs of used components, provide higher customer satisfaction and improve safety.[3]

Over the last decades a broad research activity aiming for the design of practical self-healing materials has been conducted. Multiple approaches and techniques have been invented to prevent material from permanent damage, including material able to self-repair either with or without external triggers.[3] Recent studies of self-healing materials focus on development of various materials including composites,[4] ceramics[5] or metals,[6] although one of the most promising and widely researched group of materials are polymers.

Damage of a polymer matrix may occur in two ways: irreversible, physical removal of material or breakage of chemical bonds between polymer chains. Physical removal of material often prevents restoration of its original shape and physical properties. In this instance the self-healing of the cracks may be obtained by re-filling gaps with a similar material contained within the polymer matrix and released upon breakage. When the damage results in breakage of chemical bonds within a self-healing polymer matrix, these chemical bonds can be restored and restore the integrity of the destroyed fragment.[3]

The main goal for all self-healing materials is to reach 100% healing efficiency, irrespective of the size and type of the damage or the recovery mechanism. Ideally the repaired material would have identical chemical and physical properties to the original matrix. Additionally, to provide continuous functionality of the material the recovery should be optimised to occur at the same rate as damage.[7]

Use of self-healing materials for optical purposes is one of the currently trending research fields. Protective coatings exhibiting self-healing properties could significantly extend the lifetime of many popular accessories such as smart phones. Creation of smart, transparent coatings used to protect touch screens, solar energy panels or glass surfaces is a challenging goal. Such materials, apart from their self-healing characteristics, also need to fulfil a number of specific requirements, e.g. exhibit high transparency, low haze and precise optical activity.[8]

In the introduction of this thesis an overview of the field of self-healing materials is presented. A brief historical background and general information about smart materials are presented, followed by classification of various techniques and a description of current achievements in the field. Subsequently, the use of self-healing materials for optical applications is discussed. Finally, the structure, properties, applications, synthetic routes and self-healing properties of polyurethane coatings are discussed.

1.1.1. HISTORY AND BACKGROUND

Materials with self-healing properties were first discovered in the 1970s. During tests on hard elastic polypropylene (HPP) healing of microvoids upon stretching was observed. This viscoelastic polymer was discovered to acquire stacked lamellar morphology composed of alternating layers of crystalline and amorphous phases. The recovery phenomenon was thus explained as a consequence of lamellar morphology providing an energy balance between work, strain energy, viscous dissipation and damage. It was demonstrated that the healing was achieved by the conversion of surface energies, obtained by stretching, to strain energy and subsequently to mechanical work triggering the closure of cracks.[9]

Broader research in the field of smart materials started in the 1980s. A research group from Switzerland explored crack healing and welding of poly(methyl methacrylate) (PMMA), styrene-acrylonitrile (SAN) and blends of PMMA-SAN. Mechanical tests showed that at temperatures greater than the glass transition temperature (T_g) the fracture toughness and self-diffusion constant increases rapidly, allowing the material to heal microcracks.[10] It was further explained that exceeding the T_g provides polymer chains with a sufficient amount of energy to become more flexible and mobile. The polymer in a molten or rubber-like form gains the ability to flow and fill microcracks. This discovery enabled the invention of healable materials from polymers with a low glass transition temperature. However, undesirable change of overall shape of these materials at elevated temperatures was also observed. The application of such materials on vertical surfaces could potentially result in a flow-down of the material at the high temperatures required to initiate self-repair process and subsequently cause uneven distribution of the material.

Research carried out in the 1990s introduced a new approach to design self-healing materials. Dry and Sottos' group researched controlled cracking and repair of hollow fibres.[4] This novel approach involved dispersion of cyanoacrylate-filled fibres within a composite matrix. The fibres able to release adhesive chemicals were shown to seal microcracks. Beside one-part systems containing one chemical enclosed in fibres,

more effective, two-part reagent systems were developed in the following years. For instance, fibre-reinforced polymers consisted of a system including two reagents – a resin, such as an epoxy, and a hardener, such as a diamine.[11] These two reagents were contained within adjacent fibres and upon damage of the fibres immediate mixing and hardening occurred. Further systems involved one of reagents placed within a fibre and the other embedded within the polymer matrix or encapsulated and dispersed within the matrix.

The early studies of self-healing materials aroused interest and inspired a larger group of scientists to research bioinspired, self-healing materials. Since the first discovery of smart materials a wide range of novel structures have been reported in the literature. These materials, made from several components, use various triggers to initiate the repair process obtained *via* different mechanisms.

Based on the ability of the material to initiate a self-healing process, smart materials can be divided into two groups: autonomic and non-autonomic systems. In autonomic systems, the healing is initiated automatically by a damage of the material, thus human intervention or an external trigger are not required. The autonomic materials closely resemble biological systems, where healing is triggered mechanically and chemically by the damage of a tissue. In non-autonomic systems an external trigger is required to initiate healing. The stimulus, e.g. light or heat, usually needs to be launched by a human.[7]

Based on the mechanism of healing, self-healing materials can be divided into three groups: capsule-based, vascular and intrinsic systems (**Figure 1-1**).

In capsule-based systems the healing agents, usually liquid monomers or epoxy resins, are closed in microcapsules embedded within a polymer matrix. The damage of the matrix triggers rupture of the capsules and the release of encapsulated monomers. Once the healing agent is released, a chemical reaction occurs and microcracks can be filled with hard, cross-linked material. However, multiple healing at the same location is not possible due to consumption of microcapsules.

In vascular systems the polymer matrix contains a network of capillaries or channels within its structure. The network can have 1D, 2D or 3D connectivity and is usually connected to a reservoir of the healing agent. When the network gets broken the agent can be delivered to a damaged area. Constant supply of the healing agent allows multiple repairs at the same location.

In intrinsic systems healing is possible as a result of weak interactions between polymer chains and inherent reversible and dynamic chemical bonds within the matrix. The healing of the material is triggered by latent functionality of the molecular structure of the material. Upon damage broken chemical bonds can be restored or rearranged while the polymer chains can diffuse, recombine and heal the crack. Healing obtained *via* intrinsic processes usually offers unlimited healing at the same location, however the initiation usually requires an external stimulus, e.g. application of heat, light or pressure.

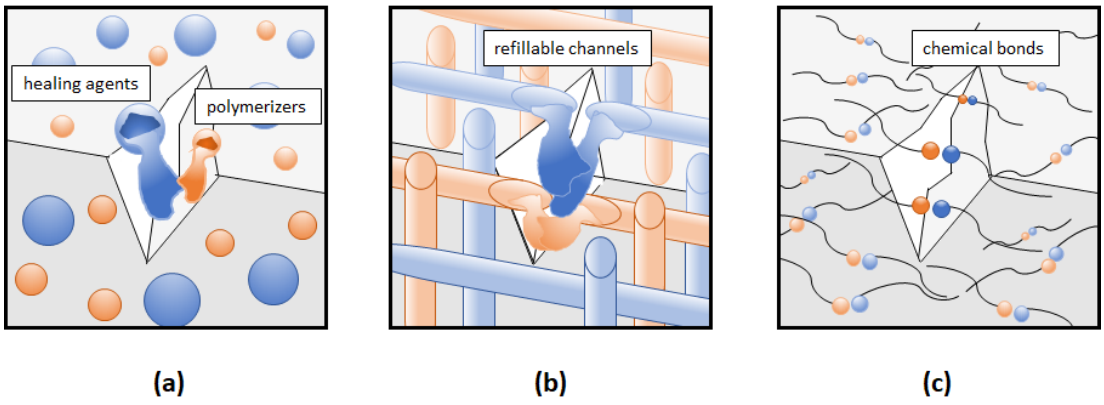

Figure 1-1 *The healing mechanisms of smart materials: a) capsule-based system, b) vascular system and c) intrinsic system.*

The creation of capsule-based and vascular self-healing systems is a suitable choice for thermosetting materials. The damage of a hard, thermosetting matrix usually involves irreversible removal of material. Release of healing agents from the capsules or reservoir provides new material capable of filling the damaged areas. In turn, intrinsic systems are considered useful for thermoplastic materials. Thermoplastic materials become mouldable above a specific temperature, thus healing can be

obtained by polymer chain rearrangement, diffusion, chemical reactions or bond rearrangements between polymer chains.

Capsule-based, vascular and intrinsic systems vary in the extent of damage they are able to heal. Capsule-based systems can recover small and moderate damage volumes. The size of damage needs to be sufficient to break the healing capsules, but not too large to exceed the volume of available healing agents. Additionally, the healing ability is confined due to a limited number of capsules within the matrix and their exhaustion upon healing. Vascular systems are able to recover small, medium and large damage volumes. The constant supply of the healing agent makes the system attractive for materials in which a large amount of material can be damaged or removed. Intrinsic systems generally can efficiently recover only small damage volumes. This limited healing ability is related to the requirement of a close proximity of damaged surfaces to provide good re-bonding. The system is attractive for materials in which small and shallow damage may occur, such as coatings. The healing rate to damage rate ratio can be optimised to the purpose of a particular material in all the systems, however it is dependent on the volume of damage (**Figure 1-2**). [7]

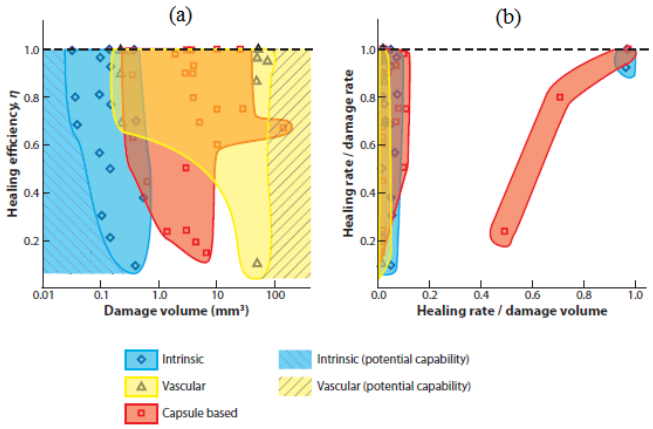

Figure 1-2. *Properties of self-healing systems: a) healing efficiency for different damage volumes and b) healing rate to damage rate ratio.*[7]

Regardless of the number of disadvantages and challenges, self-healing materials are a promising field of research. The three mentioned systems – capsule-based, vascular and intrinsic – will be reviewed further in this thesis, followed by detailed descriptions of current achievements in the field of self-healing materials for optical purposes as well as patented technologies.

1.1.2. *Review of self-healing approaches*

1.1.2.1. Capsule-based systems

In capsule-based systems the healing agents are enclosed in microcapsules, usually prepared from polyurea or poly(urea-formaldehyde), and released upon damage of the polymer matrix. The capsule-based healing is the most popular approach due to practical considerations, such as ease of microcapsule preparation and dispersion within the polymer matrix, as well as effectiveness of the system. This approach was pioneered by Dry and Sottos and their work with hollow glass fibres (HGFs). The fibres showed the ability to release adhesive chemicals capable of sealing microcracks. However, manufacturing of these materials was found to be problematic.[4] The microcapsule approach provided similar self-repair properties with an improved and facilitated manufacturing process.

The design of a functional capsule-based system has several requirements. The microcapsules must be equally dispersed within the matrix, inherently reactive to provide quick repair and should not influence the properties of the material. The encapsulated chemicals must be very stable and stay active during the lifetime of the material. Additionally, incorporation of a catalyst is usually required in order to initiate the polymerisation of released monomers (**Figure 1-3**).[12]

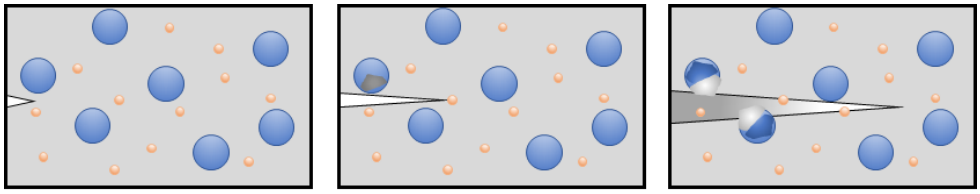

Figure 1-3. *Stages of capsule-based healing: a) initial shallow damage of material, b) damage reaches encapsulated healing agent and causes its release and c) catalyst triggered formation of hard filling material. Encapsulated healing agent is represented by large circles, while catalyst is shown by small dots.*[12]

One of the first autonomic capsule-based systems was reported by researchers from the University of Illinois at Urbana-Champaign in 2001.[13] Within the polymer matrix an epoxy resin, Grubbs' catalyst and microcapsules containing a liquid monomer,

dicyclopentane diene (DCPD) were embedded. The living ring-opening metathesis polymerisation was chosen as the most suitable polymerisation mechanism. The design of the microcapsule was optimised to achieve the highest healing efficiency. Parameters such as wall thickness, toughness, relative stiffness or the strength of the interface were modelled and optimised to provide the best properties of the material. The encapsulated healing agent, DCPD, was chosen to provide long lifetime, exhibit low monomer viscosity and volatility, provide rapid polymerisation at ambient conditions and display low shrinkage upon polymerisation. The polymer network yielded a high strength, toughness and high crosslinking. Mechanical tests showed more than 75% recovery of the material's mechanical strength. However, it was reported that the low melting temperature of DCPD influenced the mechanical properties of the material at elevated temperatures. Additionally, the initiation of polymerisation was found to require large amount of Grubbs' catalyst.[13]

Since the first development of autonomic capsule-based systems various research groups studied these materials and introduced several improvements. Further systems involved use of 5-ethylidene-2-norbornene (ENB) and Grubbs' catalyst,[14] polydimethylsiloxane and tin catalyst,[15] and more currently use of epoxy resins and curing agents.[16–20] For example, Rule and co-workers encapsulated Grubbs' catalyst in wax microspheres in order to avoid decomposition of the catalyst.[21] In further research DCPD was replaced with ENB due to its more effective healing properties and ease of handling during large-scale application.[14] Other researchers reported encapsulation of the catalyst instead of encapsulation of the monomers.[15]

Grubbs' catalyst is the most commonly used catalyst in capsule-based self-healing systems. However, some research reported the use of less common tin-based catalysts, for example di-n-butyl tin dilaurate (DBTDL) used for polycondensation reactions of hydroxyl polydimethylsiloxane and polydiethylsiloxane (PDES).[15] Keller and co-workers replaced the tin catalyst with platinum complexes used for polycondensation of PDES.[16] Furthermore, Motorola Inc. used in their patented self-healing capsule based material catalysts consisting of derivatives of aluminium (III), titanium (IV) and tin (V) attached to the surface of microcapsules.[17,18]

More recently, the cost of producing self-healing materials was reduced by the replacement of rather expensive and not stable catalysts with cheaper epoxy resins, and aromatic bis-phenols, which are cost-effective, have low toxicity, flammability and good thermal stability.[19] One of the first publications reporting the use of such resins comes from Yuan and co-workers, who prepared and characterised epoxy resin filled microcapsules.[20] Another improvement of capsule-based systems was invented by Kirk and co-workers. The group encapsulated a two part Buehler epoxy system consisting of a liquid epoxy resin and a hardener located inside nanoporous silica capsules, which additionally improved the mechanical properties of the composite.[22] Variation of capsule-based systems using epoxy resins was presented by Liu *et al*.[23] Superior shell strength of such capsules was reported due to use of diglycidyl ether of bisphenol A (DGEBA) as a resin mixed with ethylenediamine.

As the recovery time of self-healing materials is crucial, the acceleration of the recovery process in capsule-based systems was studied extensively. Neuser and Michaud reported that healing of epoxy resins was reduced from 2 hours to 10 minutes by use of microcapsules loaded with ethyl phenylacetate and the incorporation of shape memory alloy wires.[24] Later, research in Sun Yat-Sen and Jilin Universities reported a novel ultrafast self-healing material able to recover from damage within a few seconds.[25] The healing was obtained by use of a DGEBA resin encapsulated in poly(melamine formaldehyde) (PMF) spheres and accelerated by addition of silica walled microcapsules containing an antimony pentafluoride-ethanol complex acting as an instant hardener.

A novel approach eliminating the need of a catalyst was presented by Yao *et al.*[26] The described self-healing polystyrene composites contained embedded PMF capsules filled with glycidyl methacrylate (GMA). As polystyrene was synthesized by reversible addition-fragmentation chain-transfer (RAFT) polymerization, it kept its living characteristics. During the damage of the matrix GMA was released from the capsules and copolymerised with the living polystyrene chains. The damaged areas were filled by the healing agent covalently bonded to the polystyrene matrix and provided high

impact strength. Due to the living characteristics of the polymer, the healing was obtained without use of any other chemicals or catalysts.

Recently, capsule-based self-healing systems are being researched widely in industry. To date they have found applications in anti-corrosion coatings,[27,28] paints [29,30] and cementitious composites.[31] They have been reported as effective, practical, economical and easy to synthesise novel materials. Ongoing research in other fields is also being carried out.

The main drawback of capsule-based systems is the lack of repeated healing ability at the same location. Since chemical potential is exhausted by the rapture of microcapsules upon first polymerisation, further repairs at the same location are not possible. For materials required to exhibit repeatable healing the problem may be overcome by creation of a microvascular healing network.

1.1.2.2. Vascular systems

Vascular healing within a polymer matrix is obtained through a network of capillaries or channels. The network can have 1D, 2D or 3D connectivity and is usually connected to a reservoir of the healing agent. The chemicals can be delivered to the damaged area upon network breakage. The constant supply of the healing agent in this system allows multiple repairs at the same location.

One of the first self-healing materials, the hollow glass fibres (HGFs) matrix, can be considered as both capsule-based and a simple vascular system without repeatable healing properties. HGFs can be prepared using existing glass fibre synthesis techniques subsequently being filled with appropriate healing agents. Although initially the approach seemed to be promising, HGFs were found to provide only 1D connectivity and have very limited healing properties.[7]

The HGF repair and controlled cracking were pioneered by Dry and Sottos. The approach involved dispersion of cyanoacrylate-filled glass fibres able to release adhesive chemicals capable of sealing microcracks in a composite matrix.[4] The research was further expanded by Motuku *et al.* who focused on the processing

quality, the selection of storage material for the repairing solution, release and transportation of healing agents, distribution, number and type of nanotubes, self-healing material thickness, matrix material and impact energy level.[32] Alternative materials for fabrication of channels were used, such as borosilicate glass micro-capillary pipets, flint glass Pasteur pipettes, copper tubing and aluminium tubing. Further improvements were made by Pang and Bond, who fabricated highly effective fluid filling HGFs and solid glass fibres.[33] Their healing system was based on two epoxy resins that were organised into two separate layers and once broken provided quick release of healing agents and strong bonding and filling. Another approach that significantly increased material strength was introduced by Trask and Bond.[34] Quasi-isotropic HGFs at the ply interfaces were used, filled with either pre-mixed or two individual components of two-part liquid epoxy resin systems.

Due to the limited healing repeatability of the HGF approach, alternative techniques providing high connectivity of the channels had been developed. The complex network connected to a healing agent reservoir offered multiple healing of the same location, easy refilling of the channels and large amount of healing agent available to heal large volumes of damage. Multiple connection points of the microchannels allowed better self-healing properties, as a result of the presence of alternative routes for transport of healing material in case of localised channel blockage or multiple damage at the same side.[7]

One of the most common techniques used to create multidimensional networks of microchannels involves direct-write assembly using fugitive ink. The ink is deposited through a cylindrical nozzle into a multilayer 3D scaffold, which is subsequently immersed into uncured polymeric precursor. After solidification of the polymer and removal of the scaffold a multidimensional hollow channel system is formed. However, this approach is restricted to materials that can be synthesised around the fugitive scaffold (**Figure 1-4**).[35]

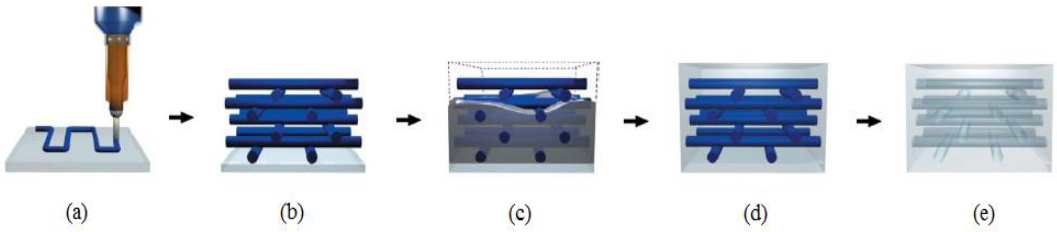

Figure 1-4. *Stages of creation of multidimensional microchannel network using direct-write assembly: a) creation of the network using fugitive ink, b) multidimensional channel network, c) immersion of network into uncured polymer, d) polymer matrix solidification and e) removal of fugitive ink.*[35]

In some vascular systems two independent networks of microchannels may be required. Hansen *et al.* reported that this type of interpenetrating microvascular networks may be created by direct-write assembly with dual ink deposition and vertical ink writing.[36] In the created system the first fugitive ink was composed of microcrystalline wax and mineral oil. The mixture melted at temperatures above 80 °C and could be removed from the matrix in order to create a network of microchannels. The second fugitive ink was composed of an aqueous, triblock-copolymer solution which softened at low temperatures. The difference in softening temperatures of these fugitive inks allowed independent removal of them and filling the networks with different substances, such as epoxy resin and epoxy hardener. The self-healing tests reported multiple healing up to 30 repeated damage-heal cycles.

Williams *et al.* reported detailed studies of the optimisation of vessel diameter and distribution of vessel lengths in order to provide the most efficient fluid flow.[37] Their further study focused on possible failure modes of vascular networks, as well as the formation of duplex and triplex of independent parallel systems.[38] Moreover, Aragon *et al.* studied microvascular flow networks and designed a multi-objective genetic algorithm used to obtain an optimal design of such networks.[39]

Another research programme explored pressurized vascular systems and use of various delivery strategies. Two parallel microchannel systems providing healing agents from an external reservoir were studied. Various pumping strategies such as static pressure, capillary flow or various dynamic pumping were examined.[40] In further research, mitigation of fatigue damage in self-healing vascular materials was studied.[41] Later, Williams *et al.* reported self-healing composite sandwich structures

manufactured by placing PVC tubes between adjusted sheets of various materials in order to create horizontal supply channels. Vertical riser channels were developed to improve the healing properties. Various configurations of the system were tested and optimised.[42]

Comparison of two delivery methods of self-healing agents in vascular systems was presented by Norris *et al.*[43] In the first one, named the single air filled system, an air-pressurised vessel was placed within the composite material. The damage of the matrix led to a loss of pressure that triggered the pump to deliver the healing agents. The healing efficiency was reported to reach 94% within 24 hours. A simplified second system was created by a continuous flow of the healing agent. The constant supply and circulation of the healing agent in the vessels provided 100% recovery of material's original strength and very strong bonding between the composite material and the healing agents. Due to high interconnectivity between the vessels. a single vessel was reported to heal large damage volumes. However, each vessel was found to provide healing agents only for one healing cycle.

Current developments in the field of vascular self-healing materials provide many manufacturing techniques and applications of these materials. The systems are being applied to a wide range of materials, including hard and rigid structures such as electronic conductors in stretchable wires,[44] as well as soft ones such as polymeric foams.[45] Patrick *et al.* focused on the healing of brittle polyisocyanurate foam using commercially available two-part polyurethane foam.[45] The study showed over 100% macro-scale recovery of fracture toughness after multiple optimised damage-recovery cycles, providing a promising self-healing concept for economical sandwich panels. Self-healing stretchable wires were studied by Palleau *et al.*[44] The wires consisted of liquid metal (eutectic gallium indium) injected into microchannels composed of self-healing polymers. The healed wires were reported to retain the same Young's modulus as undamaged material and could be stretched to up to 60% strain. However, the self-healing was reported to require mechanical alignment of the cut parts.

In the majority of SH materials with vascular systems the healing agent is introduced to the matrix after the damage. The need of an efficient flow of healing agents reduces the number of chemicals that may be used as healing agents. Factors like wettability, chemical reactivity and viscosity also need to be considered. However, the current achievements in the field of vascular self-healing technologies have proved that well optimised and adjusted systems provide excellent materials with the ability to efficiently heal multiple damage events of the matrix.[7]

1.1.2.3. Intrinsic systems

In intrinsic systems the repair properties are achieved due to inherent reversibility of chemical bonds within the polymer matrix. Intrinsic systems can be divided into four groups in which healing is obtained by: molecular diffusion or entanglement, reversible chemical reactions, ionomeric arrangements or hydrogen bonding.

The multistep mechanism of molecular diffusion and entanglement between polymer chains placed on opposite sides of the crack was discovered and explained by Wool and O'Connor. Polymer chains initially rearrange and approach each other. The next stage involves wetting of surfaces of the crack. Over the time, the chains start to diffuse between both surfaces to finally fully diffuse, equilibrate and randomise. Subsequent molecular entanglement provides full material strength (**Figure 1-5**).[46,47]

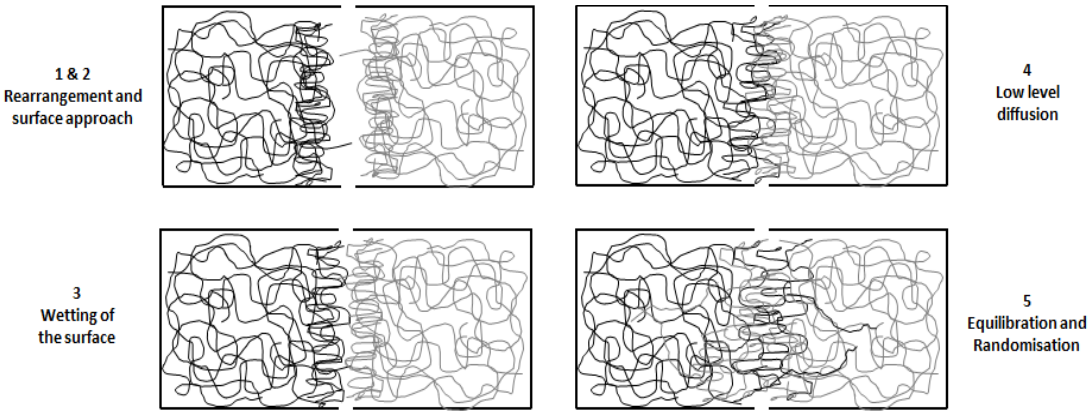

Figure 1-5. *The multistep mechanism of self-healing via molecular diffusion.*[47]

As the molecular interdiffusion is strongly time and temperature dependent, Yamagutchi *et al.* created an improved system able of healing cracks at relatively short times at room temperature.[48] Heating, immersing the matrix into solvent or utilisation of metabolic reactions between chain ends generated by molecular scission is known to accelerate molecular interdiffusion. Since liquids show repairing nature and solids keep their shape, the material displayed both solid and liquid properties. A cross-linked weak polyurethane (PU) gel created from diethylene glycol, adipic acid and hexamethylene diisocyanate showed 80% recovery of the tear strength after being healed. The healing occurred rapidly like in a liquid, although the material was reported not to flow or change shape due to the permanent, cross-linked network.

Another study explored thermally triggered molecular interdiffusion in epoxy-amine polymer thermosets. The matrix was created from DGEBA and 4,4'-methylene biscyclohexanamine and exhibited efficient and repeatable healing after 1 hour at 185°C, obtained through rearrangement of aligned free surfaces causing mechanical interlocking.[49] Further research showed that molecular interdiffusion occurs the most effectively at temperatures above the glass transition.[50]

The second type of intrinsic self-healing system involves the use of reversible chemical bonds. The healing of these systems is usually triggered by activation of dynamic chemical bonds by light or temperature. Examples of such reactions include cycloaddition reactions, dimerization of *N*-heterocyclic carbenes (NHCs) and metathesis reactions. A summary of the main self-healing techniques based on reversible chemical reactions between the chains is presented in **Figure 1-6**.

Cycloaddition reactions are used widely in these systems, especially Diels-Alder (DA) and retro-Diels-Alder (rDA) reaction. The first study of thermally-reversible DA systems with pendant furan groups cross-linked with maleimides was performed in the 1960s and patented in 1969.[51] Since then, the strategy has been greatly improved and optimised.

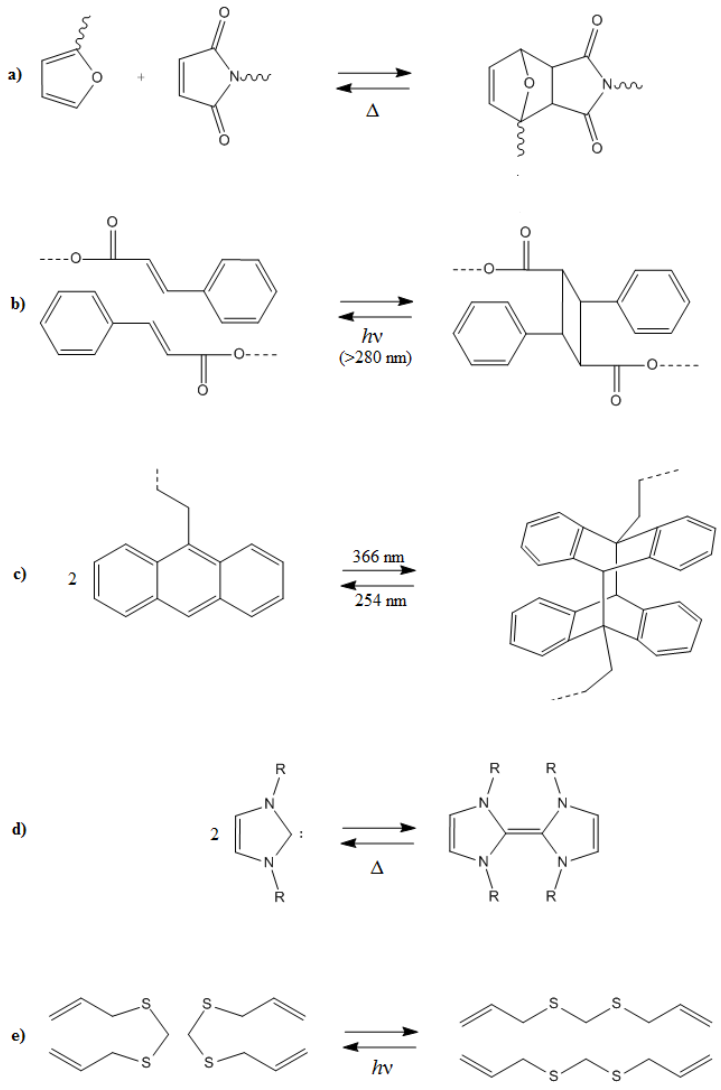

Figure 1-6. *The summary of self-healing techniques based on reversible chemical reactions between the chains: a) Diels-Alder reaction, b) [2+2] cycloaddition, c) [4+4] cycloaddition, d) dimerization of NHCs, e) metathesis reaction.*

Chen *et al.* reported formation of a transparent material from a furan tetra-linker (diene) and maleimide tri-linker (dienophile) able to disconnect approximately 30% of bonds *via* rDA at temperatures above 120 °C then reconnect upon cooling.[52] The material scraped with a razor blade was reported to reconnect after a 1 hour treatment at 130 °C, creating a homogenous material with a few minor defects and visible scars. It was reported that about 57% of the original fracture load was obtained, with a potential of full curing at an extended healing time. The process was described as fully reversible and repeatable.

Several improvements of the intrinsic cycloaddition reactions in SH systems were developed, aiming to increase the rate of DA reactions, decrease healing temperature and provide a broader application range for these materials. One of the most current achievements was reported by Oehlenschlaeger *et al.*[53] A polymer based on the hetero DA chemistry of a cyanodithioester with cyclopentadiene was created, providing extremely fast self-healing under mild conditions. The healing process occurred at temperatures as low as 70 °C and the sample stretched until break was completely reconnected within 10 minutes in a heat press at 120 °C.

Other types of cycloaddition reactions include a photo-induced self-healing approach, first reported by Chung *et al.*[54] The healing of a polymer was enabled by cinnamate monomers forming cyclobutane rings within its structure, which break upon crack formation. The efficient healing of these materials was reported to occur due to transformation of cinnamoyl C=C bonds into cyclobutane rings triggered by photoirradiation for 10 minutes with light irradiation of $\lambda > 280$ nm at 100 °C. The crosslinking *via* [2+2] cycloaddition, reverse reaction and re-photocyclisation were described as fast, simple, catalyst free and environment friendly.

A similar approach of [4+4] photocycloaddition was studied by Froimowicz *et al.*[55] Photo-reactive dendritic anthracene containing hyperbranched polyglycerol film was damaged, then irradiated with 254 nm light for 15 minutes, resulting in the backward decomposition (de-crosslinking) of the dimer and regenerating the building blocks. The treated film was kept overnight in the dark at room temperature to allow the material with a T_g below the room temperature to reorganise and equally cover the area. The process was followed by irradiation with 366 nm light for 120 minutes, inducing [4+4] dimerization of the anthracene and recreating the damaged matrix.

Dimerization of NHCs is another system using thermally reversible covalent bond formation to obtain self-healing properties, first studied by Kamplain *et al.*[56] Benzimidazole-based frameworks with bifacially opposing carbene moieties were used as monomers, supporting the formation of linear polymers and preventing the formation of cyclic species. The catalytic polymerisation created novel self-healing materials based on dynamic carbon-carbon double bonds. The research was further

explored by Neilson *et al.*[57] A library of starting materials used for electrical applications, including *bis*(azolylidene) with two NHC units, were used. The study was not focused on evaluation of self-healing properties, but it was observed that micro-cracks created on the samples disappeared after being heated at 200 °C for 60 minutes.

Most recently, metathesis reactions have been studied as promising reactions to be used in intrinsic self-healing systems. The reaction was the basis of research rewarded by the Nobel Prize in 2005.[58] In the approach based on olefin metathesis, light is used to break dynamic covalent bonds and create highly reactive radicals on damaged surfaces. The radicals on opposite sides of the crack can be subsequently recombined, resulting in recovery of the damaged surface.[3] Particularly useful metathesis reactions occur between disulphides,[59,60] allyl sulphides,[61] thiocarbonates[62] or novel disulphide-thiols.[63] To provide high efficiency of self-repair, high chain mobility is required.

The third technique involves the use of ionomers, polymers that contain up to 20 mol% of charged or ionic groups. The ions within the matrix interact with each other providing a secondary structure of the material. Under stress the ionic interactions get broken but can be recovered by restoration of the electrostatic interactions between charged groups. It was reported that self-healing ionomeric materials can be stressed and relaxed multiple times with good recovery of original features. For example, copolymers of ethylene and methacrylic acid were studied, with methacrylic acid salts used as the ionic groups. Within the ionomeric structure two phases were found – strong organic crystallites and weaker ionic aggregates. The autonomic self-healing occurred due to a friction and mechanical force present during stressing of the material, leading to an increase of temperature and destroying the ionic aggregates. Cooling of the system reversed the process and restored the molecular integrity.[12,47] A theoretical healing mechanism of ionomers is presented in **Figure 1-7.**

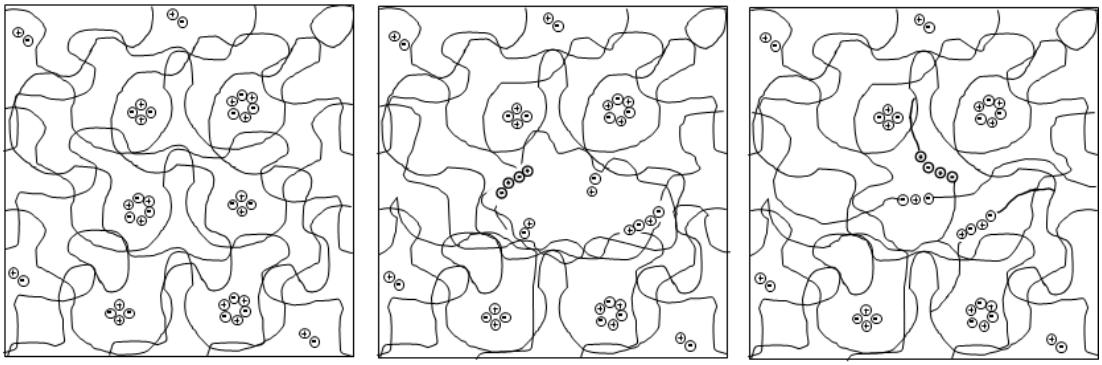

Figure 1-7. *Proposed mechanism of self-healing of ionomers: a) ionic structure in undamaged polymer matrix, b) damage causing elastic and plastic deformation and c) recovery of the overall shape with ionic rearrangements.*[47]

In the last group of intrinsic systems, the recovery properties are related to the secondary structure of a polymer matrix created by hydrogen bonds. In this approach the polymer matrix is widely cross-linked *via* hydrogen bonds. Upon damage or tear, separation of hydrogen-bonded moieties occurs. The formation of active moieties at the damaged surface allows the material to heal through restoration of the bonds. One of the materials that use crosslinking *via* hydrogen bonds to gain self-healing properties is thermoreversible rubber based on multivalent fatty acids. For example, Cordier *et al.* used three types of functional groups within the matrix to provide strong crosslinking *via* multiple hydrogen bonds, including incorporation of imidazolidone, and urea.[64] All materials showed very good healing properties during multiple break-heal cycles without creation of any visible scars. Interestingly, one of the tested materials exhibited self-healing upon bringing together two broken or cut parts at room temperature, without application of stress or increasing temperature. A broader study of the nature, dynamics and properties of hydrogen bonds, as well as ageing of supramolecular self-healing rubber was carried out by Zhang *et al.*[65]

Intrinsically healing materials using hydrogen bond breakage and restoration to recover damage have attracted a lot of attention in recent years. One of the most promising group of materials offering creation of transparent, self-healing materials using hydrogen bonding are polyurethanes. This will be discussed in detail in section 1.2, focusing on the use of polyurethanes to create self-healing materials.

1.1.3. Self-healing of optical materials

A number of factors must be considered in order to design efficient self-healing materials. An ideal self-healing material should recover all characteristics of the original material e.g. tensile strength, texture or transparency, as well as chemical properties. The mechanism of self-healing should be activated only when it is needed and only at the place of damage. The material should be long-lasting and allow repeatable healing to provide a durable structure. The self-healing should also occur at different levels of damage. Additionally, the materials used to create the material should be economical and suitable for mass production.[8]

Use of a self-healing material as a part of a transparent appliance requires precise adjustment of the physical properties. Optical devices often consist of multi-layered materials,[66,67] thus formation of a self-healing outer coating is the most suitable application. As the main function of a coating is protection of the underlying material, factors like transparency, optical activity and haze level need to match the properties of other layers and be optimised to provide minimal disturbance during use of the device. Moreover, as the coating may be exposed to a number of external stimuli, the influence of factors like UV stability, humidity or friction must be explored.[8]

Self-healing materials containing vascular networks are usually unsuitable to use as transparent coatings. Filling of large damage volumes is unnecessary for the recovery of a scratched layer of the self-healing coating. Furthermore, the physical properties of the vascular self-healing coatings may be not compatible with their applications. The presence of microchannels can also influence transparency and haze of the material, although some novel methods, e.g. femtosecond laser irradiation followed by a chemical etching process, allow the creation of 3D microchannels with retention of the material transparency,.[68,69] Additionally, the healed crack may be filled with an excess of healing agent, making the surface rough or uneven, resulting in a thickness of the coating that may affect transparency and haze.

Capsule-based systems are more suitable to use in transparent coatings and have been researched and used in the crack healing approach of transparent materials.

Coillot *et al.* created a glassy matrix containing dispersed microcapsules with vanadium bromide particles.[70] Oxidation of these particles at elevated temperatures lower than the softening point of the glass provided efficient self-healing of the material. At temperatures between 400 °C and 700 °C rapid creation of V_2O_5 and B_2O_3 and local formation of glass was observed. The very high temperature required to initiate healing of the glass excludes its commercial use for optical devices, but the technology may be potentially used in high-temperature enamelled reactors or for aerospace and military applications.

Jackson *et al.* focused on optimisation of physical and optical properties of transparent PMMA and polystyrene coatings containing urea-formaldehyde capsules filled with dibutylphthalate (DBP).[71] It was reported that the use of small capsules with DBP was effective for thin PMMA films due to the similarity of their refractive indices. The material also displayed good recovery efficiency.

However, the use of microcapsules in transparent materials has several limitations. The main disadvantage of the system is that microcapsules can scatter light causing limited transparency of the material. The reduction in light scattering can be obtained by adjusting the size of the microcapsules, their concentration and refractive index. Jackson *et al.* reported that the diameter of a single microcapsule should not exceed 1 μm and the refractive index should be as close as possible to that of the material, with a maximum difference of 4%, and the concentration of capsules needs to have the maximum value of 7-10%.[71] Unfortunately, the optimisation of size, concentration and properties of the microcapsules limits the healing properties of the materials. Moreover, multiple healing at the same place is impossible due to microcapsule exhaustion.

It may be concluded that intrinsic systems appear to be the most suitable for optical applications. Various techniques, achievements and systems will be highlighted in the next section.

1.1.3.1. Current technologies

Several transparent materials potentially suitable for optical applications have been reported in recent years. The majority of them exhibit unlimited self-healing properties, although the systems are usually non-autonomic, thus require an external trigger to initiate the healing.[8]

An example of such a self-healing system is reported by Rodriguez *et al.,* created from a blend of linear and cross-linked poly(ε-caprolactone) (PCL), known as Shape Memory Assisted Self-Healing (SMASH) (**Figure 1-8**).[72] Shape memory polymers are a class of smart materials showing reversible plasticity, able to recover their original shape from a temporarily deformed state upon heating. The created SMASH system exhibited self-healing properties obtained through diffusion of polymer chains, supported by the shape memory properties.

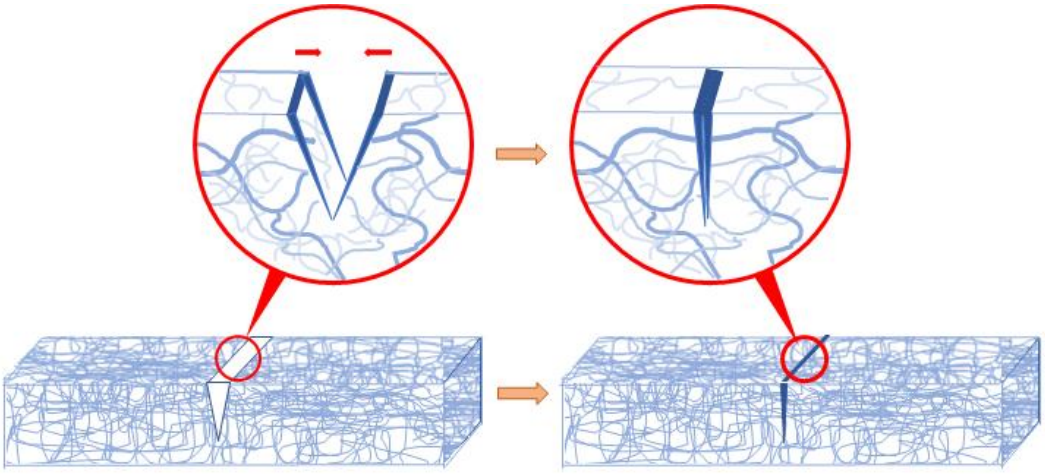

Figure 1-8. *Shape-memory assisted self-healing concept – closure of the crack upon a trigger.*[72]

This transparent material displayed self-healing properties upon heating up to 80 °C for 10 minutes and reached a healing efficiency of 95%. The healing of the SMASH material is based on molecular mobility, triggered by the presence of two different polymer chains within the structure. The branched n-PCL chains provided the material with thermosetting properties and the linear l-PCL chains provided thermoplastic properties. The semicrystalline structure and the presence of crosslinks within the structure allowed a temporary deformation of the matrix obtained by

crystallisation of linear chains at temperatures below the melting temperature (T_m) and recovery of the original shape obtained by heating up the material to above T_m. During healing the system returned to the highest conformational entropy state, followed by crack rebonding *via* diffusion.[72]

A novel type of corrosion resistant SMASH coating was presented by Luo *et al.*[73] l-PCL fibres were randomly distributed in a shape memory epoxy matrix. The material was scratched and heated up to 80 °C showing high healing efficiency and restoration of original physical properties. Scanning electron microscopy (SEM) revealed complete crack closure. It was explained that heat triggered two events: bringing the crack surfaces in closer proximity through the release of stored strain energy and providing l-PCL with enough energy to become mobile, flow and rebond the crack. However, the crack closure was limited if permanent material loss occurred.

Further improvement of SMASH was reported by Rivero *et al.*[74] The method named Diels-Alder SMASH combined three approaches: a shape memory PCL system favouring crack closure upon heating, a polyurethane chemically cross-linked with furan based groups improving mechanical properties, and a reversible Diels-Alder system offering thermally triggered self-mending. The tough, flexible, transparent and lightly coloured films were scratched with a diamond spherical tip creating micro-scratches and a razor blade creating macro-scratches. During the damage, breakage of DA bonds occurred leading to regeneration of free furan and maleimide functional groups, while upon heating to 100 °C reconnection of the groups was observed.

The healing of such systems can be improved by increasing molecular mobility. For example, a low viscosity self-healing hydrogel-based film containing cinnamate nanoparticles providing the material with reversible bonds was recently reported.[75] The scratched swellable films were immersed in an azeotropic solvent (THF/water or 2-propanol/water) and left to dry. As the re-solvation provides the polymer chains with mobility, the energetically favourable reformation of the polyelectronic interactions enabled reorganisation of the network and disappearance of the damage. Additionally, due to the presence of cinnamoyl groups, irradiation of the

films with 254 nm and 280 nm light induced decomposition and dimerization of the links through [2+2] photo-cycloaddition, respectively.

A similar system with furfuryl glycidyl ether was presented by Pratama *et al*.[76] Various polymer films were scratched with a razor blade and the healing was measured after three treatments: heat treatment at 90 °C for 2 hours, immersion in dimethylformamide (DMF) and immersion in bismaleimide (BMI) solution in DMF. The healing was evaluated using SEM and corrosion tests. The furan-functional epoxy-amine thermoset films of thickness 100 µm showed the best self-healing properties in BMI solution, with 70% recovery compared to 14% obtained for heat treatment and 28% for solvent healing. It was reported that during immersion the solvent caused swelling of the film, bringing the crack surfaces together, while *bis*-maleimide promoted the Diels-Alder reaction between furan and maleimide groups.

Other examples of systems using swelling of a polymer matrix in solvent to decrease the viscosity include sugar based organogels,[77] peptide-based organogels[78] or metallo-gels.[79]

An increase of molecular mobility can be also obtained by addition of water. Wang *et al.* reported transparent polyelectrolyte multilayer coatings made of branched poly(ethylenimine) (bPEI) and poly(acrylic acid) (PAA) displaying excellent healing properties.[80] Spraying the film with water was found to be effective for healing of small cuts up to 50 µm wide, while large scratches were healed by immersing the coatings in water at room temperature for 10-300 seconds. The healing ability was explained by the high flowability of the polymer and the interdiffusion of polyelectrolytes at the damaged surfaces. The healing was found to be repeatable, independent of the waiting time after damage and thickness-dependent. Current research involves attempts to incorporate nanofillers into the films in order to fabricate more robust films.[81]

Self-replenishing polyurethane coatings are another interesting group of self-healing materials. Coatings containing perfluoroalkyl dangling chains linked to a PCL polymeric matrix were first reported by Dikic *et al.* and offered complete recovery of

their functionality.[82] The hydrophobic films were damaged with a microtome. During the damage the dangling chains created a new air interface, orienting towards the surface and creating a depleted layer underneath the new surface. The replenishment of the surface occurred immediately after damage, spontaneously for materials with low T_g and with a temperature trigger for materials with high T_g.

Incorporation of photo-reversible bonds in transparent films allows near ultraviolet or visible light triggered self-healing. Chung *et al.* reported creation of hard transparent films formed from 1,1,1-tris(cinnamoyloxymethyl)ethane (TCE) with cinnamoyl chloride.[54] Efficient healing of cracks was obtained by irradiation of the films with a 280 nm light for 10 min *via* a [2+2] addition process. In this system internal cracks or thick scratches were reported to be unlikely to heal as the result of reaction occurring only on the surfaces exposed to light. Froimowicz *et al.* studied [4+4] reactions of anthracene derivatives.[55] Hyperbranched polyglycerol transparent polymeric films were found to heal efficiently upon irradiation at 254 nm triggering regeneration of building blocks, followed by irradiation at 366 nm restoring the crosslinks.

Metathesis is another widely studied reversible reaction enabling self-healing of polymers. Canadell *et al.* reported polymer created from epoxy-terminated aliphatic polysulphide, Bisphenol A based epoxy resin and tetrathiol.[61] The yellowish, transparent film showed high tensile strength and good healing properties upon heating to 60 °C for 1 hour. It was reported that healing efficiency was proportional to disulphide concentration.[60] Other monomers, such as diamines and dithiols containing disulphide groups, may be also used to create moieties with reversible metathesis reactions. For example, Scott *et al.* synthesised a transparent material exhibiting self-healing using allyl sulphide groups.[61] Amamoto *et al.* reported a transparent polymer synthesised using RAFT copolymerisation of trithiocarbonate (TTC) cross-linker and n-butyl acetate. The complete, repeatable healing of scratches was observed after 12 hours of UV photostimulation of the matrix immersed in acetonitrile or in the bulk state after 48 hours under nitrogen atmosphere.[59]

A novel approach for creation of self-healing materials used for optical applications was proposed recently by Burnworth *et al.*[83] Colourless and elastic metallosupramolecular polymers consisting of metal-ligand complexes forming hard segments and polymeric matrix forming soft segments were healed by reversible dissociation and reformation of bonds among Zn^{2+} and La^{3+} metal ions. The metal-ligand bonds were reported to absorb energy from UV irradiation in the 320-390 nm range and convert it into heat. The thermal energy initiated the dissociation of metal-ligand bonds, decreased the polymer's molecular mass and viscosity, and reformed metal-ligands, resulting in healing reaching up to 100% efficiency.

The use of Zn^{2+} ions was also researched by Coulibaly *et al.*[84] The transparent, light-healable materials were created from nanocomposites based on a metallosupramolecular polymer and cellulose nanocrystals used to increase stiffness and strength of such polymers. The films were cut to a depth of 50-70% and exposed to UV light in the range of 320 and 390 nm, reaching healing efficiency of up to 90%.

Skorb *et al.* exploited anticorrosive coatings made of hybrid sol-gel materials with dispersed benzotriazole filled TiO_2 or SiO_2 capsules.[85] Interestingly, the healing agents were released upon UV radiation and took place only in the damaged sites. To adjust the triggering wavelength silver particles with surface plasmon absorption bands in the visible range of the light spectrum were used. Also, Allesandri *et al.* used gold nanoparticles to enhance the UV-triggered healing of acrylic adhesives.[86]

Organosiloxanes are another group of materials known to exhibit excellent self-healing properties. The unusual behaviour of these materials was first observed in the 1950s. More recently, the chemistry of poly(dimethylsiloxane) was researched by Zheng *et al*.[87] The transparent material displayed excellent repeatable healing properties upon heating at 90 °C for 24 hours obtained through siloxane equilibration. The presence of ethylene bridges within the matrix enabled easy control of cross-link density, allowed to reach an equilibrium after damage and provided high interface strength of a healed material comparable to original. A similar material described as having the potential of self-healing, α,ω-dichloride-terminated multi-vinyl branched siloxane, was reported by Fu *et al.*[88]

A novel polysiloxane film designed for space applications was reported by Lei *et al.*[89] The polymer was created from hyperbranched polysiloxane and polyimides and displayed high optical transparency, excellent thermal stability and good mechanical strength. The self-healing was obtained through the formation of a protective SiO_2 layer triggered by contact of the damaged material with atomic oxygen.

Self-healing epoxy elastomers cured with polythiol containing alkoxyamine crosslinks were reported recently by Zhang *et al*.[90] The healing was examined visually during repeatable cut-reconnect cycles at room temperature and tensile strength measurements. Electron spin resonance spectroscopy was used to study the process and showed that the recovery was triggered by dissociation and association of the C-ON bonds.

Materials described in this section showed a broad range of chemistry used to create self-healing coatings of various applications. However, the majority of the materials were not designed as transparent coatings for optical application. Though some of the materials were reported to be suitable for optical application due to their high transparency, more detailed evaluation of properties such as haze and refractive index were not reported. Additional exploration of physical properties such as fracture toughness, strength, abrasion resistance or standardised healing evaluation would be necessary to compare these practical, efficiently self-healing coatings.

1.2. PROTECTIVE COATINGS

Polymer films are used in numerous applications, e.g. packaging, labels, construction components, photographic films etc. The films are usually formed *via* extrusion of molten polymer beads. While some films consist of one main type of material, e.g. polyethylene plastic bags or polypropylene films on microwavable food containers, others consist of a stack of various thin films, called multilayer polymer films.[91,92] Multilayer polymer films are common in applications in which a single material does not fulfil all the required specifications.[91] For example, lenses of sunglasses consist of multiple layers such as UV-protection layer, polariser layer, glare absorption layer or impact-resistant layer.

Multilayer polymer films commonly contain a wear-resistant outer layer, known as a protective coating. The protective coating applied to a substrate can provide the material with additional properties such as waterproofing, friction-resistance, scratch-resistance or water-repellence.[93]

1.2.1. COATING SYSTEMS

Protective coatings can be applied as a thin layer on a surface of a substrate, known as thin-film deposition. Deposition techniques can be divided into two main categories: chemical deposition, in which the process is mainly chemical, and physical deposition, in which the process in mainly physical. While physical deposition usually requires very high temperatures, high vacuum, and specialised and often expensive equipment, chemical deposition techniques are usually low cost and a require simple set-ups.[94] Among the various chemical deposition methods used for polymer films, knife systems, metering rod systems, roller systems and dip-coating systems are worth mentioning.

1.2.1.1. Knife systems

In knife systems the coatings are produced using an application device and a wiping device, known as a knife. The application device spreads a layer of coating on the substrate and the excess material is removed and smoothed down with a metal knife (**Figure 1-9**). The applied medium must be in a liquid form, e.g. a hot polymer melt or a liquid solution. This low-cost technique allows precise application of a coating of a desired thickness and can be used on uneven materials. In some advanced systems the knife can function simultaneously as an application device, a spreading device and a wiping device.[95]

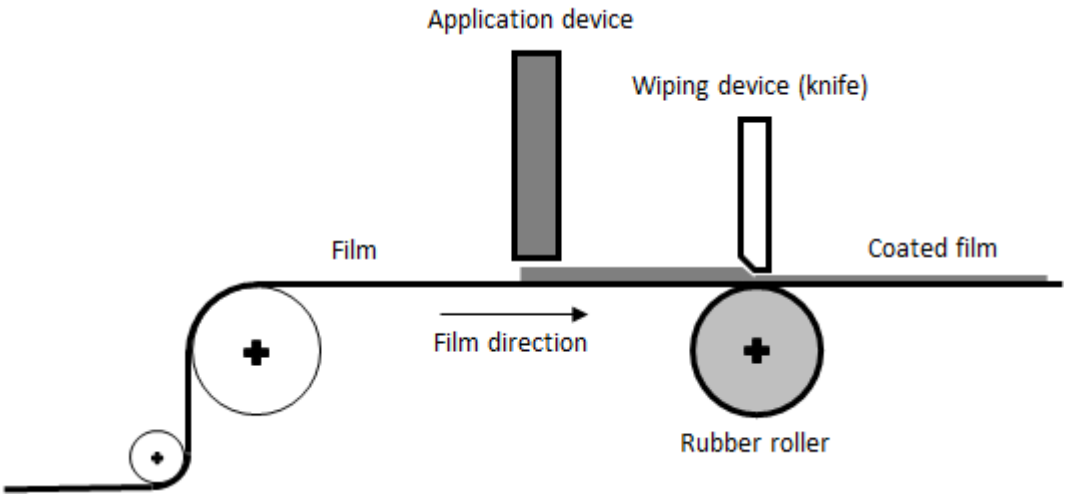

***Figure 1-9**. Roller knife coating application system.*[96]

The system is inexpensive to install and maintain and provides a good quality coating. The small amount of moving parts increases the reliability of the system. However, the maintenance of the knife itself is the main disadvantage. The blade must be kept sharp and smooth to ensure the uniformity of a coating. Furthermore, the cleaning of the knife is also time-consuming and requires precision

1.2.1.2. Metering rod systems

In another liquid surface coating technology, the knife is replaced with a metering rod, also known as a Mayer rod (**Figure 1-10**). The Mayer rod was invented by Charles W. Mayer in 1905 in New York. The rod consists of a core bar wound tightly with a stainless-steel wire of a known thickness, varying between 4.5 µm and 350 µm. The diameter of the wire coils and the size of grooves between them determines the amount of a coating applied, thus directly influencing the thickness of a coating. The theoretical value of the wet coating thickness can be calculated with accuracy within 0.1 mil (1 mil = 1/1000th of an inch) and can be related to a dried coating thickness if the percentage of solid content of a solution is known. Some other factors, such as the viscosity of a coating solution, web tension or the speed of the moving substrate can also influence the thickness of a created coating. However, all these factors introduce less than 20% difference from the theoretical coating thickness.[96] **Table 1-1** presents a conversion table of the rod size and coating thickness.

***Table 1-1**. A conversion table of the rod size and coating thickness*

Rod Size	Wet Mils	Thickness Microns	25% Solids	50% Solids	75% Solids	100% Solids
005	0.5	12.7	3.2	6.4	9.5	12.7
010	1	25.4	6.4	12.7	19.1	25.4
015	1.5	38.1	9.5	19.1	28.6	38.1
020	2	50.8	12.7	25.4	38.1	50.8
030	3	76.2	19.1	38.1	57.2	76.2
040	4	101.57	25.4	50.8	76.2	101.6

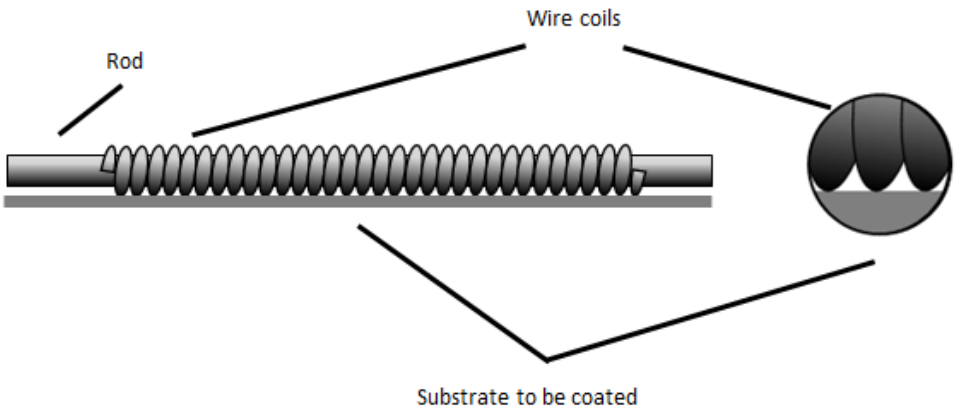

***Figure 1-10**. Wire-wound Mayer rod.*

The coating application is similar to the roller knife technique, with the knife being replaced with a Mayer rod being used to work against a rubber or a metal backup roller (**Figure 1-11**). The rod can rotate in the same direction or in the opposite direction to the movement of the film. As the Mayer rod acts as a wiping and smoothing device with an uneven surface, the initial shape of a coating on the moving film is a series of lines. Subsequently, due to a surface tension of the solution the stripes of coating collapse creating a flat surface. Therefore, the viscosity of the coating solution is crucial for efficient coating.[95]

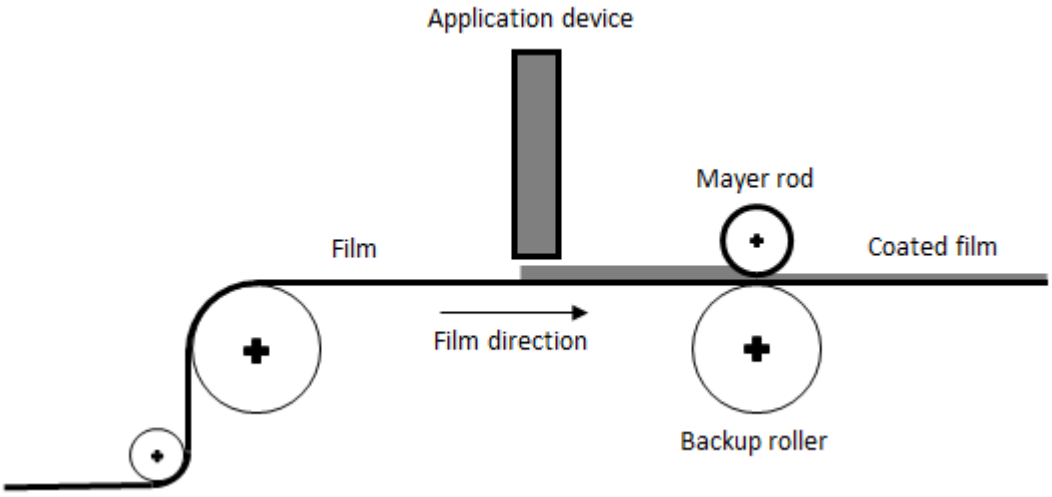

Figure 1-11. *Mayer rod roller coating application system.*[96]

The main advantage of the system is the low cost of the equipment and the ease of operation, as the Mayer rods are inexpensive and easy to clean, change or replace. Furthermore, the system allows for a precise control of a coatings' thickness, in 0.1-0.2 mil increments. The disadvantage of the system is the viscosity of coating solutions, as the Mayer rods work best with liquids of low viscosity. However, an improved version of a Mayer rod known as a grapped rod can be used with higher viscosity coatings, due to the wires being separated from each other.

1.2.1.3. Roller systems

In another coating system, known as a roller system, the coating is applied using rollers alone. An example of such system is a reverse roll coater, in which a dosing roller and an application roller contra-rotate, creating a gap filled with a coating medium (**Figure 1-12**). The application roller, loaded with an excess of coating, deposits the coating on surface of a moving film. The distance between the application roller and the rubber impression roller determines the thickness of the coating.[95]

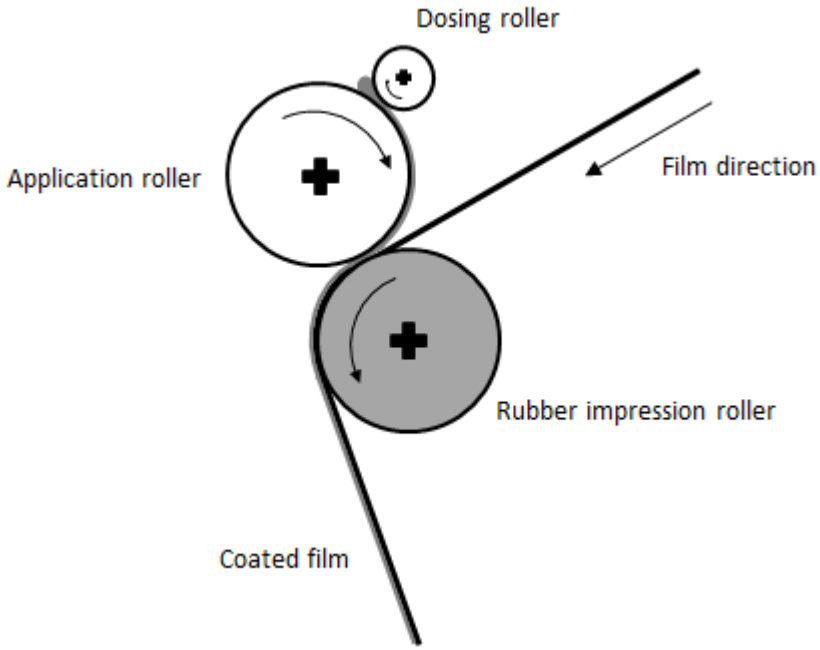

Figure 1-12. *Reverse roll coating system.*[96]

The system offers a great flexibility and precision of coating, with a wide range of coating thickness, viscosity, materials and speed of the line that can be used. However, the high cost of the instrumentation, the complexity of the system control units and the time-consuming set-up and maintenance of the system are the main disadvantages.

1.2.1.4. Dip-coating systems

The last system is a dip-coating system, in which the coating is applied on a film surface *via* immersion in a reservoir filled with a coating medium. The thickness of the coating deposited on a substrate is determined by the speed of film. The excess

coating can be further removed using a roller, a knife or a Mayer rod.[95] An example of such system is presented in **Figure 1-13**.

Moreover, the systems can also offer a three-dimensional coverage by lowering the position of the dipping roller so it remains fully immersed in the coating solution. That allows both sides of a film as well as the edges to be coated.

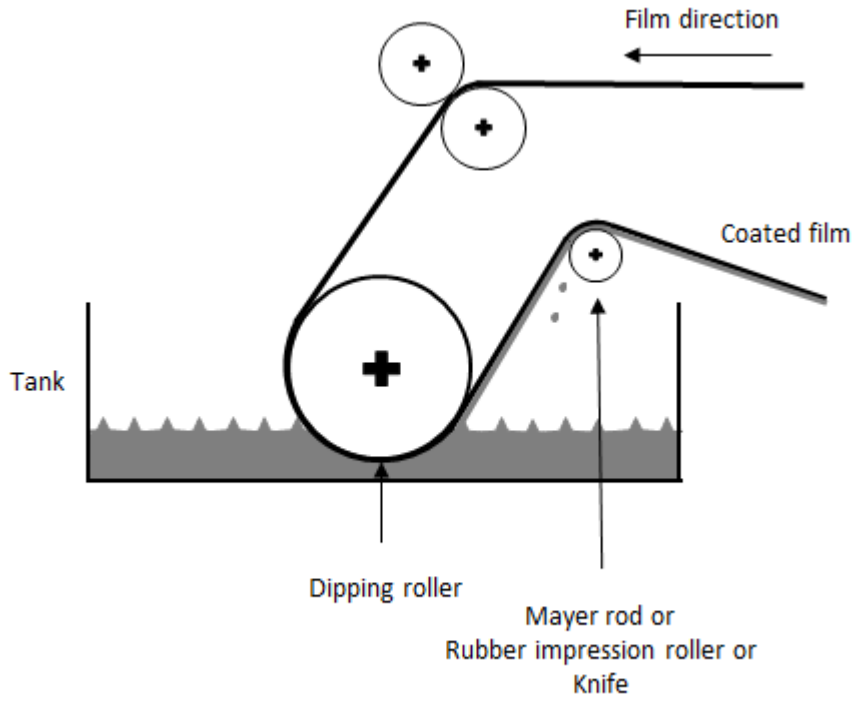

Figure 1-13. *Dip-coating system.*[96]

The dip-coating systems allow formation of uniform, high quality coatings on various substrates, including bulky and complex structures. The system is also highly efficient, minimising the amount of wasted material, as well as offering coating of both side of a substrate. However, the equipment used for dip-coating can be expensive and its cleaning can be very time consuming. Moreover, the coating process must be performed in a clean room to avoid tank contamination. Additionally, due to the relatively large size of a tank, it requires large volumes of the liquid coating, which may increase the cost and the amount of waste if the substrate volume is low.

1.2.2. CELLULOSE TRIACETATE

Among many commercially available films, cellulose triacetate (TAc) is one of high importance. The material is widely used in photography as a safe film base, first produced commercially in 1954 by the Celanese corporation. Other uses of TAc films include polariser films, projector view foils, packaging or semipermeable membranes.

TAc films are one of the organic polyesters of cellulose. TAc is produced from purified cellulose by a process known as acetylation, where acetic anhydride converts hydroxyl groups into acetyl groups in a presence of a catalyst. For the material to be called TAc at least 92% of the hydroxyl groups must be replaced with acetyl groups.[97] The structures of cellulose and cellulose triacetate are presented in **Figure 1-14.**

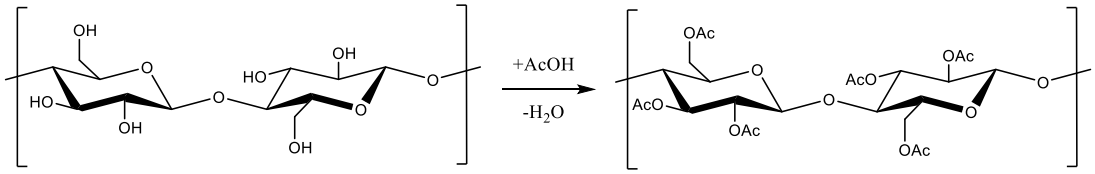

Figure 1-14*. The acetylation of cellulose to cellulose triacetate.*

Due to the high softening point of TAc, the material shows very high toughness and hardness, therefore it cannot be moulded or extruded. Moreover, it is highly resistant to most common solvents, therefore casting of TAc films require special multicomponent solvent mixtures, such as methylene chloride and methanol.[98,99]

The sheets of TAc show a number of essential properties required of an optical base film which may act as a substrate of a multilayer polymer films. The films are highly transparent and have an excellent optical clarity. Moreover, the flexible films can be easily cut, shaped, laminated and coated, thus they are used widely as base films or coating components.

1.3. POLYURETHANE COATINGS

1.3.1. STRUCTURE, PROPERTIES AND APPLICATIONS OF POLYURETHANES

Polyurethanes (PU) are widely used across a number of industries, including in vehicles, construction, furniture and electronics industry. The properties of polyurethanes vary from very soft, rubbery elastomers to hard, ceramic-like systems. The adjustment of physical properties of PUs depends mainly on their chemical structure and formulation methods. Alongside with the most popular form of polyurethanes including foams, elastomers, rubber, adhesives or gels, PUs in the form of hard coatings are in high demand in the market. Around 13% of polyurethane consumption in 2013 was accounted by the paints and coatings industry.[100] PU lacquers and coatings are broadly used for painting wood, road and rail vehicles, aircraft and ships, coating metals, papers or leather dressing.[101]

One of the most promising groups of self-healing materials is based on polyurethane (PU) chemistry. Due to the unique physical and mechanical properties of PUs, this group of polymers attract the attention of many chemists and engineers designing self-healing coatings.

PUs are used widely as coatings that are shiny, clear, resistant to abrasion and corrosion, have high mechanical strength and show good elasticity.[102] Benefits of using PU coatings over cheaper coatings include higher abrasion resistance, tensile strength, tear propagation resistance, strong adhesion and high chemical resistance.[103] A number of formulations are commercially available from various companies, including Bayer MaterialScience, Henkel, Resin Surfaces Ltd. or Metal Coatings Corp. In order to create a good PU coating exhibiting desired physical properties, good understanding of the link between chemical structure and physical properties is necessary.

PUs are formed from two basic components: a diisocyanate and a chain diol. The basic chain growth reaction of these two components leads to the production of linear polymer linked by urethane (carbamate) links.

The choice of a type of isocyanate and polyol results in the creation of polyurethanes exhibiting different properties, varying from thermoplastic PUs, such as sporting goods or footwear, flexible PUs, such as foams or packaging, to rigid PUs, such as thermal insulators. The polymeric morphology can be further adjusted by incorporation of chain extenders (CE) and cross-linkers. These low molecular weight compounds allow controll of properties such as phase-separation or phase-mixing, crystallization, chemical resistance or insulation properties.[104]

The influence of chain extender length on the properties of polyurethanes was studied by a number of groups.[105] Blackwell *et al*. observed that chain extenders with an even number of carbon atoms, except from ethylene glycol, promote crystallinity and packing.[106] That was also confirmed by Chang *et al.*[107] Introduction of an amine CE is known to create more rigid poly(urethane-urea) (PUU) coatings. PUUs had been reported to have higher melting and glass transition temperatures[108] and superior thermal and mechanical properties.[109,110] That is caused by the presence of stronger hydrogen bonding between the urea groups creating mono- and bidentate H-bonds with higher bond energy.[111]

Hard, dense systems with great adhesive properties are created by introduction of highly cross-linked networks, while softer, more elastic materials are formed from linear polymer chains with less cross linking.[112] Crosslinking is a process of linking polymer chains together. During crosslinking linear chains are covalently bonded, leading to a formation of network polymers.[113] Introduction of crosslinking is widely used to improve various properties of polymers, such as mechanical and adhesive properties, solvent resistance or thermal resistance.[114,115] Jin *et al.* observed that crosslinking improves the elastic modulus and adhesive interactions of polydimethylsiloxane.[116] The improvement of properties of crosslinked polymeric materials is caused by changes in the polymers' structure.[117] Yang *et al.* reported that in waterborne, crosslinked polyurethanes rearrangement of soft and hard segments was observed, leading to an increase of T_g and melting temperature (T_m). These changes significantly enhanced adhesive strength, tension strength, hardness and waterproof performance.[118]

Due to the internal structure of PUs two segments can be distinguished within the matrix – a hard one and a soft one. The soft segments are made of long chain diols possessing low polarity and low glass transition temperature. The hard segments are formed from isocyanate and chain extenders creating rigid segments with a high density of polar urethane groups and high glass transition temperature.[119] As a result of high polarity, the hard segments tend to attract each other and aggregate, and in some cases forming crystalline blocks connected *via* hydrogen bonds. Therefore, the flexible soft segments are reinforced with ordered hard segments *via* pseudo-net points creating thermally reversible physical crosslinks and H-bonds. Thus, the resulting copolymer can be thus described as composed of the hard segments providing toughness, dispersed in the soft segment providing flexibility and elasticity (**Figure 1-15**).[102,120]

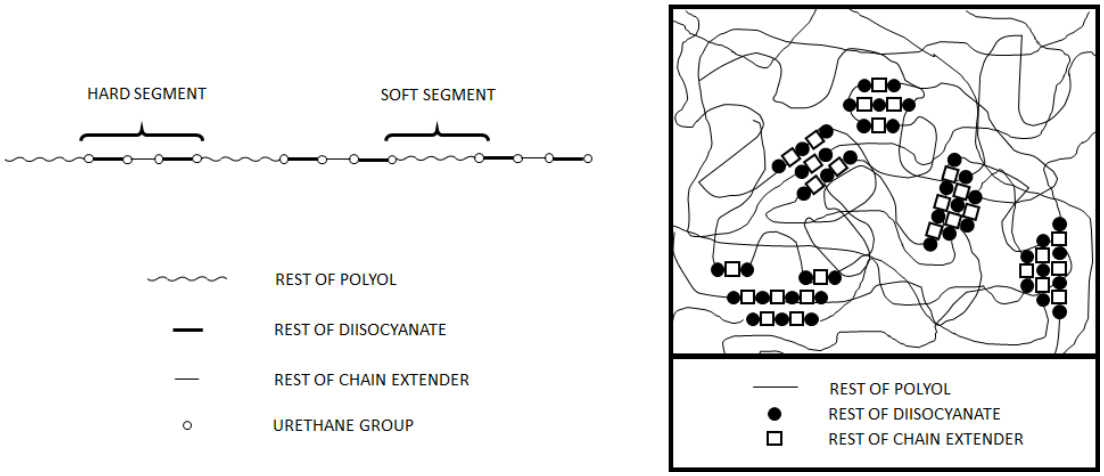

Figure 1-15. *Schematic representation of: a) chain structure of PU and b) formed block copolymer.*

The hard segment content (%HS) can be calculated using the equations derived by Flory. It is possible to calculate the %HS as the chain-extended urethane content using **Equation 1.1**, or the combine urethane and chain-extended urethane content using **Equation 1.2**. where *R* is the mole ratio of isocyanate to polyol and M_{iso}, M_{CE} and M_{ol} are respectively number average molar masses of isocyanate, CE and polyol.[121]

$$\%HS = \frac{(R-1)(M_{iso}+M_{CE})}{M_{ol}+R\times M_{iso}+(R-1)\times M_{CE}}\times 100 \qquad \textbf{Equation 1.1}$$

$$\%HS = \frac{R \times M_{iso} + (R-1)(M_{CE})}{M_{ol} + R \times M_{iso} + (R-1) \times M_{CE}} \times 100 \qquad \textbf{Equation 1.2}$$

It has been well established that the properties of polyurethanes are related to their biphasic morphology. Intermolecular interactions between the HS and SS present in PU can lead to either phase-separation or phase-mixing of the polyurethane matrix (**Figure 1-16**). In phase-separated systems HS and SS do not mix together and thus segregate into a biphasic structure consisting of SS-rich and HS-rich blocks. That promotes packing of polymer chains, leading to highly organised structures, increased crystallinity and higher haze. Phase-mixed systems create a single phase structure in which SS and HS tend to be more amorphous and have lower crystallinity and haze.[122]

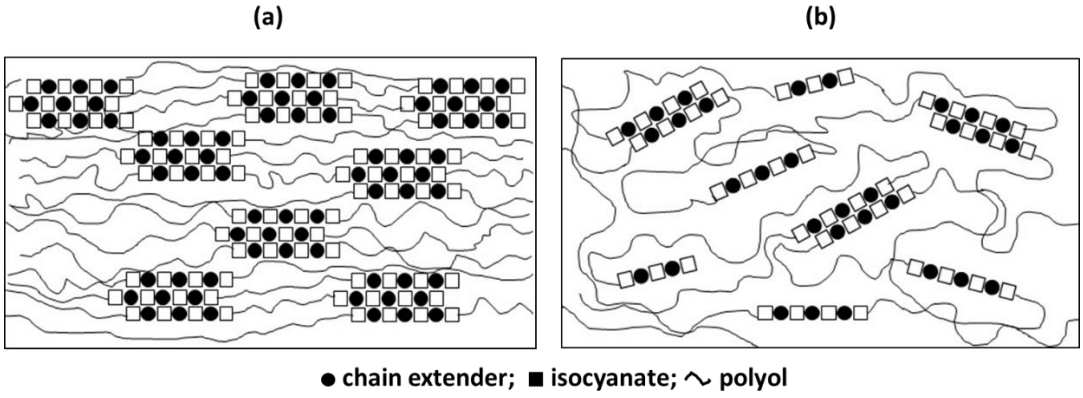

Figure 1-16. *Morphology of polyurethane matrix: (a) phase-separation and (b) phase-mixing.*

The extent of phase-separation within a polyurethane matrix depends on thermodynamics and kinetics driving forces.[123]

Usually, the thermodynamic phase incompatibility is the driving force leading to phase-separation, observed as e.g. macrophase-separated structures present in incompatible polymer blends. However, in block copolymers, such as PU, the chemically incompatible segments are confined by the covalent bonds present within the polymer chains. Therefore, the microphase separation is a localised process present in a much finer scale and is largely influenced by the forced closeness of the phases.[124] The incompatibility in PUs occurs due to the high polarity of HS leading to

stabilisation of the semi-crystalline segments *via* hydrogen bonds between the urethane groups. Therefore, the degree of phase-separation is dependent on the chemistry of HS and SS. Moreover, in systems with a low HS content the hard segments are usually well dispersed in the amorphous matrix of SS, while an increase of HS content leads to increased interactions between hard segments creating large blocks of HS. Additionally, an increase of the length of the polyol was found to increase phase-separation, caused by an increased content of SS, as well as the hydrophobicity and crystallinity of the long chain polyols.[105] Therefore, the degree of phase-separation is also dependent on the ratio of the segments and the mobility of SS.

The Flory-Huggins solution theory can be used to describe the thermodynamics of phase-separation. The theory describes the enthalpy change of mixing as:

$$\Delta H_m = kT\Phi N\chi \qquad \textbf{Equation 1.3}$$

where k is the Boltzmann's constant, T is temperature, Φ is the lattice volume fraction, N is the number of repeat units in the sequence and χ is the Flory-Huggins interaction parameter.[125]

The Flory-Huggins interaction parameter χ defines the incompatibility of HS and SS and can be expressed as:

$$\chi_{HS-SS} = V_{ref}\frac{(\delta_A + \delta_B)^2}{RT} \qquad \textbf{Equation 1.4}$$

where V_{ref} is a reference volume, and δ_A and δ_B are the Hildebrand solubility parameters of monomers, describing the ability of materials to interact or mix with each other.[125] However, even if the solubility parameters of the two monomers are relatively close, the phase-separation in PU systems is driven by the repulsion of the unlike sequences due to covalent bonds confinement of the chemically incompatible segments. The main driving force of phase-separation is the value of the χN. Therefore, higher HS content leads to longer HS, and thus greater χN and higher extent of phase-mixing.[125]The kinetics of phase-separation is temperature and time dependant. Chu *et al.* reported that the kinetics of phase-separation is mainly related

to the molecular mobility of hard segments.[126] An increase of temperature results in a breakage of H-bonds leading to phase-mixing, while decreasing temperatures leads to phase-separation.

If the amorphous HS and the amorphous SS are compatible, a single phase, phase-mixed matrix will be created. The two segments will consequently follow classical rules of mixing, for example the Flory-Fox equation for the T_g,

$$\frac{1}{T_g} = \frac{w_1}{T_{g1}} + \frac{w_2}{T_{g2}} \qquad \textbf{Equation 1.5}$$

where T_g is the glass transition of compatible mixture, T_{g1} and T_{g2} are glass transitions of HS and SS, and w_1 and w_2 are weight fractions of HS and SS. Therefore, two completely compatible HS and SS polymers will have one T_g given by the Flory-Fox equation and two incompatible phases will have two T_g.[127]

However, due to a complex structure of polyurethane matrix and formation of multiple regions with various compatibilities and ratios of HS and SS, the presence and temperatures of the glass transitions can vary. For example, in partially mixed phases the T_g of one of the segments is often affected by the other segment, therefore the two glass transitions can be described as a glass transition of a soft segment influenced by the hard segments, and a glass transition of a hard segment influenced by the soft segments.[128] The commonly observed increase of the T_g of SS within phase-mixed polyurethane matrix is related to decreased mobility of SS, caused by interactions with HS.[123] Moreover, the T_g of HS is often poorly visible in DSC due to the broad distribution of the sequence length, as well as a small change in the heat capacity of the segments.[129]

As mentioned previously, the extent of phase-separation is related to the amount and the strength of H-bonding between urethane groups present in HS, and the degree of crosslinking occurring within the matrix. If the H-bonding is very strong and occurs only between urethane groups, large extent of phase-separation can be observed. If the H-bonding can be formed between both HS and SS, more phase-mixing of segments occurs. Therefore, the information about H-bonding within a PU

system, obtained *via* various analytical techniques such as DSC or ATR FT-IR, allows determination of the extent of phase-separation.

PU coatings can be divided into two main groups – thermoplastic and thermosetting. Thermoplastic materials usually exhibit lower resistance towards mechanical strains and thermal degradation than thermosetting PUs. Considering chemical structure, the hardness is mainly linked to the presence of crosslinks that provides thermosets with enhanced tensile strength, mechanical wear and chemical resistance.[130] The main structural difference between thermosetting and thermoplastic PU is the presence of hard and soft segments in the thermoplastics. Therefore, the PU thermoset coatings are not suitable materials for the creation of self-healing coatings.

The properties of thermoplastic PUs depend on a number of factors. The most important ones include: 1) polymerisation procedure and reaction conditions leading to various molecular weight of polymers and morphology of the solid state, 2) HS and SS properties, such as composition of the segments, their length or the sequence of length distribution and 3) the chemistry of starting materials, such as chemical composition of segments or presence and chemical structure of crosslinks and chain extenders.[130]

1.3.2. SYNTHESIS AND SYNTHETIC CHALLENGES

PUs are formed from two basic components: a diisocyanate and a diol. The basic chain growth reaction of these two components leads to the production of a linear polymer linked by urethane (carbamate) links. A reaction scheme for the polyurethane formation reaction is presented below (**Figure 1-17**).

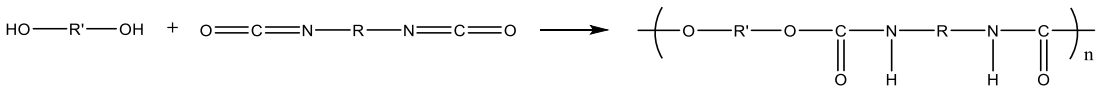

Figure 1-17. *Reaction scheme of diol and diisocyanate forming polyurethane.*

PUs are commonly prepared using single-step methods or multi-stage methods. In the single-step methods all the starting materials are added together.[131] Different rates of reactions between various chemical groups lead to formation of a polymer with a random block sequence. The multi-stage method, also known as the pre-polymer method, is a two-stage reaction. In the first step the excess diisocyanate is reacted with a diol, leading to creation of isocyanate end-capped blocks. Secondly, during a chain extension step, a reaction with a short chain diol or diamine is carried out, leading to a formation of urethane or urea linkage (**Figure 1-18**). If short, polyfunctional diols or diamines are used, the formation of highly crosslinked PUs can be observed. Additionally, the multi-stage method of PU synthesis gives some control over the length of the segments.[112]

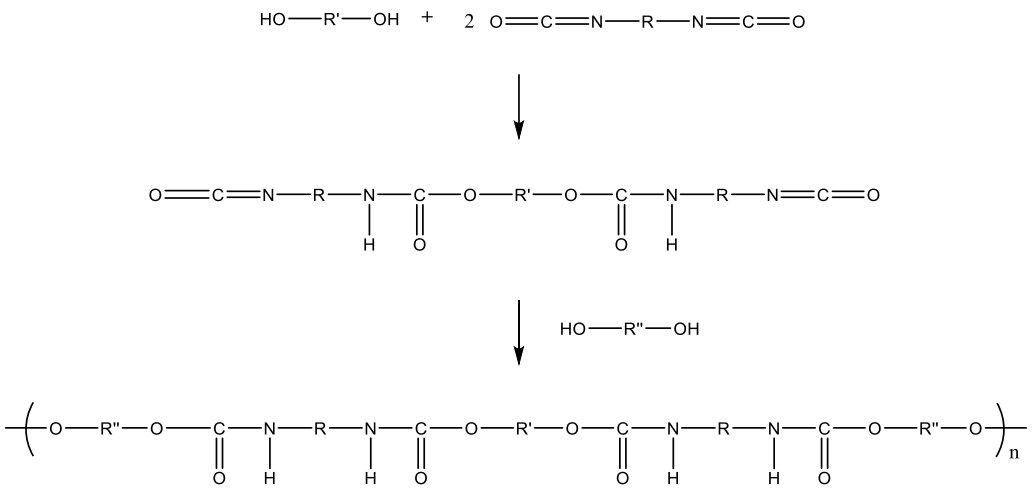

Figure 1-18. *The pre-polymer method of polyurethane synthesis.*[131]

During the polymerisation reaction a number of side reactions can occur. The most significant process involves the reaction of isocyanate with water, leading to a formation of an amine *via* carbamic acid. The highly reactive primary amine can further react with isocyanates, leading to a formation of urea groups and a urea-urethane polymer.[132] The process, known as a 'moisture curing', can be used to complete the polymerisation reaction of polyurethane prepolymers during various applications such as coating or lamination. The formation of highly polar urea groups leads to toughening and hardening of the materials. In a polyurethane-urea copolymer bidentate hydrogen bonds with carboxyl groups can be formed, exhibiting

higher hydrogen bond strength comparing to monodentate urethane bonds (58.5 kJ/mol vs 46.5 kJ/mol). In general, materials containing high urea content exhibit higher modulus, tensile strength and hardness, as well as reduced flexibility and elongation.[104] Moreover, a number of other reactions involving the isocyanate group can occur. The relative reaction rates of isocyanate with various chemical groups is presented in the **Table 1-2**.

Table 1-2. *Relative reaction rates of isocyanate with various chemical groups.*[127]

Chemical group	Chemical structure	Relative reaction rate
Primary aliphatic amine	R-NH_2	100,000
Secondary aliphatic amine	R-NH-R'	20,000-50,000
Primary aromatic amine	Ar-NH_2	200-300
Primary hydroxyl	R-OH	100
Water	H_2O	100
Urea	R-NH-CO-NH-R'	15
Urethane	R-NH-CO-O-R'	0.3

In order to create materials with desired physical properties the side reactions need to be controlled. The presence of allophanate groups and biuret groups is undesirable, although urethane groups can improve the toughness of materials. It was reported that due to the formation of allophanate groups and biuret groups polymers form a gel-like structure or strongly covalently cross-linked networks.[123] Such reactions dramatically influence the morphology of the final product. These reactions need to be controlled and they are strongly influenced by isocyanate type, reaction temperature, solvent used and type and concentration of catalyst. Side reactions are especially favoured at temperatures above 60 °C for aromatic isocyanates and in the presence of catalyst for aliphatic isocyanates. The most common solvents, DMF, dimethylacetamide (DMAC) and *n*-methyl pyrrolidine (NMP) can also act as catalysts and trigger side reactions.

The prepolymer method is known to give a control of the amount of side products formation. The reaction can be carried out in bulk, which reduces the risk of organic solvents and the residual water catalysing side reactions, such as urea formation.

To reduce the viscosity of PUs during the manufacturing process, as well as to the practical requirements of some PU-based materials such as coatings, paints,

varnishes or adhesives, organic solvents are commonly added to these formulations.[133]

Due to a number of Volatile Organic Compounds (VOCs) directives, low VOCs technologies have been gaining increasing interest in a number of applications.[134] The aqueous polyurethane dispersions (PUDs) are one of the most commonly used environment friendly systems, containing no VOCs and using water as a dispersion medium to create a colloidal suspension of polymer.[135] The dispersions are superior to solvent based products as due to lack of solvent they are cheaper to manufacture and being non-toxic and non-flammable are safer to use for a broad range of applications.[136]

To provide a suitable dispersibility of polyurethane in water, a modification of the polymer structure is necessary. The usual approach involves incorporation of internal emulsifiers with hydrophilic groups, which provide solubility in the aqueous phase.[137] Among many of the popular emulsifiers, three main groups can be distinguished – PU anionomers, cationomers and zwitterions. One of the commonly used anionomers is dimethylol propionic acid (DMPA), containing an ionic functionality, a carboxylic acid group that can be neutralized with a basic group such as triethylamine (TEA). Due to the low molecular weight of DMPA, it can be used as a fraction of the chain extenders used during the reaction.[138] To reduce the viscosity of the polymer, acetone is usually added to the reaction. Upon completion of the reaction, water is added, and a dispersion is created *via* a high speed stirring process. Finally, the low boiling point acetone can be removed to obtain a waterborne polyurethane dispersion.[139] The reaction scheme of synthesis of waterborne PUDs is presented below (**Figure 1-19**).

Due to severe health hazards associated with raw isocyanates alternative polyurethane synthesis techniques were also developed. Among these methods a non-isocyanate method is worth mentioning. The three main methods include step-growth polyaddition, polycondensation, and ring-opening polymerisation.[140]

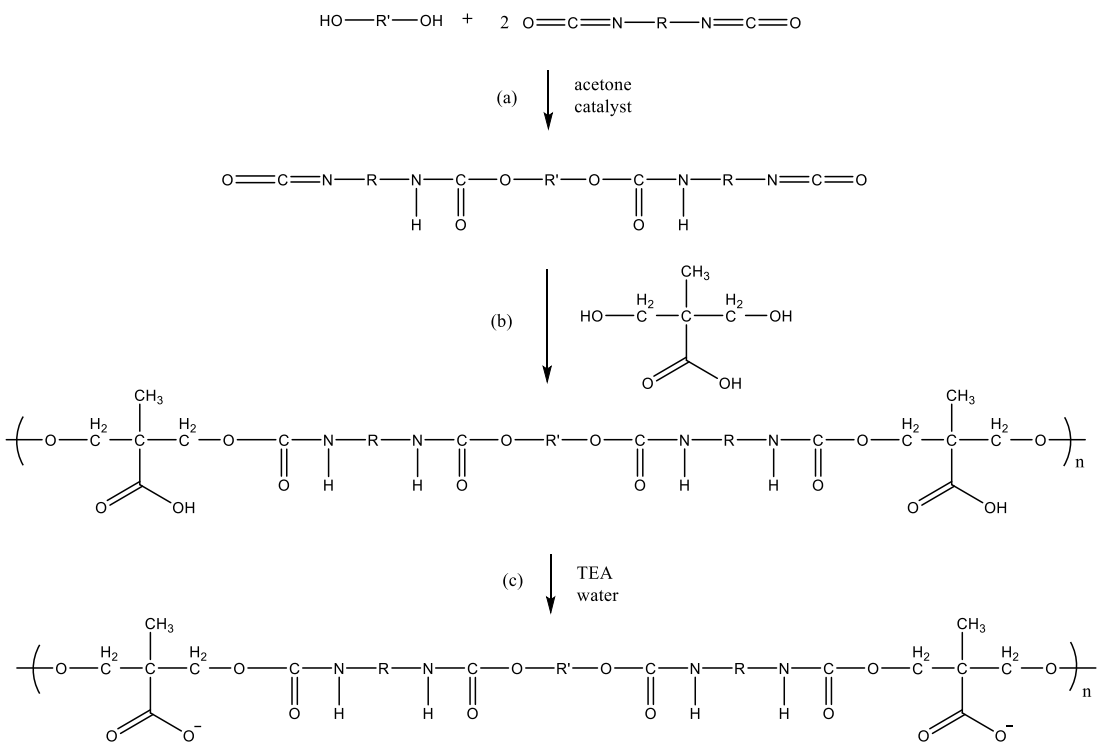

Figure 1-19. *The pre-polymer method of waterborne polyurethane dispersion: (a) pre-polymerisation of diols and isocyanates in the presence of a catalyst, (b) chain extension and crosslinking by the addition of internal emulsifier (DMPA) and (c) creation of a dispersion in the presence of TEA.*

Step-growth polyaddition involves a reaction of cyclic carbonates with diamines. In the polycondensation method, the isocyanate is replaced with chloroformates and reacted with diamines, or with carbamates reacting with alcohols. In the ring-opening reaction strained rings of aliphatic cyclic urethanes are opened using catalysts and polymerised with each other or other raw materials. Other environment-friendly techniques involve use of carbon dioxide or simple esters of carbonic acid used to obtain polyurethanes.[140]

The novel non-isocyanate routes of PU synthesis appear to be very promising. However, a number of adjustments and further research in the field is required and the techniques have no practical use so far.[131] The waterborne polyurethane synthesis method remains the most commonly used approach minimising the risks and environmental concerns associated with polyurethane synthesis.[131]

The common problem occurring during the polyurethane synthesis reaction is a reaction mixture separation.[141] As the reaction proceeds, the chemical and physical

properties of the initially homogenous reaction mixture changes, due to formation of oligomer and polymer chains resulting in an increase of the molecular weight of the present species, and due to the variety of chemical modifications resulting in the change of the interactions between the species. These changes may lead to creation of thermodynamic phase boundaries and induce microphase separation of the system.[142] The reaction mixture separation, often occurring by spinodal decomposition, can lead further to formation of a blend of species, including unreacted monomers, homopolymers or various block copolymers.

A significant amount of a multiblock block polyurethane copolymer can be formed only when the phase-separation of the system is prevented. To prevent the spinodal decomposition in polymer reaction mixtures, the incipient surface energy of the system has to be increased.[143] That can be obtained by the use of solvents and an increase of reaction temperature.

1.3.3. SELF-HEALING PROPERTIES OF POLYURETHANES

The healing of supramolecular materials can be obtained *via* dynamic and reversible networks of noncovalent bonds, including hydrogen bonds,[64,65] ionomers[47] or π-π interactions.[144,145] Reversible hydrogen bonds were reported to be the most suitable for transparent coatings.[146] The concept was studied extensively in various polymers including elastic rubbers. Herbst *et al.* report the influence of hydrogen bonds in poly(isobutylene) leading to supramolecular association of polar moieties, enabling dynamic rearrangement of the aggregates and exhibiting self-healing properties.[147] Cordier *et al.* reports the self-healing of rubber being linked to a large number of groups ready to form hydrogen bonds and a subsequent slow association of these clusters leading to healing of the materials.[64] A theoretical model of an autonomic self-healing of unentangled polymer networks with reversible bonds was studied by Stukalin *et al.* The reaction kinetics at different stages of the repairing process was analysed and described as a self-adhesion of separated surfaces followed by a diffusion of chains.[148]

The large number of reversible hydrogen bonds present within polyurethane structures allow them to display self-healing properties. Hydrogen bonds provide the PU matrix with secondary structure and high elastic strength. When the surface of a PU matrix is scratched, the elastic strength of flexible SS prevents the material from crumbling and being irreversibly removed. The scratch appears due to realignment and breakage of H-bonds. Reorientation of polymer chains is possible when the glass transition of the soft phase is exceeded, providing the soft phase with sufficient energy to become mobile. The rubber-like form of the soft phase allows the polymer chains to flow and restore the broken hydrogen bonds (**Figure 1-20**).[149] If during the process the glass transition temperature of the hard phase is not exceeded, the phase can maintain the overall shape of the matrix.[150]

Severe damage of polymer matrix can also induce covalent bond scission, leading to a decrease of polymer molecular mass in the vicinity of the damage.[151] However, in the case of relatively light scratching, such an effect is localised on the surface of the polymer and only severely damaged samples show a change in their overall molecular mass.

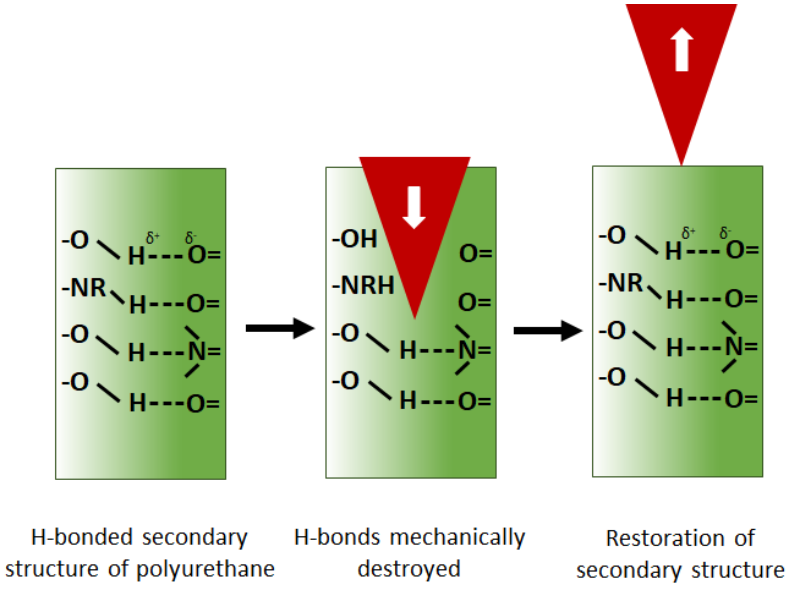

Figure 1-20. *The self-healing mechanism of PU coating – realignment, breakage and restoration of broken hydrogen bonds.*[152]

Bayer MaterialScience reported that an increase of the polymer network density can improve scratch resistance. Denser polymer networks can resist higher forces prior to

breakage and provide better chemical resistance. However, as the density of the network increases, the material becomes more brittle and this may result in irreversible fine brittle fracture. It was also reported that flexibility of the network has a large influence on self-healing efficiency. Applying force to highly flexible networks causes deformation rather than irreversible breakage of covalent bonds and removal of some material. As mentioned previously, the plastic deformation can be removed within a few hours at temperatures exceeding the lower glass transition temperature of the soft phase. However, an increase of flexibility results in decrease of the chemical resistance of the matrix.[150] The creation of highly effective self-healing PU coatings requires finding the right balance between hardness and flexibility, which can be obtained by careful selection of starting materials and a combination of UV and thermal urethane curing methods.

The unique properties of PUs make them a very attractive candidate to create self-healing coatings. The ratio of hard to soft segments, as well as their glass transition temperatures, can be modified by use of different types and ratios of isocyanates and diols. The control of these factors gives a great opportunity to adjust the physical properties of a polyurethane matrix, such as toughness, strength, abrasion resistance or recovery of damage, and potentially allows creation of highly efficient self-sealing materials.[102]

For example, Hood *et al.* showed that different proportions of hard and soft segments allowed adjustment of mechanical properties, such as intrinsic viscosity, thermal transition temperature, degree of crystallinity or storage modulus.[119] Chang *et al.* explored transparent PUs based on polytetramethylene glycol reacted with methylene diphenyl diisocyanate (MDI) or hexamethylene diisocyanate (HDI), various bulky diols containing ether and aromatic groups as CEs.[153] It was observed that use of a bulky CE in the hard segment disrupted hydrogen bonds and changed thermal and mechanical properties.

Extensive studies between the relationship of the PU composition and the healing efficiency were performed by Ardjmand *et al.*[102] The group explored self-healing properties of coatings synthesised from HDI trimer combined with a polyester polyol

or polyacrylate and ethylene glycol as a CE. The hardness, gloss and self-healing efficiency of the materials was compared. Coatings with a 2:1 ratio of diisocyanate to diol and a chain extender showed the lowest hardness, while coatings without any chain extenders showed the highest hardness. Coatings with chain extenders were found to have minimally lower gloss than the coatings without any chain extenders. It was also discovered that the use of chain extenders significantly increased recovery of samples after damage. The most efficient self-healing coatings with acceptable hardness and gloss were created from a polyacrylate polyol with chain extender.[102]

Another research study explored the self-healing properties of PU coatings using mechanical analysis and microscopy techniques. The examined material consisted of two-segmented block co-polymers. Linear poly(ε-caprolactone) (PCL) was used to form the soft segment, while polyurethane segments created the hard segment. A film of 5 µm thickness consisting of 8 wt% of hard segments was scratched with a razor blade and healed in an oven at 40 °C and 80 °C for 24 hours. Laser scanning confocal microscopy (LSCM) was used to obtain a 3D image of the surface before and after healing of the scratch. It was concluded that the glass transition temperature of the soft segments was 70 °C, thus at temperatures above 70 °C the PCL soft segment transformed from the semi-crystalline into an amorphous state. The higher mobility of the soft segment allowed the polymer to flow locally and heal the defects, while the hard segments maintained the overall shape of the matrix. The LSCM analysis confirmed that heating the material to 80 °C caused significant decrease in the damage and partial filling of the scratch, while treatment at 40 °C showed no changes of scratches.[154] Moreover the coatings were found to hinder corrosion activity at the damage site.[155]

The effect of hard-soft segment separation on SH properties was studied by Chen *et al.*[156] The microphase separation was found to enhance stiffness and toughness while retaining dynamic supramolecular properties leading to self-healing properties. Similar systems of block copolymers were widely studied. Hentschel *et al.* reported on a block copolymer created from poly(*n*-butyl acetate) as the soft block and polystyrene as the hard block.[157] The hard/soft microphase-separation resulted in the

polymer exhibiting hardness of thermoplastic elastomer and dynamic self-healing properties of supramolecular materials. Chen *et al.* presented soft-hard-soft triblock copolymers and supramolecular block copolymers exhibiting phase-separated morphologies, linked to their efficient self-healing properties.[158]

An adjustment of mechanical properties of PUs to the desired specifications can be obtained using multiple strategies. An improvement of mechanical strength by introduction of carbon nanotubes to electrically conductive and optically transparent shape-memory PU films was reported by Jung *et al*.[159] The introduction of 0.5 wt% of multiwalled carbon nanotubes into the matrix prepared from MDI, PCL diol and butanediol (BD) provided the films with superior mechanical properties: increasing modulus and tensile strength. Another study showed that the addition of 0.1 wt% of high-quality graphene to a transparent shape-memory PU matrix significantly improves physical properties such as modulus, tensile strength, thermal conductivity, electric conductivity, shape retention and recovery.[160]

Further adjustments of PU structure include incorporation of additional chemical groups which *via* various mechanisms may improve self-healing efficiency. Such groups may include moieties introducing reversible cycloaddition reactions e.g. Diels-Alder, radical reactions or metathesis reactions.

Thermally healed PU coatings with a Diels-Alder moiety were studied by Du *et al.*[161] The self-healing, transparent material was synthesised *via* Diels-Alder reaction between BMI and linear PU prepolymer comprised of MDI and poly(1,4-butylene adipate glycol) (PBA) end-capped with furan groups. The films were cut into half and treated at 120 °C for 300 s on a heating plate under N_2 flow. The treatment resulted in complete healing and disappearance of the crack. Tests of similar PUs without DA moiety showed no self-healing properties, proving that the healing was attributed to thermally triggered debonding of DA moiety (rDA), rearrangement of furan groups and BMI fragments and re-bonding *via* DA reaction upon cooling (**Figure 1-21**). An improvement of mechanical properties after healing was obtained by extending the healing time to 20 minutes at 120°C, followed by 48 hours treatment at 60 °C. After

two damage-repair cycles the samples were reported to maintain 66% of their original mechanical properties.

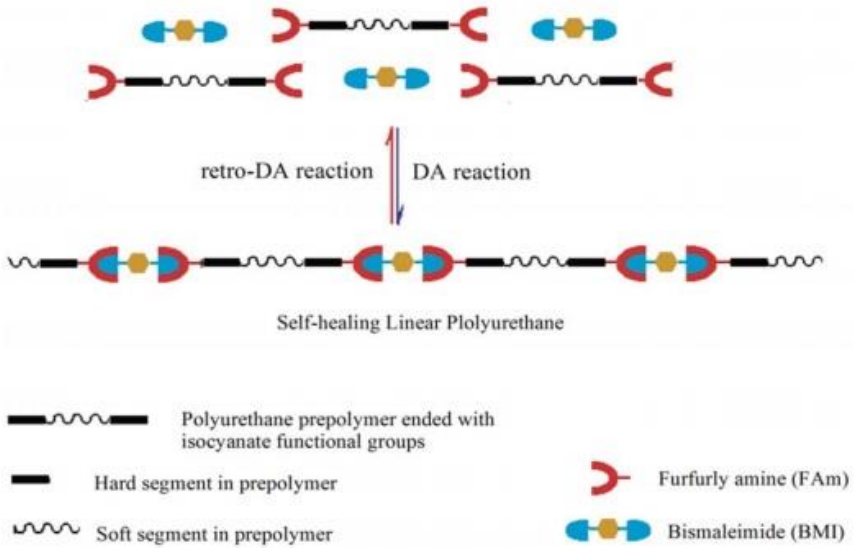

Figure 1-21. *The scheme of DA and rDA reactions in PU-DA.*[161]

In further research of these materials an improvement of the healing efficiency and reduction of healing time was achieved.[162] Replacement of monomeric MDI with a prepolymer mixture of MDI and introduction of longer PBA chains provided the material with a higher number of crosslinks and higher tensile strength. The healing time was reduced to 5 minutes at 130 °C, followed by 24 hours at 55 °C and the healing efficiency increased to 92% after the first damage-heal cycle and 65% after third cycle.

Yuan *et al.* presented an efficiently self-healing PU consisting of alkoxyamine-based diol, HDI trimer and polyethylene glycol (PEG).[163] The healing was observed after 2.5 hours at 80 °C and was explained by a one-step dynamic equilibrium of C-ON within alkoxyamine crosslinks. However, due to the alkoxyamine radicals' sensitivity to oxygen the healing was reported to require an argon atmosphere. Moreover, the healing efficiency was reported to decrease after several break-heal cycles.

PU consisting of IPDI, PEG and a photo-reversible coumarin moiety was reported by Ling *et al.*[164] Repeated UV-triggered crosslinking and de-crosslinking was observed under successive irradiations at 350 and 254 nm (**Figure 1-22**). Thin films stretched to

failure were exposed to 254 nm light for 1 minute, placed back together and irradiated with 350 nm light for 90 minutes. The healing efficiency was reported to reach 65% and be dependent on the polymer chains mobility. In further research the influence of molecular weight of PEG was studied.[165] A lower molecular weight PEG was found

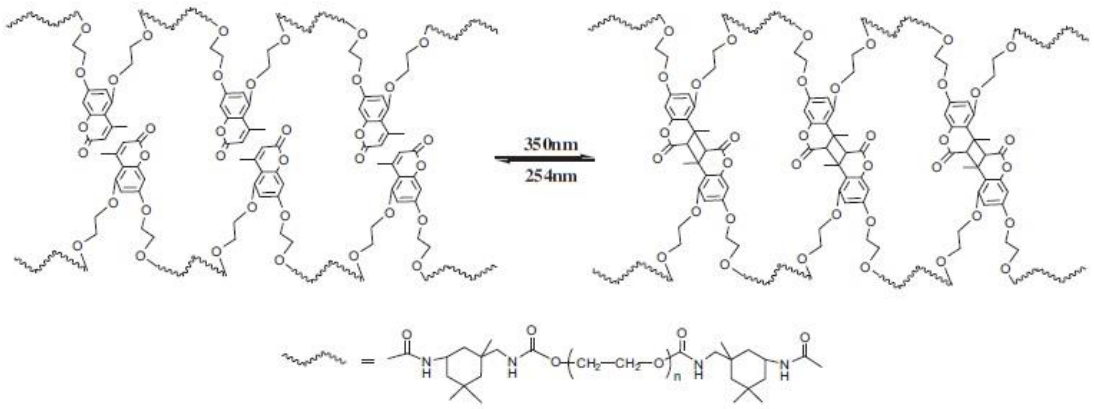

Figure 1-22. *Reversible photodimerization and photocleavage reactions of coumarin moieties upon irradiation with UV light.* [164]

to increase healing efficiency due to creation of small soft segments with a high concentration of coumarin groups.

The broad scope of intrinsically healing approaches used in PUs presented in this section shows a significant potential to create efficiently self-healing, commercial coatings for optical applications.

1.3.4. EVALUATION OF SELF-HEALING PROPERTIES

To evaluate the self-healing of coatings, a controllable and measurable amount of damage needs to be introduced. Over the years a number of techniques used to determine scratch resistance of coatings have been developed. These techniques can also be employed to damage coatings prior to evaluation of their self-repair properties. Among these methods micro-abrasion techniques can be used to introduce scratches to a transparent, protective coating (**Figure 1-23**). Micro-abrasion damages a large area, creating a high density of small scratches more shallow than the coating thickness. [166]

Figure 1-23. *An example of a micro-abrasion instrument - an automatic scratch tester BGD 520.*[166]

A sand trickle test is one of the micro-abrasion techniques. The technique involves a slow, controlled release of standardised-particle size sand onto the sample from a pre-set height. The sand is placed in a funnel at the top of a shielding tube and, when released, introduces damage to a sample attached to a spinning disc at the bottom of the tube. The size of the sand particles, the distance from the funnel to the sample and the speed of the spinning disc allow determination of the extent of damage. However, due to the small size of sand particles the samples tested using this technique require post-testing cleaning of the surface, thus introducing an additional factor that might increase the extent of damage or affect the healing properties.

Another technique, called a cheesecloth test, is performed using a cheesecloth scratch instrument. The damage to a sample attached to a flat surface is introduced by a moving arm of the instrument covered with a piece of standardised grade cheesecloth. Due to the rough structure of the cheesecloth scratching of the surface can be obtained. The movement of the arm can be pre-set to a number of back-and-forth cycles and a weight of a bearing load can be adjusted, allowing a controlled damage introduction. However, due to the relatively low hardness and roughness of the cheesecloth compared to other micro-abrasion techniques, the amount of introduced scratching is small. Therefore, the technique is usually used to test materials with a very low hardness.

In a Taber scratch test micro-abrasion is induced with a Taber apparatus equipped with a rubber turntable containing fine aluminium oxide particles. A sample is placed against the rough surface of the wheel and secured with an intender allowing control of the load. The weight of the load and the rotation frequency of the turntable determines the extent of damage introduced to the tested material.[166] However, the monodirectional rotation of the turntable introduces a constant force which might lead to flaking or peeling of a tested material.

The last technique, an automated steel wool test, is also performed using a specially designed scratch instrument. The instrument consists of (i) a moving arm covered with a standardised grade steel wool and can be loaded with various weights, (ii) a stand where a sample can be attached to a flat surface and (iii) a control unit allowing adjustment of the number of back-and-forth cycles and velocity. The weight of the load and the grade of the wool determines the extent of damage introduced to the material. The constant load and velocity of the arm provides control over the repeatability and reproducibility of scratching of the same material. Moreover, a sample that underwent damage does not require any clean-up and is easily accessible to perform any further tests.

While all the mentioned techniques offer some advantages and disadvantages, a careful choice of a technique used to damage the materials of interest allows a suitable testing protocol to be established.

The damage and recovery of self-healing materials can be monitored using various techniques. The most popular methods include measurements of gloss, transparency and haze.[167–174] Comparison of these properties measured during evaluation of self-healing allows quantification of the amount of introduced damage and the extent of recovery.

Gloss is an optical property which indicates how well a surface reflects light. This property is dependent on the amount of specular reflection, i.e. the amount of light reflected in a symmetrical angle to the one of incoming light without getting scattered.[97] Gloss is primarily affected by the surface topography. A damaged and

scratched surface exhibits lower gloss values due to decreased light reflection and increased light scattering. Therefore, the measurement of gloss before damage, after damage and during recovery provides information about the efficiency of self-healing.

Transparency is the amount of light that passes through an object without being absorbed, scattered or reflected.[97] Transparency of a coating is largely influenced by its defects, thus a scratched surface exhibits lower transparency than a smooth, undamaged surface. Therefore, the measurement of transparency is also used to evaluate the self-healing properties of coatings.

Haze is defined as the cloudiness or haziness of a body.[97] It is measured with a wide angle scattering test and calculated as the percentage of light that is deflected by more than 2.5° from the direction of the incoming light. Diffusion and scattering of the light in all directions leads to a loss of contrast, resulting in the cloudy appearance of a scratched coating, thus indicating the level of surface damage. Therefore, the measurement of haze of coatings can be also used to describe the amount of damage introduced to a coating, as well as the extent of recovery from damage.

Measurement of the gloss, transparency or haze values before damaging, immediately after damaging and during the healing of the materials allows for a precise characterisation of the process. Moreover, the variety of methods used to monitor damaging and recovery of self-healing materials enables design of the most suitable testing protocol for particular materials.

1.3.5. PATENTS

In recent years several self-healing materials has been patented. A review of these patents focusing on transparent materials with potential use as coatings for optical applications is presented below.

PU materials repairable by introduction of energy were patented by BASF in 2008 and 2014.[167,173] Thin, self-healing coatings were created from various fatty acid based

polyols, nonblocked or blocked di- or poly-isocyanate, various polyol chain extenders and polyhydroxy compounds, with pigments or fillers added. The materials were reported to have T_g values between -10 °C and 100 °C. The repair of the coatings was obtained by a thermal treatment for at least 15 minutes at temperatures exceeding T_g and/or by exposure to near-IR radiation (900-1500 nm). A comparative example describes healing of a clear film of 200 µm thickness created from fossil plant wax and hexafunctional polypropylene oxide, HDI, IPDI and polyacrylate-ol at 130 °C, showing 95% gloss recovery after the first damage-heal cycle, 90% after the second, 54% after the third and 64% after the fourth.

In 2009 PPG patented similar systems describing curable film-forming compositions with self-healing properties.[168] The films comprised of a polymer binder formed from various polyesters containing hydroxyl functional groups and various polyisocyanates having at least three isocyanate groups were reported to have T_g above 35 °C. The damage was introduced using a dry abrasion test (DAT) and a wet abrasion test (WAT). The healing was obtained by a thermal treatment of the samples at elevated temperatures and monitored by measurement of gloss before and after scratching. Samples damaged using DAT showed gloss recovery of above 75%, while WAT achieved at least 60- 95% gloss recovery after the first scratch and up to 80% after 4 damage-heal cycles. A comparative example described four films healed by immersing in water at 53 °C for 10 minutes, showing 91-96% recovery of samples damaged with DAT, while WAT displayed 92-95%, 84-90%, 74-84% and 69-79% recovery for respectively the first, the second, the third and the fourth damage-heal cycle.

Inexpensive self-healing polymer coatings consisting of two phases, thermosetting and thermoplastic, were recently patented by NEI Corporation.[170] The thermosetting phase with superior strength was created from various materials including polyurethane, epoxy, polyimide, unsaturated polyester, silicone, fluoropolymers, polyvinyl formal or their blends. A thermoplastic phase allowing flowable agents to repair the structure was created from materials including PCL, poly(acrylic acid), poly(acrylonitrile), poly(ether ketone), polystyrene, PU or poly(vinyl acetate). The

transparent coatings scratched with steel wool or sandpaper were treated with short heat gun hot air bursts causing raise of surface temperature to 70-80 °C. The gloss measurement showed 85-95% recovery of damage. The low T_g thermoplastic phase was reported to lose its mechanical strength and integrity when heated, gaining free flowing properties enabling self-healing, while the thermosetting phase with a high T_g provided strength and stability. The technology was reported to repeatedly heal both scratches and deep cracks.

Transparent materials designed to be used as coatings for optical lenses were also patented by Essilor International.[171] The self-healing coatings made of various poly-isocyanates and polythiol-enes were reported to have the T_g between 40 °C and 70 °C. The damage was introduced using a Manual Brass Brush Test (MBB Test) and an Automated Steel Wool Test (ASW Test). The healing was obtained by immersion of damaged coatings in warm water at 60°C for 15 minutes and monitored by haze measurements. The two coatings reported in the patent displayed healing levels of 87% and 86% in the MBB test, but reached only 36% and 37% recovery in the ASW test. Incorporation of conductive mineral colloids e.g. S_2O_5 or SnO_2 improved the healing efficiency, reaching up to 80% recovery efficiency using both damage methods. More recent improvement of their system involved an addition of an abrasion-resistant layer place beneath the self-healing outer layer.[174] The multi-layered coatings exhibited higher scratch resistance, lower haze value and improved SH properties.

1.4. SUMMARY AND AIM OF RESEARCH

The number of techniques and approaches used to create self-healing materials increases every year. As presented in the above discussions, multiple autonomic or non-autonomic systems have been found to show excellent healing properties. Adjustment of their features such as healing efficiency, repeatability, initiating trigger, maximal filling volume or sensitivity allows creation of materials suitable to their specific application. Such materials are already being used in industry as anti-corrosion coatings, self-healing insulators, protective layers, micro-damage-removing ceramics and aerospace materials.

The creation of self-healing materials for optical applications remains one of the most challenging tasks. Such coatings need to fulfil several requirements, such as having high transparency, low haze or suitable hardness. They also need to allow repeatable healing, display high tear strength and long life-time. The review of achievements and current findings in the field suggests that the most suitable materials for the application mainly involve co-polymeric matrices consisting of two phases – thermosetting and thermoplastic. Careful choice of materials used for formation of these phases and an appropriate ratio of the segments, can lead to creation of highly efficient, useful and practical self-healing coatings. Polyurethanes, due to their versatility and complex chemical structure influencing their physical properties, are one of the most promising fields for research of self-healing materials for optical applications.

Based on the polyurethane coating systems used for optical application four main requirements of the research were identified:

- Development of an optically clear, transparent coating with haze below 2%.
- Development of a coating with a pencil hardness of B or above.
- Development of a coating with the glass transition temperature above room temperature and below 80 °C.
- Development of a coating exhibiting rapid, thermally-triggered self-healing properties, allowing above 90% recovery from damage within less than 10 min.

To fulfil the above requirements a library of polyurethane formulations was created from various starting materials, including seven polyols, two diisocyanates, one triisocyanate, diol, diamine, alkanolamine and triol chain extenders as well as various amounts of the internal emulsifier, DMPA. The coatings were characterised using several techniques and tested to determine their self-healing properties. The relationship between their composition, morphology and self-healing properties was established.

In the next chapter, **Chapter 3**, the first set of formulations will be presented, focusing on a choice of a polyol. The influence of various soft segment blocks on morphology and self-healing properties will be determined. In the following chapters the most suitable polyol, PH50 polycarbonate with a MW of 500 g mol^{-1}, will be used as the SS building block, and the influence of other polyurethane building blocks will be determined (**Figure 1-24**).

A second set of formulations prepared with two isocyanates, linear HDI and bulky IPDI, and their blends, is presented in **Chapter 4**. **Chapter 5** reports the third set of formulations and shows the influence of diol chain extenders with various numbers of carbons on the self-healing properties and morphology of polyurethane. In **Chapter 6** the fourth set of coatings is presented. The effect of various amounts of urea groups on the formulations, introduced by using chain extenders containing amine groups, is reported. **Chapter 7** shows the fifth set of materials and focuses on the introduction of trimers by using trimeric-IPDI and triol chain extenders and the effect of crosslinking on properties and self-healing behaviour of polyurethane coatings. In **Chapter 8** the last set of coatings is presented, in which the amount of the ionic content is varied by incorporation of different amounts of the internal emulsifier, DMPA. Various modes of evaluation of SH properties are presented in **Chapter 9**. Finally, the findings are summarised and discussed in **Chapter 10**.

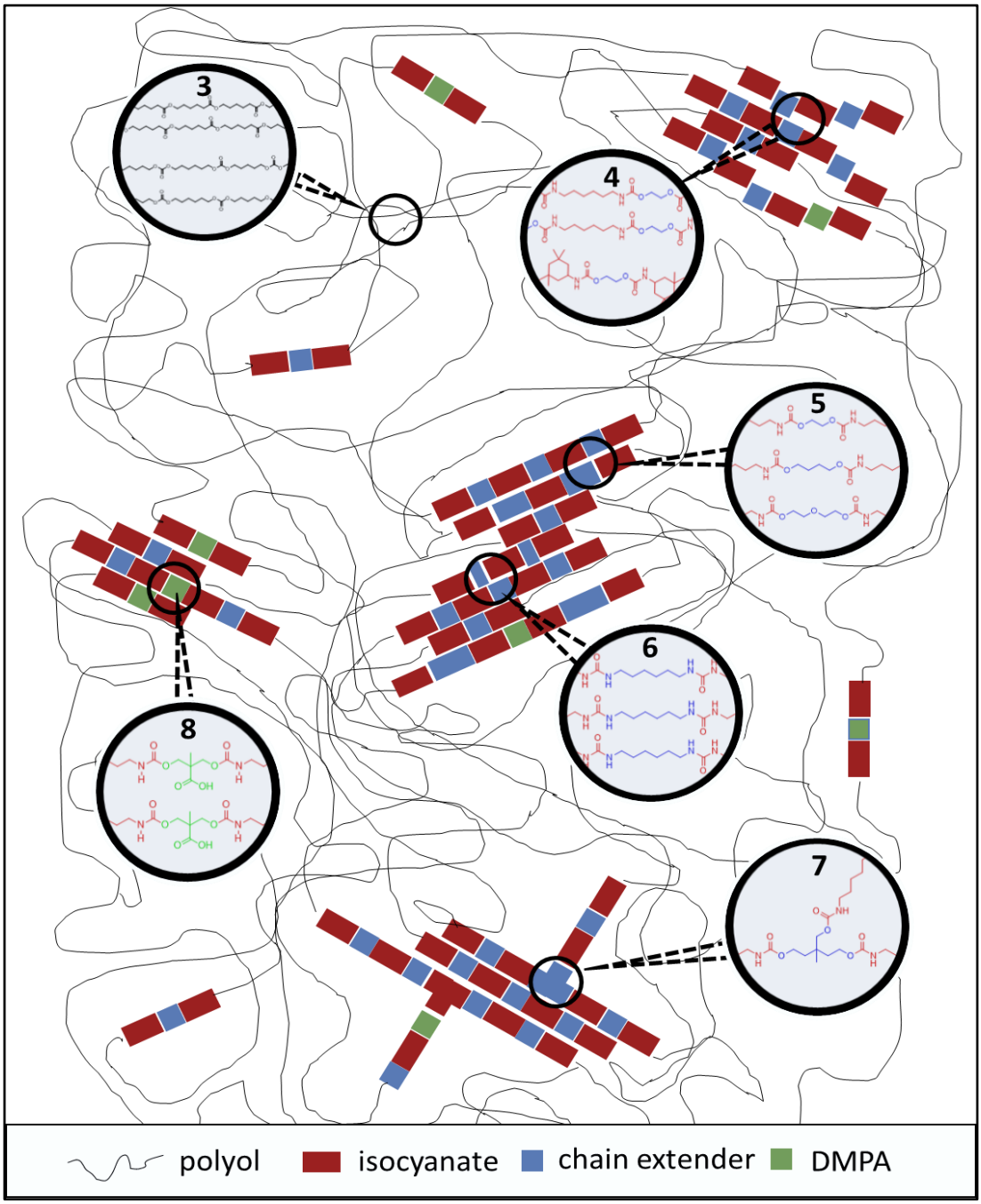

Figure 1-24. *Model of polyurethane microphase morphology and visualisation of composition of various blocks discussed in Chapters 3 to 8: (3) polyol, (4) isocyanate, (5) diol chain extender, (6) amine chain extender, (7) crosslinking and (8) ionic content.*

1.5. REFERENCES

1 P. Martin, *Science (80-.).*, 1997, **276**, 75–81.
2 D. J. Leaper and K. G. Harding, *Wounds: Biology and Management*, Oxford University Press, Oxford, 1998.
3 D. Habault, H. Zhang and Y. Zhao, *Chem. Soc. Rev.*, 2013, **42**, 7244–7256.
4 C. M. Dry and N. R. Sottos, *Proc. SPIE*, 1993, **1916**, 438–444.
5 W. Nakao, *Mater. Sci. Forum*, 2010, **638**–**642**, 2133–2137.
6 R. D. Deshpande, J. Li, Y.-T. Cheng and M. W. Verbrugge, *J. Electrochem. Soc.*, 2011, **158**, 845–849.
7 B. J. Blaiszik, S. L. B. Kramer, S. C. Olugebefola, J. S. Moore, N. R. Sottos and S. R. White, *Annu. Rev. Mater. Res.*, 2010, **40**, 179–211.
8 V. Amendola and M. Meneghetti, *J. Mater. Chem.*, 2012, **22**, 24501–24508.
9 R. P. Wool, *Polym. Eng. Sci.*, 1978, **18**, 1056–1061.
10 K. Jud, H. H. Kausch and J. G. Williams, *J. Mater. Sci.*, 1981, **16**, 204–210.
11 S. M. Bleay, C. B. Loader, V. J. Hawyes, L. Humberstone and P. T. Curtis, *Compos. Part A*, 2001, **32**, 1767–1776.
12 K. A. Williams, D. R. Dreyer and C. W. Bielawski, *MRS Bull.*, 2008, **33**, 759–765.
13 S. R. White, N. R. Sottos, P. H. Geubelle, J. S. Moore, M. R. Kessler, S. R. Sriram, E. N. Brown and S. Viswanathan, *Nature*, 2001, **409**, 794–797.
14 J. K. Lee, S. J. Hong, X. Liu and S. H. Yoon, *Macromol. Res.*, 2004, **12**, 478–483.
15 S. H. Cho, H. M. Andersson, S. R. White, N. R. Sottos and P. V. Braun, *Adv. Mater.*, 2006, **18**, 997–1000.
16 M. W. Keller, S. R. White and N. R. Sottos, *Adv. Funct. Mater.*, 2007, **17**, 2399–2404.
17 A. Skipor, S. Scheifer and B. Olson, *Self-healing polymer compositions*, US20040007784, 2004.
18 S. M. Scheifers, A. F. Skipor and A. Brown, *Method and chemistry for automatic self-joining of failures in polymers*, US20050027078, 2005.
19 B. J. Blaiszik, M. M. Caruso, D. A. McIlroy, J. S. Moore, S. R. White and N. R. Sottos, *Polym.*, 2009, **50**, 990–997.
20 L. Yuan, G. Liang, J. Xie, L. Li and J. Guo, *Polym.*, 2006, **47**, 5338–5349.
21 J. D. Rule, E. N. Brown, N. R. Sottos, S. R. White and J. S. Moore, *Adv. Mater.*, 2005, **17**, 205–208.
22 J. G. Kirk, S. Naik, J. C. Moosbrugger, D. J. Morrison, D. Volkov and I. Sokolov, *Int. J. Fract.*, 2009, **159**, 101–102.
23 X. Liu, H. Zhang, J. Wang, Z. Wang and S. Wang, *Surf. Coatings Technol.*, 2012, **206**, 4976–4980.
24 S. Neuser and V. Michaud, *Exp. Mech.*, 2013, **54**, 293–304.
25 X. J. Ye, J.-L. Zhang, Y. Zhu, M. Z. Rong, M. Q. Zhang, Y. X. Song and H.-X. Zhang, *ACS Appl. Mater. Interfaces*, 2014, **6**, 3661–3670.
26 L. Yao, Y. C. Yuan, M. Z. Rong and M. Q. Zhang, *Polym.*, 2011, **52**, 3137–3145.
27 H. Choi, K. Y. Kim and J. M. Park, *Prog. Org. Coatings*, 2013, **76**, 1316–1324.

28 L.-P. Lv, Y. Zhao, N. Vilbrandt, M. Gallei, A. Vimalanandan, M. Rohwerder, K. Landfester and D. Crespy, *J. Am. Chem. Soc.*, 2013, **135**, 14198–14205.
29 E. Koh, N.-K. Kim, J. Shin and Y.-W. Kim, *RSC Adv.*, 2014, **4**, 16214–16223.
30 Y. Zhao, W. Zhang, L. Liao, S. Wang and W. Li, *Appl. Surf. Sci.*, 2012, **258**, 1915–1918.
31 M. Wu, B. Johannesson and M. Geiker, *Constr. Build. Mater.*, 2012, **28**, 571–583.
32 M. Motuku, U. K. Vaidya and G. M. Janowski, *Smart Mater. Struct.*, 1999, **8**, 623–638.
33 J. W. C. Pang and I. P. Bond, *Compos. Sci. Technol.*, 2005, **65**, 1791–1799.
34 R. S. Trask and I. P. Bond, *Smart Mater. Struct.*, 2006, **15**, 704–710.
35 D. Therriault, R. F. Shepherd, S. R. White and J. A. Lewis, *Adv. Mater.*, 2005, **17**, 395–399.
36 C. J. Hansen, W. Wu, K. S. Toohey, N. R. Sottos, S. R. White and J. A. Lewis, *Adv. Mater.*, 2009, **21**, 4143–4147.
37 H. R. Williams, R. S. Trask, P. M. Weaver and I. P. Bond, *J. R. Soc. Interface*, 2008, **5**, 55–65.
38 H. R. Williams, R. S. Trask, A. C. Knights, E. R. Williams and I. P. Bond, *J. R. Soc. Interface*, 2008, **5**, 735–747.
39 A. M. Aragón, J. K. Wayer, P. H. Geubelle, D. E. Goldberg and S. R. White, *Comput. Methods Appl. Mech. Eng.*, 2008, **197**, 4399–4410.
40 A. R. Hamilton, N. R. Sottos and S. R. White, *J. R. Soc. Interface*, 2012, **9**, 1020–1028.
41 A. R. Hamilton, N. R. Sottos and S. R. White, *Polym.*, 2012, **53**, 5575–5581.
42 H. R. Williams, R. S. Trask and I. P. Bond, *Smart Mater. Struct.*, 2007, **16**, 1198–1207.
43 C. J. Norris, J. A. P. White, G. McCombe, P. Chatterjee, I. P. Bond and R. S. Trask, *Smart Mater. Struct.*, 2012, **21**, 1–10.
44 E. Palleau, S. Reece, S. C. Desai, M. E. Smith and M. D. Dickey, *Adv. Mater.*, 2013, **25**, 1589–1592.
45 J. F. Patrick, N. R. Sottos and S. R. White, *Polym.*, 2012, **53**, 4231–4240.
46 R. P. Wool and K. M. O'Connor, *J. Appl. Phys.*, 1981, **52**, 5953–5963.
47 D. Y. Wu, S. Meure and D. Solomon, *Prog. Polym. Sci.*, 2008, **33**, 479–522.
48 M. Yamaguchi, S. Ono and K. Okamoto, *Mater. Sci. Eng. B*, 2009, **162**, 189–194.
49 M. A. M. Rahmathullah and G. R. Palmese, *J. Appl. Polym. Sci.*, 2009, **113**, 2191–2201.
50 O. J. McGarel and R. P. Wool, *J. Polym. Sci. Part B Polym. Phys.*, 1987, **25**, 2541–2560.
51 J. M. Craven, *Cross-linked thermally reversible polymers produced from condensation polymers with pendant furan groups cross-linked with maleimides*, US3435003, 1969.
52 X. Chen, M. A. Dam, K. Ono, A. Mal, H. Shen, S. R. Nutt, K. Sheran and F. Wudl, *Science*, 2002, **295**, 1698–1702.
53 K. K. Oehlenschlaeger, J. O. Mueller, J. Brandt, S. Hilf, A. Lederer, M. Wilhelm,

R. Graf, M. L. Coote, F. G. Schmidt and C. Barner-Kowollik, *Adv. Mater.*, 2014, **26**, 3561–3566.
54 C. Chung, Y. Roh, S. Cho and J. Kim, *Chem. Mater.*, 2004, **16**, 3982–3984.
55 P. Froimowicz, H. Frey and K. Landfester, *Macromol. Rapid Commun.*, 2011, **32**, 468–473.
56 J. W. Kamplain and C. W. Bielawski, *Chem. Commun.*, 2006, 1727–1729.
57 B. M. Neilson, A. G. Tennyson and C. W. Bielawski, *J. Phys. Org. Chem.*, 2012, **25**, 531–543.
58 R. H. Grubbs, *Tetrahedron*, 2004, **60**, 7117–7140.
59 Y. Amamoto, H. Otsuka, A. Takahara and K. Matyjaszewski, *Adv. Mater.*, 2012, **24**, 3975–3980.
60 J. Canadell, H. Goossens and B. Klumperman, *Macromolecules*, 2011, **44**, 2536–2541.
61 T. F. Scott, R. B. Draughon and C. N. Bowman, *Adv. Mater.*, 2006, **18**, 2128–2132.
62 Y. Amamoto, J. Kamada, H. Otsuka, A. Takahara and K. Matyjaszewski, *Angew. Chem.*, 2011, **50**, 1660–1663.
63 M. Pepels, I. Filot, B. Klumperman and H. Goossens, *Polym. Chem.*, 2013, **4**, 4955–4965.
64 P. Cordier, F. Tournilhac, C. Soulié-Ziakovic and L. Leibler, *Nature*, 2008, **451**, 977–980.
65 R. Zhang, T. Yan, B. Lechner, K. Schroeter, Y. Liang and B. Li, *Macromolecules*, 2013, **46**, 1841–1850.
66 J. F. Monllor, J. R. Soriano, J. A. Fernandez, E. E. S. Eulogio and J. V. Guarinos, in *Proceedings of the European Conference on Noise Control*, 2008, vol. 123, pp. 937–942.
67 C. D. Wood and P. A. Green, *Method and Device for Detecting Fascia Damage and Repairing the Same*, US20170228094, 2017.
68 D. J. Hwang, M. Kim, K. Hiromatsu, H. Jeon and C. P. Grigoropoulos, *Appl. Phys. A*, 2009, **96**, 385–390.
69 S. He, F. Chen, K. Liu, Q. Yang, H. Liu, H. Bian, X. Meng, C. Shan, J. Si, Y. Zhao and X. Hou, *Opt. Lett.*, 2012, **37**, 3825–3827.
70 D. Coillot, F. O. Méar, R. Podor and L. Montagne, *Adv. Funct. Mater.*, 2010, **20**, 4371–4374.
71 A. C. Jackson, J. A. Bartelt and P. V. Braun, *Adv. Funct. Mater.*, 2011, **21**, 4705–4711.
72 E. D. Rodriguez, X. Luo and P. T. Mather, *ACS Appl. Mater. Interfaces*, 2011, **3**, 152–161.
73 X. Luo and P. T. Mather, *ACS Macro Lett.*, 2013, **2**, 152–156.
74 G. Rivero, L.-T. T. Nguyen, X. K. D. Hillewaere and F. E. Du Prez, *Macromolecules*, 2014, **47**, 2010–2018.
75 P. Froimowicz, D. Klinger and K. Landfester, *Chem. Eur. J*, 2011, **17**, 12465–12475.
76 P. A. Pratama, A. M. Peterson and G. R. Palmese, *Macromol. Chem. Phys.*, 2012, **213**, 173–181.

77 A. Vidyasagar, K. Handore and K. M. Sureshan, *Angew. Chem.*, 2011, **50**, 8021–8024.
78 X. Yu, X. Cao, L. Chen, H. Lan, B. Liu and T. Yi, *Soft Matter*, 2012, **8**, 3329–3334.
79 P. Terech, M. Yan, M. Maréchal, G. Royal, J. Galvez and S. K. P. Velu, *Phys. Chem. Chem. Phys.*, 2013, **15**, 7338–7344.
80 X. Wang, F. Liu, X. Zheng and J. Sun, *Angew. Chem.*, 2011, **50**, 11378–11381.
81 X. Wang, Y. Wang, S. Bi, Y. Wang, X. Chen, L. Qiu and J. Sun, *Adv. Funct. Mater.*, 2014, **24**, 403–411.
82 T. Dikić, W. Ming, R. A. T. M. van Benthem, A. C. C. Esteves and G. de With, *Adv. Mater.*, 2012, **24**, 3701–3704.
83 M. Burnworth, L. Tang, J. R. Kumpfer, A. J. Duncan, F. L. Beyer, G. L. Fiore, S. J. Rowan and C. Weder, *Nature*, 2011, **472**, 334–337.
84 S. Coulibaly, A. Roulin, S. Balog, M. V. Biyani, E. J. Foster, S. J. Rowan, G. L. Fiore and C. Weder, *Macromolecules*, 2014, **47**, 152–160.
85 E. V Skorb, D. V Sviridov, H. Möhwald and D. G. Shchukin, *Chem. Commun.*, 2009, 6041–6043.
86 I. Alessandri, *Small*, 2010, **6**, 1679–1685.
87 P. Zheng and T. J. McCarthy, *J. Am. Chem. Soc.*, 2012, **134**, 2024–2027.
88 X. Y. Fu, Z. P. Fang, H. T. Yang and L. F. Tong, *Chinese Chem. Lett.*, 2008, **19**, 655–657.
89 X. F. Lei, Y. Chen, H. P. Zhang, X. J. Li, P. Yao and Q. Y. Zhang, *ACS Appl. Mater. Interfaces*, 2013, **5**, 10207–10220.
90 Z. P. Zhang, M. Z. Rong and M. Q. Zhang, *Polym.*, 2014, 3936–3943.
91 D. Langhe and M. Ponting, *Manufacturing and Novel Applications of Multilayer Polymer Films*, William Andrew, Ohio, USA, 2016.
92 M. Stamm, *Polymer Surfaces and Interfaces*, Springer, Dresden, Germany, 1st edn., 2008.
93 Y. Fujii, H. Morita, A. Takahara and K. Tanaka, *Adv Polym Sci*, 2013, **252**, 1–28.
94 W. Knoll and R. Advincula, *Functional Polymer Films*, Willey-VCH, 1st edn., 2011.
95 A. Giessmann, *Coating Substrates and Textiles - A Practical Guide to Coating and Laminating Technologies*, Springer, Berlin, Germany, 2nd edn., 2012.
96 D. Satas and A. Tracon, *Coating Technology Handbook*, CRC Press, 2nd edn., 2000.
97 J. W. Gooch, *Encyclopedic Dictionary of Polymers*, Springer, 2007.
98 G. P. Denisova, S. E. Artemenko, T. P. Ustinova and N. N. Chervonnaya, *Fibre Chem.*, 1992, 19–21.
99 P. Howard and R. S. Parikh, *Polym. Chem.*, 1968, **6**, 537–546.
100 Markets and Markets, http://www.marketsandmarkets.com/Market-Reports%0A/mdi-tdi-polyurethane-market-381.html%0A, (accessed 27 March 2015).
101 K. Uhlig, *Discovering Polyurethanes*, Hanser, Munich, 1999.
102 M. Ardjmand and A. S. Rad, *Arab. J. Sci. Eng.*, 2012, **38**, 1005–1009.
103 D. B. Marghitu, *Mechanical Engineer's Handbook*, Academic Presscsc, 2001.

104 I. Yilgör, E. Yilgör and G. L. Wilkes, *Polym.*, 2015, **58**, A1–A36.
105 K. Gisselfält and B. Helgee, *Macromol. Mater. Eng.*, 2003, **288**, 265–271.
106 J. Blackwell, M. R. Nagarajan and T. B. Hoitink, *Polym.*, 1982, **23**, 950–956.
107 C.-C. Chang, K.-S. Chen, T. L. Yu, Y.-S. Chen, C.-L. Tsai and Y.-H. Tseng, *Polym. J.*, 1999, 31, 1205–1210.
108 G. J. E. Biemond, K. Brasspenning and R. J. Gaymans, *J. Appl. Polym. Sci.*, 2211, **124**, 1302–1315.
109 M. Shoaib and A. Bahadur, *E-Polymers*, 2016, **16**, 411–418.
110 A. Eyvazzadeh Kalajahi, M. Rezaei, F. Abbasi and G. Mir Mohamad Sadeghi, *Polym. Plast. Technol. Eng.*, 2017, **0**, 1–9.
111 R. A. Azzam, S. K. Mohamed, R. Tol, V. Everaert, H. Reynaers and B. Goderis, *Polym. Degrad. Stab.*, 2007, **92**, 1316–1325.
112 J. M. G. Cowie, *Polymers: Chemistry and Physics of Modern Materials*, CRC Press, Boca Raton, Florida, 2nd edn., 2000.
113 J. Csernica, *Standard Experiments in Engineering Materials Science and Technology: Mechanical Properties of Crosslinked Polymer*, Lewisburg, PA, United States, 1994.
114 J. Hu, K. Peng, J. Guo, D. Shan, G. B. Kim, Q. Li, E. Gerhard, L. Zhu, W. Tu, W. Lv, M. A. Hickner and J. Yang, *ACS Appl. Mater. Interfaces*, 2016, **8**, 17499–17510.
115 M. M. Rahman, H. Do Kim and W. K. Lee, *Fibers Polym.*, 2009, **10**, 6–13.
116 C. Jin, Z. Wang, A. A. Volinsky, A. Sharfeddin and N. D. Gallant, *Polym. Test.*, 2016, **56**, 329–336.
117 J. Pavlinec, M. Lazár and I. Janigová, *J. Macromol. Sci. - Pure Appl. Chem.*, 1997, **34**, 81–90.
118 D. Yang, L. Han, H. Zhang and F. Qiu, *J. Macromol. Sci. Part A Pure Appl. Chem.*, 2011, **48**, 277–283.
119 M. A. Hood, B. Wang, J. M. Sands, J. J. La Scala, F. L. Beyer and C. Y. Li, *Polym.*, 2010, **51**, 2191–2198.
120 Merquinsa, *http://www.merquinsa.com/whats/whatsaPU.pdf*, (accessed August 2014).
121 M. J. O'Sickey, *Characterization of Structure-Property Relationships of Poly(urethane-urea)s for Fiber Applications, Doctoral Dissertation*, Virginia Polytechnic Institute and State University, 2002.
122 C. Prisacariu, in *Polyurethane Elastomers*, Springer-Verlag, Wien, 1st edn., 2011, pp. 23–60.
123 T. J. Touchet and E. M. Cosgriff-Hernandez, *Hierarchal Structure-Property Relationships of Segmented Polyurethanes*, Elsevier Ltd, 2016.
124 A. J. Ryan, C. W. Macosko and W. Bras, *Macromolecules*, 1992, **25**, 6277–6283.
125 Y. Camberlin and J. P. Pascault, *J. Polym. Sci. Part A Polym. Chem.*, 1984, **22**, 1835–1844.
126 B. Chu, T. Gao, Y. Li, J. Wang, C. R. Desper and C. A. Byrne, *Macromolecules*, 1992, **25**, 5724–5729.
127 K. N. Edwards, *Urethane Chemistry and Applications*, American Chemical

Society, York, PA, US, 1981.
128 H. Jeong, J. Park, S. Kim, J. Lee, N. Ahn and H. Roh, *Fibers Polym.*, 2013, **14**, 1082–1093.
129 V. P. Joshi, *Studies on Synthesis and Characterization of Thermoplastic Polyurethane-urea Copolymers*, PhD thesis, University of Pune, 2009.
130 D. K. Chattopadhyay, B. Sreedhar and K. V. S. N. Raju, *J. Polym. Sci.*, 2006, **44**, 102–118.
131 P. Król, *Prog. Mater. Sci.*, 2007, **52**, 915–1015.
132 S. V. Romanov, Y. T. Panov and K. A. Timakova, *Polym. Sci. Ser. D*, 2013, **6**, 175–180.
133 J. O. Akindoyo, M. D. H. Beg, S. Ghazali, M. R. Islam, N. Jeyaratnam and A. R. Yuvaraj, *RSC Adv.*, 2016, **6**, 114453–114482.
134 X. Zhou, Y. Li, C. Fang, S. Li, Y. Cheng, W. Lei and X. Meng, *J. Mater. Sci. Technol.*, 2015, **31**, 708–722.
135 A. Noreen, K. M. Zia, M. Zuber, S. Tabasum and M. J. Saif, *Korean J. Chem. Eng.*, 2016, **33**, 388–400.
136 J. Rosthauser and K. Nachtkamp, *J. Coat. Fabr.*, 1986, **16**, 39–79.
137 L. Marcus, *Organic reactions in water: principles, strategies and applications*, Blackwell Publishing Ltd, Oxford, 1st edn., 2007.
138 L. Lei, Z. Xia, G. Cao and L. Zhong, *Colloid Polym. Sci.*, 2014, **292**, 527–532.
139 H. Honarkar, *J. Dispers. Sci. Technol.*, 2017, **0**, 1–10.
140 G. Rokicki, P. G. Parzuchowski and M. Mazurek, *Polym. Adv. Technol.*, 2015, **26**, 707–761.
141 M. J. Elwell, S. Mortimer, A. J. Ryan and W. Bras, 1995, **97**, 261–264.
142 W. Li, A. J. Ryan and I. K. Meier, *Macromolecules*, 2002, **35**, 5034–5042.
143 J. W. Cahn and J. E. Hilliard, *J. Chem. Phys.*, 1958, **28**, 258–267.
144 S. Burattini, H. Merino, W. Weng and S. J. Rowan, *J. Am. Chem. Soc.*, 2010, **132**, 12051–12058.
145 P. Michael, D. Döhler and W. H. Binder, *Polym.*, 2015, **69**, 216–227.
146 A. E. Hughes, *Self-healing coatings*, Elsevier Ltd., 2015.
147 F. Herbst, S. Seiffert and W. H. Binder, *Polym. Chem.*, 2012, **3**, 3084–3092.
148 E. B. Stukalin, L. H. Cai, N. A. Kumar, L. Leibler and M. Rubinstein, *Macromolecules*, 2013, **46**, 7525–7541.
149 W. Fischer and N. Yuva, *Self-healing UV-Coatings, RadTech EUROPE, Conference Proceedings*, Basel, 2011.
150 M. Mechel, *Shining prospects for two-component polyurethane clearcoats*, Bayer Materials Science, www.bayercoatings.com, accessed August, 2004.
151 B. Ghosh, K. V. Chellappan and M. W. Urban, *J. Mater. Chem.*, 2012, **22**, 16104–16113.
152 Bayer MaterialScience, *http://www.bayercoatings.com*, (accessed August 2014).
153 Z. Chang, M. Zhang, A. G. Hudson, E. B. Orler, R. B. Moore, G. L. Wilkes and S. R. Turner, *Polym.*, 2013, **54**, 6910–6917.
154 Y. González-García, J. M. C. Mol, T. Muselle, I. De Graeve, G. Van Assche, G. Scheltjens, B. Van Mele and H. Terryn, *Electrochim. Acta*, 2011, **56**, 9619–

9626.
155 Y. González-García, J. M. C. Mol, T. Muselle, I. De Graeve, G. Van Assche, G. Scheltjens, B. Van Mele and H. Terryn, *Electrochem. commun.*, 2011, **13**, 169–173.
156 Y. Chen, A. M. Kushner, G. A. Williams and Z. Guan, *Nat. Chem.*, 2012, **4**, 467–472.
157 J. Hentschel, A. M. Kushner, J. Ziller and Z. Guan, *Angew. Chem.*, 2012, **51**, 10561–10565.
158 S. Chen, N. Mahmood, M. Beiner and W. H. Binder, *Angew. Chem.*, 2015, **54**, 10188–10192.
159 Y. C. Jung, H. H. Kim, Y. A. Kim, J. H. Kim, J. W. Cho, M. Endo and M. S. Dresselhaus, *Macromolecules*, 2010, **43**, 6106–6112.
160 Y. C. Jung, J. H. Kim, T. Hayashi, Y. A. Kim, M. Endo, M. Terrones and M. S. Dresselhaus, *Macromol. Rapid Commun.*, 2012, **33**, 628–634.
161 P. Du, X. Liu, Z. Zheng, X. Wang, T. Joncheray and Y. Zhang, *RSC Adv.*, 2013, **3**, 15475–15482.
162 P. Du, M. Wu, X. Liu, Z. Zheng, X. Wang, T. Joncheray and Y. Zhang, *J. Appl. Polym. Sci.*, 2014, **131**, 1–7.
163 C. Yuan, M. Z. Rong and M. Q. Zhang, *Polym.*, 2014, **55**, 1782–1791.
164 J. Ling, M. Z. Rong and M. Q. Zhang, *Polym.*, 2012, **53**, 2691–2698.
165 J. Ling, M. Z. Rong and M. Q. Zhang, *Chinese J. Polym. Sci.*, 2014, **32**, 1286–1297.
166 S. Smeets, in *Evaluation of Scratch Resistance Test Methods for Organic Coatings*, 7th Nürnberg Congress, European Coatings Show, Nürnberg, 2003.
167 Y. Heischkel, H. Larbig, E. Beck, N. Gruber and R. Schwalm, *Coatings Reparable by Introduction of Energy*, US20080207793, 2008.
168 L. L. Foringer, C. A. Kondos, R. J. Sadvary, K. G. Olson and D. A. Simpson, *Curable film-forming compositions demonstrating self-healing properties*, US20090062453, 2009.
169 H. Zheng and J. Hazle, *Optical Article Containing A Self-Healing Coating And Improved Initial Haze*, US20140037964, 2014.
170 G. Mirchandani, M. A. Paravakkal, D. Puthran, S. Das and K. S. Mandal, *A one component self-healing coating composition*, US8664298, 2014.
171 H. Zheng, *Self-healing transparent coatings containing mineral conductive colloids*, US20140036223, 2014.
172 U. Numrich, W. Kanzler, M. Szallies, J. Ackermann and M. Olbrich, *Polymeric materials for external applications with self-healing surface properties after scratches or abrasion damage*, US20140144427, 2014.
173 O. Elizalde, F. Lucas, A. M. Steinbrecher, L. Tuchbreiter, A. Pfahler and R. Muelhaupt, *Coatings repairable by introduction of energy*, US20140031483, 2014.
174 H. Zheng, *Optical article containing self-healing and abrasion-resistant coatings*, US20140092360, 2014.

2. EXPERIMENTAL AND INSTRUMENTATION

In this work a broad range of synthetic, characterisation, spectroscopic and thermal analysis techniques was used. Most techniques will be familiar to the reader. However, the theory behind all techniques, as well as details of the experimental work, will be discussed in some detail in this section.

The majority of formulations, with two exceptions, were prepared using the so-called acetone procedure, described in Section 1.3.2., to obtain polyurethane waterborne dispersions (PUD). The dispersions were applied on cellulose triacetate (TAc) sheets using a Mayer rod and dried in an oven. The main techniques used to characterise the morphology and properties of coatings were Attenuated Total Reflectance Fourier Transform Infrared Spectroscopy (ATR FT-IR) and Differential Scanning Calorimetry (DSC). Scanning Electron Microscopy (SEM) and Atomic Force Microscopy (AFM) were secondary techniques used for some of the materials to gain additional insight into the morphology of the polymers. The damage of coatings was introduced using an Automated Steel Wool instrument, and the damage and recovery were monitored using haze measurements. The materials were also characterised using the Pencil Hardness test, Cross-cut Adhesion test, Solvent Resistance test and Contact Angle measurements and viscosity measurements. Additionally, the UV degradation of some samples was tested using a weatherometer.

2.1 SYNTHESIS AND PREPARATION OF MATERIALS

2.1.1. MATERIALS

Polyols: polydiethylene adipate glycol Desmophen 1700 (D1700, MW = 2550 g mol^{-1}) and a branched hydroxyl bearing polyester of unknown structure Desmophen 670 (D670, MW = 750 g mol^{-1}), generously donated by Bayer Materials Science, polycaprolactones CAPA2101A (PCL1000, MW = 1000 g mol^{-1}) and CAPA2201A (PCL1000, MW = 2000 g mol^{-1}), generously donated by Perstorp, and co-polycarbonates of pentanediol and hexanediol PH50 (MW = 500 g mol^{-1}), PH200 (MW

= 2000 $gmol^{-1}$) and PH300 (MW = 3000 $gmol^{-1}$), generously donated by UBS Industries, were dried overnight in a vacuum oven at 80 ˚C prior to use as a polyol.

Isocyanates: hexamethylene diisocyanate (HDI, >98%) and isophorone diisocyanate (IPDI, >98%) were purchased from Sigma Aldrich, and isophorone diisocyanate trimer Desmodur Z 4470 BA (t-IPDI, 70% in *n*-butyl acetate) was generously donated by Bayer Materials Science.

Chain extenders: 1,2-ethanediol (ethylene glycol, 1,2-EG, 99%), 1,3-propanediol (1,3-PrD, 99%), 1,4-butanediol (1,4-BD, 99%), 1,5-pentanediol (1,5-PeD, 99%), diethylene glycol (DEG, 99%), ethanolamine (EA, 98%), hexamethylene diamine (HDA, 70% solution in water), trimethylolpropane (TMP, 99%), dimethylol propionic acid (DMPA, 98%) were purchased from Sigma Aldrich and used without further purification.

Dibutyltin dilaurate (DBTDL, 95%), triethylamine (TEA, 99.5%) and 1,7-dichloro-octamethyltetrasiloxane (1,7-DCOMTS, 95%) were purchased from Sigma Aldrich and used without further purification.

Solvents: acetone (99%), distilled before use, anhydrous *n*-butyl acetate (BA, >99%) and methyl isobutyl ketone (MIBK, 98.5%) were purchased from Sigma Aldrich. Additionally, deionised water was used as the dispersing phase.

2.1.2. SYNTHESIS OF SOLVENT-BORNE FORMULATIONS

Dried polyol D1700 (45.4 g, 17.8 mmol) and DBTDL (0.06 mL, 0.09 mmol) were placed in an oven-dried reaction vessel and stirred at 100 rpm under an argon atmosphere at 75 ˚C. Next, anhydrous BA (30 mL), HDI (8.60 mL, 53.5 mmol) and 1,2-EG (1.54 mL, 27.6 mmol) were added and the mixture was stirred for 3 hours (**Figure 2-1**). Subsequently, the mixture was cooled down to room temperature (RT) and transferred to a 20 mL syringe used to apply the coating on the TAc sheets.

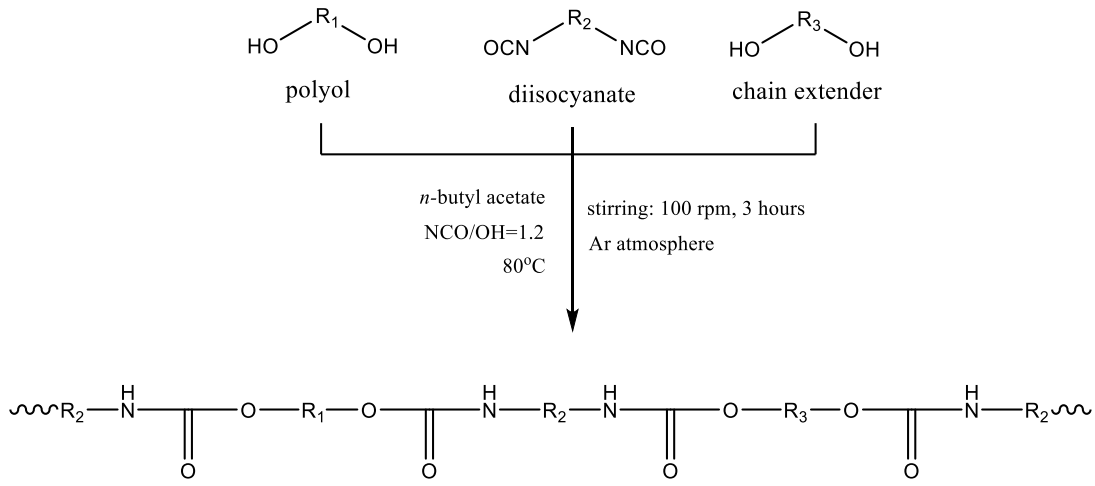

***Figure 2-1**. Scheme of the synthesis of the solvent-borne polyurethane.*

2.1.3. PREPARATION OF FORMULATIONS USING DUAL CARTRIDGE

Dried polyol D670 (25.0 g, 33.3 mmol), 1,2-EG (1.30 g, 22.2 mmol), DBTDL (0.04 mL, 0.06 mmol) and MIBK (8.14 mL) were mixed together and loaded into the first cylindrical chamber of a dual cartridge on-demand mixing and dispersing system (Figure 2-2). HDI (11.08g, 66.6 mmol) and MIBK (29.0 mL) were mixed together and loaded into the second chamber of the dual cartridge. The coatings were applied onto TAc sheets from the cartridge using an applicator gun and a static mixer nozzle.

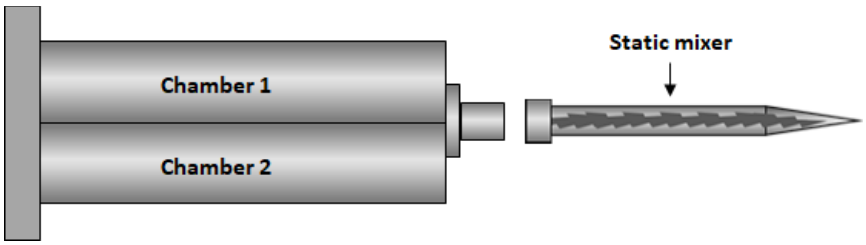

***Figure 2-2.** Dual cartridge on-demand mixing and dispersing system with static mixer.*

2.1.4. SYNTHESIS OF WATERBORNE FORMULATIONS

PUDs were prepared using the so-called *acetone process,* described in Section 1.3.2..[1] Dry polyol (10 g, 20 mmol), DBTDL (0.02 mL, 0.03 mmol) and a pre-calculated amount of DMPA were placed in an oven-dried reaction vessel. 20-40 mL of anhydrous acetone and TEA (1.4 times the number of mmol of DMPA used) were subsequently added.

The mixture was stirred under nitrogen at 200 rpm for 30 minutes at 50 °C, after which a pre-calculated amount of isocyanate or blend of isocyanates was added drop-wise. Optionally, after 2-4 hours a pre-calculated amount of CEs was added. The progress of the reaction was monitored by ATR FT-IR spectroscopy until complete disappearance of the NCO peak was observed. Subsequently the mixture was cooled down to RT, 40 mL of deionised water was added, and the solution was stirred at 600 rpm for 30 minutes to create a polyurethane dispersion. Acetone was removed in a rotary evaporator over 60 minutes at 50 °C and 300 mbar pressure (Figure 2-3).

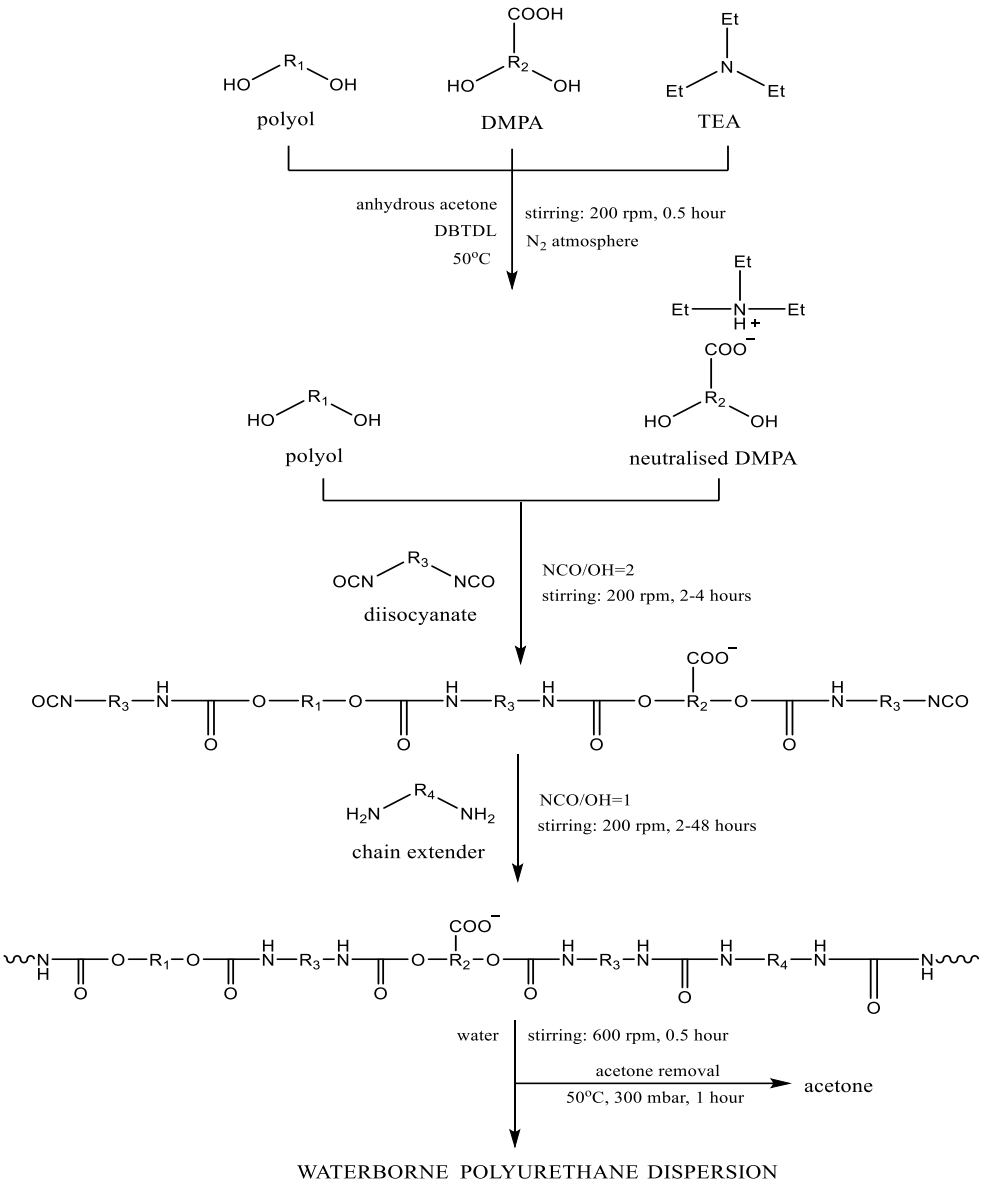

Figure 2-3. *Simplified scheme of the synthesis of diamine chain-extended polyurethane dispersions.*

2.1.5. PREPARATION OF SOLID SAMPLES

Solid samples were prepared by placing approximately 10 mL of PUD in a Petri dish and leaving to dry at RT for 24 hours followed by 1 hour in the oven at 60 °C. Solid samples of about 1 mm thickness were used for further tests including DSC, TVA and BDS.

2.1.6. PREPARATION OF COATINGS

Approximately 2 mL of PUDs were applied on a TAc sheet of 400 x 600 mm using a dual cartridge gun equipped with a mixer, or a syringe filled with a PUD dispersion. The solution was spread and smoothed with a wirewound Mayer rod 020 (20 mils, 50.8 microns wet coating thickness). The coated sheets were placed in an oven at 60 °C for 1 hour to ensure complete removal of water. Subsequently, samples of 40x60 mm size were cut and used for further tests including ATR FT-IR, haze, hardness or adhesion.

2.2 CHARACTERISATION OF DISPERSIONS

2.2.1. DETERMINATION OF SOLID CONTENT

2.2.1.1 Theory

Solid content (%S) is the amount of a non-volatile material in a solution or dispersion. It can be measured by weighing the amount of solid left after vaporisation of the volatile solvent. The solid content of PUDs ranges usually between 20 and 40%, although some researchers report dispersions with a solid content of over 50%.[2] The estimation of dry coating thickness prepared with a Mayer rod can be calculated from the controllable thickness of a wet coating if the solid content of a dispersion is known. Therefore, the measurement of solid content is crucial for coating processes.

2.2.1.2 Method

A pre-calculated volume of the dispersion was placed in a dish of known weight (m_d). Subsequently, the dish was weighed (m_{d+PUD}), left overnight in an oven at 80˚C and re-weighed (m_{d+S}). The solid content was calculated as an average of three measurements performed for every dispersion using **Equation 2.1**.

$$\%S = \frac{m_{d+S} - m_d}{m_{d+PUD} - m_d}\ x\ 100 \qquad \text{Equation 2.1}$$

2.2.2. DETERMINATION OF HARD SEGMENT CONTENT

2.2.2.1. Theory

As highlighted in the introduction, the properties of PUs are linked to their morphology. In turn, the morphology is related to the amount of HS and SS within the polymer matrix. Therefore, determination of the amount of hard and soft segments is crucial for the design of materials with desired properties.

The HS content can be calculated as chain-extended urethane content (isocyanate-CE-isocyanate), or the combined urethane (in polyol-isocyanate-polyol) and chain extended urethane (isocyanate-CE-isocyanate) content. The former method is commonly used for poly(urethane-urea) formulations due to the higher polarity of urea, and for formulations created with high MW polyols, due to the unlikelihood of urethane groups in polyol-isocyanate-polyol blocks forming HS.[3] The majority of formulations reported in this thesis were prepared with a low MW polyol PH50 and were found to contain small amounts of urethane groups. Therefore, the latter method of calculating %HS as combined urethane and CE urethane content will be used.

2.2.2.2. Method

The hard segment content (%HS) was calculated using the equations derived by Flory (**Equation 2.2**) where R is the mole ratio of isocyanate to polyol, M_{iso} is the number

average molecular weight of isocyanate, M_{CE} is number average molecular weight of chain extender and M_{ol} is number average molecular weight of polyol.[3]

$$\%HS = \frac{R \times M_{iso} + (R-1)(M_{CE})}{M_{ol} + R \times M_{iso} + (R-1) \times M_{CE}} \times 100 \qquad \text{Equation 2.2}$$

The equation was found to give a reliable estimation of HS percentage and allowed calculation of %HS in formulations prepared without any CE. The M_{CE} was calculated as a weighted arithmetic mean of molecular weights of CE, DMPA and, if used, cross-linkers.

2.2.3. Determination of contact angle

2.2.3.1 Theory

The angle of the intersection at a solid-liquid interface, known as the contact angle, is widely used to measure the wettability of a solid or the molecular interactions of a liquid. The profile of a liquid droplet can be described as a tangential angle at the interface, known as the Young's angle, $\boldsymbol{\theta}$. The contact angle is influenced by three factors: the liquid surface tension (γ_{LV}), the solid surface tension (γ_{SV}), the liquid-solid surface tension (γ_{SL}) (**Figure 2-4**).[4]

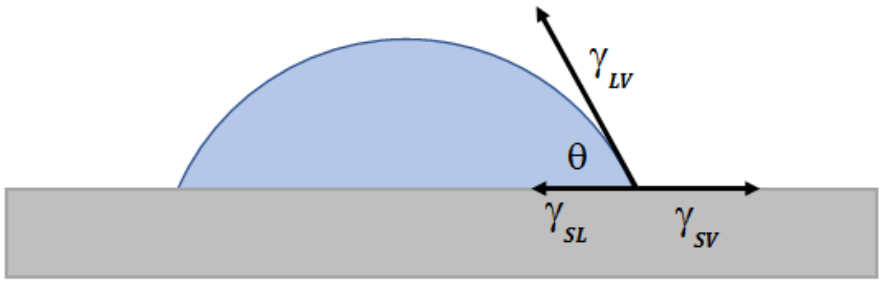

Figure 2-4. Vector representation of a contact angle.[4]

The equilibrium, first described by Young two centuries ago, can be expressed by the Young's equation:[4]

$$\gamma_{SV} = \gamma_{LV}\, x\, cos\theta + \gamma_{SL} \qquad \text{Equation 2.3}$$

The sessile drop technique is a method commonly used to measure the contact angle. The technique involves deposition of a drop of a pure liquid on a solid substrate, followed by the contact angle measurement performed with an optical capture system. As the contact angles are very sensitive to any contamination, the solid substrate must be carefully cleaned and dried prior to the test, commonly performed by soaking in ethanol to dissolve impurities and grease. To ensure reliable results, the analysis should be repeated 5 to 10 times in different areas of the sample and the dissimilarity of the results should be less than 2°.

Strong interactions between the liquid and solid molecules lead to the drop being flat and spread-out, resulting in a contact angle of 0°, commonly observed on ceramic surfaces. The higher contact angle values indicate less strong liquid-solid interactions, as well as stronger liquid intermolecular interactions. The use of water as the liquid phase allows determination of hydrophilicity of a solid. The contact angle below 90° indicates a hydrophilic surface, while above 90° indicates a hydrophobic surface, seen e.g. in low surface energy fluorinated polymers.

The contact angle is also related to surface tension of the liquid. Therefore, measurement of the contact angle of various dispersions deposited on the same substrate provides information about intermolecular interactions of the dispersions.

2.2.3.2 Method

The contact angle of the PUDs was measured at room temperature with a Kruss Drop Shape Analyser DSA25. The Sessile Drop Method was used on a cleaned with water and ethanol glass slide, with a probe liquid of a dispersion standardised to 25% of solid content. The results were calculated as an average of five measurements.

2.3. CHARACTERISATION OF COATINGS

2.3.1. ATTENUATED TOTAL REFLECTANCE FOURIER TRANSFORM INFRARED SPECTROSCOPY (ATR FT-IR)

2.3.1.1. Theory

Infrared spectroscopy involves a use of infrared (IR) radiation to identify and study chemicals and their major structural groups. The technique uses the property of molecules being able to transmit, absorb or reflect frequencies characteristic to their structure. The energy of the IR electromagnetic waves that had interacted with the sample can be measured, recorded and plotted as the absorbance against the wavelength. That allows an easy identification of functional groups present in the sample.[5]

The most common IR spectrometers use the transmission sampling mode, in which the IR beam passes through the sample and collects information about the chemical groups within the whole depth of the sample. However, this technique requires sample preparation, for example the use of potassium bromide, sodium chloride or quartz disks, or commonly the use of solvents.[6] Moreover, as the IR beam passes through the whole depth of the sample, a detailed analysis of multi-layered materials becomes complex and often impossible due to a large amount of overlaying signals.

Another IR spectroscopy technique uses a diffused reflection sampling method. In this technique an IR beam is reflected from the surface and an IR detector detects diffuse reflections. The method does not require any sample preparation and is most suitable for rough solid surfaces or powdered samples.[6] However, it is not suitable for multi-layered transparent materials due to the irradiation occurring though the entire depth of the sample.

Attenuated Total Reflectance (ATR) is a third commonly use sampling method which allows examining samples in the solid or liquid state without any preparation. The technique uses a property of total internal reflection, creating an evanescent wave within a sample. The advantages of this non-destructive spectroscopic technique

include the ease of sample preparation and quick measurement. Moreover, due to a limited penetration depth, the technique allows information about chemical groups present only in the outer layer, e.g. in multi-layered coatings.

Attenuated Total Reflectance Fourier Transform Infrared Spectroscopy (ATR FT-IR) is broadly used to analyse chemical structure of materials as well as to monitor changes occurring during chemical reactions. In comparison with traditional IR spectroscopy measuring transmission of IR light, this technique is based on the property of total internal reflection.

When a beam of light passes through an optically dense material, e.g. a diamond, with a high refractive index n_1, and then comes into a contact with another material, e.g. PU coating, with a lower refractive index n_2, total internal reflectance occurs. If the angle of incidence of the beam of light exceeds the critical angle Θ_{crit} the reflectance creates an evanescent wave. The value of the critical angle can be calculated using **Equation 2.4**, where n_1 is the refractive index of the ATR crystal and n_2 is the refractive index of a sample.[7]

$$\Theta_{crit} = sin^{-1}\frac{n_2}{n_1} \qquad \text{Equation 2.4}$$

The evanescent wave that has the ability to penetrate the sample and return as a reflected wave (Figure 2-5). ATR instruments can be either multi-reflection, as shown in the figure below, or a single-reflection.[8]

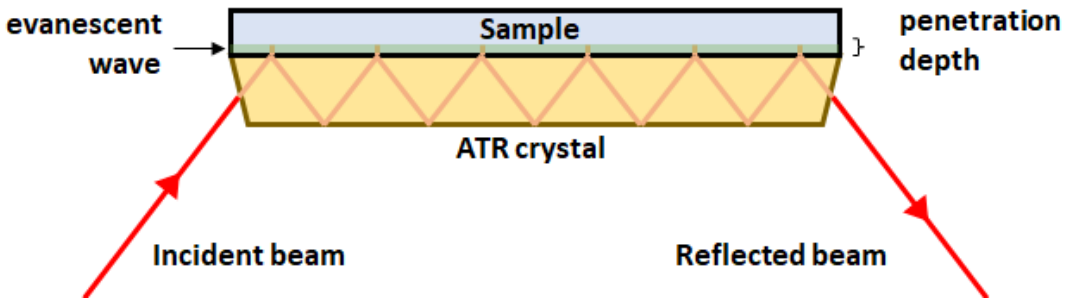

Figure 2-5. *A graph of a multi-reflection ATR instrument. The occurrence of the total reflectance is shown within the ATR crystal and the creation of the evanescence wave on the crystal-sample interface.*[8]

The evanescent wave can interact with chemical groups that possess a dipole and is absorbed at specific wavelengths. These interactions result in an informative probe of the analysed material, which can be translated into an IR spectrum. The wavelength of the absorption can be translated into information about specific chemical groups and their environment.

The penetration depth (d_p) is typically between 0.5 and 2 µm and depends on the wavelength of the light (λ), the angle of incidence (Θ), as well as refraction indices of the ATR crystal (n_1) and the sample (n_2), and can be described using **Equation 2.5**.[9]

$$d_p = \frac{\lambda}{2\pi\sqrt{n_1^2 sin^2\Theta - n_2^2}} \qquad \text{Equation 2.5}$$

Samples analysed with ATR FT-IR spectroscopy show absorption at particular wavelengths which can be related to specific chemical groups, e.g. urethane C=O groups show a stretch band in the 1750-1700 cm^{-1} region, while the N-H stretch can be observed in the 3500-3200 cm^{-1} region. As the N-H group can act as a hydrogen bond donor and the C=O group as a hydrogen bond acceptor, the urethane groups can create H-bonded segments. The H-bonding leads to electron delocalisation within the urethane, which can be detected by ATR FT-IR spectroscopy as a shift of a peak to lower wavenumber values. The strength and the environment of H-bonding determines the magnitude of the shift. For example, the stretching of free urethane N-H bond appears at 3500-3400 cm^{-1}, while H-bonded N-H occurs to lower wavenumber, between 3400 and 3200 cm^{-1}. Therefore, ATR-FTIR can be used to characterise both the strength and the order of H-bonding in PU, and indicate the extent of phase-separation or phase-mixing.

2.3.1.2 Method

Analysis was carried out with single reflection instrument Agilent 5500 Series Portable FTIR Spherical Diamond ATR. The spectra were recorded using the following parameters:

- Background valid time limit: 10 minutes

- Absorbance minimum Y threshold: 0.1 Abs
- Spectral range: 4700 cm^{-1} to 650 cm^{-1}
- Number of scans: 128
- Resolution: 2 cm^{-1}
- Sampling technology: ATR
- Sampling subtype: 1-bounce.

To confirm consistency of the structure within the film and to eliminate measurement errors, three measurements at random positions of each of the samples were taken. The recorded spectra were baseline-corrected, normalised and subsequently averaged using KnowItAll Academic Edition 2017. The graphs were plotted using Origin Pro 9.0.

2.3.2. Differential Scanning Calorimetry (DSC)

2.3.2.1 Theory

DSC is a technique developed in 1962, used to measure thermal properties of materials. The technique is used to monitor the heat capacity of a sample during a heating or cooling process, which allows determination of temperatures and enthalpies of various thermal processes such as the glass transition, melting, recrystallisation or degradation.

The instrument consists of a measuring cell where a sample pan and reference pan are placed (Figure 2-6). The analysis involves both samples kept at the same temperature during a linear increase or decrease of the temperature of the cell. When the sample undergoes a physical or chemical transformation, the heat capacity of the sample changes. The heat-flux sensor is capable to detect the difference in the amount of heat that needs to be provided to keep both pans at the same temperature. The difference can be related to a process the sample underwent, e.g. exothermic crystallisation or endothermic melting. During the DSC run the cell is being flushed with a purge gas, usually nitrogen, which eliminates localised hot-spots.[5]

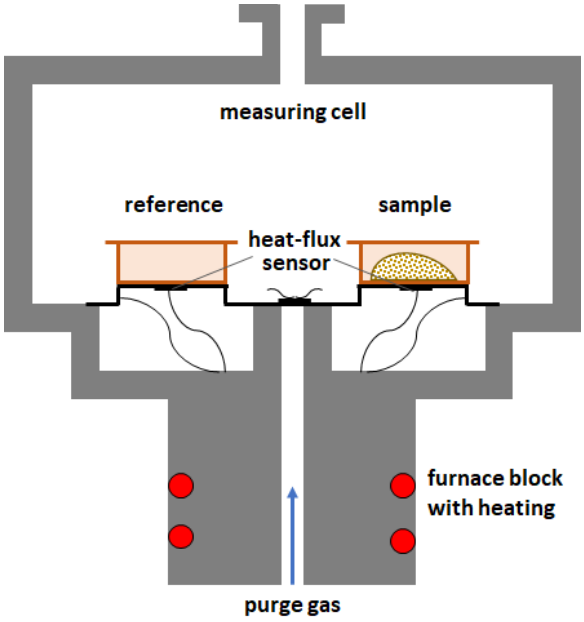

Figure 2-6. *A graph representing a DSC measuring cell – a reference and a sample pans are kept at the same temperature during a change of temperature, while the heat-flux sensor measures the amount of heat required to maintain the pans at the same temperature.*[5]

DSC is widely used to analyse thermal properties of polymers. The crystalline regions of a polymer matrix show primary transitions in the form of endothermic melting upon heating and exothermic recrystallisation upon cooling. The amorphous regions show secondary phase transitions, e.g. glass transition. These transitions can be observed when a graph of heat flux versus temperature is plotted (Figure 2-7).

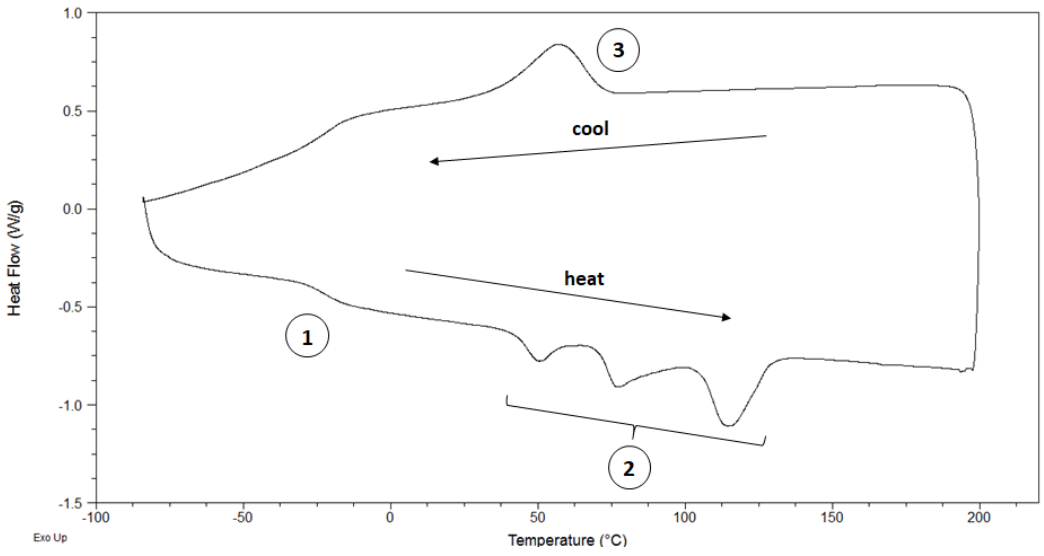

Figure 2-7. DSC heat-cool thermogram of a typical, semi-crystalline polyurethane: 1) glass transition, 2) multiple melting peaks and 3) recrystallisation.

Polymer chains within a polymer matrix can have two various internal organisation patterns – amorphous and crystalline. However, polymers often show both phases and are therefore called semi-crystalline. The fraction of ordered molecules within a polymer matrix can be described as the degree of crystallinity, which usually varies from 10% to 80%. At sufficiently low temperatures the chain motion of a polymer is frozen, and the materials appear as hard, glassy solids. When they are heated, they pass from the solid to the liquid phase. However, this process occurs in different ways for amorphous and crystalline regions (Figure 2-8).[10]

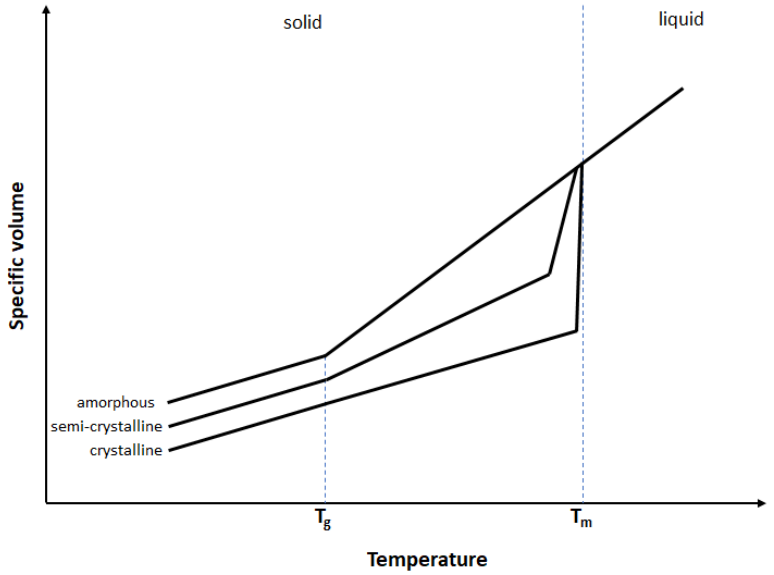

Figure 2-8. *Schematic representation of the change in specific volume of a polymer with temperature for a completely amorphous sample, a semi-crystalline sample and a completely crystalline sample.*[10]

A completely amorphous polymer has all the chains arranged randomly. In the glassy state the chains are immobilised, and the materials are rigid, brittle and optically transparent due to the absence of boundaries which could reflect the light. When the amorphous polymer is heated it obtains sufficient thermal energy to overcome the rotational energy barrier of the chains and allows the chain segments to move co-operatively. Due to the molecular motion the material softens and becomes rubbery. This transition occurs at the temperature known as the glass transition temperature (T_g) and depends on multiple factors such as chain flexibility, steric effects, configurational effects or crosslinking. Initially the molecular motion of polymer chains beyond the T_g is restricted, but as the temperature increases the chains obtain greater

freedom of movement, leading to further softening, until the material becomes a viscous liquid. Therefore, a change in the rate of specific volume change in amorphous polymers can be observed at the temperature of their glass transition.

A completely crystalline polymer in a frozen state would have all the chains in a close proximity, with the secondary valence forces acting between them triggering the organisation of three-dimensional crystallites. Upon heating, the chains reach a point where sufficient thermal energy to break the interactions is obtained and the chain segments can start moving freely. The process of melting, which changes the crystalline polymer into a viscous liquid, requires a higher input of thermal energy than the glass transition. Due to the absence of amorphous regions within a completely crystalline polymer matrix, no glass transition would be observed. Therefore, a sharp increase in the rate of specific volume change in crystalline polymers occurs at their melting temperature (T_m).

However, more commonly seen semi-crystalline polymers contain both amorphous and crystalline regions, therefore both T_g and T_m can be observed. The melting process of semi-crystalline polymers usually occurs over a broader range, and often at lower temperatures. The depression of their melting point is due to the presence of crystallites of different sizes with many defects. Therefore, changes in the rate of specific volume change in crystalline polymers occurs twice, at their T_g and T_m.

The glass transition is particularly useful to characterise the morphology of a PU moiety. Due to the multi-phase structure of PU, DSC studies often show two T_g values, a lower one associated with the SS, and a higher one associated with HS. In phase-separated systems the T_g of SS appears at lower temperatures, while in phase-mixed systems the movement of SS is restricted, thus the T_g appears at higher temperatures. The glass transition of HS is usually less visible than the one of SS, or not present at all in the DSC thermogram. This occurs due to a typical high HS sequence length distribution, resulting in a very broad transition signal, and due to a low heat capacity of HS, resulting in a poor resolution of the signal. However, the breadth of the T_g of SS and the comparison of the T_g of a pure soft segment, i.e. the polyol, with the T_g of a PU allows identification of the extent of phase-separation or phase-mixing.

Moreover, the analysis of melting and crystallisation transitions provide additional insight into the morphology.

2.3.2.2 Method

DSC measurements were carried out using TA Q1000 DSC instrument. 5-15 mg of sample was placed at the bottom of a pre-weighted DSC pan. The lid was placed at the top and the pan was sealed. A hole was punctured at the lid and the pan was weighed. The mass of a sample was obtained by extracting the two weights. The reference pan was prepared using a similar method, without placing any sample in it. For the dried samples a heat-cool-heat cycle was adopted, with the first heating cycle going from -90 ˚C to 150 ˚C, the cooling cycle from 150 ˚C to -90˚C, and the second heating cycle from -90 ˚C to 300 ˚C, under nitrogen atmosphere with a flow rate of 40 mL/min. The heating rate was set at 20 ˚C/min.

DSC data was analysed and plotted using TA Universal Analysis 4.3. The glass transition temperatures are reported as a midpoint between the onset and the end points of the transition, at half-height. Crystallisation and melting peaks are characterised using the peak temperature of the transition. All reported temperatures are rounded to the nearest integer, resulting in the maximum roundoff error of ± 0.5 ˚C. The enthalpies of melting are calculated by integration of the area under the peak. All reported enthalpy values are rounded to one decimal place, resulting in the maximum roundoff error of ± 0.05 J g^{-1}. If not stated otherwise, the DSC histograms are presented in the fashion showed in Figure 2-9.

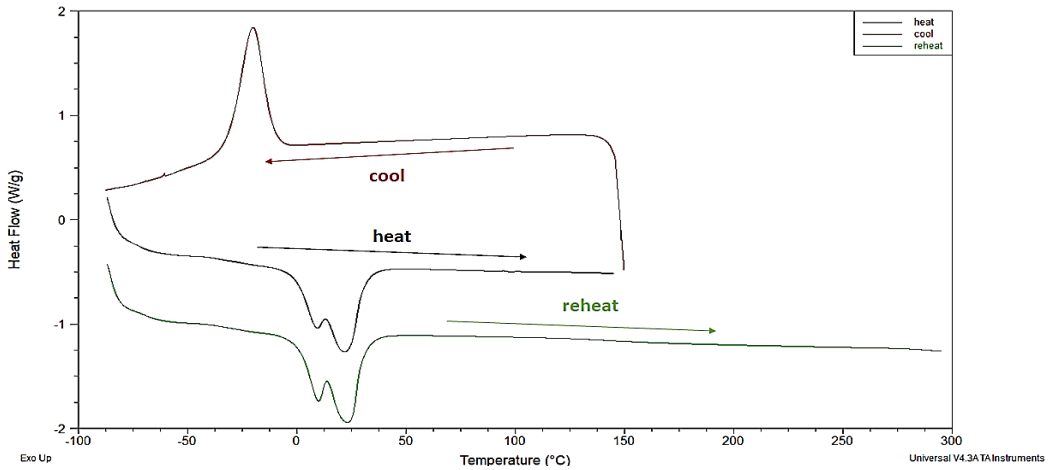

Figure 2-9. *A typical heat (black) – cool (red) – reheat (green) DSC thermogram.*

2.3.3. SCANNING ELECTRON MICROSCOPY (SEM)

2.3.3.1 Theory

SEM is a type of electron microscopy using beam of electrons to obtain the image of a sample in high vacuum and allows characterisation of the surface topography and composition of the surface. The interaction of the electron beam with the surface of a sample evokes signals of various intensity, allowing creation of an image.

The electrons must be generated, accelerated, focused and guided towards the sample, thus the system must be kept in an ultra-high vacuum to avoid contamination or discharge of the high voltage. The beam of primary electrons (PE) is emitted towards the sample and interact with the sample's surface. During the interaction, a process called an inelastic scattering occurs. The PE lose some of the energy and secondary electrons (SE) with a lower energy formed and scattered. The SE, as well as the backscattered electrons, are collected and amplified by detectors, and the signals are translated into a topographic image of the sample.[11]

To obtain an image, the sample must be electrically conductive and electrically grounded. Therefore, the specimens need to be coated with metal, e.g. silver or gold, and mounted onto an SEM stub. The SEM images can get a resolution better than 1 nm and magnification of up to 500,000 times. However, SEM does not produce colour images.

SEM images of PU coatings can provide information about topography and composition of the surface, hence the properties such as surface roughness, cracking of a coating or thickness of a coating can be determined.

2.3.3.2 Method

Coated TAc sheets were cut into 10x10 mm pieces and covered with a thin layer of silver using a sputter coater. The samples were analysed using a Cambridge Scanning Electron Microscopy Stereoscan 90.

2.3.4. PENCIL HARDNESS

2.3.5.1 Theory

Determination of the hardness of a protective coating is crucial to ensure its durability towards abrasion and functionality. A hardness is considered as a measure of durability and rigidity of the material, and its resistance to indentation or abrasion. Among the three main types of hardness, i.e. indentation hardness, scratch hardness and rebound hardness, the scratch hardness of a coating is the most important from a practical point of view. The scratch hardness describes the resistance of a sample to a fracture or deformation caused by a friction.[12]

The scratch hardness of a coating or a film can be easily determined by a method known as a pencil hardness test. This rapid, inexpensive technique involves a pencil containing a lead centre being pushed against the film while held firmly at a 45° angle. The process starts with the hardest pencil and continues down the scale of hardness. The first pencil that does not scratch or gauge the film determines scratch hardness.

2.3.5.2 Method

The hardness of PU coatings was performed with a certified Elcometer 501 Pencil Hardness Tester (Figure 2-10), following the ISO 15184:2012 standard. Coated TAc sheets were placed on a firm horizontal surface. The pencil was placed in a pencil hardness test device designed to keep the pencil at a 45° angle. The tester was placed on the surface of the coating and pushed in two parallel 20-50 mm strokes. The process was started with the hardest pencil and continued down the scale of hardness until the pencil did not cause damage of the coating.

Figure 2-10. *Pencil hardness tester set – Elcometer 501.*[13]

2.3.5. CROSS-CUT ADHESION

2.3.6.1 Theory

The adhesion of a coating to a substrate describes the tendency of the two materials to cling to each other. A good coating adhesion depends on chemical and physical properties of both coating and a substrate, e.g. their atomic bonding structure, elastic moduli or thickness.

Adhesion can be split into two factors: basic adhesion and a practical adhesion. The basic adhesion describes all interfacial intermolecular interaction between the two substrates, including chemical bonding, hydrogen bonding or Van der Waals forces. The practical adhesion describes the forces required to disrupt the adhering system. While the basic adhesion cannot be determined, the practical adhesion can be measured using various techniques, e.g. scrape adhesion test, a pull-off test or a cross-cut adhesion test.[14]

The cross-cut adhesion test can be especially useful for determination of a resistance of a coating to separation from a substrate. The test involves a device used to cut through the coating, ensuring the surface gets damaged all the way to the substrate. Subsequently, a tape is placed over the cut and pulled off rapidly. The adhesion might be assessed visually by determination of the extent of coating removal.

This simple and straight-forward technique allows for a rapid and reliable determination of a coatings' practical adhesion.

2.3.6.2 Method

The adhesion of PU coatings was performed with an Elcometer 107 Cross-Hatch Cutter (Figure 2-11) following the ISO 2409:2007 standard. Two cuts at 90˚ to each other were made through the coating. The detached coating was removed with a soft brush, followed by placing of an adhesive tape over the cut and smoothing the surface using the brush. Subsequently, the tape was removed by pulling it off rapidly at 60˚ and delamination of the coating was evaluated under a magnifying glass. Adhesion was assessed on a 0 to 5 scale (0 – 0% flaking, 5 – more than 65% flaking).

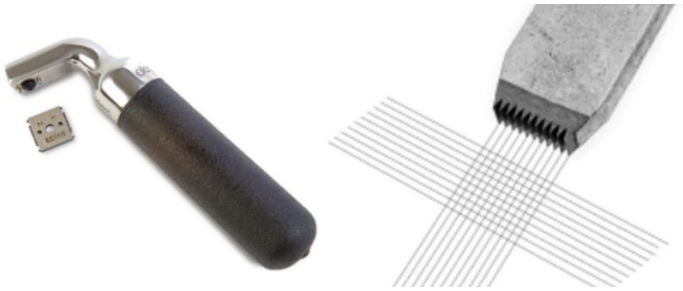

***Figure 2-11**. Elcometer 107 cross-hatch cutter.*[13]

2.3.6. HAZE

2.3.7.1 Theory

Haze is defined as the cloudiness or haziness of a body. Haze, together with transparency, clarity and refractive index, are important factors that influence properties and functionality of transparent, optical materials.

When a beam of light passes through a transparent medium, a number of interactions occur. The interactions include the light being reflected from the surface, refracted within the material and reflected from the other surface, or passing through the material. The light that passes through the material is affected by the refractive index of the material as well as the internal structure of the transparent medium. All irregularities within the material, including contamination, air bubbles, poor particles dispersion or surface damage, can lead to the beam being scattered or diffused in all directions, a process known as a Wide-Angle Scattering. Large irregularities lead to the light getting scattered in a narrow cone shape, known as a Narrow Angle Scattering. The measurement of the scattering and the intensity of the transmitted light allows determination of the medium transparency, haze and clarity. Therefore:

- **Transparency** can be measured by a total transmittance of an object.
- **Transmittance** is the amount of light that passes through an object without being absorbed, scattered or reflected. It can be calculated as the ratio of the incident light and the transmitted light.

- **Haze** is the amount of light that underwent the Wide-Angle Scattering. It determines the transmissive contrast and can be measured as the percentage of the transmittance of light that has deviated by more than 2.5° angle from the incident beam.
- **Clarity** is the amount of light that underwent the Narrow Angle Scattering. It determines the sharpness of the image and can be measured as the percentage of the transmittance of light that has deviated by less than 2.5° angle from the incident beam.

Haze can be rapidly measured using a haze meter, an instrument that also measures total transmittance. A haze meter emits a collimated single beam of light that passes through a sample and gets scattered. The light enters a spherical cell coated with a highly reflective material. At 90° from the entrance port a photodetector is placed. A light trap, placed on the opposite side to the entrance port, absorbs all the light that has not been scattered, absorbed and reflected. When the light trap is closed the total transmittance of the light is measured, while when the light trap is open the portion of light that underwent the Wide-Angle Scattering is measured (Figure 2-12).[15]

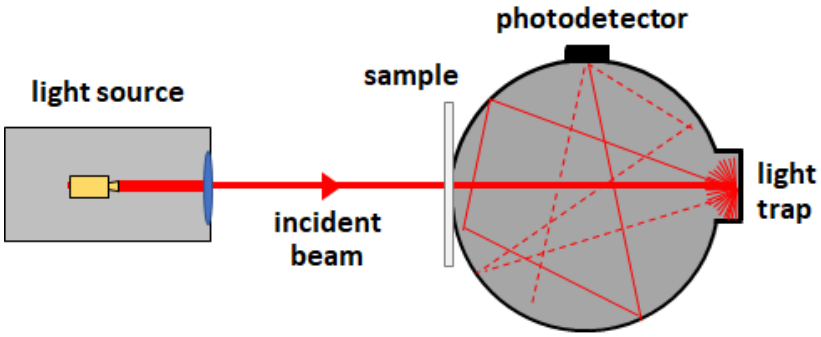

Figure 2-12. *A graph representing a typical set-up of a haze meter. The incident beam passes throughout the sample and the amount of the light is measured* [15]

2.3.7.2 Method

All haze measurements were performed with a BYK Gardner Haze-Guard Dual instrument. The haze was calculated as an average of three measurements, each with a measurement error of ± 0.01. Therefore, all reported haze values carry the standard error of the mean equal to ± 0.02.

2.3.7. SOLVENT RESISTANCE

2.3.8.1 Theory

The chemical resistance of polymers is crucial to determine the life-time of consumer goods. Protective coatings can be exposed to various chemicals which over time might lead to discoloration, softening, swelling, blistering or detachment. For example, protective coating on sunglasses can be easily exposed to water, alcohol, solvents used in sunscreens or hand creams, as well as various cleaning products.

The solubility of polymers depends on their physical and chemical properties. Critical properties that influence the solubility of polymers, and therefore their solvent-resistance, include the polymer's molecular weight, polarity, crosslinking density, hardness, glass transition and melting temperature, crystallinity or permeability. The solubility of polymers can be partially predicted using Hildebrand solubility parameters, describing polarity and the amount of H-bonding in materials, and Hansen solubility parameters, describing the 'volume' of solubility. The parameters can be calculated *via* measurement of polymer's properties, e.g. molecular weight, atomic dispersion forces, molecular dipole-dipole forces or H-bonding.[16]

Among various solvent-resistance measurement techniques, rub test and immersion tests are among the most popular. *Evaluation for Solvent Resistance by Solvent Rub Test* involves rubbing the surface of a film with solvent soaked cheesecloth, usually methyl ethyl ketone, and assessment of solvent-induced damage. *ISO 2812 Paints and varnishes – Determination of resistance to liquids – Part 1: Immersion in liquids other than water* test involves immersion of a material in a solvent for a defined period of time and assessment of the influence of the solvent on the material. Factors such as the amount and size of damage and intensity of alteration are taken into the account.

The rub test allows a quick, relative estimation of solvent resistance of a coating and simulates the possible damage caused by wiping of the surface with a solvent. However, factors like the type of cheesecloth, the stroke distance and rate or the applied pressure significantly influence the results of the test. The immersion test

provides more precise measurement and simulates a possible damage caused by a spillage of a solvent over the coating

2.3.8.2 Method

250-350 mg of samples were immersed in 5 mL of various solvents for 30 minutes. The solvent resistance was assessed by physical changes of the coatings as follows: solvent resistance if no change in appearance, poor solvent resistance if swelling was observed, and no solvent resistance if the coating was dissolved.

2.3.8. CONTACT ANGLE

2.3.9.1 Theory

The angle of the intersection of the solid-liquid interface is widely used to measure the wettability of a solid. Therefore, the contact angle of water deposited on various coatings provides information about polarity and molecular interactions of the coatings. A more detailed description of the technique is presented in Section 2.2.3.1.

2.3.9.2 Method

The contact angle of the coatings was measured at room temperature with a Kruss Drop Shape Analyser DSA25. The Sessile Drop Method was used on a cleaned with water and ethanol coated TAc sheets, with a probe liquid of a deionised water. The results were calculated as an average of five measurements.

2.3.9. WEATHERING OF THE COATINGS

2.3.12.1 Theory

Polymer degradation has been studied since the 1950s. The process of degradation involves various environmental factors, such as light, heat, moisture or chemicals, which trigger a change in the physical and chemical properties of a polymer. The most common processes are thermal, chemical and photoinduced degradation.

Thermal degradation, also known as thermolysis, is induced by heat triggering the breakage of chemical bonds. The process usually gets initiated by an auto-oxidation process involving loss of H atoms and creation of radicals. The radicals, upon reactions

with atmospheric oxygen create peroxy radicals, react further with hydrogen atoms of the polymer backbone chain, propagate formation of new free radicals and create new products. Other possible reactions include depolymerisation, random chain scission, side group elimination or oxidation of the polymer. Thermolysis is often observed in chain-growth polymers, e.g. poly(methyl methacrylate) which degrades to monomers, gases and oils.[17]

The chemical degradation of polymers involves chemical reactions with chemical substances present in the surroundings of the polymer. The most common reactions, e.g. degradation of polyamide by acids, ozonolysis, e.g. decomposition of natural rubber by ozone, oxidation, e.g. oxidation of tertiary carbon atoms in polypropylene, or chlorine-induced cracking of polybutylene.[18]

Photoinduced degradation occurs under the influence of electromagnetic waves, e.g. visible light or UV radiation and is commonly observed in materials exposed to a direct sunlight. Susceptible polymers include polymers with tertiary carbon atoms in their backbone structure, e.g. polyethylene, or aromatic rings, e.g. Kevlar. Commonly observed reactions include photooxidative degradation, leading to breakage of polymer chains and reduced molecular weight of the polymer, e.g. photolysis of polystyrene. [19]

Materials exposed to outdoor conditions often display weathering processes involving combined effects of multiple external factors. Therefore, for practical reasons, estimation of the stability of polymer to various modes of degradation is crucial during development of consumer goods.

Controlled polymer degradation, known as weathering, is a commonly used technique to study the stability of polymers. Natural weathering can be obtained by exposing the samples to the direct sunlight or using accelerators such as amplifying UV radiation mirrors. Artificial weathering involves solar concentrator instruments, allowing the control over temperature, humidity and amount of UV radiation. The temperature of weathering is usually controlled by a Black Standard Temperature (BST) sensors that absorbs at least 90% of radiation received during exposure used to represent the

maximum surface temperature achieved. Carefully optimised conditions allow accelerated exposure tests, stimulating up to 63 years of natural UV exposure in one year.[20]

2.3.12.2 Method

Weathering tests were carried out using an Atlas Suntest XLS+ weatherometer equipped with a daylight filter with a cut-off at 290 nm, following the ASTM D5071-06 standard. The coated TAc sheets were placed in the chamber using a metal frame and exposed to an irradiation intensity of (365 ± 35) W m^{-2}, measured between 290-800 nm, and the BST of (37.5 ± 2.5)°C. The samples were left for 4 weeks under constant UV-vis exposure, comparable to 30 weeks of external weathering, calculated as follows:

$$Weatherometer\ intensity = 365\ W\ m^{-2}$$

$$Intensity\ outside = 1541x\ 10^{6}\ J\ m^{-2} = 1541\ x\ 10^{6}\ W\ s\ m^{-2} = 48.86\ W\ m^{-2}$$

$$Therefore\colon\ \frac{365\ W\ m^{-2}}{48.86\ W\ m^{-2}} = 7.5$$

$$And\colon 4\ weeks\ x\ 7.5 = 30\ weeks$$

The intensity value for outside in Redcar, England, was provided by DuPont Teijin Films. ATR FT-IR spectra of the coatings were taken before and after weathering.

2.3.10. DAMAGE OF COATINGS

2.3.14.1 Theory

To evaluate the self-healing of coatings, a controllable and measurable amount of damage needs to be introduced. Over the years a number of techniques used to determine the scratch resistance of coatings have been developed. These techniques can be also employed to damage coatings prior to evaluation of their self-repair properties.

An automated steel wool test is a widely used technique to introduce damage to a coating. The specially designed scratch instrument consists of (i) a moving arm covered with a standardised grade steel wool and can be loaded with various weights,

(ii) a stand where a sample can be attached to a flat surface and (iii) a control unit allowing adjustment of the number of back-and-forth cycles and velocity. The weight of the load and the grade of the wool determines the extent of damage introduced to the material. The constant load and velocity of the arm provides a control over the repeatability and reproducibility of scratching. The sample that underwent damage does not require any clean-up and is easily accessible to perform any further tests.

2.3.14.2 Method

The PU coatings were damaged using a Lima TRS Automated Steel Wool Instrument. The samples were placed underneath the moving arm and introduction of damage was performed by 40 back-and-forth scratch cycles using 000 grade steel wool and a 500 g load. The initial haze of a coating (iH) was measured before the scratching, while the haze of scratched coatings (sH) was measured immediately after the scratching. The percentage of damage was calculated as a ratio of total damage introduced by scratching, that is the difference between the measured haze values of damaged (sH) and undamaged sample (iH), to the haze of undamaged sample (iH) **(Equation 2.6).**

$$\%Damage = \frac{sH - iH}{iH} \times 100\% \qquad \text{Equation 2.6}$$

2.3.11. SELF-HEALING EVALUATION

2.3.15.1 Theory

Quantitative evaluation of the extent of damage and recovery of coatings can be performed using various techniques, including the measurement of transparency, gloss or haze.

Transparency, the amount of light that passes through an object without being absorbed, scattered or reflected, can be easily measured with a haze meter. Structural defects, such as cracks or scratches can influence the transparency, thus the technique can be employed to monitor the damage and recovery of transparent objects. Gloss, the optical property which indicates how well a surface reflects the

light, is primarily affected by the surface topography. Surfaces that have been scratched exhibit lower gloss value due to decreased light reflection and increased light scattering. Haze, the amount of light that has diffused by more than 2.5°, determines the transmissive contrast of a transparent object. Therefore, the diffusion of the light resulting in the loss of contest, can indicate the level of surface damage.

The transparency, gloss and haze can be easily and rapidly measured and provide a good insight into the level of damage introduced to transparent, protective coatings.

2.3.15.2 Method

The self-healing efficiency was determined by monitoring haze of samples after scratching, measured with a BYK Gardner Haze-Guard Dual instrument.

The measurements of haze of samples healing at 60 °C were performed every 10 minutes for the first 30 minutes, while the measurements of samples healing at room the temperature were performed every 10 minutes for the first 30 minutes, followed by every 30 minutes for the next 150 minutes.

The percentage of recovery was calculated as a ratio of change in haze value during recovery, which is a difference between the haze values of damaged (sH) and recovering (H) sample at time, to a total damage caused by scratching, which is a difference between the haze value of the damaged (sH) and undamaged (iH) sample **(Equation 2.7).**

$$Recovery = \frac{sH - H}{sH - iH} \times 100\% \qquad \text{Equation 2.7}$$

2.4 References

1 D. Dieterich, *Prog. Org. Coatings*, 1981, **9**, 281–340.
2 Q.-A. Li and D.-C. Sun, *J. Appl. Polym. Sci.*, 2007, **150**, 2516–2524.
3 M. J. O'Sickey, *Characterization of Structure-Property Relationships of Poly(urethane-urea)s for Fiber Applications, Doctoral Dissertation*, Virginia Polytechnic Institute and State University, 2002.
4 K.-Y. Law and Z. Zhao, *Surface Wetting - Characterisation, Contact Angle, and Fundamentals*, Springer, Switzerland, 2016.
5 T. R. Crompton, *Analysis of Polymers*, Pergamon Press, Exeter, 1st edn., 1989.
6 I. Yut, A. Bernier and A. Zofka, in *Asphalt Paving Technology: Association of Asphalt Paving Technologists-Proceedings of the Technical Sessions*, 2012, pp. 1–28.
7 R. Brown, *Handbook of Polymer Testing*, Marcel Dekker, Inc., New York, 1st edn., 1999.
8 T. Hasegawa, *Quantitative Infrared Spectroscopy for Understanding of a Condensed Matter*, Springer, Tokyo, 2017.
9 L. A. Averett, P. R. Griffiths and K. Nishikida, *Anal. Chem.*, 2008, **80**, 3045–3049.
10 J. M. G. Cowie, *Polymers: Chemistry and Physics of Modern Materials*, CRC Press, Boca Raton, Florida, 2nd edn., 2000.
11 S. Thomas, R. Thomas, A. K. Zachariah and R. K. Mishra, *Microscopy Methods in Nanomaterials Characterisation*, Elsevier, 1st edn., 2015.
12 K. Sato, *Prog. Org. Coatings*, 1980, **8**, 1–18.
13 Elcometer Ltd., http://www.elcometer.com/, (accessed 19 April 2018).
14 K. L. Mittal, in *Adhesion Measurement of Thin Films, Thick Films, and Bulk Coatings*, American Society for Testing and Materials, Philadelphia, 1976, pp. 5–17.
15 BYK-Gardner GmbH, https://www.byk.com, (accessed 19 April 2018).
16 A. Eckelt, J. Eckelt and B. Wolf, *Solubility of Polymers*, Willey, 1st edn., 2011.
17 M. A. Villetti, J. S. Crespo, M. S. Soldi, A. T. N. Pires, R. Borsali and V. Soldi, *J. Therm. Anal. Calorim.*, 2002, **27**, 295–303.
18 P. Lewis and C. Gagg, *Forensic polymer engineering: why polymer products fail in service*, Woodhead Publishing Limited, Cambridge, 1st edn., 2010.
19 E. Yousif and R. Haddad, *Springerplus*, 2013, **2**, 1–32.
20 J. DeVries, *Paint Coatings Ind.*, 2006, 22, 54–58.

3. THE INFLUENCE OF POLYOL ON MORPHOLOGY AND SELF-HEALING PROPERTIES

Segmented polyurethanes (PU) can be considered as block copolymers, consisting of soft segments (SS) composed of oligomer polyols and hard segments (HS) composed of isocyanate and chain extenders.[1] In a typical PU the amount of SS varies between 40% and 80%, thus the chemistry and length of the SS will have a large influence on the morphology and properties of the created materials.[2]

In general, oligomer polyols have low glass transition temperatures in the range of -120 °C to -30 °C, therefore they are in the rubbery form at ambient temperatures.[3] Since the content and the length of HS (χN), as well as the immiscibility of HS and SS triggers phase-separation of the two segments, the length and the chemical structure of polyols plays an important role in the properties of the resulting polymers. There is a wide range of polyols that can be used as SS building blocks, allowing to obtain materials with desired properties. Polyester diols, for example polycaprolactone (PCL), are commonly used, as they offer excellent mechanical properties and allow creation of biodegradable materials due to their ability to undergo hydrolysis. Polyether diols, for example polyethylene glycol, are often used to improve flexibility, hydrophilicity and hydrolytic stability of PU.[2] Polycarbonate diols impart high water, solvent and oil resistance, improved ageing, as well as high mechanical strength and heat resistance.[4,5] Aliphatic oligomers offer high UV stability and durability. However, aliphatic polyesters and polyethers are known to induce higher degrees of phase separation than polycarbonates.[6] Aromatic oligomers possess excellent physical and mechanical properties; however, they also exhibit low degradability and yellowing.[7]

The length of the oligomeric polyol also plays an important role and influences the morphology and properties of polyurethanes. An increase of the SS length was found to lead to increased phase-separation, order and crystallinity of HS and overall stiffness.[8,9] Therefore, in this chapter the influence of the length and the chemistry of oligomer polyols on the morphology and self-healing behaviour of PU coatings will be investigated.

3.1. SYNTHESIS INFORMATION

In the first set of formulations the composition of soft segments was varied by use of seven different polyols of various length and chemical structure, and the influence of the SS building blocks on the morphology and the self-healing properties of polyurethane coatings was examined. The formulations were prepared using two diisocyanates, HDI and IPDI, and two chain extenders, BD and EG. Structures of the polyols are shown in **Figure 3-1** and their description can be found in **Table 3-1**.

Table 3-1. *List of polyols used.*

Polyol	Polyurethane	MW (g mol^{-1})
D1700	polydiethylene adipate glycol	2550
D670	branched hydroxyl bearing polyester	750
PCL2000	polycaprolactone	2000
PCL1000	polycaprolactone	1000
PH50	polycarbonate	500
PH200	polycarbonate	2000
PH300	polycarbonate	3000

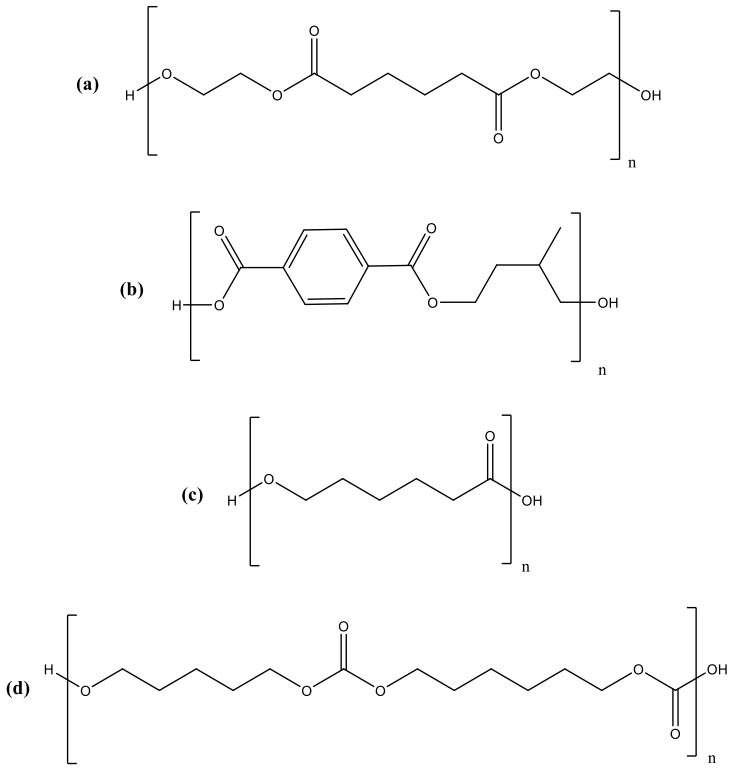

Figure 3-1. *Structure of polyols: (a) D1700, (b) example structure of a polyester similar to D670, (c) polycaprolactone and (d) PH polycarbonates.*

Formulation B1 was prepared as a solvent-borne coating in anhydrous *n*-butyl acetate, as described in Section 2.2.3. Formulation B2 was prepared using a dual cartridge, as described in Section 2.2.4. The remaining formulations were prepared using the acetone process, using DMPA (25mol% of the total number of moles of CE) and a CE (75mol% of the total number of moles of CE), as described in Section 2.2.5.

Octamethyltetrasiloxane-1,7-diol (1,7-SD), used as a CE in formulation B5, was prepared by hydrolysis of the corresponding siloxane dichloride (1,7-DCOMTS) in an ice-cold mixture of pH 7 buffered water and diethyl ether, and purified by distillation (**Figure 3-2**).

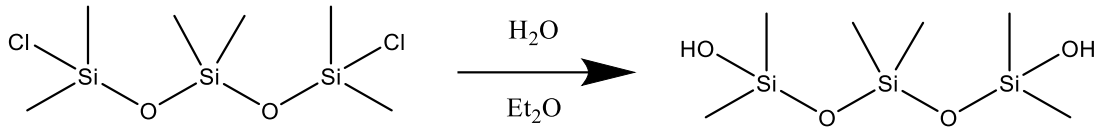

***Figure 3-2**. Synthesis scheme of 1,7-SD from 1,7-DCOMTS.*

All coatings were prepared using a wire round Mayer rod, as described in Section 2.2.7. A detailed description of the structure of the eight formulations is presented in **Table 3-2**.

***Table 3-2.** Structure and details of formulations prepared.*

Code	Polyol	Isocyanate	Chain extender	NCO:OH (mole ratio, before CE)	NCO:OH (mol ratio, total)	Synthesis method
B1	D1700	HDI	1,2-EG	3:1	1.2:1	solvent-borne
B2	D670	HDI	1,2-EG	3:1	1.2:1	dual cartridge
B3	PCL2000	HDI	1,4-BD	3.5:1	1:1	waterborne
B4	PCL1000	HDI	1,4-BD	2:1	1:1	waterborne
B5	PCL1000	HDI	1,7-SD	2:1	1:1	waterborne
B6	PCL1000	IPDI	1,4-BD	2:1	1:1	waterborne
B7	PH50	HDI	1,4-BD	2:1	1:1	waterborne
B8	PH50	IPDI	1,4-BD	2:1	1:1	waterborne
B9	PH200	IPDI	1,2-EG	2:1	1:1	waterborne
B10	PH300	IPDI	1,2-EG	2:1	1:1	waterborne

The progress of reactions was monitored using ATR FT-IR. An example of the 2500-2000 cm^{-1} region of the spectra obtained during the synthesis of formulation B1 is presented in **Figure 3-3**.

In the first step of the reaction, occurring between the polyol and diisocyanate, a rapid disappearance of the isocyanate peak at 2260 cm^{-1} can be observed. After 90 minutes the reduction of the size of the peak stops due to consumption of all hydroxyl groups of the polyol. After the addition of the chain extender a further decrease of the amount of isocyanate can be seen. A complete disappearance of the peak was observed after 5320 minutes, upon the completion of the reaction.

While the reaction monitored by ATR FT-IR, presented in **Figure 3-3**, was carried out in *n*-butyl acetate and took nearly 90 hours to complete, all remaining formulations were prepared in acetone as a part of waterborne PU dispersion synthesis and showed a complete consumption of the isocyanate groups within 24-48 hours.

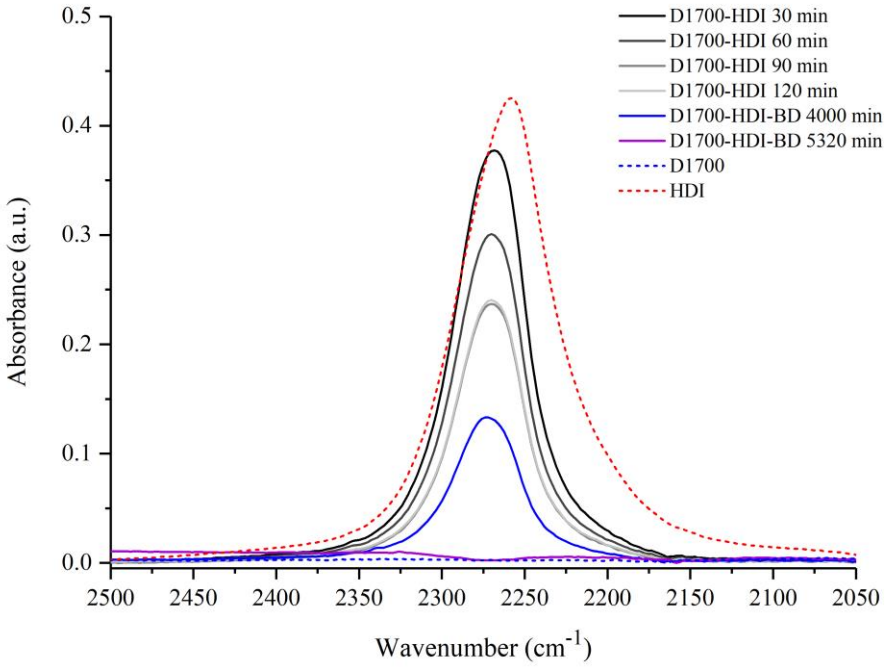

Figure 3-3. *Changes in the intensity of NCO peak during the reaction, monitored by ATR FT-IR. The intensity of the NCO peak decreases during the first 90 minutes of the reaction between the polyol and the isocyanate. Upon exhaustion of available hydroxyl groups, confirmed by the measurement taken at 120 minutes, the chain extender (BD) is added and the reaction is continued until the complete disappearance of the NCO peak (5320 min).*

3.2. CHARACTERISATION OF COATINGS

The percentage of HS within the first set of formulation varied significantly and was influenced mainly by the MW of the polyol (**Table 3-3**). Formulations prepared with long polyols: B1 (MW of polyol 2550 g mol^{-1}), B3 (MW of polyol 2000 g mol^{-1}), B9 (MW of polyol 2000 g mol^{-1}) and B10 (MW of polyol 3000 g mol^{-1}) contained 19.8%, 29.0%, 29.3% and 21.6% of HS respectively. Formulations prepared with average length polyol PCL1000 were found to contain 31.0-35.8% of HS, while formulations prepared with short polyols D670 and PH50 contained 34.4-52.2% of HS.

Coatings B1, B3, B9 and B10, prepared with polyols with MW over 2000 g mol^{-1}, were found to be very soft, exhibiting pencil hardness of 6B or 3B, which is linked to the low percentage of HS responsible for the hardness of materials.[8] Coatings prepared with shorter polyols, and therefore containing more HS increasing the amount of H-bonds, were harder, with pencil hardness varying between 2B and HB.[10]

The high haze of coatings B1 and B3, prepared with long polyols, was found to be linked to the high crystallinity of SS and phase-separation of the systems.[11] Replacement of the long chain polyols with short chain polyols, as well as the use of bulky and non-symmetrical IPDI, was found to reduce the haze to levels below 3%. Interestingly, coating B5 prepared with siloxane CE showed a high haze of almost 35%, indicative of the large influence of polar siloxane CE on phase-separation of the system, as shown by Chuang *et al*.[12] Formulation B7 showed the highest haze reaching almost 70%, also linked to the high crystallinity and phase-separation (discussed in detail in Section 3.2.2).

***Table 3-3**. Characterisation of coatings B1-B10.*

Code	Polyurethane	Hard Segments (%)	Pencil Hardness	Haze (%)
B1	D1700-HDI-1,2-EG	19.8	6B	22.3
B2	D670-HDI-1,2-EG	34.4	HB	1.1
B3	PCL2000-HDI-1,4-BD	29.0	6B	22.1
B4	PCL1000-HDI-1,4-BD	31.0	HB	3.0
B5	PCL1000-HDI-1,7-SD	35.9	B	34.8
B6	PCL1000-IPDI-1,4-BD	35.8	2B	0.8
B7	PH50-HDI-1,4-BD	46.7	2B	69.0
B8	PH50-IPDI-1,4-BD	52.2	B	0.4
B9	PH200-IPDI-1,4-BD	29.3	3B	1.4
B10	PH300-IPDI-1,4-BD	21.6	3B	0.8

3.3. CHARACTERISATION OF COATINGS' MORPHOLOGIES

ATR FT-IR spectra of the first two polyols, D1700 and D670, and corresponding coatings B1 and B2 are presented in **Figure 3-4**. The spectra of polyols show the main peaks: OH stretch at 3550 cm^{-1}, asymmetric stretch of alkane CH at 2950 cm^{-1} and symmetric stretch at 2870 cm^{-1}, carbonyl stretches at 1730 cm^{-1} (D1700) and 1720 cm^{-1} (D670), and several CH signals below 1500 cm^{-1}. Moreover, the D670 polyol of unknown structure also showed peaks associated with the presence of aromatic ring at 1615 cm^{-1} (aromatic C-C stretching) and 725 cm^{-1} (aromatic CH bending). Important absorption wavenumber regions are shown in **Table 3-4**.[13,14]

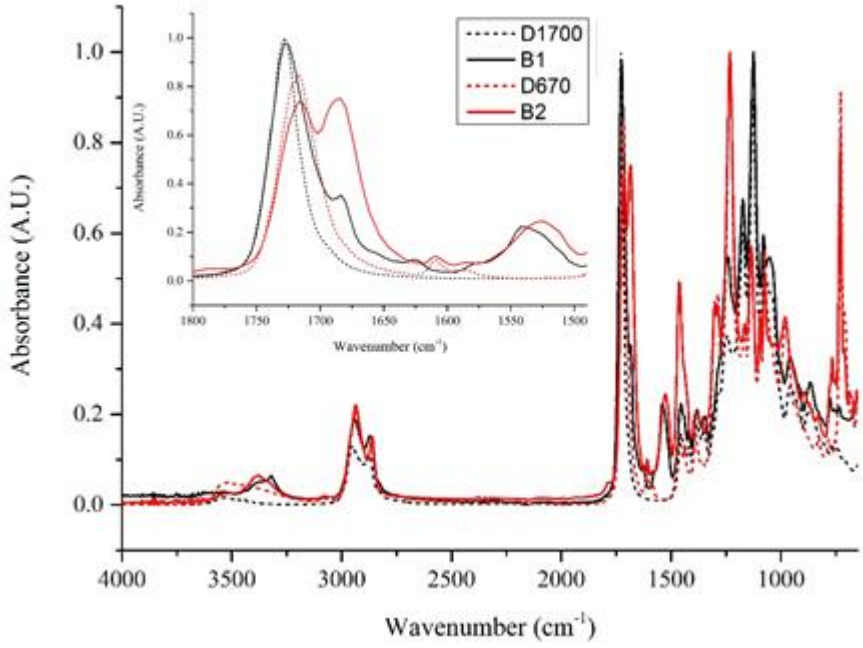

Figure 3-4. *ATR FT-IR spectra of polyols D1700 and D670, and coatings B1 and B2.*

Comparison of the spectra of polyols, acting as building blocks of SS within the formulations, and the corresponding spectra of the coatings, shows significant changes in the spectra profile, found mainly in the amine and carbonyl stretch regions. The OH stretch at 3550 cm^{-1} present in the spectra of polyols is not present in the spectra of the coatings due to the consumption of hydroxyl groups during the reaction. However, new peaks appear at 3380 cm^{-1} and 3320 cm^{-1}, associated with H-bonded urethane and H-bonded monodentate urea NH stretch respectively.[15,16]

The peaks originating from the carbonate groups of polyols can be observed at the same wavelengths in the spectra of the two coatings. Additionally, some carbonyl stretch peaks of newly formed urea and urethane groups can be seen in the 1700-1600 cm^{-1} region. In the spectrum of coating B1 a shoulder peak at 1700 cm^{-1} can be associated with H-bonded urethane CO stretch, while the peaks at 1670 cm^{-1}, 1625 cm^{-1} and at 1540 cm^{-1} indicate the presence of H-bonded monodentate and bidentate urea.[17] The spectrum of coating B2 shows two large peaks at 1670 cm^{-1} and 1525 cm^{-1} associated with the presence of mainly H-bonded monodentate urea, caused by the moisture cure process resulting in formation of urea groups.[18]

Table 3-4. *The ATR FT-IR absorption regions.*[13,14]
$\bar{\upsilon}$ – stretching, δ – bending, ω – wagging, a – asymmetric, s - symmetric

Wavenumber (cm^{-1})	Functional group	Group assignment
3550-3200	$\bar{\upsilon}$(OH)	Polyol
3500-2250	$\bar{\upsilon}$(OH)	Carboxylic acid
3500-3400	$\bar{\upsilon}$(NH) free	Urethane/Urea
3400-3300	$\bar{\upsilon}$(NH) bonded	Urethane
3340-3320	$\bar{\upsilon}$(NH) bonded, bidentate	Urea
3240	$\bar{\upsilon}$(NH) bonded, monodentate	Urea
2940	$\bar{\upsilon}_a(CH_2)$	CH_2
2860-2790	$\bar{\upsilon}_s(CH_2)$	CH_2
1745-1730	$\bar{\upsilon}$(C=O)	Polyol
1733-1730	$\bar{\upsilon}$(C=O) free	Urethane
1723-1680	$\bar{\upsilon}$(C=O) bonded	Urethane
1700-1680	$\bar{\upsilon}$(C=O) free	Urea
1680-1635	$\bar{\upsilon}$(C=O) bonded, monodentate	Urea
1616-1627	$\bar{\upsilon}$(C=O) bonded, bidentate	Urea
1615	$\bar{\upsilon}$(C=C) aromatic	Aromatic
1580-1576	$\bar{\upsilon}$(CN) + δ(NH) bonded, bidentate	Urea
1570-1540	$\bar{\upsilon}$(CN) + δ(NH) bonded, monodentate	Urea
1539-1510	$\bar{\upsilon}$(CN) + δ(NH) bonded	Urethane
1450	δ_a(CH)	CH_3
1370	ω(CH)	CH_2
1365	δ_s(CH)	CH_3
1240	$\bar{\upsilon}$(CN) + δ(NH)	Urethane/urea
1100	$\bar{\upsilon}$(C-O-C)	Ether
725	δ_a(CH) aromatic	Aromatic

The DSC heat-cool-reheat cycle of the first polyol, D1700, and sample B1 prepared with this polyol, are presented in **Figure 3-5**. The polyol showed a glass transition at -51 °C in both heating cycles. Moreover, a broad melting endotherm can be seen in the first heat cycle at 74 °C with the enthalpy of 7.5 J g^{-1}, indicative of a semi-crystalline morphology of the polyol. The melting endotherm is not present in the second cycle, suggesting that crystallinity within the polyol develops slowly.

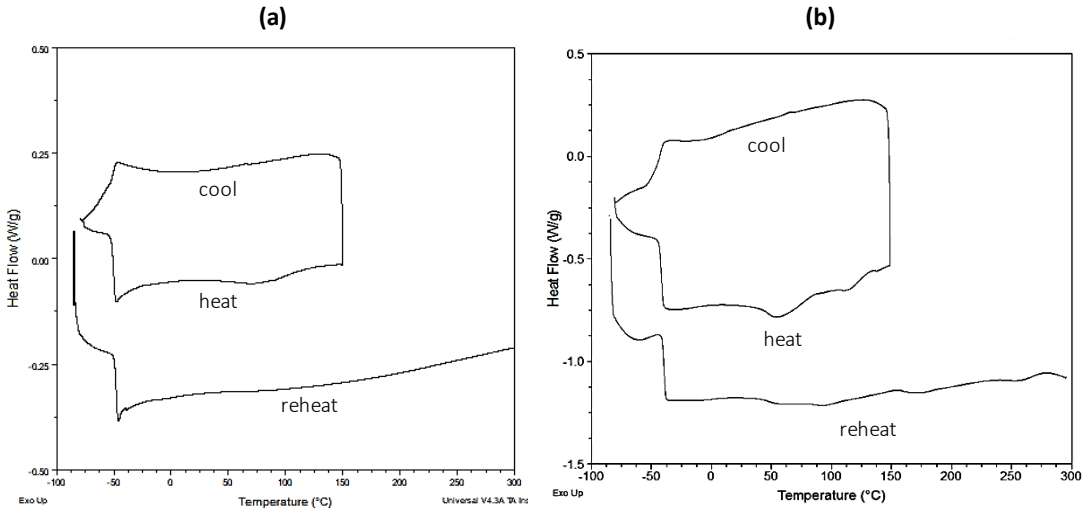

Figure 3-5. *DSC heat-cool-reheat cycles of (a) polyols D1700 and (b) formulation B1.*

The DSC analysis of the coatings showed important changes in the curves, indicative of the polymers' morphologies.

Sample B1 showed a shift in the glass transition of the amorphous regions of SS from -51 °C to -42 °C in the first heat cycle, and to -40 °C in the second heat cycle (**Figure 3-5b**). The change in the T_g occurs due to two factors. First, when the polyols react with isocyanates, the chemistry of their end groups changes, and they become chemically bonded with the HS. The newly created urethane groups exhibit high polarity and can interact with other urethane groups, therefore a restriction of the mobility of the polyol can be observed.[3] Second, some small amounts of HS present within the polyurethane matrix can get trapped within SS regions.[19] Therefore, the SS get contaminated with the dissolved HS, creating a so-called 'soft segment rich' phase, and the presence of HS causes a shit of the phase transition to higher temperatures.[20] The two factors have a large influence on the T_g and the effect increases with the decrease of the molecular weight of the polyol.[3] Sample B1,

prepared with the polyol D1700, with a large molecular weight of 2550 g mol^{-1}, is composed of 80% SS. Therefore, the shift of T_g in both heat cycles can be attributed to the presence of a small amount of HS dispersed within the SS-rich region, due to a small amount of phase-mixing, and in a lesser extent to the change of the chemistry of the polyol end groups. The small shift indicates almost fully phase-separated morphology of the system, expected for a PU prepared with a long polyol, and thus small HS content (χN).[9] The glass transition of HS is not visible in the DSC curves, due to mainly crystalline structure of the HS and their low percentage of the HS within the polymer matrix.

Formulation B1 also showed multiple melting endotherms, commonly observed in phase-separated PU.[21] Three endotherms are generally observed. A low temperature endotherm, typically occurring below 60 °C, is usually assigned to the melting of SS in the case of polyols with a tendency to crystallise, or to a short-range reorganisation of the HS dispersed within SS-rich phases.[19,21] The second endotherm is usually assigned to a breakup of a short-range ordering of HS.[19] The third endotherm, occurring usually above 200 °C, corresponds to the melting of HS with long-range ordering. The crystalline HS are also known to show multiple endotherms in systems with a large percentage of HS, due to different crystal structures and segment sizes, as well as melting endotherms associated with microphase mixing of SS and HS.[8]

The first endotherm, present at 55 °C in the first heat cycle can be therefore assigned to the melting of SS. The depression of the endotherm comparing to the melting temperature of pure polyol (74 °C) occurs due to the presence of HS within the SS-rich phase, acting as impurities and decreasing the melting point.[15] The enthalpy of the SS endotherm was found to be 5.8 J g^{-1}. As 80.2 wt% of the formulation consists of SS, the recorded enthalpy expressed in 'Joules per gram of polymer' can be recalculated to 'Joules per gram of polyol', using Equation 3.1:

$$\Delta H_{mSS} = \frac{\Delta H_m \text{ x } 100\%}{\%SS} \qquad \textbf{Equation 3.1}$$

where ΔH_{mSS} is the enthalpy of melting of SS, ΔH_m is the enthalpy of melting of the PU, and $\%SS$ is the percentage of SS.

The equivalent value allows comparison of enthalpies and reflects the changes in the crystallinity of the polyol and the SS block. Therefore, the enthalpy of 5.8 J g^{-1} of the polymer provides the equivalent of 7.2 J g^{-1} of the polyol creating SS blocks. The small decrease of the value (compared against 7.5 J g^{-1} of pure polyol D1700) can be attributed to the HS 'impurities' contaminating the SS-rich phase.[20] Unlike the pure polyol, formulation B1 also shows the endotherms in a second cycle at 58 °C, which can be associated with the change of the chemistry of the end groups of polyol facilitating the recrystallisation process.[3] However, the enthalpy of melting is significantly lower than in the first cycle, 1.4 J g^{-1} (the equivalent of 1.7 J g^{-1}).

The second endotherm, present at 115 °C in the first heat cycle and at 92 °C in the second, can be assigned to a short-range reorganisation of the crystalline HS. The increase of the enthalpy of the process from 1.1 J g^{-1} in the first heat cycle to 5.7 J g^{-1} in the second can be related to a thermally induced reorganisation of HS and SS and increased phase-separation of the system.[21] In the second heat cycle two additional endotherms can be seen at 178 °C and 257 °C with the combined enthalpy of 2.8 J g^{-1}, associated with the crystalline regions of HS. The presence of multiple melts indicates polymorphism of the crystalline regions of HS, influenced by the presence of urethane and urea groups creating different crystalline regions.

The DSC heat cycle of the second polyol, D670, and sample B2 prepared with this polyol, are presented in **Figure 3-6**. The polyol showed a glass transition at -31 °C in both heating cycles. Moreover, a broad melting endotherm can be seen in the first heat cycle at 91 °C with the enthalpy of 11.7 J g^{-1}, indicative of a semi-crystalline morphology of the polyol. The endotherm is not present in the second cycle, suggesting that crystallinity within the polyol develops slowly.

Sample B2, prepared with a polyol D670 with a molecular weight of 750 g mol^{-1}, showed a large shift of the glass transition of the amorphous SS regions (**Figure 3-6b**). The shift of the temperature from -31 °C to 13 °C in the first heat cycle and to 16 °C

in the second is consistent with the lower MW of the polyol and therefore a larger percentage of HS interacting with SS-rich segments.[3] The shift of T_g by 44 °C indicates a significantly larger amount of phase-mixing within the system and reflects an increase of the interactions between the high amount of HS (χN) and the low molecular weight polyol. The glass transition of HS is not observed in the graph due to the dominantly crystalline structure of the HS.

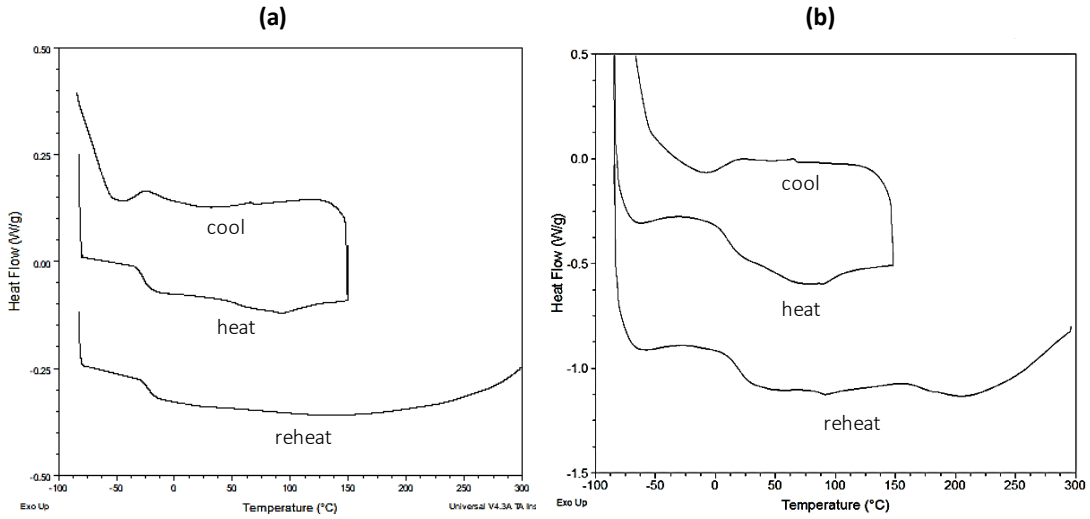

***Figure 3-6**. DSC heat-cool-reheat cycles of (a) polyols D670 and (b) formulation B2.*

The first broad endotherm, present in the first heat cycle of sample B2 at 77 °C, can be associated with melting of SS-rich phases. The depression of the endotherm comparing to the melting temperature of pure polyol (91 °C) occurs due to the presence of HS within the SS-rich phase, acting as impurities and causing the depression of the melting point.[15] The enthalpy of the SS endotherm was found to be 13.0 J g^{-1}, giving the equivalent of 19.8 J g^{-1} of SS. The increase of the enthalpy (11.7 J g^{-1} for polyol D670) reflects the effect of the change of chemistry of the end groups in the short polyol, restricting mobility of SS and facilitating crystallisation process.[3] The width of the endotherm suggest the presence of crystals of various size and different degrees of perfection.[22] In the second heat cycle the endotherm at 92 °C is significantly smaller than in the first cycle, showing the enthalpy of 1.1 J g^{-1} (the equivalent of 1.7 J g^{-1} of SS). The lower enthalpy value suggests that, similar to the pure polyol, crystallinity within the SS develops slowly over time, while the increased

temperature of melting can be explained by thermally induced reorganisation of HS and SS.[8]

The second endotherm, present in the second heat cycle at 219 °C with the enthalpy of 36.4 J g^{-1}, can be associated with melting of the crystalline regions of HS. The high enthalpy of melting confirms predominant formation of strongly bonding urea groups, expected for a moisture-cured coating. The breadth of the melting peak indicates the presence of strongly bonded crystals of various size and different degrees of perfection.[22] The broad distribution of crystal sizes can be related to the presence of large amount of urea groups within HS, able to create both monodentate and bidentate interactions, as well as the presence of aromatic groups within the SS, capable to interact with other SS and partially disturb the crystallinity of the HS.

ATR FT-IR spectra of the third polyol, long polycaprolactone PCL2000, and the corresponding coating B3, are presented in **Figure 3-7**. The spectra of the polyols show the main peaks: OH stretch at 3550 cm^{-1}, alkane CH stretches at 2950 cm^{-1} and 2870 cm^{-1}, carbonyl stretches of ester groups at 1730 cm^{-1}, and several CH signals below 1500 cm^{-1}.[13]

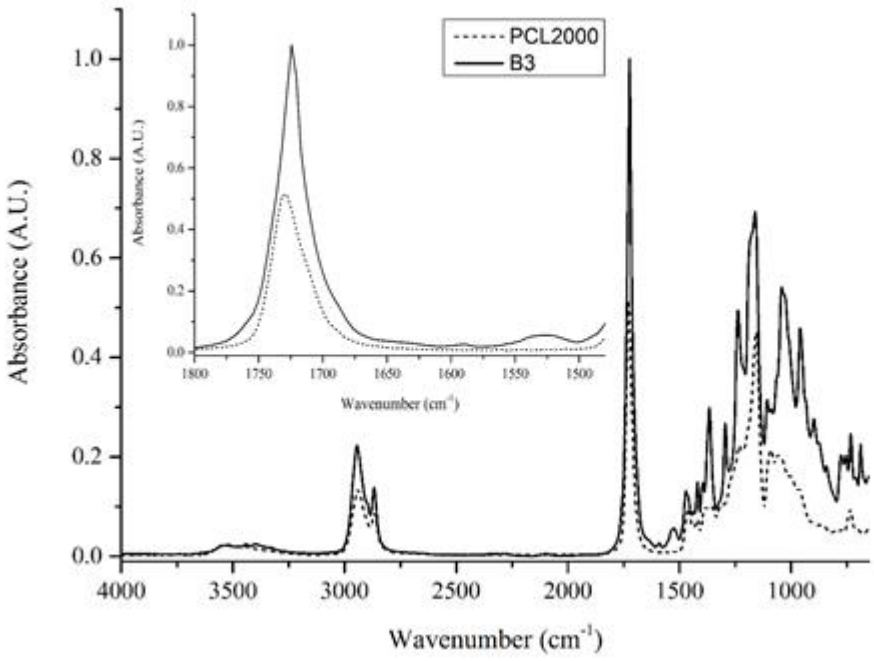

Figure 3-7. *ATR FT-IR spectra of polyol PCL2000 and coatings B3.*

In the spectrum of coating B3, a new peak, NH stretch at 3380 cm^{-1} can be seen, associated with H-bonded urethane and urea groups. Moreover, the peak at 3350 cm^{-1} indicates presence of non H-bonded urethane and urea groups. The presence of the newly formed groups can be also seen in the carbonyl region of the spectra. The peak originating from PCL2000 can be observed at 1720 cm^{-1} as a shoulder peak of the large H-bonded urethane stretch peak at 1720 cm^{-1}. Another shoulder peak at 1680 cm^{-1} can be observed, associated with H-bonded monodentate urea groups, as well as a small peak at 1625 cm^{-1} associated with H-bonded bidentate urea groups.[17] Additionally, a peak at 1525 cm^{-1} can be seen, a C-N stretch and NH bend of H-bonded monodentate urea and urethane.[18] The peaks related to the urea groups are significantly smaller than in the spectra of formulations B1 and B2, indicating the smaller amount of urea groups.

The glass transition of the long polycaprolactone diol, PCL2000, was found at -64 °C (**Figure 3-8a**). The transition is not well defined, suggesting only a small amount of amorphous segments. The crystalline regions of the polyol were found to be polymorphous, indicated by the presence of two melting peaks in the first heat cycle: a smaller one at 31 °C with the enthalpy of 16.1 J g^{-1} and a larger one at 53 °C with the enthalpy of 79.8 J g^{-1}. The large recrystallisation peak observed in the cooling cycle at 10 °C shows the tendency of the polyol to easily crystallize. The two melts at 34 °C and 41 °C found in the second heat cycle were found to have similar size and the overall enthalpy of 83.7 J g^{-1}, showing almost complete restoration of crystallinity during the cooling cycle. The high crystallinity of PCL is well known and established in the literature, and related to the regularity of the molecule and strong intermolecular interaction.[23]

The coating prepared with PCL2000, B3, showed a small shift of the glass transition of the amorphous SS regions from -63 °C to -49 °C, caused by the presence of HS within SS-rich blocks (**Figure 3-8b**).[19] However, the shift of the T_g is relatively small, indicating a large extent of phase-separation within the formulation, expected for a formulation prepared with a small amount of HS (χN). Two melting peaks, associated with the polymorphous crystalline SS blocks, can be seen at 34 °C and 44 °C in the

first heat cycle, with the combined enthalpy of 32.9 J g^{-1} (the equivalent of 46.3 J g^{-1} of polyol), reflecting the influence of 'HS impurities' present within SS-rich blocks and lowering the melting temperature and the enthalpy.[9]

Moreover, similar to a pure PCL2000, an exothermic recrystallisation peak at 0 °C in the cooling cycle and one melting peak at 39 °C with the enthalpy of 25.7 J g^{-1} (the equivalent of 36.2 J g^{-1} of polyol) in the second heat cycle can be observed. Another two melting peaks at 115 °C and 143 °C in the first heat cycle and at 143 °C and 159 °C in the second heat cycle, as well as recrystallisation at 76 °C and 118 °C, can be associated with polymorphous crystalline HS blocks and their interactions with SS. The first endotherm can be assigned to melting of a crystalline HS blocks, while the second to the microphase mixing of the SS and HS. Comparing formulation B3 with B1 and B2, it appears that the melting of HS occurs at significantly lower temperatures. That can be explained by the effect of a low amount of urea groups, a lower percentage of HS content as well as the crystalline nature of SS able to restrain small fragments of HS and prevent their growth. No glass transition of the crystalline regions of HS was found, indicating a mainly crystalline morphology of HS.

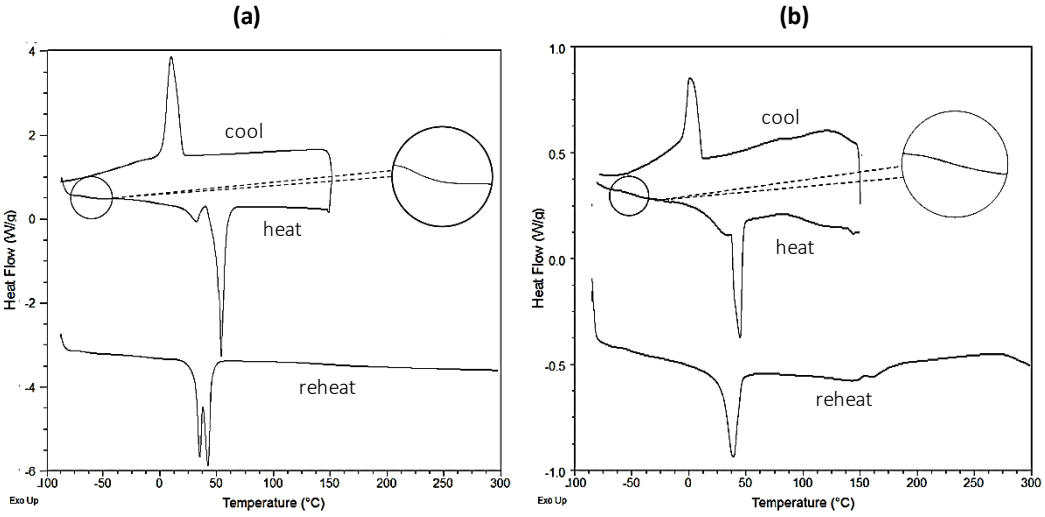

Figure 3-8. *DSC heat-cool-heat cycle of (a) polyol PCL2000 and (b) formulation B3.*

ATR FT-IR spectra of the fourth polyol, the shorter polycaprolactone, PCL1000, and the three coatings prepared with this polyol, B4, B5 and B6, are presented in **Figure 3-9**. The spectrum of the polyol shows similar peaks to the spectrum of PCL2000: OH

stretch at 3550 cm^{-1}, alkane CH stretches at 2950 cm^{-1} and 2870 cm^{-1}, ester carbonyl stretch at 1730 cm^{-1} and several CH signals below 1500 cm^{-1}.[13]

In the spectra of the three coatings the OH stretch peak at 3550 cm^{-1} is not present due to consumption of the hydroxyl groups. A new peak formed in the 3380-3320 cm^{-1} region can be associated with an NH stretch of H-bonded urethane groups. Interestingly, the NH stretch peak of coating B4 at 3325 cm^{-1} is narrower and sharper than the broader NH stretch peak of coatings B5 and B6 at 3380 cm^{-1}, indicating a more phase-separated morphology of the coating B4.[16] The broad peak between 3500 cm^{-1} and 2250 cm^{-1} was assigned to carboxylic acid of DMPA. In the carbonyl region of the spectra the carbonyl peak of polyol can be seen at the same wavenumbers as in the spectrum of pure PCL1000. Additionally, several H-bonded urethane peaks appear at 1715 cm^{-1} and 1690 cm^{-1}. A small amount of H-bonded monodentate urea groups can be indicated by the peak at 1660 cm^{-1}. Moreover, coating B5 shows peaks associated with H-bonded bidentate urea groups at 1625 cm^{-1}. In the C-N stretch and NH bend region, peaks associated with urethane groups can be seen at 1530 cm^{-1}, and in the spectrum of B5 at 1575 cm^{-1}, associated with H-bonded bidentate urea groups.[17]

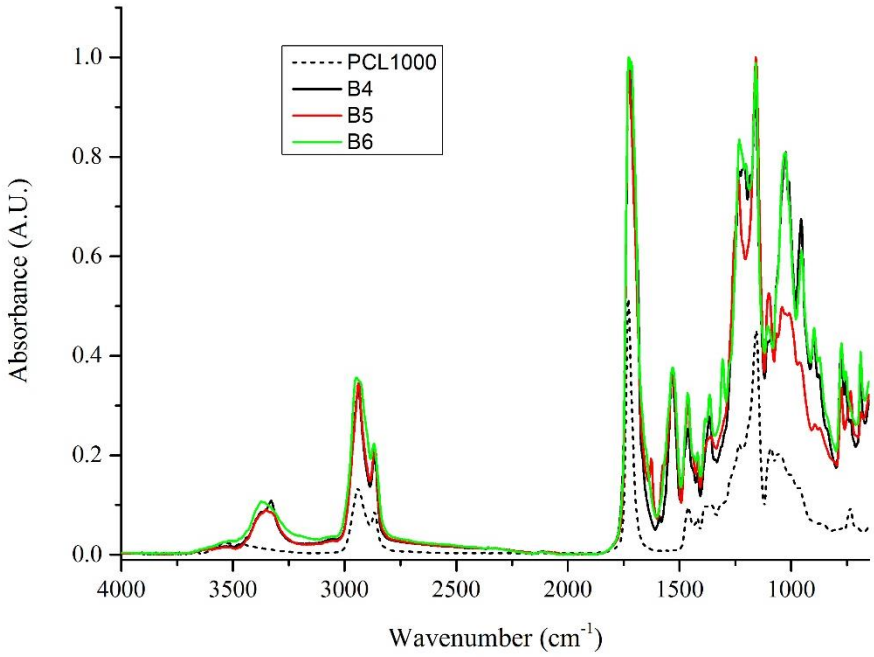

Figure 3-9. *ATR FT-IR spectra of polyol PCL1000 and coatings B4, B5 and B6.*

In the DSC analysis the polyol PCL1000 showed a glass transition at -31 °C in the first heat cycle, and -25 °C in the second (**Figure 3-10a**). The transition is broader and defined somewhat better than in the trace for PCL2000, and occurs 30 °C higher, which is expected with the decrease of the PCL length, resulting in restricted mobility of the oligomer chains.[9] Similar to PCL2000, two melts can be seen in the first heat cycles, but they appear at lower temperatures due to the shorter chain length of PCL1000 creating smaller crystallites. The two peaks, a smaller one at 10 °C and a larger one at 22 °C have the combined enthalpy of 53.6 J g^{-1}. The recrystallisation peak at -20 °C in the cooling cycle and the presence of two melting peaks at 10 °C and 23 °C in the second heat cycle with the combined enthalpy of 54.0 J g^{-1} indicate polymorphism of the crystallites and the tendency of the polyol to crystallize.[23]

The DSC curves of samples prepared with PCL1000 were found to have very similar profiles (**Figure 3-10 b-d**). Samples B4 and B5, prepared with 1,4-BD and 1,7-SD respectively, showed a small decrease of T_g of the amorphous regions of SS, by approximately 5 °C, possibly due to formation of hydrogen bonding between the carbonyl groups in PCL and the urethane groups, known as the antiplasticisation effect and commonly observed in PCL based systems.[24] The low T_g indicates a large extent of phase-separation of the systems. Sample B5, in which HDI was replaced with IPDI, showed a small increase of T_g by approximately 5 °C. The influence of asymmetrical isocyanates on phase-mixing is well established in the literature. They are reported to reduce phase-separation and hinder development of crystallinity due to their bulky and asymmetric structure.[5] However, the influence of IPDI on formulation B6 was found to be small, due to the large amount of crystalline and strongly phase-separation promoting nature of the PCL, as well as the crystallinity promoting nature of 1,4-butanediol.[25]

All samples showed one endotherm in the first heat cycle, which can be associated with melting of the crystalline regions of SS, at 54 °C for sample B4 with the enthalpy of 32.9 J g^{-1} (the equivalent of 47.7 J g^{-1} of polyol), at 56 °C for sample B4 with the enthalpy of 7.4 J g^{-1} (the equivalent of 11.5 J g^{-1} of polyol), and at 78 °C for sample B6 with the enthalpy of 5.8 J g^{-1} (the equivalent of 9.0 J g^{-1} of polyol). The increase of the

melting temperatures and the decrease of the melting enthalpy (53.6 J g^{-1} for PCL1000) can be related to the change of the chemistry of the end groups in the polyol upon formation of urethane.[3] In the second heat cycle only sample B5 showed a broad melting peak associated with SS, present at 99 °C (44 °C - 150 °C), with the high enthalpy of 10.7 J g^{-1} (the equivalent of 16.7 J g^{-1} of polyol), reflective of the influence of the polar siloxane CE reinforcing the SS-rich blocks.[12]

The three samples also showed an onset on the melting endotherm of the HS at temperatures near 300 °C. The increase of the melting temperature comparing to formulations prepared with PCL2000 can be related to the larger percentage of HS present within the matrix being able to form large crystallites with a long-range ordering. The glass transition of the amorphous regions of HS is not observed in the curves due to high crystallinity of the HS.

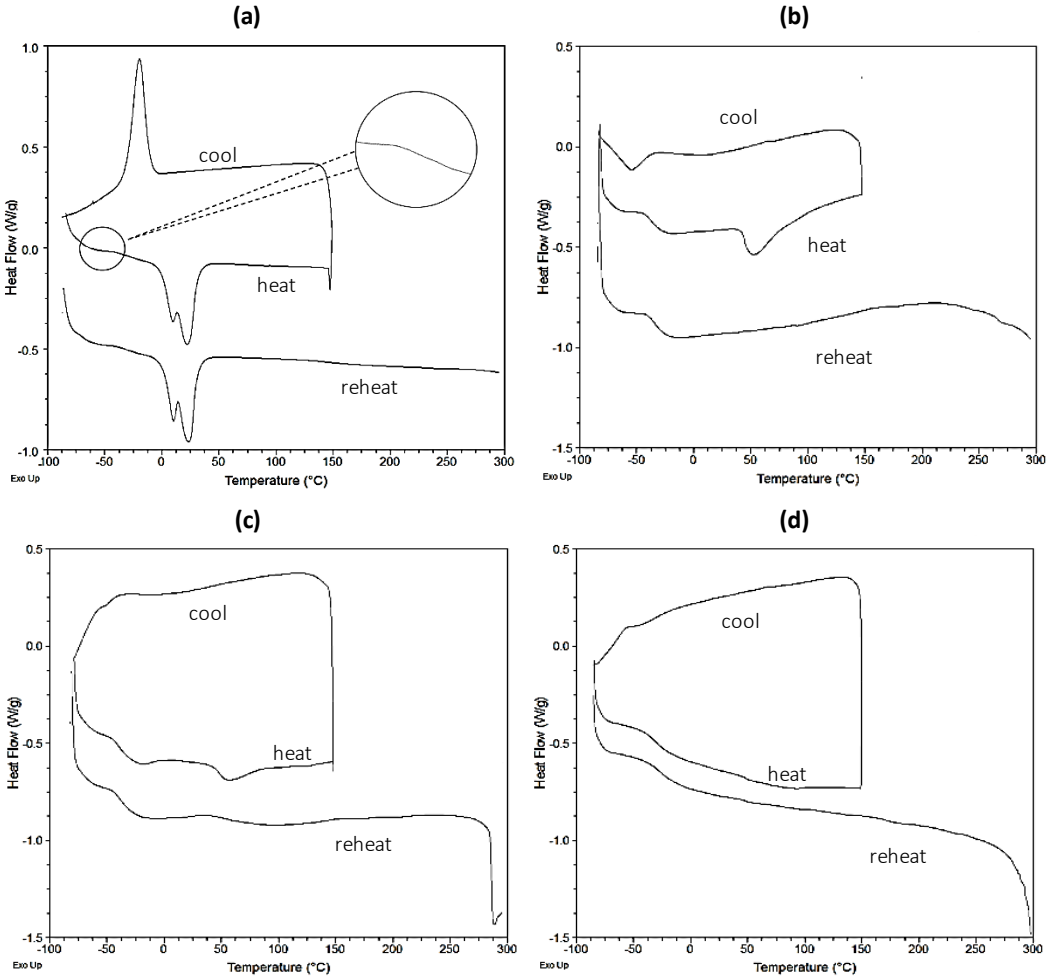

Figure 3-10. *DSC heat-cool-heat cycle of (a) polyol PCL1000, (b) formulation B4, (c) formulation B5 and (d) formulation B6.*

ATR FT-IR spectra of the short polycarbonate polyol PH50 and the corresponding coatings B7 and B8 are presented in Error! Reference source not found.. The spectrum of polyol shows OH stretch at 3500 cm^{-1}, alkane CH stretches at 2950 cm^{-1} and 2870 cm^{-1}, carbonate stretch at 1740 cm^{-1} and several CH signals below 1500 cm^{-1}.[13]

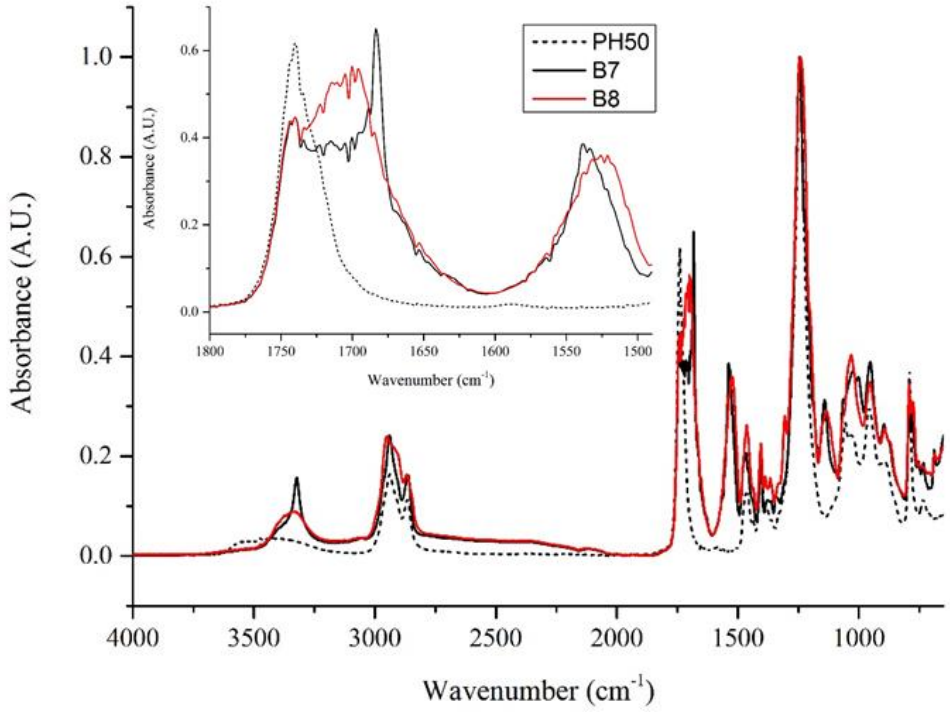

Figure 3-11. *ATR FT-IR spectra of polyol PH50 and coatings B7 and B8.*

The OH stretch at 3350 cm^{-1} is not present in the spectra of the coatings due to consumption of the hydroxyl groups during the reaction. The broad peak between 3500 cm^{-1} and 2250 cm^{-1} was assigned to the carboxylic acid groups of DMPA. As in the spectra of coatings B4 and B6, the NH stretch of H-bonded urethane groups of HDI-based coating B7 appears at 3325 cm^{-1} and is narrow and sharp, indicating phase-separation of the system. However, in the spectra of IPDI-based coating PH8 a broader peak at 3340 cm^{-1} can be seen, indicating a larger extent of phase-mixing.[14,19,26] In the carbonyl region, the carbonate stretch of polyol appears at the same wavenumber as in the spectrum of pure PH50. The spectrum of coating B7 shows the largest carbonyl peak at 1690 cm^{-1}, associated with H-bonded urethane and a phase-separated morphology. Coating B8 shows large, multiple peaks in the

1715-1700 cm^{-1} region, associated with phase-mixed urethane groups.[14,19,26] The C-N stretch and NH bend of urethane groups can be observed in the phase-separated system at 1540 cm^{-1} and in the phase-mixed system at 1525 cm^{-1}. More detailed explanation and the analysis of the effect of H-bonding on the ATR FT-IR spectroscopy shifts will be provided in Chapter 4.

The fifth polyol, polycarbonate PH50, showed a glass transition at -68 °C (**Figure 3-12**). Moreover, in the first heating cycle a broad melting peak can be observed at 66 °C, with the onset of the endotherm at 25 °C and the end at 140 °C. The breadth of the transition indicates a large size distribution of crystallites with various imperfections, expected for a random copolymer of pentanediol and hexanediol. The enthalpy of the transition was found to be 13.7 J g^{-1}. No melting endotherms were observed in the second cycle.

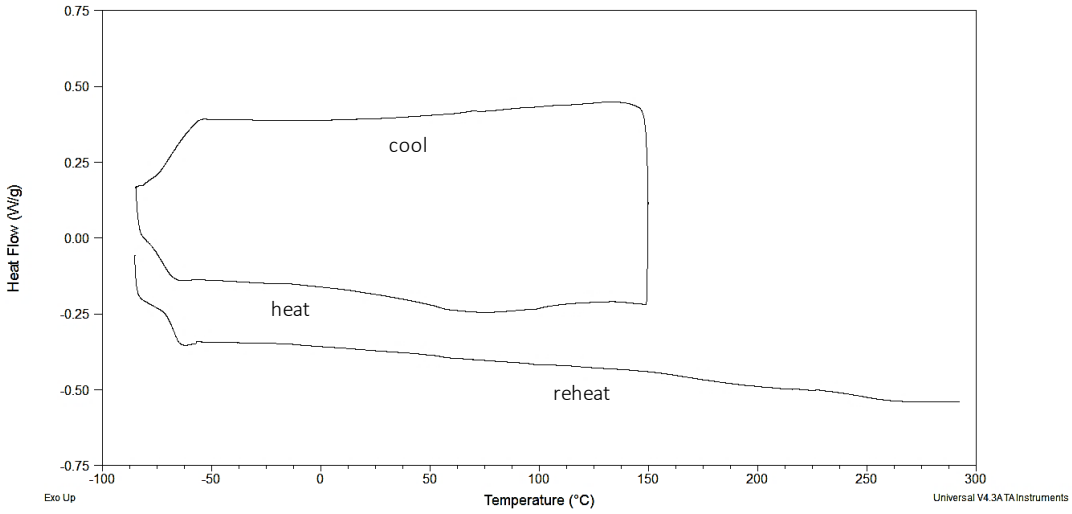

***Figure 3-12**. DSC heat-cool-heat cycle of polycarbonate polyol PH50.*

Coatings B7 and B8 prepared with PH50 showed very different DSC profiles, indicating the large influence of the isocyanate (**Figure 3-13**). The sample prepared with the linear HDI, B7, showed a moderate shift of the glass transition of the amorphous regions of SS to -22 °C, and the shift can be related to HS being 'dissolved' in the SS-rich phase, causing a delay of the phase transition as predicted by **Equation 1.5** (see page 39).[19] The sample prepared with IPDI, B8, showed a large shift of the T_g to 37 °C. The large shift, exceeding 100 °C, as well as the width of the transition, indicate

homogeneity of the phase and large extent of phase-mixing.[20] Therefore, the glass transition can be considered as a transition of a homogenously mixed and fully compatible HS-SS phase.[27]

In the first heat cycle of sample B7 multiple melting peaks of the crystalline SS can be observed at 50 °C, 77 °C and 114 °C, with the overall enthalpy of 42.7 J g^{-1}. The enthalpy can be recalculated as the equivalent of 80.1 J g^{-1} of polyol. The large increase of the enthalpy of melting shows the significance of modification of end groups of the polyol during formation of urethane, restricting the molecular motion of polymer chains and facilitating crystallinity.[3] Moreover, the polycarbonate polyols were shown to exhibit interactions between the carbonate groups and HS. The HS, acting as physical crosslinks, enforce the overall strength of SS-rich phase and increase the enthalpy of melting.[6] Sample B8 showed significantly smaller melting peak at 106 °C, with the enthalpy of 3.0 J g^{-1} (the equivalent of 6.3 J g^{-1} of polyol), present only in the first heating cycle. That indicates a high extent of phase-mixing and low crystallinity.

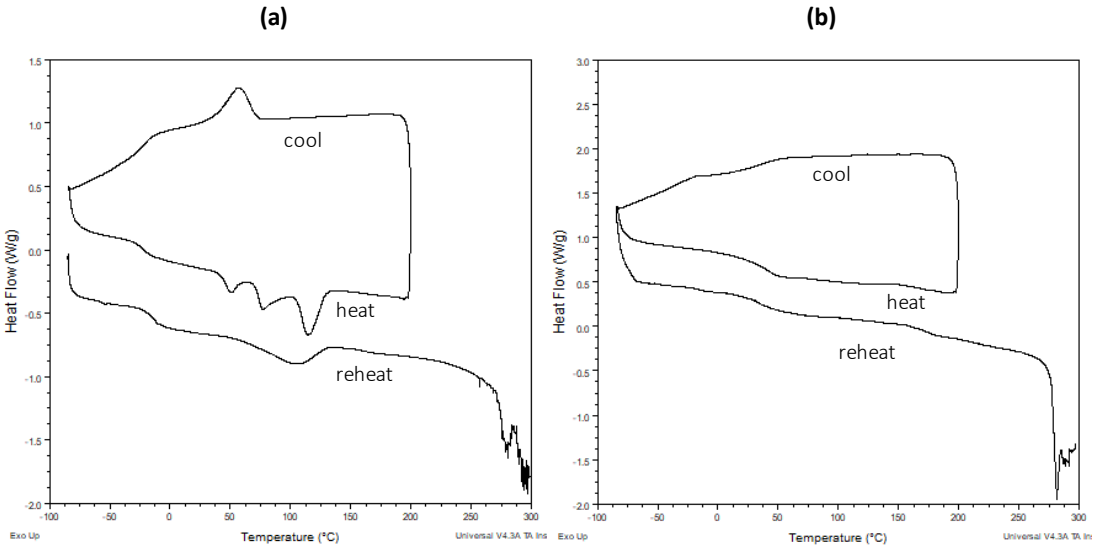

Figure 3-13. *DSC heat-cool-heat cycle of formulations (a) B7 and (b) B8.*

The recrystallisation process seen as an exotherm during cooling of sample B7, as well as the melting peak in the second heating cycle at 106 °C with the enthalpy of 23.3 J g^{-1} (the equivalent of 43.7 J g^{-1} of polyol) reflects the crystallinity promoting nature of 1,4-butanediol.[25] Interestingly, both samples shown a second glass transition in the

second heat cycle, at 160 °C and 171 °C respectively, associated with the amorphous regions of HS, as well as melting endotherms of the crystalline regions of HS at temperatures above 270 °C. The presence of the second glass transition can be related to the high percentage and length of HS (χN), allowing creation of multiple phases and arrangements of the segments.

The large difference in the lower glass transition temperatures of the two samples, as well as the difference in their crystallinity, show the significant influence of the diisocyanate on the morphology of polyurethanes. The symmetrical and linear HDI promotes crystallinity and phase-separation of PU, while the asymmetrical and bulky IPDI disturbs crystallinity as well as promoting phase-mixing.[3,11,28] The effect is more significant in coatings prepared with PH50 than in coatings prepared with PCL1000 due to the lower crystallinity of the polycarbonate polyol and the higher percentage of HS within formulations B7 and B8.

As the ATR FT-IR spectra of PH200 and PH300 were found to be identical, only one of them is presented in Error! Reference source not found.. The spectrum of PH200 and PH300 shows, similarly to PH50: OH stretch at 3550 cm^{-1}, alkane CH stretches at 2950 cm^{-1} and 2870 cm^{-1}, carbonate stretch at 1740 cm^{-1} and several CH signals below 1500 cm^{-1}.[13]

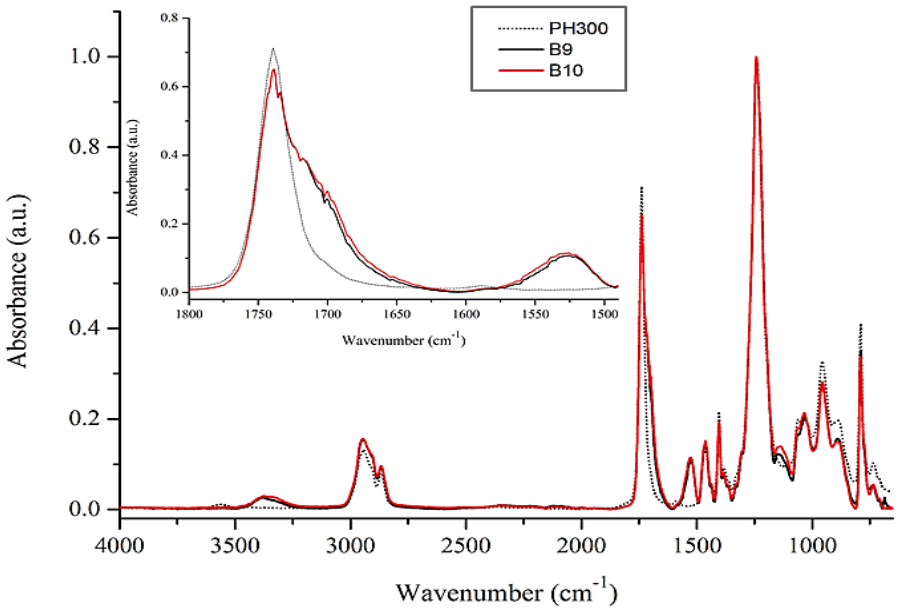

Figure 3-14. *ATR FT-IR spectra of polyol PH50 and coatings B7 and B8.*

The spectra of coatings B9 and B10, composed from over 70% of SS, were found to be very similar. The OH stretch at 3350 cm^{-1} is not present in the spectra of the coatings due to the consumption of hydroxyl groups during the reaction. A broad NH stretch of H-bonded urethane groups can be seen at 3350 cm^{-1} and the H-boned urethane carbonyl peaks can be seen at 1720 cm^{-1} and 1700 cm^{-1}. [15] The C-N stretch and the NH bend peak of urethane groups is present at 1525 cm^{-1}. The broad peak between 3500 cm^{-1} and 2250 cm^{-1}, assigned to the carboxylic acid groups, appears to be smaller than in the spectra of coatings B7 and B8 due to the significantly larger amount of SS, and thus in a comparison smaller percentage of DMPA.

The DSC analysis of the first longer polycarbonate, PH200, showed the glass transition at -51 °C in the first and second heat cycle (**Figure 3-15a**). No melting endotherms were observed in the histogram. Formulation B9 showed a T_g of SS at -28 °C, thus over 20 °C higher than in the pure polyol (**Figure 3-15b**). The shift of the transition is influenced by the presence of HS within the SS-rich segments, indicating some amount of phase-mixing.[19] Additionally, formulation B9 showed a melting peak of HS at 290 °C, indicating the presence of pure HS within the polymer matrix.

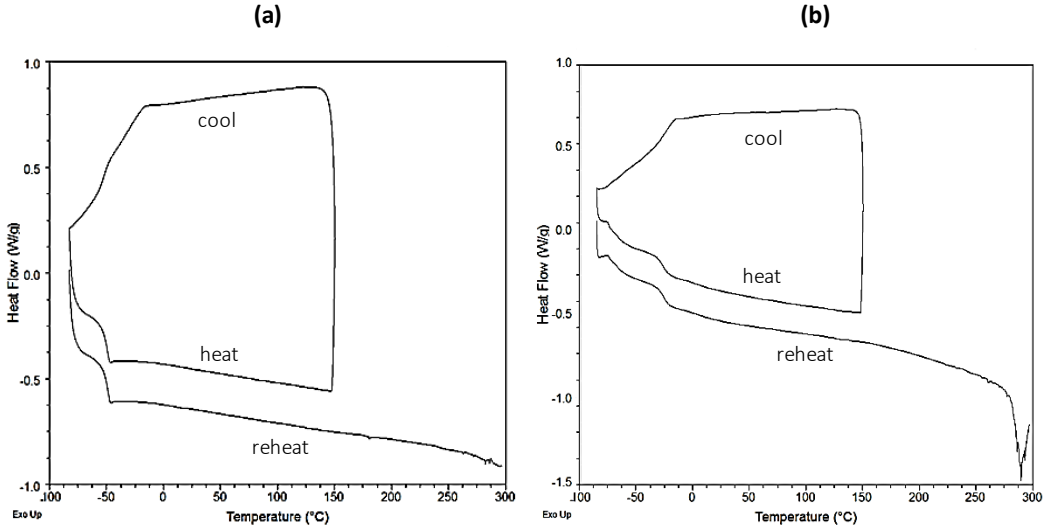

Figure 3-15. *DSC heat-cool-heat cycle of (a) polyol PH200 and (b) formulation B9.*

The DSC analysis of the second longer polycarbonate, PH300, showed the glass transition at -50 °C in the first heat cycle and at -49 °C in the second (Error! Reference source not found.**a**). No melting endotherms were observed in the histogram. Formulation B10 showed a T_g of SS at -32 °C, thus almost 20 °C higher than in the pure polyol (Error! Reference source not found.**b**). The shift of the transition is influenced by the presence of HS within the SS-rich segments, indicating some amount of phase-mixing.[19] A melting peak of HS at 290 °C is also present, indicating the presence of pure HS within the polymer matrix.

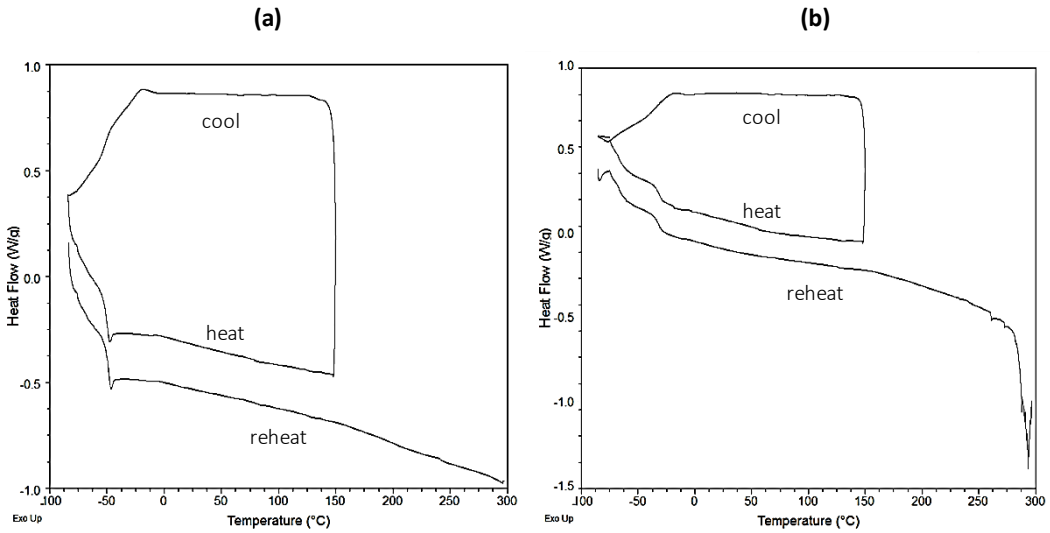

Figure 3-16. *DSC heat-cool-heat cycle of (a) polyol PH300 and (b) formulation B10.*

The presented differences in the ATR FT-IR and DSC of formulations prepared with a short polycarbonate PH50 and the two longer polycarbonates PH200 and PH300 reflect the significant influence of the length of the polyol on the morphology and the properties of PU. The summary of derived DSC data is presented in **Table 3-5**.

Table 3-5. *Summary of DSC data of formulations prepared with various long chain polyols (the melting enthalpy values in the brackets represent the recalculated enthalpy in J per gram of polyol within the formulation).*

Code	Polyurethane	Cycle 1			Cycle 2		
		T_g (°C)	T_m (°C)	ΔH_m (Jg^{-1})	T_g (°C)	T_m (°C)	ΔH_m (Jg^{-1})
	D1700	-51	74	7.5	-51	-	-
B1	D1700-HDI-EG	-42	55 115	5.8 [7.2] 1.1	-40	58 92	1.4 [1.7] 5.7
						178 257	2.8
	D670	-31	91	11.7	-31	-	-
B2	D670-HDI-EG	13	77	13.0 [19.8]	16	92	1.1 [1.7]
						219	36.4
	PCL2000	-64	31 53	16.1 79.8	-64	34 41	83.7
B3	PCL2000-HDI-BD	-49	34 44	32.9 [46.3]	-50	39	25.7 [36.2]
			115 143	-		143 159	17.7
	PCL1000	-31	10 22	53.6	-30	10 23	54.0
B4	PCL1000-HDI-BD	-36	54	32.9 [47.7]	-32	-	-
B5	PCL1000-HDI-siloxane	-38	56	7.4 [11.5]	-36	99	10.7 [16.7]
B6	PCL1000-IPDI-BD	-28	78	5.8 [9.0]	-25	-	-
	PH50	-69	67	13.7	-67	-	-
B7	PH50-HDI-BD	-22	50 77 114	42.8 [80.1]	-17 160	106	23.3 [43.7]
B8	PH50-IPDI-BD	37	106 188	3.0 [6.3] 0.7	35 171	-	-
	PH200	-51	-	-	-51	-	-
B9	PH200-IPDI-BD	-28	-	-	-27	-	-
	PH300	-50	-	-	-49	-	-
B10	PH300-IPDI-BD	-32	-	-	-32	-	-

3.4. EVALUATION OF SELF-HEALING PROPERTIES

Among the ten coatings prepared in the first set of materials, coatings B1, B3, B4, B5, B6 and B7 exhibited high haze values above the required 2%, thus they were not tested to evaluate their SH properties. Among the remaining four coatings exhibiting haze values below 2% only coating B8 fulfilled the other two main requirements, i.e. showed a pencil hardness of B or above and showed a T_g above the RT and below 80 °C. However, in order to investigate the relationship between the morphology and the SH properties of polyurethane coatings, all the four materials were scratched using the automated steel wool instrument and left to heal at RT for 120 minutes. The haze measurement data of the four coatings is presented in **Table 3-6**. A visual representation of the haze values is shown in **Figure 3-17**. The calculated percentage recovery of the remaining samples is presented in **Figure 3-18**.

Table 3-6. *Haze values of samples tested for SH properties.*

Sample	Haze							
	Initial	After scratching	10 min healing	20 min healing	30 min healing	60 min healing	90 min healing	120 min healing
B2	1.77	2.74	2.53	2.46	2.54	2.66	2.69	2.60
B8	0.44	4.17	3.52	3.46	3.36	3.23	3.12	3.11
B9	0.60	3.40	2.91	3.09	3.21	2.81	2.81	2.55
B10	0.83	3.72	2.39	2.23	2.13	2.08	2.02	2.00

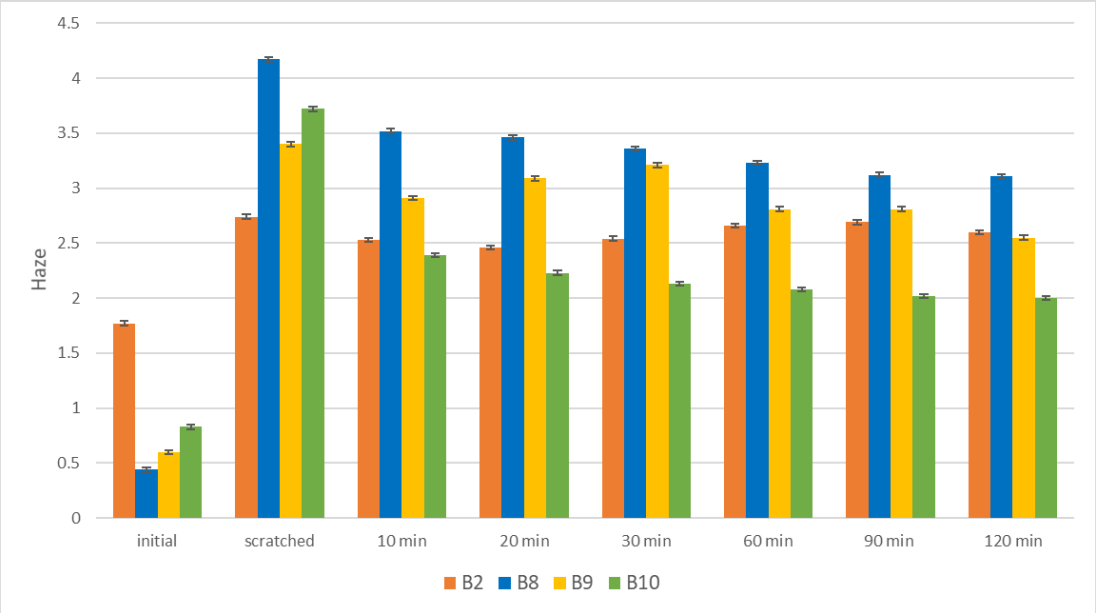

Figure 3-17. *Graphs of haze values of samples tested for SH properties.*

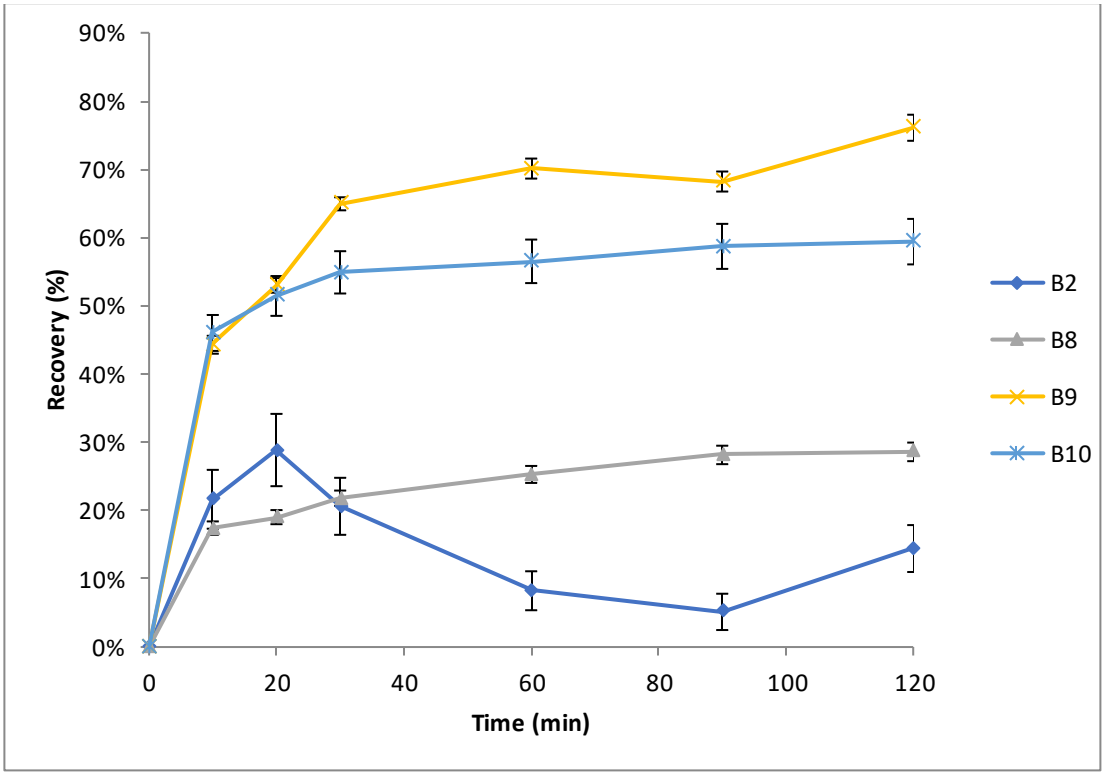

Figure 3-18. *Percentage recovery at RT of coatings prepared with various polyols.*

Coatings prepared with the two long polycarbonate polyols, B9 and B10, were found to exhibit the highest recovery, reaching 80% and 60% respectively. The efficient healing can be associated with the low T_g of SS-rich phases, allowing them to be in their rubbery state at RT. The molecular mobility of SS allowed them to flow and restore the secondary structure of PU damaged during scratching. The healing process was also supported by a relatively phase-mixed morphology of the polymers and their low crystallinity, facilitating the rearrangement of the segments and restoring the properties. However, the T_g occurring below RT resulted in a low pencil hardness of the two coatings, thus they were found to be unsuitable to be used as self-healing coatings.

Coating B2, with a T_g just below RT, showed an initial recovery of 30% followed by a decrease of recovery. The increase of the haze values in the moisture-cured coating might be associated with a large amount of polar urea groups forming monodentate and bidentate interactions within HS and increasing the crystallinity of the coating over time. Additionally, the presence of aromatic groups within the SS, able to self-

organise into crystalline regions *via* π-π stacking and interacting with HS, reduced the amount of phase-mixing within the polymer and thus hindered the healing process.[29]

Coating B8, prepared with a short polycarbonate polyol, showed a promising, steady recovery from damage reaching 30%. During the healing process the sample remained below the lower T_g, associated with the phase-mixed homogenous blend of HS and SS. However, due to the width of the transition, with the onset at approximately 10 °C, some mobility of the phase-mixed segment was obtained at RT, allowing the small recovery from damage. Therefore, in the following chapters the influence of the healing temperature on the recovery of coating B8, as well as similar coatings prepared with the polycarbonate polyol PH50, will be investigated.

3.5. SUMMARY AND DISCUSSION

The initial study of SH PU materials focused on the investigation of the chemistry and the length of polyol, acting as the soft segment building block within polyurethane matrix, on the morphology and the properties of the coatings. Four main factors having the largest influence of the prepared and tested materials were identified :

- **MW of polyol.** Polyols with MW ≥ 2000 g mol^{-1} were found to reduce the hardness of coatings. The low hardness of coatings B1, B3, as well as B9 and B10, can be associated with the low percentage of HS, below 30%, within the formulations prepared with the long polyols D1700, PCL2000, PH200 and PH300. Coatings prepared with shorter polyols, thus exhibiting higher percentage of HS, showed a better hardness.

  Moreover, longer polyols were found to reduce the effect of other building blocks of PU, such as diisocyanate or CE. For example, the phase-mixing inducing IPDI in coating B8, prepared with a short polyol, significantly increased mixing of the system, apparent by the large increase of the lower T_g. In coating B9 and B10, prepared with polyols with MW ≥ 2000 g mol^{-1}, the effect was largely reduced. The difference in the T_g and the extent of phase-mixing can be therefore related to the percentage of SS, and thus to the MW of polyol. A detailed investigation of

the influence of the symmetry of diisocyanates on the morphology and performance of SH PU coatings will be presented in Chapter 4.

Additionally, shorter polyols were found to create more phase-separated systems. That can be related by a low HS content and length, leading to lower χN values triggering separation.

- **Crystallinity of polyol**. Crystallinity of the pure polyols was found to have a significant effect on crystallinity of SS and SS-rich segments within the PU. Highly crystalline polyols PCL1000 and PCL2000 resulted in formation of crystalline coatings, indicated by the presence of melting peaks with large enthalpy values, and hindering phase-mixing of the segments, indicated by the small shift of T_g. Moreover, crystalline polymers are known to be opaquer due to the large number of amorphous-crystalline blocks interfaces, seen in the high haze values of coatings B1, B3, B5 and B7. The four coatings showed melting of SS in both DSC cycles, indicating a rapid recrystallisation of SS during cooling and high thermodynamic stability of the semi-crystalline matrices. Therefore, the crystalline regions with different refractive indices as well as the large number of the blocks' interfaces led to increase of the overall haze.
- **Symmetry of polyol**. The high crystallinity of polycaprolactone can be explained by the symmetrical structure and the short repeating unit of the polymer. Polyols prepared with less regular structures, such as co-polycarbonates of pentanediol and hexanediol PH50, PH200 and PH300, showed less crystalline structure and allowed better adjustment of the properties by varying other building blocks of PU. Therefore, the symmetry and regular sequence of the polyol, acting as SS in PU, plays an important role in a design of functional polymers.
- **Compatibility of polyol (SS) and HS**. To create a phase-mixed polymer matrix the repulsive interactions between HS and SS need to be minimised. The effect can be seen in samples B2 and B7, which showed a similar shift of the T_g of SS by approximately 40 °C. Coating B2, prepared with a short polyester polyol D670 and linear HDI exhibited high compatibility between HS and SS indicated by a low haze. Coating B7, prepared with a short polycarbonate PH50 and linear HDI

showed lack of compatibility, indicated by a very high haze. However, coating B8 showed a great compatibility of PH50 and IPDI. Therefore, the interactions between the HS and SS can be optimised by varying all building blocks of PU.

Moreover, the chemistry and the length of polyol, acting as the soft segment building block within polyurethane matrix, was found to have a significant effect on the self-healing behaviour of the coatings.

Sample B2, prepared with a short oligomeric polyester D670 containing aromatic groups, exhibited low haze, acceptable hardness and a phase-mixed morphology. However, the sample showed a T_g below RT, indicative of insufficient compatibility between HS and SS. Even though the coating was found to have the T_g below RT, only moderate recovery from damage at RT was observed. The low recovery was associated with the presence of large amount of urea groups within the structure of PU created during moisture-curing, as well as the aromatic groups within the polyol.

Coatings B9 and B10, prepared with long polyol PH200 and PH300, were found to be too soft, largely phase-separated and showed the T_g at very low temperatures. However, the coatings showed very efficient healing at RT, above their T_g, largely influenced by the structure of the polycarbonate polyol and the phase-mixing promoting nature of IPDI.

Coating B8, prepared with a short polycarbonate polyol, showed a promising, steady SH behaviour at RT, reaching 30% within 120 minutes, associated with a phase-mixed morphology and the onset of T_g just below the RT. Moreover, the sample showed a low haze value, within the required 0-2% and an acceptable pencil hardness above B.

The large shift of the temperature of the lower glass transition of sample B8 compared to the T_g of the polyol and the low crystallinity suggest that the sample is comprised of a compatible mixture of SS and HS, and pure HS segments.[27] The homogeneity of the phase-mixed segment resulted in the T_g shifting to above RT, while the presence of separate HS segments reinforced the overall strength and shape of the coating. Therefore, further investigation of materials prepared with the polycarbonate polyol PH50 will be presented in the remainder of the thesis.

3.6. REFERENCES

1 Z. Wirpsza, *Polyurethanes. Chemistry, Technology and Applications*, Ellis Hornwood Ltd, Midsomer Norton, 1st edn., 1993.

2 T. J. Touchet and E. M. Cosgriff-Hernandez, *Hierarchal Structure-Property Relationships of Segmented Polyurethanes*, Elsevier Ltd, 2016.

3 I. Yilgör, E. Yilgör and G. L. Wilkes, *Polymer*, 2015, **58**, A1–A36.

4 V. Garcia-Pacios, V. Costa, M. Colera and J. M. Martin-Martinez, *Prog. Org. Coatings*, 2011, **71**, 136–146.

5 C. M. Gomez, D. Gutierrez, M. Asensio, V. Costa and A. Nohales, *J. Elastomers Plast.*, 2017, **49**, 77–95.

6 V. García-Pacios, M. Colera, Y. Iwata and J. M. Martín-Martínez, *Prog. Org. Coatings*, 2013, **76**, 1726–1729.

7 Y. Chen, L. Tan, L. Chen, Y. Yang and X. Wang, *Brazilian J. Chem. Eng.*, 2008, **25**, 321–335.

8 A. Eceiza, M. D. Martin, K. de la Caba, G. Kortaberria, N. Gabilondo, M. A. Corcuera and I. Mondragon, *Polym. Eng. Sci.*, 2008, **2**, 297–306.

9 K. Gisselfält and B. Helgee, *Macromol. Mater. Eng.*, 2003, **288**, 265–271.

10 V. García-Pacios, J. A. Jofre-Reche, V. Costa, M. Colera and J. M. Martín-Martínez, *Prog. Org. Coatings*, 2013, **76**, 1484–1493.

11 C. Prisacariu, in *Polyurethane Elastomers*, Springer-Verlag, Wien, 1st edn., 2011, pp. 23–60.

12 F. S. Chuang, W. C. Tsen and Y. C. Shu, *Polym. Degrad. Stab.*, 2004, **84**, 69–77.

13 F. Sen Yen, L. L. Lin and J. L. Hong, *Macromolecules*, 1999, **32**, 3068–3079.

14 E. Princi, S. Vicini, K. Castro, D. Capitani, N. Proietti and L. Mannina, *Macromol. Chem. Phys.*, 2009, **210**, 879–889.

15 J. Mattia and P. Painter, *Macromolecules*, 2007, **40**, 1546–1554.

16 H. S. Lee, Y. K. Wang and S. L. Hsu, *Macromolecules*, 1987, **20**, 2089–2095.

17 E. Ylgor, I. Ylgor and E. Yurtsever, *Polymer*, 2002, **43**, 6551–6559.

18 E. Yilgör, E. Yurtsever and I. Yilgör, *Polymer*, 2002, **43**, 6561–6568.

19 C.-C. Chang, K.-S. Chen, T. L. Yu, Y.-S. Chen, C.-L. Tsai and Y.-H. Tseng, *Polym. J.*, 1999, 31, 1205–1210.

20 I. M. Pereira and R. L. Oréfice, *Macromol. Symp.*, 2011, **299–300**, 190–198.

21 L. M. Leung and J. T. Koberstein, *Macromolecules*, 1986, **19**, 706–713.

22 M. Reading and D. J. Hourston, *Modulated Temperature Differential Scanning Calorimetry. Theoretical and Practical Applications in Polymer Characterisation*, Springer, Dordrecht, the Netherlands, 1st edn., 2006.

23 S. Velankar and S. L. Cooper, *Macromolecules*, 1998, **31**, 9181–9192.

24 T. M. Don, J. P. Bell and M. Narkis, *Polym. Eng. Sci.,* 1996, **36**, 2601-2613.

25 J. Blackwell, M. R. Nagarajan and T. B. Hoitink, *Polymer*, 1982, **23**, 950–956.

26 C. S. Paik Sung and N. S. Schneider, *J. Mater. Sci.*, 1978, **13**, 1689–1699.

27 H. Jeong, J. Park, S. Kim, J. Lee, N. Ahn and H. gyoo Roh, *Fibers Polym.*, 2013, **14**, 1082–1093.

28 P. Król, *Prog. Mater. Sci.*, 2007, **52**, 915–1015.

29 S. Burattini, H. Merino, W. Weng and S. J. Rowan, *J. Am. Chem. Soc.*, 2010, **132**, 12051–12058.

4. THE INFLUENCE OF ISOCYANATE ON MORPHOLOGY AND SELF-HEALING PROPERTIES

As polyurethanes are composed of soft segments and hard segments, the adjustment of the chemistry of these two phases has a crucial influence on the morphology and the properties of created materials.[1]

In the previous chapter the chemistry and the length of polyols, the soft segments building blocks, was explored. It was established that self-healing of polyurethane coatings requires a well phase-mixed polyurethane matrix with a high compatibility between hard and soft segments. Long polyols were found to reduce the hardness of coatings and minimise the effect of HS, related to a large percentage of SS. Crystallinity of polyols was found to be unfavourable due to introduction of crystallinity of SS within PU, increasing the overall haze and facilitating phase-separation. The symmetry of polyols was also found to be unsuitable due to their increased crystallinity and phase-separation inducing nature. Therefore, the polycarbonate polyol, co-polymer of pentanediol and hexanediol with MW of 500 g mol^{-1}, was chosen as the most suitable polyol to be used as a soft segment of efficiently self-healing polyurethane coatings.

The hard segment content in a typical PU varies between 20% and 60%.[2] HS are formed during the reaction of isocyanates with chain extenders and possess high densities of polar urethane groups. As the result of the high polarity, the HS attract each other and form semi-crystalline blocks with high glass transition and melting temperatures.[3] The HS reinforce the structure of PU and have a large influence on the overall properties of the materials. Therefore, the choice of suitable building blocks used to create HS of efficiently healing PU coatings is equally important.

In this chapter the influence of the chemistry of the diisocyanate used to create the HS blocks of PU moiety will be investigated. Two diisocyanates, linear and symmetrical HDI and bulky and asymmetrical IPDI, were used to create a library of coatings with various ratios of the two mentioned isocyanates. Their effect on the morphology and self-healing behaviour will be further discussed.

4.1. SYNTHESIS INFORMATION

In the second set of formulations the influence of two diisocyanates, linear and symmetrical HDI and bulky and non-symmetrical IPDI, was investigated in detail by preparing coatings with various ratios of the two materials (**Figure 4-1**). All formulations were prepared using polycarbonate polyol PH50 and EG chain extender.

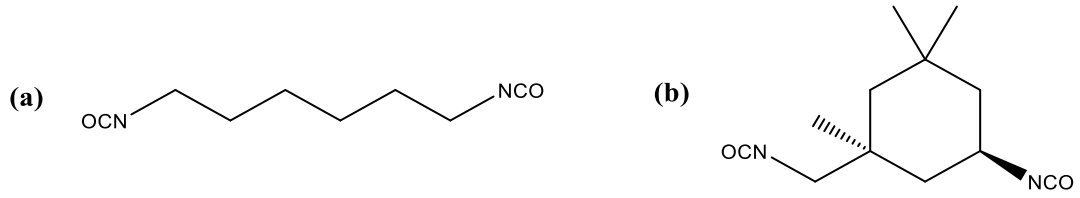

Figure 4-1. *Structure of (a) HDI and (b) IPDI.*

All formulations were prepared using the acetone process, using DMPA (25mol% of the total number of moles of CE) and 1,2-EG (75mol% of the total number of moles of CE), as described in Section 2.2.5.

4.2. CHARACTERISATION OF DISPERSIONS

Five formulations with various ratios of isocyanates were prepared. The first formulation was synthesised with HDI only. Subsequently, in the following formulations an increasing amount of HDI was replaced with IPDI. The last formulation was prepared with IPDI only.

The dispersions showed experimental solid contents between 16.0% and 31.1%, dependent on the solubility of polymer in water and the viscosity of a dispersion. The full list of formulations and the percentage of solid content of the dispersions are presented in **Table 4-1**.

Table 4-1. *Composition and solid content of the dispersions.*

Polyurethane	HDI (%)	IPDI (%)	Solid content (wt%)
PH50-HDI-1,2-EG	100	0	27.4 ± 1.7
PH50-HDI/IPDI(90:10)-1,2-EG	90	10	16.0 ± 0.9
PH50-HDI/IPDI(50:50)-1,2-EG	50	50	29.2 ± 1.0
PH50-HDI/IPDI(10:90)-1,2-EG	10	90	31.1 ± 2.9
PH50-IPDI-1,2-EG	0	100	23.1 ± 1.1

4.3. CHARACTERISATION OF COATINGS

The percentage of hard segments within formulations varied insignificantly, reaching between 45.4% and 51.2%, influenced by the ratio of diisocyanates used and their molecular weight (**Table 4-2**). The coating prepared with HDI only, despite the lowest percentage of HS, was found to be the hardest one (HB). The remaining coatings showed somewhat better pencil hardness of B. The cross-cut adhesion of all the samples was found to be 0, indicating excellent adhesion properties between the coating and TAc sheets.

The majority of coatings exhibited very low haze values, within the acceptable 0-2% level (**Table 4-2**). However, the coating prepared with 90% of HDI and 10% of IPDI showed an unexpectedly high haze value.

The high haze can be explained by the presence of multiple crystalline regions of different refractive indices within the polymer matrix. The small amount of IPDI can promote a fast crystallisation occurring close to the surface of the coating, leading to a formation of segments with a different refractive index. Slower crystallisation of the coating synthesised with HDI only led to a more homogenous coating with a lower haze value.[4,5] Further investigation of the relationship between the morphology and the haze values of the coatings will be presented in Section 4.4.

Table 4-2. *Characterisation of coatings.*

Polyurethane	Hard segments (%)	Pencil Hardness	Cross-Cut Adhesion	Haze (%)
PH50-HDI-1,2-EG	45.4	HB	0	1.04
PH50-HDI/IPDI(90:10)-1,2-EG	46.1	B	0	17.10
PH50-HDI/IPDI(50:50)-1,2-EG	48.5	B	0	0.88
PH50-HDI/IPDI(10:90)-1,2-EG	50.7	B	0	0.72
PH50-IPDI-1,2-EG	51.2	B	0	0.77

4.4. CHARACTERISATION OF COATINGS' MORPHOLOGIES

Figure 4-2 presents spectra of the five coatings prepared with various rations of HDI and IPDI. Among the important signals, a broad NH stretch can be observed at 3500-3250 cm^{-1}, CH_2 stretches at 2935 cm^{-1} and 2860 cm^{-1}, and a broad peak at 3500-2250 cm^{-1} assigned to the carboxylic acid groups of DMPA. Furthermore, multiple carbonyl stretches at 1740-1650 cm^{-1}, C-N stretch and NH bend at 1600-1500 cm^{-1}, and several CH signals below 1500 cm^{-1} can be observed.[6]

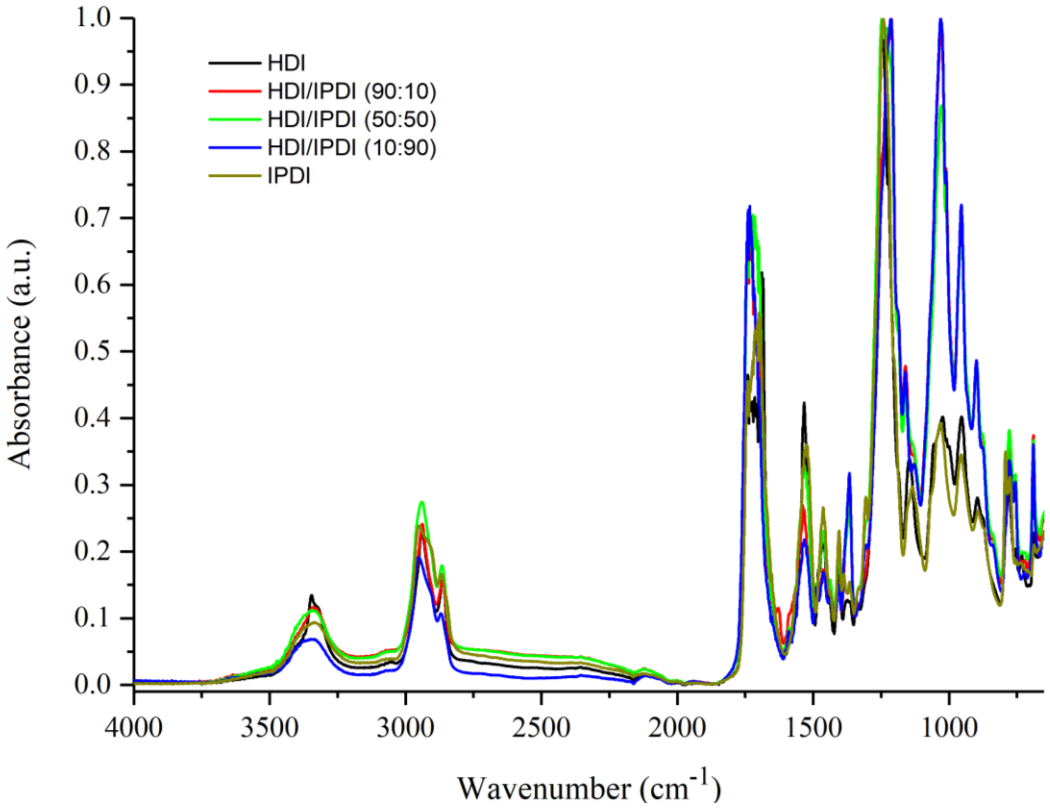

Figure 4-2. *ATR FT-IR spectra of the five coatings prepared with blends of isocyanates.*

Interactions between HS and SS lead to thermodynamic incompatibility of the segments, leading to phase-separation.[7–9] As HS-SS hydrogen bonding is a driving force for phase-mixing, the amount of phase-separation and phase-mixing can be determined by investigation of N-H and C=O stretching regions of ATR FT-IR.[10–13]

Free N-H groups of urethane and urea are known to show stretching vibration in the 3500-3400 cm^{-1} region, while H-bonded groups show the signals at lower values, usually at 3350-3200 cm^{-1}.

The H-bonding interactions between HS, dominant within phase-separated systems, occur between the secondary amine and carbonyl groups of urethanes (**Figure 4-3**). The interactions between HS and SS, present within phase-separated systems, occur between the secondary amine of urethane groups and carbonyl groups of polyols. As the strength of H-bonding between HS is stronger than between HS and SS, the stretching vibration of groups involved in the HS-HS interactions can be observed at higher wavelengths, in the 3350-3300 cm^{-1} region, while groups involved in HS-SS interactions appear at higher lower wavelengths, in the 3400-3350 cm^{-1} region. A similar trend can be seen in the carbonyl region, with the HS-HS signals appearing below 1700 cm^{-1} and the HS-SS signals above 1700 cm^{-1} (**Table 4-3**).[14]

The urea groups can also interact with both HS and SS. The urea groups can interact between each other creating two distinct structures – monodentate and bidentate blocks. However, the amount of urea groups within the presented systems is minimal. Therefore, the signals from the urea groups will not be used to analyse the microphase morphology of the coatings.

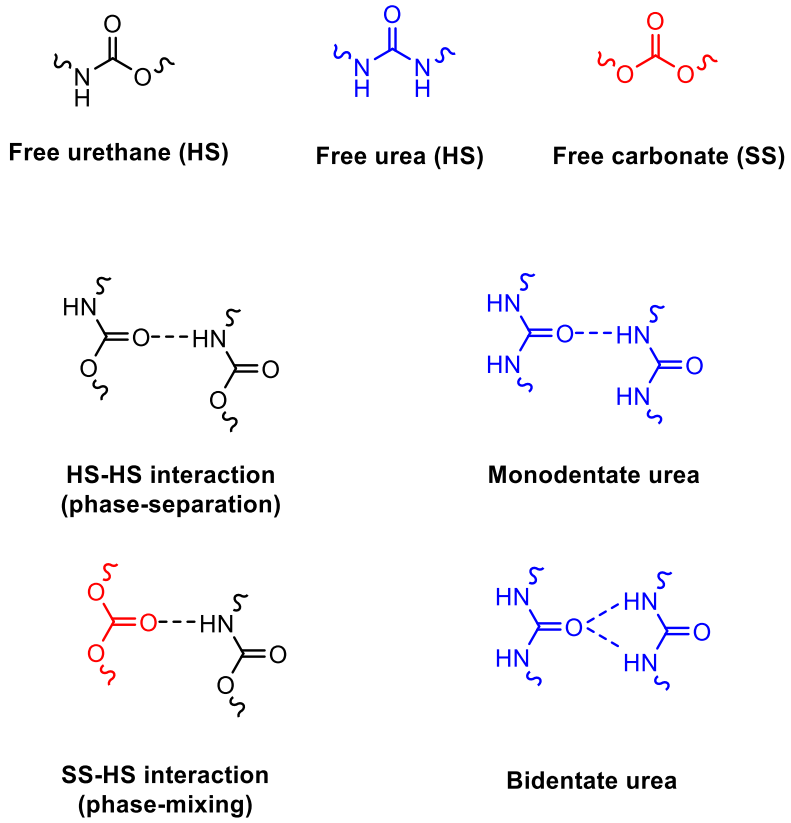

Figure 4-3. *The interactions between N-H and C=O within polyurethanes*

Table 4-3. *Characteristic IR bands for phase-mixed and phase-separated systems.*[10,15-20]

Wavenumber (cm^{-1})	Functional group ($\bar{\upsilon}$ – stretching, δ – bending)	Group assignment	Morphology
3500-3400	$\bar{\upsilon}$(NH) free	Urethane/Urea	Free
3400-3350	$\bar{\upsilon}$(NH) bonded	Urethane	Phase-mixed
3350-3300	$\bar{\upsilon}$(NH) bonded	Urethane	Phase-separated
3340-3320	$\bar{\upsilon}$(NH) bonded, bidentate	Urea	Phase-separated
3240	$\bar{\upsilon}$(NH) bonded, monodentate	Urea	Phase-separated
1743	$\bar{\upsilon}$(C=O) free	Polyol	Free
1740-1730	$\bar{\upsilon}$(C=O) bonded	Polyol	Phase-mixed
1733-1730	$\bar{\upsilon}$(C=O) free	Urethane	Free
1723-1705	$\bar{\upsilon}$(C=O) bonded	Urethane	Phase-mixed
1700-1683	$\bar{\upsilon}$(C=O) bonded	Urethane	Phase-separated
1700-1680	$\bar{\upsilon}$(C=O) free	Urea	Free
1660-1635	$\bar{\upsilon}$(C=O) bonded, monodentate	Urea	Phase-mixed
1616-1627	$\bar{\upsilon}$(C=O) bonded, bidentate	Urea	Phase-separated
1580-1576	$\bar{\upsilon}$(CN) + δ(NH) bonded, bidentate	Urea	Phase-separated
1570-1554	$\bar{\upsilon}$(CN) + δ(NH) bonded, monodentate	Urea	Phase-mixed
1539-1530	$\bar{\upsilon}$(CN) + δ(NH) bonded	Urethane	Phase-separated
1526-1507	$\bar{\upsilon}$(CN) + δ(NH) bonded	Urethane	Phase-mixed

Figure 4-4a presents the NH region of ATR FT-IR spectra of the five samples. All samples show a small amount of non H-bonded NH groups present as the 3500-3400 cm^{-1} shoulder peak, suggesting that the majority of NH groups are involved in H-bonding.[10] The NH peak of the sample prepared with HDI only in the 3350-3300 cm^{-1} region is sharp and narrow, indicating that the HS-HS interactions dominate within the phase-separated polymer matrix. With the increase of the percentage of IPDI, the NH stretch peak shifts to the left, becomes wider and more prominent, indicating an increase of HS-SS interactions within a more phase-mixed matrix.[15]

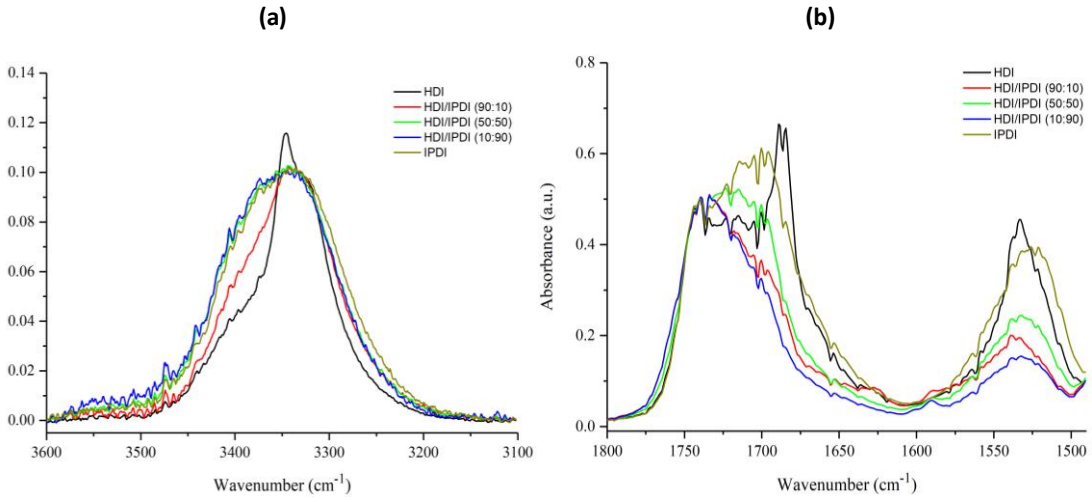

Figure 4-4. *ATR FT-IR spectra of the samples: (a) the NH region and (b) the carbonyl region.*

A similar observation can be made by the analysis of the carbonyl region of the ATR FT-IR spectra (**Figure 4-4b**). All spectra show the peak associated with the free carbonyl groups of PH50 in the 1740-1720 cm^{-1} region, partially overlapped with signal from the free urethane groups. The largest carbonyl peak in the spectrum of the coating prepared with only HDI, present at 1690 cm^{-1}, can be associated with H-bonded urethane groups within HS-HS blocks. Several significantly smaller peaks in the 1720-1700 cm^{-1} region, associated with HS-SS interactions, suggest a largely phase-separated morphology.[15] The remaining samples show the majority of the carbonyl peaks associated with the H-bonded urethane in the 1720-1700 cm^{-1} region, indicating more HS-SS interactions and a phase-mixed morphology influenced by the increased amount of IPDI.[7]

To confirm the relationship between the morphology of the samples and their spectra, the sample prepared with HDI/IPDI (50:50) was tested at various temperatures (**Figure 4-5**). It is well known that an increase of temperature causes breakdown of H-bonding, induces the disruption of short range order and organisation of HS, and promotes phase-mixing.[8] As the sample gets heated, the H-bonded amine stretch at 3340 cm^{-1} decreases, indicating reduced phase-separation, as shown by Cipriani *et al.*[16] In the carbonyl region a decrease of the peak at 1690 cm^{-1}, associated with a strongly H-bonded groups within phase-separated HS, and an increase of a peak at 1720 cm^{-1}, associated with a loosely bonded H-bonded groups within phase-mixed segments, can be observed.[17,18]

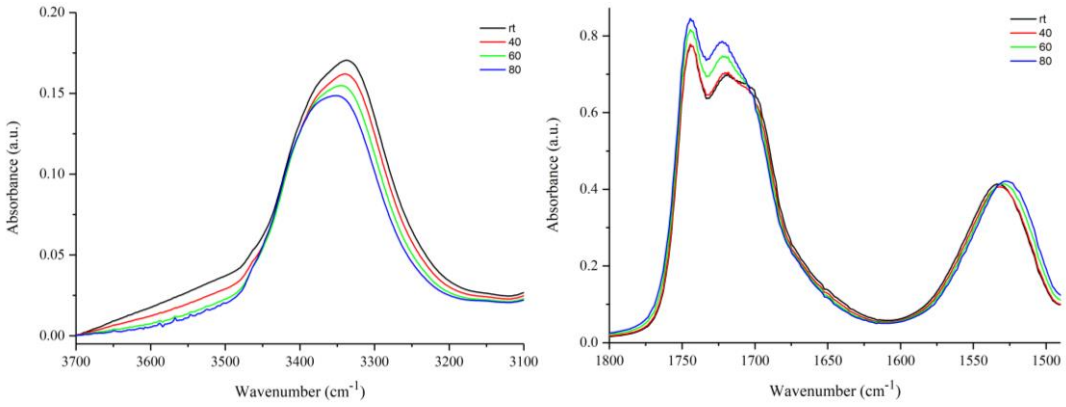

Figure 4-5. *Studies of temperature dependant phase-mixing of sample prepared with HDI/IPDI (50:50).*

This effect of the symmetry of diisocyanate is well established in the literature. Sami *et al.* reported that symmetrical diisocyanates allow formation of long-range ordering of H-bonds between HS leading to a phase-separated morphology. Bulky diisocyanate did not display such behaviour and could not form such ordered structures[19]. Gomez *et al.* reported an increase of phase-separation in systems with increasing HDI/IPDI ratio. Similar to formulations reported here, the change was indicated by an increase in the sharpness and intensity of the band at 3320 cm^{-1}, assigned to the formation of more ordered HS structures. Moreover, the increase of a band at 1685 cm^{-1} was reported, assigned to urethanes associated within HS blocks.[20]

Figure 4-6 presents DSC curves of the samples. It is important to consider both first and second heating cycles. The first heat cycle shows the morphology and hence the thermal properties of the samples "as-coated", whilst the second heat cycle provides information on the morphology subsequent to the imposition of an identical thermal history on all samples.

Considering the T_g of pure polyol, -69 ˚C, a significant change in the lower T_g of the formulations prepared with this polyol can be observed. The glass transition among the samples was found to shift to higher temperatures with an increase of IPDI content, moving from -21 ˚C to 17 ˚C in the first heat cycle, and from -8˚C to 30 ˚C in the second heat cycle (**Table 4-4**). Moreover, broadening of the glass transition can be observed. The difference between the T_g of pure polyol and the T_g of SS within the formulations can be related in part to the change of the chemistry of the polyol end groups, restricting the mobility of polymer chains.[21] Moreover, the restriction of chain mobility is also a result of the polymerisation of the polyol. The variation of the T_g among the samples reflects the influence of the ratio of the diisocyanates used. The low temperature (-8 °C) and the width of the transition (-17 °C to 2 °C) observed in the second heat cycle of the formulation prepared with the linear and symmetrical HDI suggests, that the SS comprise mainly of the polyol and some small amount of HS fragments 'dissolved' within the phase.[7] As the amount of IPDI increases, the temperature of glass transition raises, indicating larger amount of HS present within SS-rich blocks.[9] Therefore, the higher amount of IPDI increases the extent of phase-

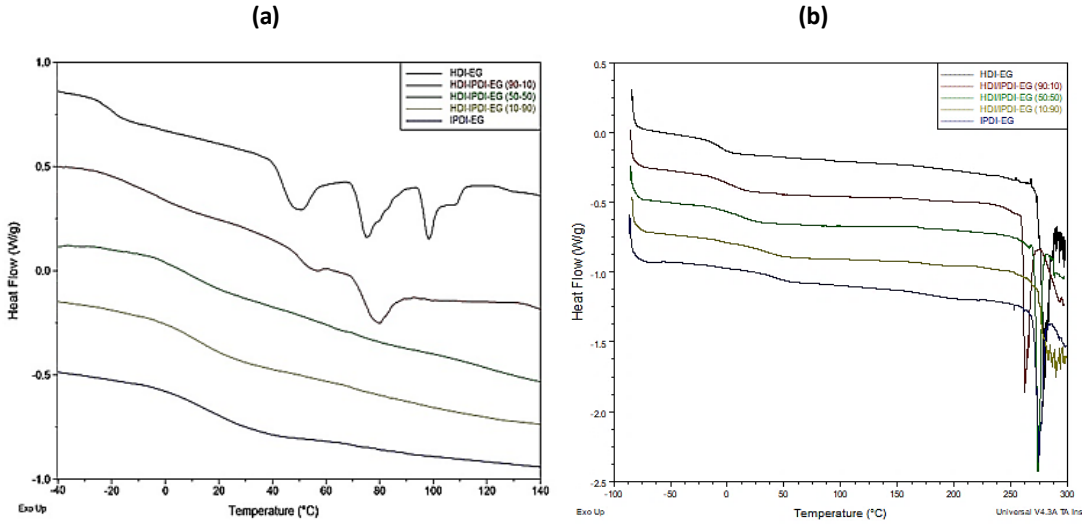

Figure 4-6. *DSC curves of formulations: (a) the first heat cycle and (b) the second heat cycle.*

mixing of the systems. The high temperature (30 °C) and the width of the transition (14-48 °C) observed in the formulation prepared with the bulky and non-symmetrical IPDI may suggest that the phase comprise of homogenous blend of HS and SS.[22]

Moreover, the samples prepared with HDI only and 90:10 HDI:IPDI show multiple melting peaks of the SS-rich phase in the first heating cycle, in a similar temperature range to the pure polyol. The melting peaks can be observed in the sample prepared with HDI at 49 °C, 75 °C and 98 °C with the overall enthalpy of 31.0 J g^{-1} (the equivalent of 63.1 J g^{-1} of polyol), and in the sample prepared with 90:10 HDI:IPDI at 56 °C and 80 °C with the overall enthalpy of 9.4 J g^{-1} (the equivalent of 18.2 J g^{-1} of polyol). The increase of the melting enthalpy, compared with the enthalpy obtained for a pure polyol PH50 (7.5 J g^{-1}) shows the influence of polymerisation and modification of end groups of the polyol, leading to restricted chain mobility and facilitating crystallinity.[21] The presence of multiple melting peaks indicates a complex morphology of the semi-crystalline SS, showing a significant level of crystallinity, promoted by the large amount of linear HDI within the structure. The remaining samples show no melting peaks, thus indicate an amorphous morphology of the SS, triggered by an increased content of bulky, non-symmetrical IPDI disturbing the packing of polymer chains.[20] The absence of melting peaks can also indicate that, rather than being considered as a SS-rich phase, the phase comprises of amorphous and homogenous blend of HS and SS, as indicated by the analysis of their T_g.[22]

Table 4-4. *The DSC data obtained from histograms (the T_g values reported in the brackets refer to the range of the transition, while ΔH_m values in the brackets represent the recalculated enthalpy in J per gram of polyol within the formulation).*

PU	Heat 1			Heat 2		
	T_g (°C)	T_m (°C)	ΔH_m (J/g)	T_g (°C)	T_m (°C)	ΔH_m (J/g)
PH50	-69 (-71 to -66)	74	7.5	-67 (-70 to -65)	-	-
HDI	-21 (-26 to 16)	49 75 98	31.0 [63.1]	-8 (-17 to 2) 198 (174 to 223)	294	-
HDI/IPDI (90:10)	-8 (-21 to 6)	56 80	9.4 [18.2]	4 (-9 to 17) 172 (166 to 180)	294	-
HDI/IPDI (50:50)	8 (-4 to 20)	-	-	10 (0 to 21) 170 (166 to 175)	262	-
HDI/IPDI (10:90)	11 (-2 to 24)	-	-	23 (9 to 37) 185 (177 to 194)	274	-
IPDI	17 (0 to 33)	-	-	31 (14 to 48) 182 (164 to 200)	293	-

The glass transition of HS is present in the DSC plots in the 170 °C to 200 °C region. However, the transition is not well defined due to the mainly crystalline structure of the HS. All samples show melting endotherms of the HS with the onset of the transition at temperatures above 250 °C. Therefore, the presence of semi-crystalline HS reinforcing the SS can be confirmed by the DSC analysis.

Images obtained by AFM showed the changes in the morphology of polyurethanes with an increase of IPDI content (**Figure 4-7**). AFM topography imaging showed an intermediate roughness of the phase-separated coating prepared with HDI only, while larger mounding structures of HDI/IPDI (90:10) and HDI/IPDI (50:50), and relatively smooth surface of phase-mixed coatings prepared with HDI/IPDI (10:90) and IPDI only were observed. Moreover, the AFR phase contrast imaging (**Figure 4-8**) showed that the phase-separated coating prepared with HDI only is composed of platelets. Smaller amount of platelets was found in formulations HDI/IPDI (90:10) and

HDI/IPDI (50:50), and no platelets in the phase-mixed coatings prepared with HDI/IPDI (10:90) and IPDI only.

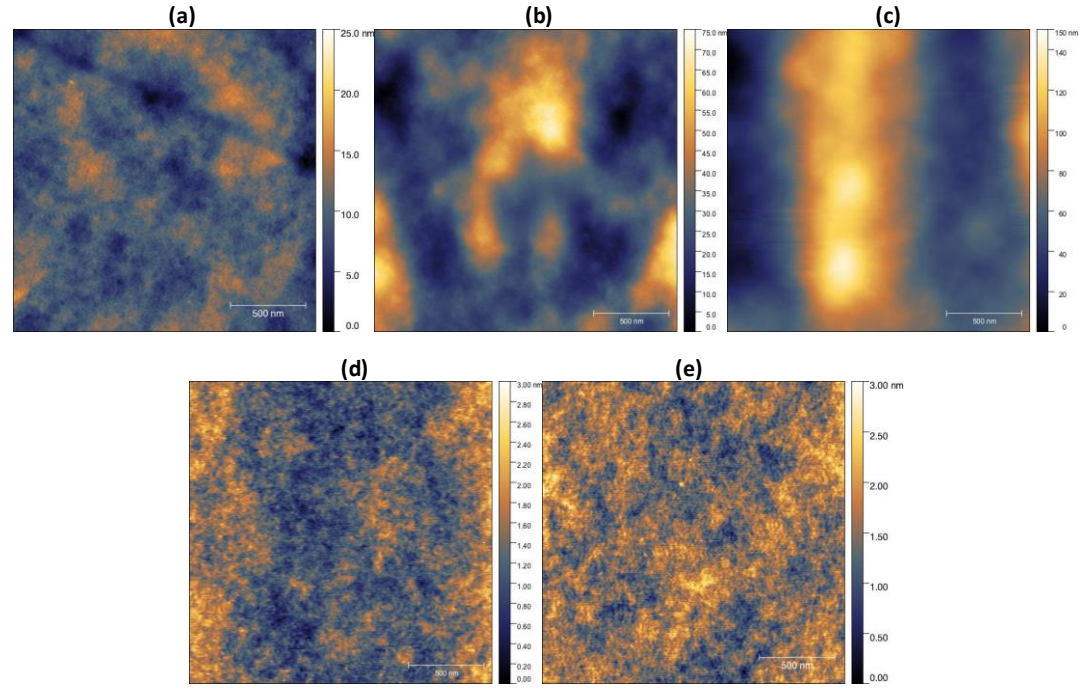

Figure 4-7. *Height, 2 µm AFM images of coatings (a) HDI-EG, (b) HDI/IPDI(90:10)-EG (c) HDI/IPDI(50:50)-EG, (d) HDI/IPDI(10:90)-EG and (e) IPDI-EG*

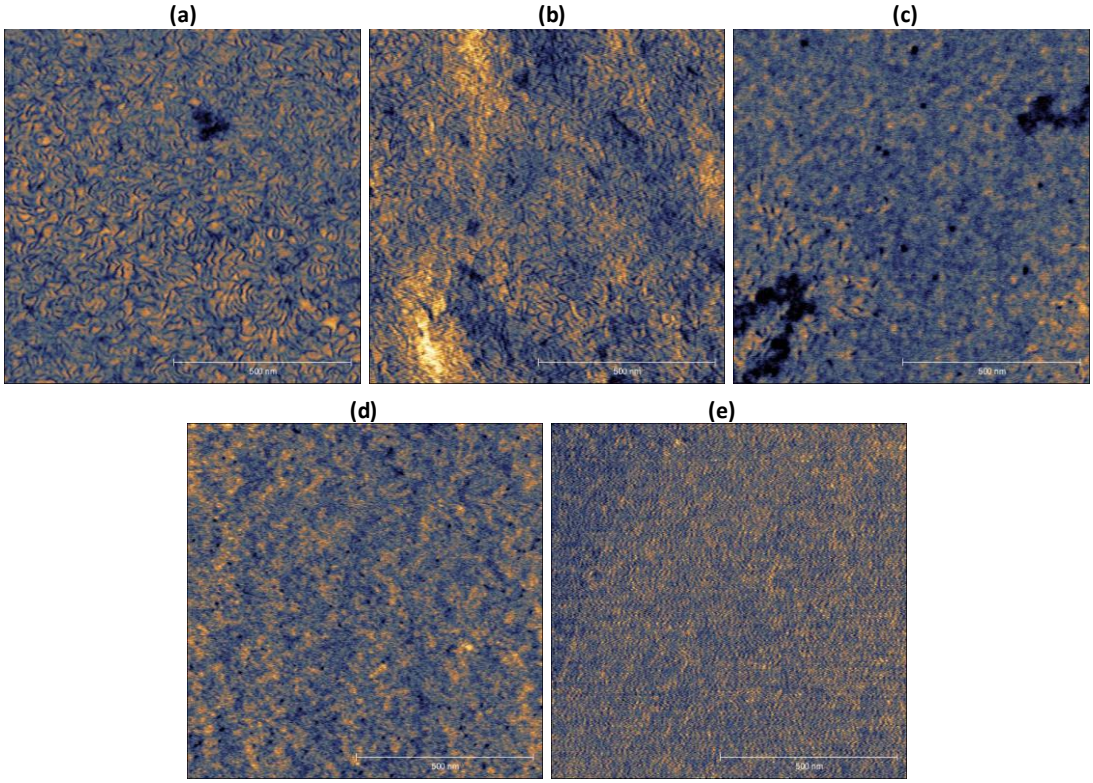

Figure 4-8. *Phase contrast, 1 µm AFM images of coatings (a) HDI-EG, (b) HDI/IPDI(90:10)-EG (c) HDI/IPDI(50:50)-EG, (d) HDI/IPDI(10:90)-EG and (e) IPDI-EG*

4.5. EVALUATION OF SELF-HEALING PROPERTIES

Two sets of samples were scratched using the automated steel wool instrument and left to heal at RT and at 60 °C. The sample prepared with HDI/IPDI (90:10) exhibited very high initial haze value, thus it was not tested to evaluate the SH properties. The percentage recovery of the other four samples (**Figure 4-9**), as well as the recorded haze values (**Table 4-5** and **Table 4-6**) are presented below.

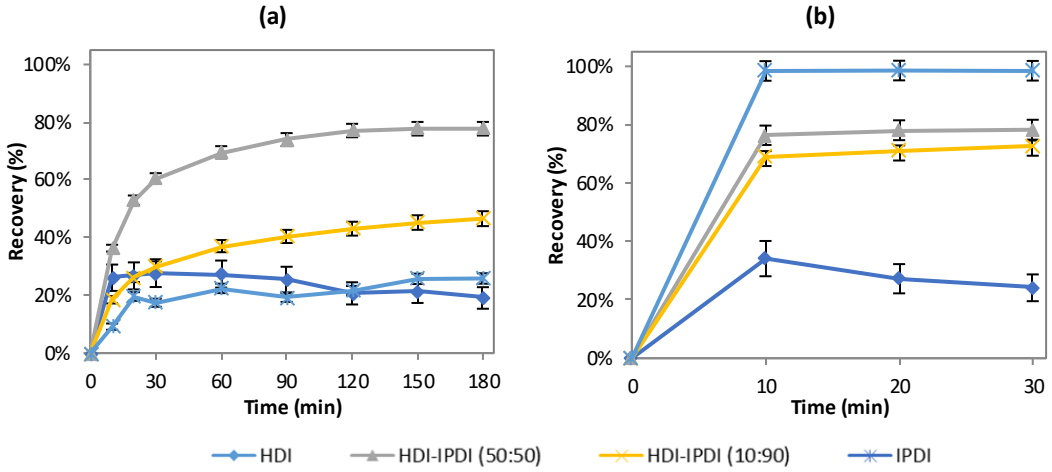

Figure 4-9. *Percentage recovery of the samples healing at (a) RT and (b) 60˚C.*

Table 4-5. *Haze values of samples tested for SH properties at RT.*

Sample	Haze									
	Initial	Scratched	10 min	20 min	30 min	60 min	90 min	120 min	150 min	180 min
HDI	0.33	1.37	1.10	1.09	1.08	1.09	1.11	1.16	1.15	1.17
HDI/IPDI(50:50)	0.29	1.35	0.96	0.79	0.71	0.61	0.56	0.53	0.52	0.52
HDI/IPDI(10:90)	0.27	3.25	2.70	2.47	2.36	2.15	2.05	1.97	1.90	1.86
IPDI	0.22	2.83	2.59	2.32	2.38	2.25	2.33	2.27	2.16	2.16

Table 4-6. *Haze values of samples tested for SH properties at 60 ˚C.*

Sample	Haze				
	Initial	Scratched	10 min	20 min	30 min
PH50-HDI-1,2-EG	0.47	1.44	1.11	1.18	1.21
PH50-HDI/IPDI(50:50)-1,2-EG	0.69	4.36	1.56	1.49	1.49
PH50-HDI/IPDI(10:90)-1,2-EG	0.37	6.68	2.32	2.20	2.09
PH50-IPDI-1,2-EG	0.24	4.88	0.32	0.31	0.31

All formulations, with the exception of the coating prepared with IPDI only, showed their glass transition below RT, therefore the SS were in their rubbery state during healing. The coating prepared with HDI only showed very limited recovery from damage at RT, reaching 30% within the first 30 minutes. The low recovery of the sample can be associated with the large extent of phase-separation of the system, reducing the mobility of polymer chains and inhibiting mixing of the phases. However, as the SS-rich phase was above the T_g, some mobility of the SS allowed limited rearrangement of the phase present by some healing. After the initial 30 minutes a slow increase of the haze of the coating (thus decrease of recovery) was observed, indicative of a slow rearrangement of the polymer matrix leading to the increase of haze.

Sample prepared with an equal number of moles of HDI and IPDI showed a very efficient healing process, reaching 75% recovery within 180 minutes. That can be explained by the mobility of SS in their rubbery state, supported by a moderate amount of phase-mixing induced by IPDI, more significant than in the sample prepared with HDI only. The coating prepared with HDI/IPDI (10:90) was found to have a smaller recovery efficiency, reaching 50% after 180 minutes. That can be related to the higher T_g, leading to reduced mobility of SS at RT.

The coating prepared with IPDI showed a small recovery of 25% after 180 minutes, associated with the SS having very limited mobility below their T_g, thus disabling rearrangement of polymer chains. However, as the onset of the T_g was observed to be below the RT, some mobility of the SS allowed limited healing of the sample.

At 60˚C all coatings were above their lower T_g, therefore the SS, SS-rich phase or the phase-mixed HS-SS blocks were in their rubbery state, allowing an efficient rearrangement of the segments. In the case of the coating prepared with HDI-only, the healing at 60 °C occurred above the lower melting point of the SS-rich phase. However, the recovery from damage at elevated temperature was not greatly improved. Therefore, the healing process at elevated temperatures can be mainly linked to the macroorganisation of HS and SS and the extent of phase-mixing. The recovery of coatings was the most significant within the first 10 minutes, after which

a recovery plateau was reached. The healing efficiency was found to increase with the increase of IPDI content and thus the extent of phase-mixing, reaching approximately 30% recovery of sample prepared with HDI only, nearly 75% recovery of samples HDI/IPDI (50:50) and HDI/IPDI (10:90) and 100% recovery of coating prepared with IPDI only.

4.6. *SUMMARY AND DISCUSSION*

The study of materials prepared with various ratios of two diisocyanates, HDI and IPDI, showed the influence of IPDI on phase-mixing between HS and SS. An increase of IPDI content resulted in a lower crystallinity level and higher T_g of SS, indicating an increased mixing of the phases. The effect was also confirmed by a shift of NH and CO peaks in the FTR AT-IR spectra, as well as by images obtained by AFM.

- **The structure of diisocyanate**. As shown in multiple studies, the increase of phase-mixing and higher T_g relate to the unsymmetrical, nonplanar and bulky structure of the IPDI.[8,19,20] The spatial arrangement urethane groups as well as the presence of three methyl groups on the cyclohexane ring hinders the alignment of the chains and prevents formation of large blocks of HS and averts crystallisation. HDI, due to the linear, symmetrical and planar structure allows easier alignment of HS, thus induces phase-separation and facilitate aggregation and crystallisation of the blocks (**Figure 4-10**).

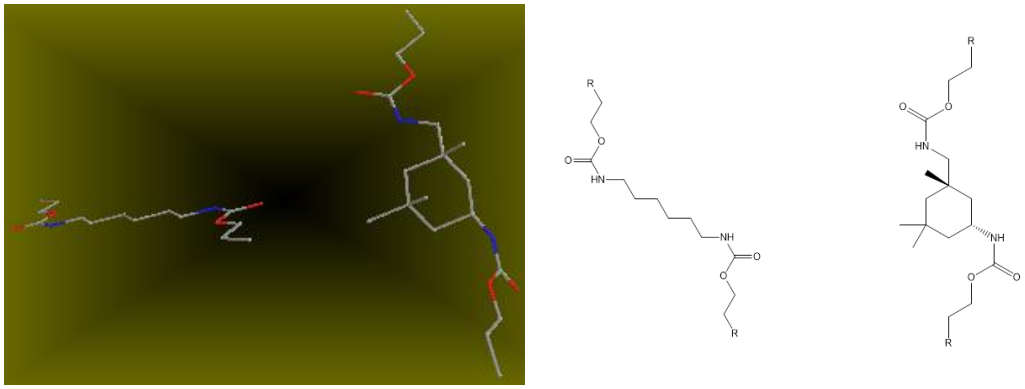

Figure 4-10. *Stick models of the linear HDI- and the bulky IPDI-based fragments of HS.*

The effect of the chemistry and the symmetry of diisocyanate on the morphology of PU is well established in the literature. However, the relationship between the morphology of transparent, protective coatings prepared with various diisocyanates and their self-healing behaviour was never studied.

The mixing of HS and SS and the low crystallinity of SS were found to be crucial to enable the movement of polymer chains during healing from damage. Coatings prepared with the extent of a linear and symmetrical HDI exhibited a phase-separated morphology, apparent by the high crystallinity of SS and low T_g of the SS-rich phase. The amorphous SS-rich phase was found to have a limited mobility and lacking the ability to fully restore the damage, even at temperatures above the T_g. That can be related to the restriction of movement induced by the crystalline regions of SS-rich phase, as well as the presence of mainly crystalline HS separated from the SS. With the increase of IPDI content, an increase of phase-mixing was observed, apparent by the decrease of crystallinity levels and an increase of the T_g. In the almost fully phase-mixed system prepared with IPDI, the mixing of phases allowed an efficient and rapid rearrangement of damaged surfaces above the T_g and almost full recovery.

Therefore, coating PH50-IPDI-EG was found to fulfil the four requirements of the research: exhibiting haze below 2%, pencil hardness of B and above, suitable T_g and thermally-triggered SH properties reaching over 90% recovery from damage.

4.7. REFERENCES

1 Z. Wirpsza, *Polyurethanes. Chemistry, Technology and Applications*, Ellis Hornwood Ltd, Midsomer Norton, 1st edn., 1993.

2 T. J. Touchet and E. M. Cosgriff-Hernandez, *Hierarchal Structure-Property Relationships of Segmented Polyurethanes*, Elsevier Ltd, 2016.

3 Merquinsa, *http://www.merquinsa.com/whats/whatsaPU.pdf*, (accessed August 2014).

4 F. C. Stehling, C. S. Speed and L. Westerman, *Macromolecules*, 1981, **14**, 698–708.

5 E. Andreassen, A. Larsen, K. Nord-Varhaug, M. Skar and H. Emptysd, *Polym. Eng. Sci.*, 2002, **42**, 1082–1097.

6 F. Sen Yen, L. L. Lin and J. L. Hong, *Macromolecules*, 1999, **32**, 3068–3079.

7 C.-C. Chang, K.-S. Chen, T. L. Yu, Y.-S. Chen, C.-L. Tsai and Y.-H. Tseng, *Polym. J.*, 1999, 31, 1205–1210.

8 C. Prisacariu, in *Polyurethane Elastomers*, Springer-Verlag, Wien, 1st edn., 2011, pp. 23–60.

9 I. M. Pereira and R. L. Oréfice, *Macromol. Symp.*, 2011, **299**–**300**, 190–198.

10 E. Princi, S. Vicini, K. Castro, D. Capitani, N. Proietti and L. Mannina, *Macromol. Chem. Phys.*, 2009, **210**, 879–889.

11 E. Ylgor, I. Ylgor and E. Yurtsever, *Polymer*, 2002, **43**, 6551–6559.

12 C. S. P. Sung and N. S. Schneider, *Macromolecules*, 1974, **8**, 68–73.

13 A. G. Strikovsky, *Macromol. Symp.*, 1995, **94**, 181–188.

14 S. M. Cakić, M. Špírková, I. S. Ristić, J. K. B-Simendić, M. M-Cincović and R. Poręba, *Mater. Chem. Phys.*, 2013, **138**, 277–285.

15 J. Mattia and P. Painter, *Macromolecules*, 2007, **40**, 1546–1554.

16 E. Cipriani, M. Zanetti, V. Brunella, L. Costa and P. Bracco, *Polym. Degrad. Stab.*, 2012, **97**, 1794–1800.

17 H. S. Lee, Y. K. Wang and S. L. Hsu, *Macromolecules*, 1987, **20**, 2089–2095.

18 S. Pongkitwitoon, R. Hernández, J. Weksler, A. Padsalgikar, T. Choi and J. Runt, *Polymer*, 2009, **50**, 6305–6311.

19 S. Sami, E. Yildirim, M. Yurtsever, E. Yurtsever, E. Yilgor, I. Yilgor and G. L. Wilkes, *Polymer*, 2014, **55**, 4563–4576.

20 C. M. Gomez, D. Gutierrez, M. Asensio, V. Costa and A. Nohales, *J. Elastomers Plast.*, 2017, **49**, 77–95.

21 I. Yilgör, E. Yilgör and G. L. Wilkes, *Polymer*, 2015, **58**, A1–A36.

22 H. Jeong, J. Park, S. Kim, J. Lee, N. Ahn and H. gyoo Roh, *Fibers Polym.*, 2013, **14**, 1082–1093.

5. THE INFLUENCE OF DIOL CHAIN EXTENDER ON MORPHOLOGY AND SELF-HEALING PROPERTIES

The adjustment of the chemistry of hard and soft segments in polyurethanes has a crucial influence on the morphology and the properties of created materials.[1]

In Chapter 3 of this thesis the effect of chemistry and the length of polyols, the SS building blocks, was explored. It was established that self-healing of polyurethane coatings requires a well phase-mixed polyurethane matrix with a high compatibility between hard and soft segments. That can be obtained by using polyols with low crystallinity and symmetry. Therefore, the polycarbonate polyol, co-polymer of pentanediol and hexanediol with MW of 500 g mol^{-1}, was chosen as the most suitable polyol to be used as a soft segment of efficiently self-healing polyurethane coatings.

In Chapter 4 the influence of the chemistry of the diisocyanate used to create the HS blocks of PU moiety was investigated. Two diisocyanates, linear and symmetrical HDI and bulky and non-symmetrical IPDI, were used to create a library of coatings with various ratios of the two mentioned isocyanates. As reported in the literature, the symmetrical HDI was found to promote phase-separation, apparent by the presence of crystallinity and low T_g of the SS-rich phase. Bulky IPDI was found to promote phase-mixing, apparent by the absence of crystallinity and higher T_g of the homogenous, phase-mixed phase composed of HS and SS. Phase-mixing of the segments was found to enable self-healing of damaged coatings, reaching 100% recovery at temperatures above their lower T_g.

It has been well established that the structure and the length of chain extenders, one of the building blocks of HS, influence the morphology of PU.[2,3] In this chapter two subsets of formulations were prepared. Each consists of six samples prepared with or without various chain extenders. The first subset was prepared with HDI to further explore the relationship between the chemistry of the segments and the properties of materials. The second subset was prepared with IPDI to explore the self-healing behaviour of well phase-mixed PU systems. The effect of the chain extender on the morphology and self-healing behaviour will be discussed in detail.

5.1. SYNTHESIS INFORMATION

The third set of formulations was designed to establish the influence of diol chain extenders on the morphology and the properties of PU coatings. All materials were prepared using the polycarbonate polyol PH50 with MW of 500 g mol^{-1}. Two subsets of formulations were prepared, one with HDI and one with IPDI. Each subset consists of six samples prepared without a chain extender, with one of aliphatic diol and with diethylene glycol (**Figure 5-1**).

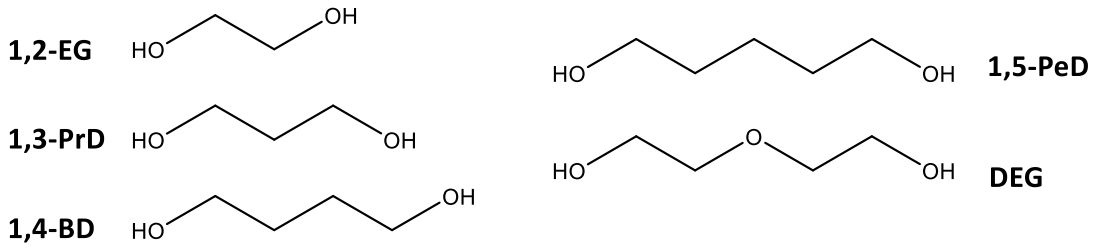

Figure 5-1. *Structures of the CE used.*

All formulations were prepared using the acetone process, using DMPA (25mol% of the total number of moles of CE) and various CE (75mol% of the total number of moles of CE), as described in Section 2.2.5. The samples were tested using various techniques immediately after preparation and drying of the coatings. Additionally, DSC and ATR FT-IR tests were repeated after 12 weeks to investigate ageing of the polymers. Samples were also tested for their stability to weathering.

5.2. CHARACTERISATION OF DISPERSIONS

Two subsets of materials were prepared – HDI-based formulations and IPDI-based formulations. Each subset has six formulations – without a chain extender, with 1,2-EG, 1,3-PrD, 1,4-BD, 1,5-PeD and 1,5-DEG. The experimental solid content of dispersions varied between 11.8% and 32.9% depending on the solubility of polymers in water and the viscosities of dispersions. The list of formulations and percentage content solid of the dispersions are presented in **Table 5-1**.

Table 5-1. *Composition and solid content of the dispersions.*

Polyurethane	Solid content (wt%)
PH50-HDI	32.9 ± 2.7
PH50-HDI-1,2-EG	27.4 ± 1.7
PH50-HDI-1,3-PrD	15.8 ± 7.5
PH50-HDI-1,4-BD	27.5 ± 2.6
PH50-HDI-1,5-PeD	11.8 ± 2.1
PH50-HDI-DEG	27.8 ± 2.8
PH50-IPDI	29.4 ± 3.1
PH50-IPDI-1,2-EG	23.1 ± 1.1
PH50-IPDI-1,3-PrD	26.8 ± 4.2
PH50-IPDI-1,4-BD	24.3 ± 1.0
PH50-IPDI-1,5-PeD	27.4 ± 3.6
PH50-IPDI-DEG	23.5 ± 1.0

5.3. CHARACTERISATION OF COATINGS

The percentage of hard segments within formulations varied from 39.0% to 52.7%, depending on diisocyanate and CE used (**Table 5-2**). The hardness of coatings varied insignificantly between HB and 2B. The cross-cut adhesion was found to be 0 for HDI-based coatings prepared with no CE, a short 1,2-EG and DEG, and 5 for coatings prepared with longer CE. The lower adhesion of the coatings prepared with longer CE was related to the increased brittleness of the samples. The cross-cut adhesion of IPDI-based samples was found to be 0 for coatings prepared with no CE and with a short 1,2-EG, and 5 for coatings prepared with longer CE. The lower adhesion of the coatings prepared with longer CE was related to the increased phase-mixing of the samples, known to reduce reinforcement from HS due to lower availability of groups able to form H-bonding.[4,5]

Table 5-2. *Characterisation of coatings.*

Polyurethane	Hard segments (%)	Pencil Hardness	Cross-Cut Adhesion	Haze
PH50-HDI	39.0	B	0	1.08
PH50-HDI-1,2-EG	45.4	HB	0	1.04
PH50-HDI-1,3-PrD	46.1	2B	5	34.83
PH50-HDI-1,4-BD	46.7	2B	5	69.00
PH50-HDI-1,5-PeD	47.3	2B	5	92.93
PH50-HDI-DEG	47.3	HB	0	0.45
PH50-IPDI	44.5	2B	0	0.21
PH50-IPDI-1,2-EG	51.2	B	0	0.77
PH50-IPDI-1,3-PrD	51.7	2B	5	0.44
PH50-IPDI-1,4-BD	52.2	B	5	0.44
PH50-IPDI-1,5-PeD	52.7	2B	5	0.60
PH50-IPDI-DEG	52.7	2B	5	0.33

All coatings prepared with IPDI exhibited very low haze values within the acceptable 0-2% haze level, indicative of low crystallinity and a phase-mixed morphology influenced by a bulky, non-symmetrical structure of the diisocyanate used.[6] Coatings prepared with HDI showed a broad scope of haze values, increasing with the length of CE. The linear and symmetrical structure of HDI facilitates packing of the polymer chains in the HS, thus promoting crystallinity and phase-separation.[7] As the HS consist of diisocyanate and CE, the length of CE will influence the size of hard blocks, and the size of the phase segments, thus increasing haze. Interestingly, the presence of heteroatom within the structure of DEG significantly lowered the haze of coatings due to disturbance of the packing of HS.

The SEM images showed a relationship between the haze and the coating's surface morphology (**Figure 5-2**). The high-haze coatings prepared with HDI showed an uneven and grainy surface. The roughness, caused by a fast crystallisation of large HS blocks close to the surface of coatings, leads to formation of regions of different refractive index and increases overall haze value.[8,9] Such an effect was not observed in more phase-mixed and amorphous coatings prepared with IPDI (**Figure 5-3**).

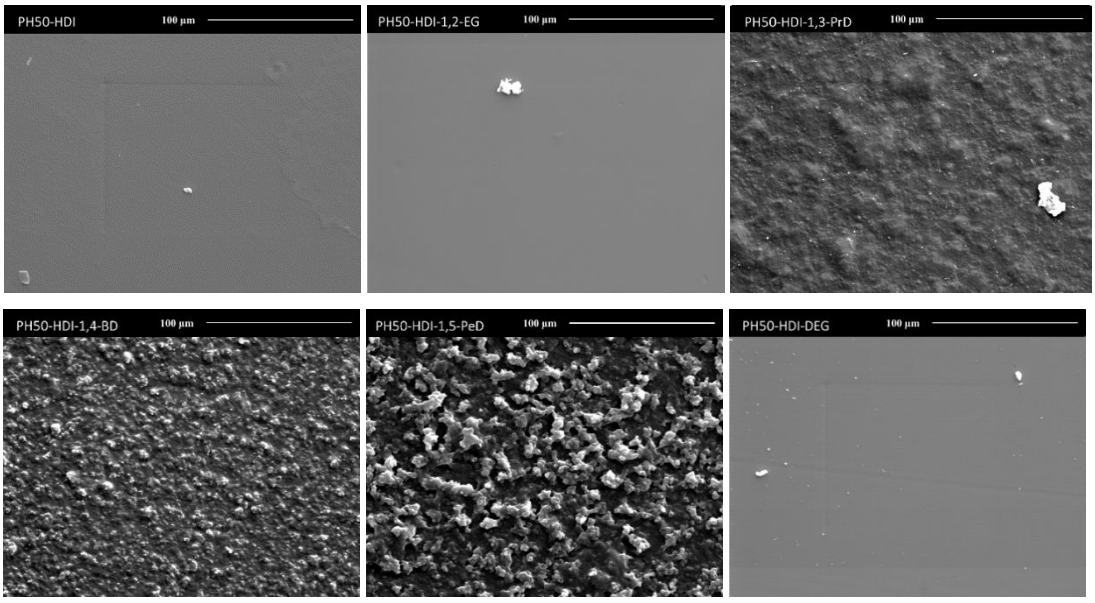

Figure 5-2. *SEM images of coatings prepared with HDI.*

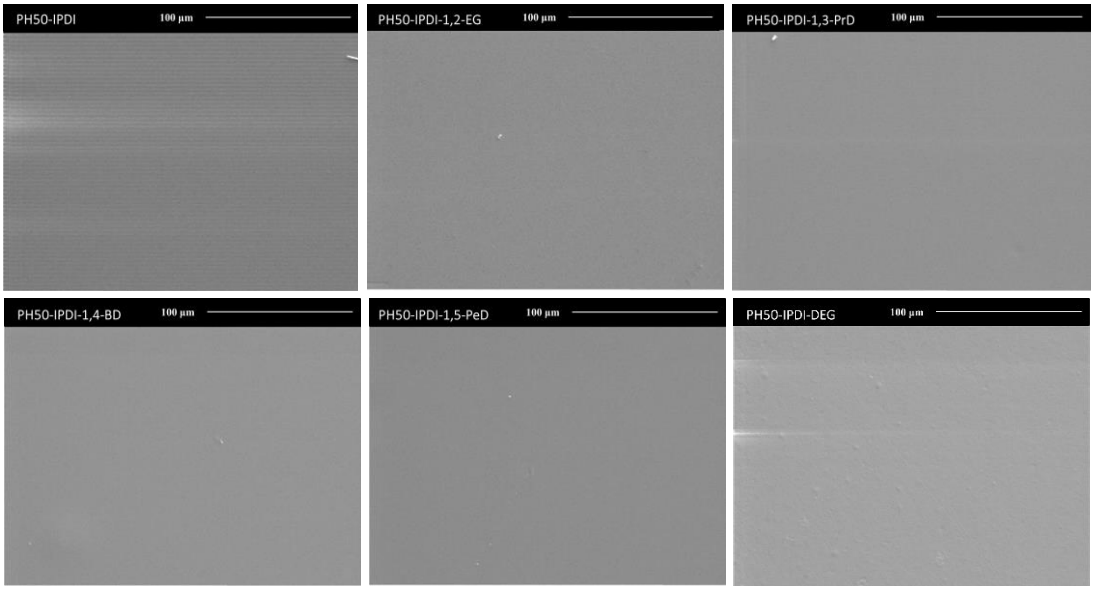

Figure 5-3. *SEM images of coatings prepared with IPDI.*

5.4. CHARACTERISATION OF COATINGS' MORPHOLOGIES

Figure 5-4 presents FT-IR spectra of the two sets of coatings. Among the important signals, a broad NH stretch can be observed between 3500 cm^{-1} and 3250 cm^{-1}, CH_2 stretches at 2935 cm^{-1} and 2860 cm^{-1}, and a broad peak between 3500 cm^{-1} and 2250 cm^{-1} assigned to carboxylic acid. Furthermore, multiple carbonyl stretches between 1740 cm^{-1} and 1650 cm^{-1}, C-N stretch and NH bend between 1600 cm^{-1}, and several CH signals below 1500 cm^{-1} can be observed.[10]

Both sets of samples show a small amount of non-H-bonded NH groups of urethane, present as a shoulder peak at 3500-3400 cm^{-1} (**Figure 5-5**), suggesting that most of the NH groups are involved into H-bonding (**Table 5-3**). Samples prepared with HDI and various CE showed a sharp, narrow NH stretch signals in the 3350-3300 cm^{-1} region, indicating the excess of HS-HS interactions and hence phase-separation of the systems. The sample prepared without CE showed a smaller, less sharp peak at a marginally higher wavenumber, confirming that the presence of CE promotes phase-separation. While the NH signal of the coatings prepared with 1,3-PrD, 1,4-BD and 1,5-PeD are very similar and occur at 3325 cm^{-1}, the sample prepared with 1,2-EG shows an additional peak at 3345 cm^{-1}.[6] The presence of two peaks indicates two

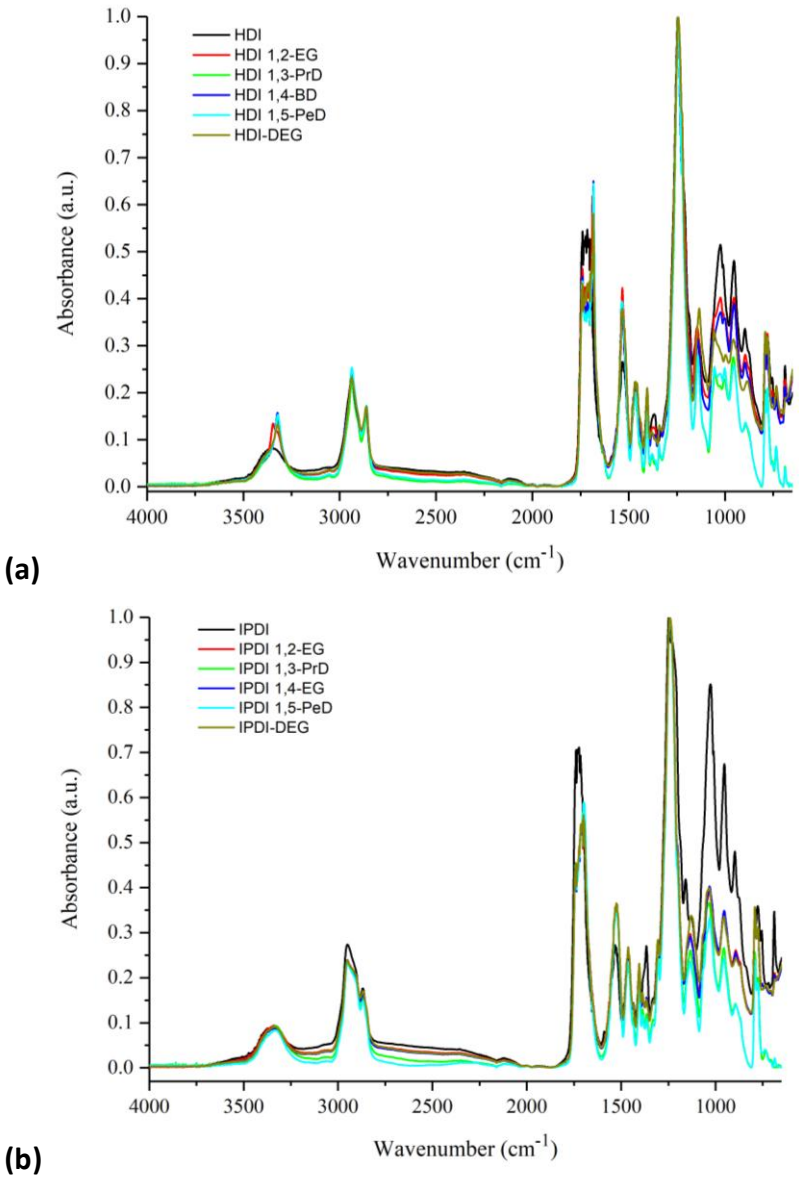

***Figure 5-4**. ATR FT-IR spectra of (a) HDI based coatings and (b) IPDI based coatings.*

distinct structures of HS within the matrix of the polymer, while the remaining formulations have more heterogenous structure. Interestingly, the low haze coating prepared with DEG shows significantly larger NH shoulder peak at 3380 cm^{-1} associated with phase-mixing, influenced by the presence of the heteroatom within the structure of the CE.

Samples prepared with IPDI showed a broader urethane NH stretch peak with a more prominent shoulder at 3400-3350 cm^{-1}, indicating mainly the presence of HS-SS interactions and phase-mixing. The variation of the length and the structure of CE

was not found to influence the interactions between HS and SS within the IPDI-based materials. However, the sample prepared without a CE showed a smaller, less sharp peak at a marginally higher wavenumber.

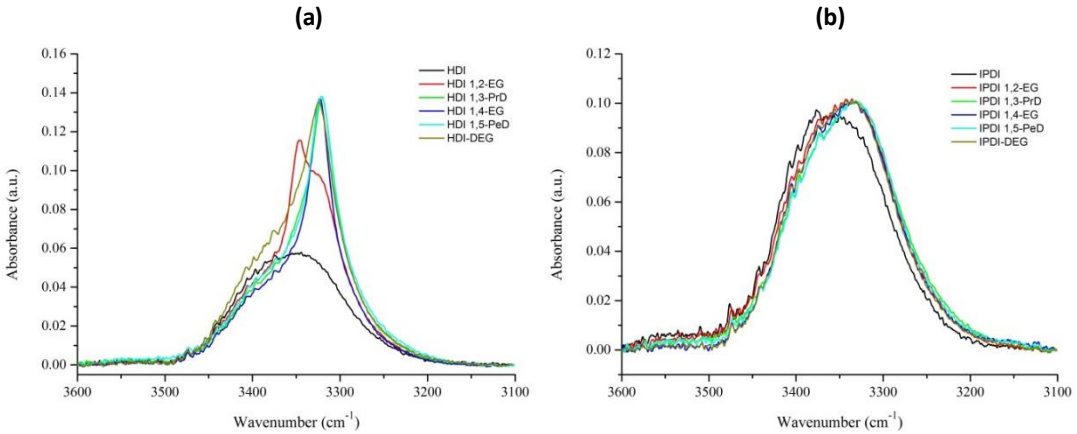

Figure 5-5. *The NH region of ATR FT-IR spectra of samples prepared with (a) HDI and (b) IPDI.*

Table 5-3. *Characteristic IR bands for phase-mixed and phase-separated systems.*[10,11]

Wavenumber (cm^{-1})	**Functional group ($\bar{\upsilon}$ – stretching, δ – bending)**	**Group assignment**	**Morphology**
3500-3400	$\bar{\upsilon}$(NH) free	Urethane/Urea	Free
3400-3350	$\bar{\upsilon}$(NH) bonded	Urethane	Phase-mixed
3350-3300	$\bar{\upsilon}$(NH) bonded	Urethane	Phase-separated
3340-3320	$\bar{\upsilon}$(NH) bonded, bidentate	Urea	Phase-separated
3240	$\bar{\upsilon}$(NH) bonded, monodentate	Urea	Phase-separated
1743	$\bar{\upsilon}$(C=O) free	Polyol	Free
1740-1730	$\bar{\upsilon}$(C=O) bonded	Polyol	Phase-mixed
1733-1730	$\bar{\upsilon}$(C=O) free	Urethane	Free
1723-1705	$\bar{\upsilon}$(C=O) bonded	Urethane	Phase-mixed
1700-1683	$\bar{\upsilon}$(C=O) bonded	Urethane	Phase-separated
1700-1680	$\bar{\upsilon}$(C=O) free	Urea	Free
1660-1635	$\bar{\upsilon}$(C=O) bonded, monodentate	Urea	Phase-mixed
1616-1627	$\bar{\upsilon}$(C=O) bonded, bidentate	Urea	Phase-separated
1580-1576	$\bar{\upsilon}$(CN) + δ(NH) bonded, bidentate	Urea	Phase-separated
1570-1554	$\bar{\upsilon}$(CN) + δ(NH) bonded, monodentate	Urea	Phase-mixed
1539-1530	$\bar{\upsilon}$(CN) + δ(NH) bonded	Urethane	Phase-separated
1526-1507	$\bar{\upsilon}$(CN) + δ(NH) bonded	Urethane	Phase-mixed

In the carbonyl region, the peak at 1743 cm^{-1} can be assigned to a non-H-bonded CO stretch of SS, while the peak at 1740-1730 cm^{-1} shows the loosely H-bonded carbonyl of phase-mixed SS (**Figure 5-6**). In the spectra of coatings prepared with HDI and various CE the largest peak at 1680 cm^{-1} can be associated with HS-HS interactions of urethane groups, indicating a large extent of phase-separation. The peaks in the 1725-1700 cm^{-1} region, associated with a phase-mixed morphology, are significantly

smaller.[11] Interestingly, similarly to the NH region, the coating prepared with EG shows a second peak in the phase-separated CO stretch region, at 1690 cm^{-1}. In the spectrum of coating prepared without a CE the peak at 1680 cm^{-1} is not present, while the peaks in the 1725-1700 cm^{-1} region are larger, thus confirming the phase-separation promoting nature of CE. The effect of the presence of CE can be also seen in the C-N stretch and NH bend region (1550-1500 cm^{-1}), with the peak of the sample prepared without CE being broader and less sharp compared to the samples prepared with various CE.

In the spectra of coatings prepared with IPDI and various CE the peaks in the 1720-1700 cm^{-1} region, associated with HS-SS interactions of phase-mixed urethane groups, are significantly larger than in the spectra of HDI-based materials. The peaks in the 1700-1680 cm^{-1} region, associated with HS-HS interactions of phase-separated urethane groups, are smaller than in spectra of HDI-based materials. Additionally, similarly to the NH region of the spectra, the peaks in this region of the sample prepared without CE are significantly smaller, indicating even larger extent of phase-mixing due to the smaller amount of HS.

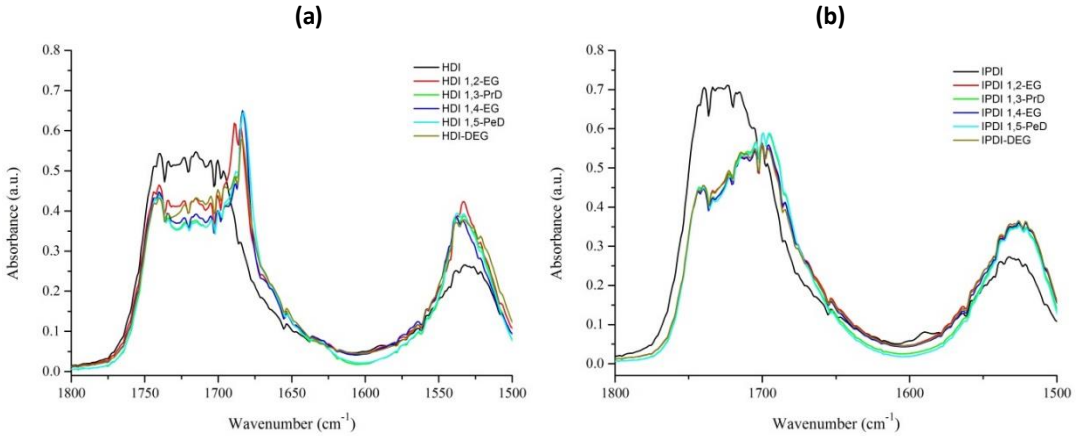

***Figure 5-6**. The carbonyl region of ATR FT-IR spectra of samples prepared with (a) HDI and (b) IPDI.*

DSC plots of coatings prepared with HDI are presented in **Figure 5-7**. The T_g of SS of all samples were found to be below 0 °C, varying from -22 °C to -17 °C in the first heat cycle and from -17 °C to -8 °C in the second (**Table 5-4**). The samples showed higher T_g than the one of pure polyol PH50 (-69 °C) due to the restriction of mobility as a consequence of the polymerisation.[12] In the second cycle, T_g values were found

mostly to decrease with the increase of the CE length. The T_g is that of the amorphous region of the SS-rich phase and lower values are associated with increased phase-separation, induced by longer chain extenders forming larger HS.[2] The samples prepared without CE or with DEG show a deviation from this trend due to increased phase-mixing after the thermal cycling.

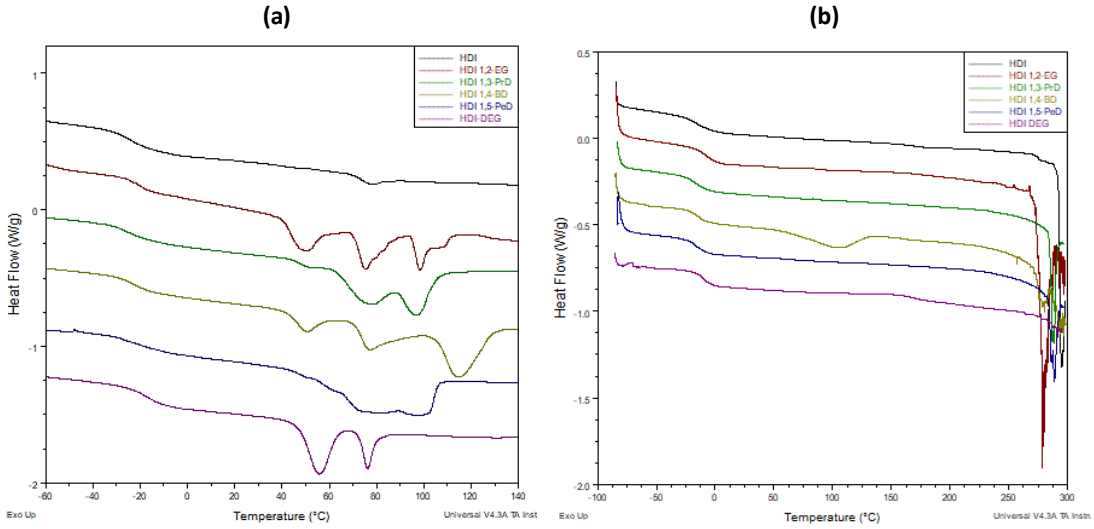

Figure 5-7. *DSC curves of coatings prepared with HDI: (a) first heating cycle and (b) second heating cycle.*

Multiple melting endotherms observed in the first heat cycle of all samples can be associated with crystalline regions of semi-crystalline SS-rich phase. The smallest enthalpy of melting was observed for the formulation prepared without CE, with the enthalpy of 1.8 J g^{-1} (the equivalent of 3.0 J g^{-1} of polyol), indicative of a more phase-mixed and hence less crystalline morphology. The low enthalpy of melting of the single endotherm present at a similar temperature to the one of pure polyol can be related to the smaller amount of HS able to disperse within SS-rich phase and change the properties of the phase.[13] The remaining samples showed multiple endotherms with the enthalpies significantly larger than the enthalpy of melting of the pure polyol, reflecting the influence of larger HS blocks 'dissolved' within the SS-rich phase, in small amount capable to disturb the crystallinity of the SS-rich phase apparent by the endotherms with depressed melting temperature, and in larger amounts able to form more homogenous, phase-mixed blocks, apparent by the endotherms at higher temperatures.[14]

Interestingly, in the second heat cycle, only the sample prepared with 1,4-BD shows cold crystallisation and melting. The behaviour can be explained by the presence of 1,4-BD particularly known to promote phase-separation.[3] All samples showed a second glass transition at approximately 165 °C, associated with the amorphous regions of HS. However, the transition is not well defined, suggesting a small amount of amorphous HS present in the PU. The presence of crystalline regions of HS is apparent by the large melting endotherms at temperatures above 275 °C.

Formulations prepared with IPDI showed broader glass transition of SS at significantly higher temperatures, varying from 4˚C to 36˚C in the first heat cycle and 19˚C to 36˚C in the second (**Figure 5-8**). The increase of the breadth and the temperature indicates a larger extent of phase-mixing of homogenously mixed, partially compatible blocks of HS and SS.[14] The formulation prepared without any CE was found to have the lowest T_g due to the smallest percentage of HS and less HS-SS interactions. The variation of T_g in the first heat cycle reflects the influence of a thermal history on the samples. However, in the second cycle, T_g values were found mostly to decrease with the increase of the CE length. The T_g is that of the amorphous region of the mixed SS-HS phase and higher temperatures are associated with longer chain extenders forming larger HS and increasing the overall transition temperature.[2]

The samples showed small and broad melting peaks in the first heat cycle, between 84 °C and 123 °C, associated with the homogenous HS-SS phase. The temperatures

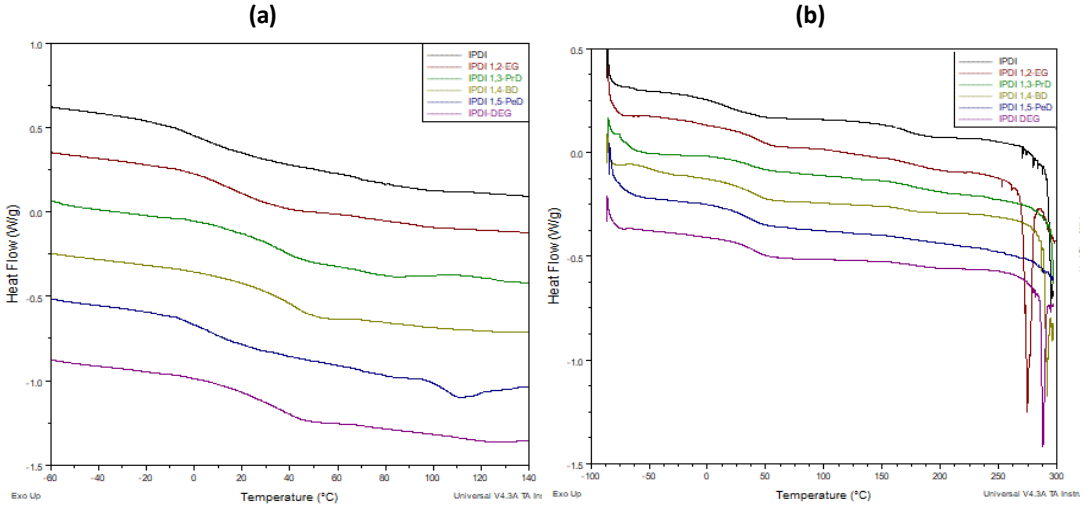

Figure 5-8. *DSC curves of coatings prepared with IPDI: (a) first heating cycle and (b) second heating cycle.*

of the endotherms were found to mainly increase with the increase of the CE length, reflecting the influence of the size of the HS blocks. The enthalpy of melting was smaller than the one of pure polyol for all samples but PH50-IPDI-1,5-PeD, forming the largest HS blocks and increasing the enthalpy of melting. The absence of melting peaks in the second cycle indicates a mainly amorphous morphology of SS, caused by the bulky isocyanate preventing crystallisation of SS in the phase-mixed region.

All samples showed a second glass transition in the 165 °C to 180 °C region, associated with the amorphous regions of HS. However, the transition is not well defined, suggesting a small amount of amorphous HS present in the PU. The presence of crystalline regions of HS is apparent by the large melting endotherms at temperatures above 275 °C.[14] The summary of data obtained from DSC is presented below.

Table 5-4. *The DSC data obtained from histograms (the ΔH_m values in the brackets represent the recalculated enthalpy in J per gram of polyol within the formulation).*

PU	Heat 1			Heat 2		
	T_g (°C)	T_m (°C)	ΔH_m (J/g)	T_g (°C)	T_m (°C)	ΔH_m (J/g)
PH50	-69	74	7.5	-67	-	-
PH50-HDI	-22	77	1.8 [3.0]	-14 168	294	-
PH50-HDI-1,2-EG	-21	49 75 98 108	29.4 [53.8]	-8 169	278	-
PH50-HDI-1,3-PrD	-21	64 95	35.6 [66.0]	-11 169	288	-
PH50-HDI-1,4-BD	-22	50 77 114	41.2 [77.3]	-15 168	106 280	21.0 [39.4] -
PH50-HDI-1,5-PeD	-21	55 99	36.0 [68.3]	-17 167	289	-
PH50-HDI-DEG	-17	56 76	18.2 [34.5]	-11 165	292	-
PH50-IPDI	4	95	3.7 [6.7]	19 171	295	-
PH50-IPDI-1,2-EG	17	98	2.3 [4.7]	31 181	275	-
PH50-IPDI-1,3-PrD	31	84	2.8 [5.8]	33 176	294	-
PH50-IPDI-1,4-BD	36	99	2.3 [4.8]	35 172	281	-
PH50-IPDI-1,5-PeD	7	110	5.8 [12.3]	32 162	299	-
PH50-IPDI-DEG	28	123	1.0 [2.1]	36 172	279	-

5.5. EVALUATION OF SELF-HEALING PROPERTIES

SH efficiency tests performed on the first set of samples prepared with HDI are presented below, with the percentage recovery graphs shown in **Figure 5-9**. The recovery of samples prepared with HDI and 1,3-PrD, 1,4-BD and 1,5-PeD can be neglected due to very high initial haze which renders them unsuitable for optical coatings. However, their measured haze values are shown in **Table 5-5** and **Table 5-6**.

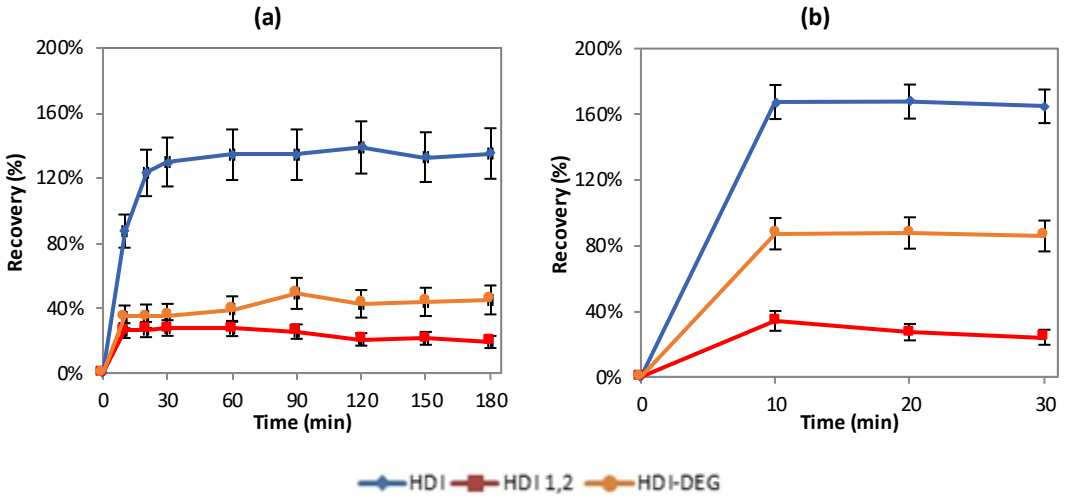

Figure 5-9. *Percentage recovery of samples prepared with HDI at (a) RT and (b) 60˚C.*

Table 5-5. *Haze values of HDI-based coatings healed at room temperature.*

Sample	Haze									
	Initial	Scratched	10 min	20 min	30 min	60 min	90 min	120 min	150 min	180 min
HDI	1.08	1.53	1.14	0.98	0.95	0.93	0.93	0.91	0.94	0.93
HDI-1,2-EG	0.33	1.37	1.10	1.09	1.08	1.09	1.11	1.16	1.15	1.17
HDI-1,3-PrD	34.83	26.77	25.13	25.03	25.03	24.97	24.87	24.90	24.83	24.67
HDI-1,4-BD	69.00	65.60	65.70	65.60	65.60	65.67	65.73	65.67	65.70	65.97
HDI-1,5-PeD	92.93	92.20	92.20	92.07	92.13	92.43	92.20	92.23	92.20	92.23
HDI-DEG	0.45	1.28	1.00	0.99	0.99	0.96	0.88	0.93	0.92	0.91

Table 5-6. *Haze values of HDI-based coatings healed at 60 ˚C.*

Sample	Haze				
	Initial	Scratched	10 min	20 min	30 min
HDI	1.88	3.15	1.02	1.02	1.05
HDI-1,2-EG	0.47	1.44	1.11	1.18	1.21
HDI-1,3-PrD	37.73	32.40	30.97	30.83	30.67
HDI-1,4-BD	68.73	64.90	64.93	64.87	65.20
HDI-1,5-PeD	92.40	92.37	92.37	92.33	92.27
HDI-DEG	0.40	1.13	0.49	0.49	0.50

Healing of the three HDI-based materials occurred readily, both at RT and 60˚C, as the coatings were above the T_g of the SS-rich phase. The sample prepared without CE showed the highest recovery, due to the higher amount of phase-mixing that maximises the HS-SS H-bonding interactions driving the healing, whilst lowering HS segment sizes and SS crystalline content, which would otherwise act as physical cross-links, limiting mobility. The coating obtained recoveries of up to 150% at RT and 165% at 60 °C, thus exhibiting even lower haze after healing than before scratching due to the efficient rearrangement of polymer chains.

The coating prepared with DEG, due to the higher amount of phase-separation, had a more limited recovery efficiency of approximately 50% at RT and 90% at elevated temperature. The significant difference between healing at RT and 60 °C can be associated with the healing at elevated temperature occurring above the melting point of the sample prepared with DEG and the efficient rearrangement of the molten SS-rich phase. Such effect was not seen for the sample prepared without a CE, reflecting the effect of DEG on phase-mixing of the phases.

The coating prepared with 1,2-EG, showing most phase-separation, recovered only 25% of the original haze value at RT and 34% at elevated temperature. Interestingly, the coating prepared with 1,2-EG showed a small decrease in recovery after the initial healing, which indicates an increase of crystallinity through annealing at the elevated temperature. The recovery of coatings appeared to be the largest within the first 30 minutes of healing at RT, and within the first 10 minutes at 60 °C.

SH efficiency tests performed on the second set of samples prepared with IPDI are presented below, with the percentage recovery graphs shown in **Figure 5-10**, while the measured haze values are shown in **Table 5-6** and **Table 5-8**.

Coatings prepared with IPDI showed only limited recovery from scratches at RT. As with the HDI-based formulations, the most efficient healing, reaching up to 54% within 180 minutes, was observed for the coating prepared without CE. Again, this is due to the high amount of phase-mixing that maximises the HS-SS hydrogen-bonding interactions and lowers the size of HS segments that restrict molecular motion.

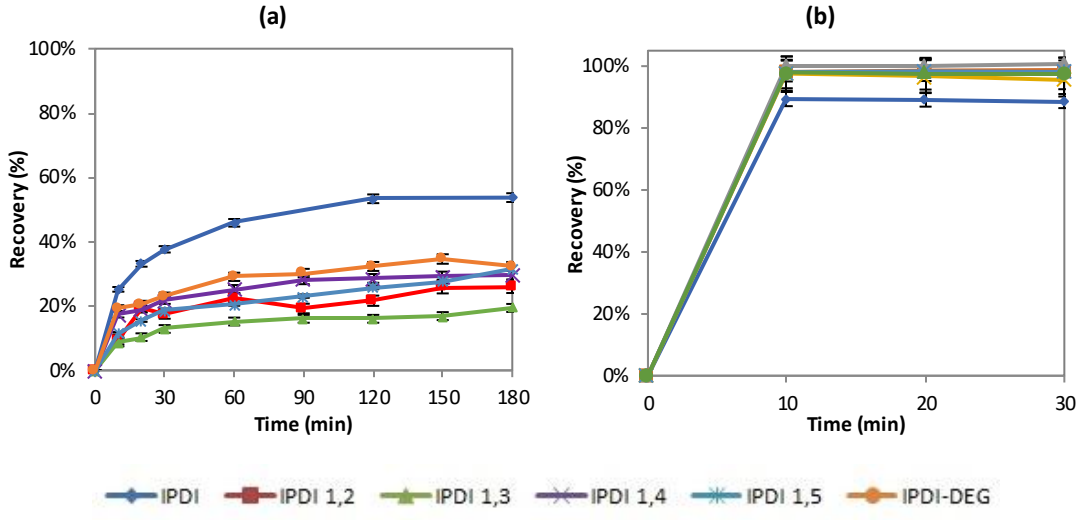

Figure 5-10. *Percentage recovery of samples prepared with IPDI at (a) RT and (b) 60˚C.*

Table 5-7. *Haze values of IPDI-based coatings healed at room temperature.*

Sample	Haze									
	Initial	Scratched	10 min	20 min	30 min	60 min	90 min	120 min	150 min	180 min
IPDI	0.21	6.64	5.02	4.51	4.22	3.69	-	3.21	-	3.18
IPDI-1,2-EG	0.22	2.83	2.59	2.32	2.38	2.25	2.33	2.27	2.16	2.16
IPDI-1,3-PrD	0.44	16.23	14.87	14.60	14.20	13.83	13.70	13.70	13.57	13.17
IPDI-1,4-BD	0.44	4.17	3.52	3.46	3.36	3.23	3.12	3.11	3.08	3.07
IPDI-1,5-PeD	0.60	8.86	7.90	7.58	7.31	7.16	6.95	6.73	6.58	6.25
IPDI-DEG	0.33	4.36	3.58	3.53	3.43	3.19	3.14	3.06	2.96	3.06

Table 5-8. *Haze values of IPDI-based coatings healed at 60 ˚C.*

Sample	Haze				
	Initial	Scratched	10 min	20 min	30 min
IPDI	0.27	6.48	0.93	0.94	0.97
IPDI-1,2-EG	0.24	4.88	0.32	0.31	0.31
IPDI-1,3-PrD	0.58	8.55	0.58	0.55	0.53
IPDI-1,4-BD	0.31	3.11	0.38	0.40	0.44
IPDI-1,5-PeD	0.57	13.30	0.81	0.78	0.79
IPDI-DEG	0.33	3.35	0.39	0.40	0.40

In the phase-mixed IPDI formulations crystallisation of the homogenous HS-SS phase is also largely supressed, as the DSC data shows. Recovery at RT is more limited than in the HDI formulations due to the higher T_g of the better phase-mixed systems. However, as the onset of the broad glass transition occurs below RT, some mobility of the homogenous phase occurs, thus some recovery from damage can be observed, reaching between 20 and 32%.

At 60˚C, all the IPDI-based samples showed almost full recovery, reaching 98% recovery for samples prepared with the various CEs, and 89% recovery for the coating without CE. The significant improvement of the healing properties at elevated temperatures can be explained by the healing process taking place above the lower T_g, allowing the polymer chains to move and rearrange freely.

5.6. *AGEING AND WEATHERING OF POLYMERS*

The haze value of selected samples measured after 12 weeks was found to somewhat increase, indicative of continued rearrangement of the phase-mixed polymer matrices and increase of phase-separation (**Table 5-9**). The largest change is observed for HDI-based samples prepared without CE and with DEG. The significant increase of the haze value of the sample prepared without CE can be associated with the low crystallinity of the SS-rich phase as well as the low T_g, enabling rearrangement of the polymer chains at RT and increase of phase-separation. Similarly, the sample prepared with DEG exhibited low T_g but higher crystallinity, thus the increase of the haze value is smaller.

Table 5-9. *Change in haze of samples over 12 weeks*

Polyurethane	Haze – original (%)	Haze – 12 weeks (%)
PH50-HDI	1.08	7.77
PH50-HDI-1,2-EG	1.04	1.57
PH50-HDI-1,3-PrD	34.83	-
PH50-HDI-1,4-BD	69.00	71.53
PH50-HDI-1,5-PeD	92.93	-
PH50-HDI-DEG	0.45	1.51
PH50-IPDI	0.21	1.16
PH50-IPDI-1,2-EG	0.77	0.94
PH50-IPDI-1,3-PrD	0.44	-
PH50-IPDI-1,4-BD	0.44	1.34
PH50-IPDI-1,5-PeD	0.60	-
PH50-IPDI-DEG	0.33	1.05

The samples that showed a moderate increase in the haze values did not show any changes in the ATR FT-IR spectra taken after 12 weeks. However, the PH50-HDI and PH50-HDI-DEG samples showed significant changes in the amine stretch and carbonyl stretch signals. The coatings showed a narrowing of the amine stretch signal due to

a combined effect of a decrease of a stretch of phase-mixed NH groups at 3375 cm^{-1} and an increase of a stretch of phase-separated NH groups at 3325 cm^{-1}, consistent with the increase of haze (**Figure 5-11**).[6]

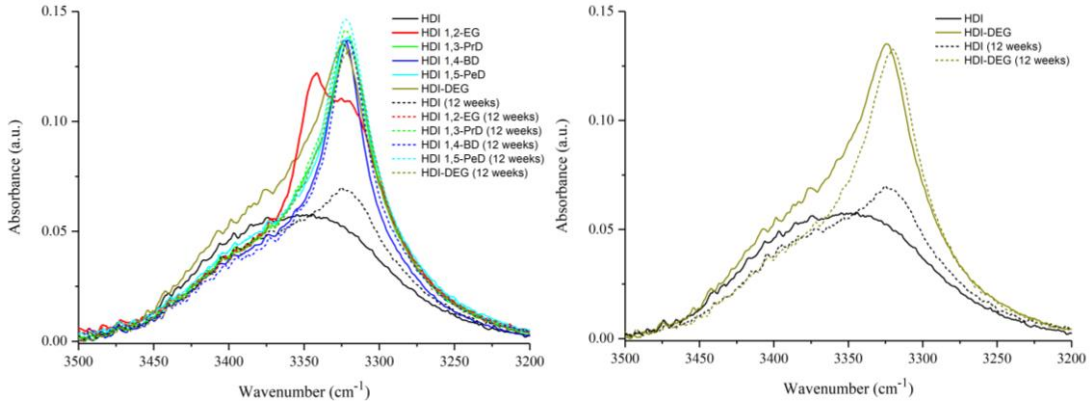

Figure 5-11. *ATR FT-IR NH region of original (solid line) and aged (dotted line) HDI-based coatings.*

In the carbonyl stretch region an increase in intensity of the HS-HS signal at 1700-1680 cm^{-1} and decrease of HS-SS signal 1720-1700 cm^{-1} of PH50-HDI and PH50-HDI-DEG samples was observed (**Figure 5-12**). That confirms the increase of phase-separation over time, leading to bigger segment sizes, higher crystallinity and haze.[6]

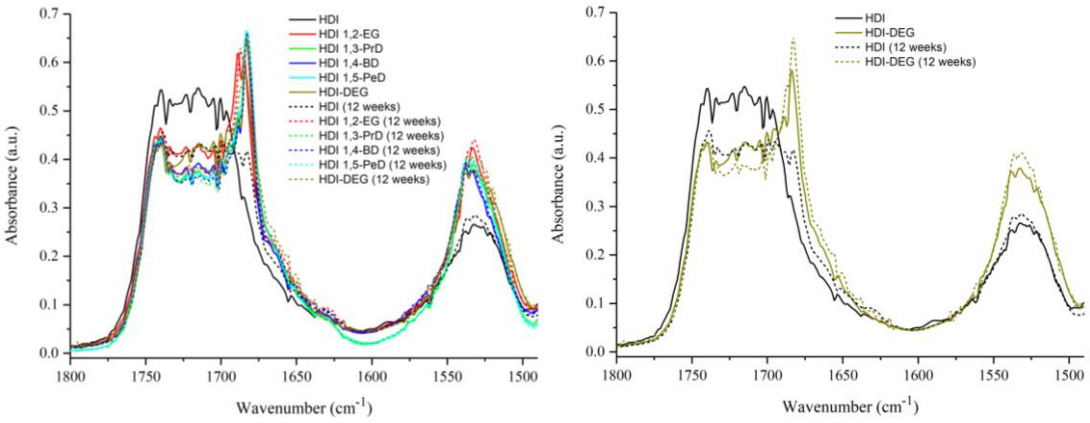

Figure 5-12. *ATR FT-IR carbonyl region of original (solid) and aged (dotted line) HDI-based coatings.*

The samples prepared with IPDI did not show any significant changes in their ATR FT-IR spectra, confirming lower mobility and higher morphological stability of the polymers at RT (**Figure 5-13**).

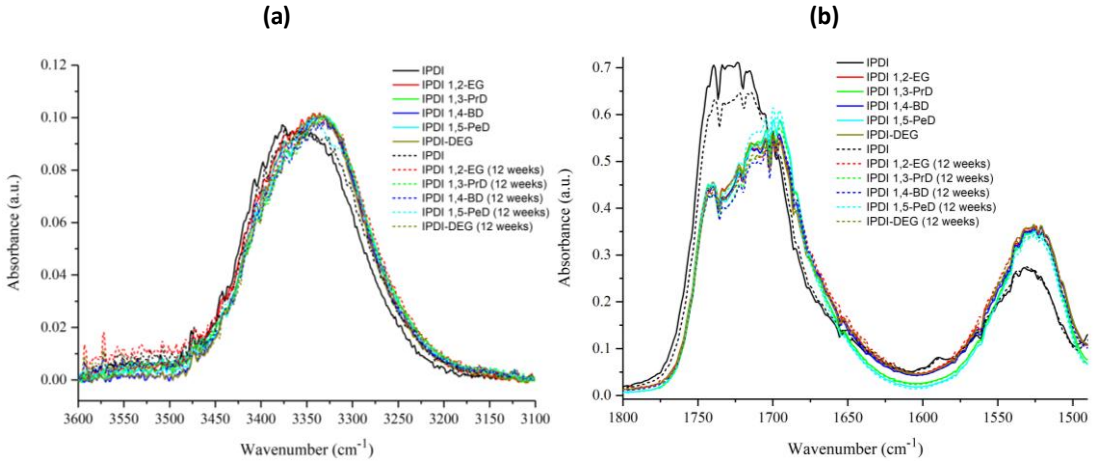

Figure 5-13. *ATR FT-IR spectra of original (solid) and aged (dotted line) IPDI-based coatings: (a) amine stretch and (b) carbonyl stretch region.*

The DSC analysis of HDI-based samples after 12 weeks did not show any significant changes in their T_g (**Figure 5-14**). However, the samples showed a shift and change in the number of melting peaks, indicative of continuous rearrangement of the SS-rich phase, enabled by the low T_g below RT. While the overall melting enthalpy of majority of samples remained unchanged, the more phase-mixed samples PH50-HDI and PH50-HDI-DEG showed a large increase in enthalpies of melting, related to the increase of phase-separation over time, leading to bigger segment sizes, higher crystallinity and haze (**Table 5-10**).

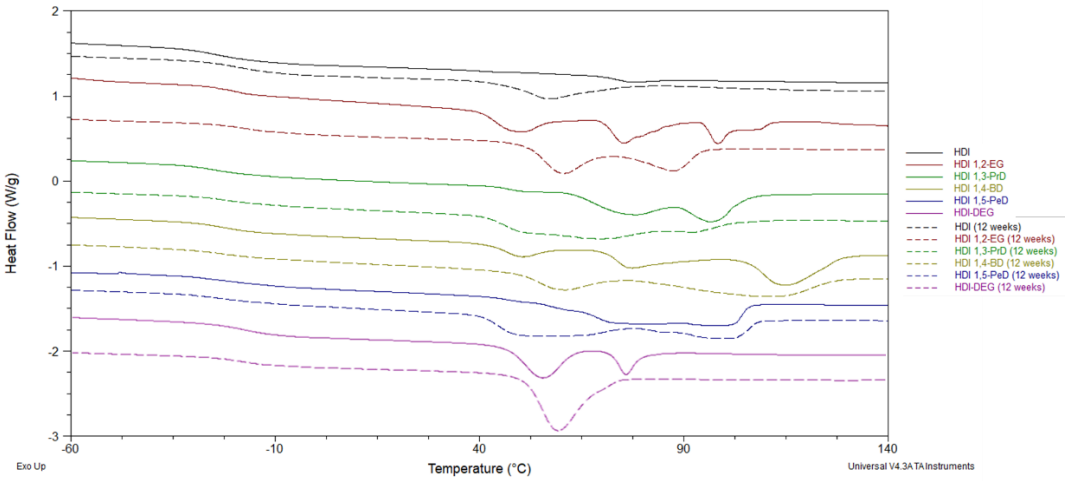

Figure 5-14. *DSC curves of HDI-based coatings tested after 12 weeks, first heat cycle.*

***Table 5-10**. DSC characterisation data of HDI-based samples.*

PU	T_g (°C)				T_m (°C)				ΔH_m (J/g)			
	0 weeks		12 weeks		0 weeks		12 weeks		0 weeks		12 weeks	
	H1	H2	H1	H2	H1	H2	H1	H2	H1	H2	H1	H2
HDI	-22	-14	-19	-13	77	-	58	-	1.8	-	11.0	
HDI-1,2EG	-21	-8	-16	-7	49 75 98 108	-	60 85	-	29.4	-	29.6	-
HDI-1,3PrD	-21	-11	-21	-13	64 95	-	50 69 93	-	35.6	-	35.5	-
HDI-1,4BD	-22	-15	-21	-17	50 77 114	106	61 110	109	41.2	21.0	39.4	22.1
HDI-1,5PeD	-21	-17	-23	-16	55 99	-	51 84 98	-	36.0	-	37.7	-
HDI-DEG	-17	-11	-18	-10	56 76	-	60	-	18.2	-	26.0	-

Samples prepared with IPDI showed minimal changes in the melting temperature (**Figure 5-15**) and enthalpy (**Table 5-11**), showing high morphological stability of the systems at RT.

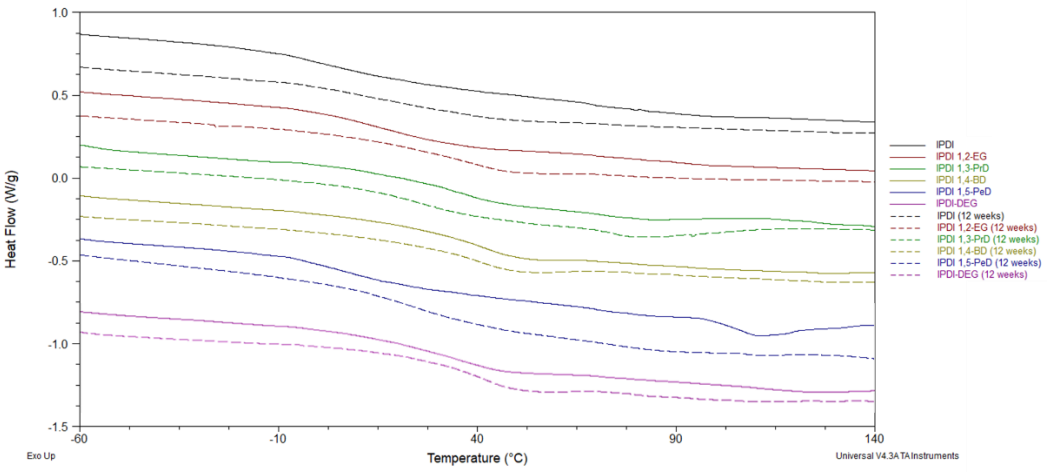

***Figure 5-15.** DSC curves of HDI-based coatings tested after 12 weeks, first heat cycle.*

***Table 5-11**. DSC characterisation data of IPDI-based samples.*

PU	T_g (°C)				T_m (°C)				ΔH_m (J/g)			
	0 weeks		12 weeks		0 weeks		12 weeks		0 weeks		12 weeks	
	H1	H2	H1	H2	H1	H2	H1	H2	H1	H2	H1	H2
IPDI	4	19	20	23	95	-	-	-	3.7	-	-	-
IPDI-1,2EG	17	31	30	32	98	-	95	-	2.3	-	1.1	-
IPDI-1,3PrD	31	33	24	33	84	-	80	-	2.8	-	5.6	-
IPDI-1,4BD	36	35	32	30	99	-	-	-	2.3	-	-	-
IPDI-1,5PeD	7	32	22	31	110	-	89	-	5.8	-	3.8	-
IPDI-DEG	28	36	37	34	123	-	107	-	1.0	-	3.0	-

The SH tests of HDI-based samples performed after 12 weeks showed some small differences in the recovery profiles at RT (**Figure 5-16**). The recovery of sample prepared without CE did not exceed 100% due to higher original haze value (**Table 5-12**). The coating prepared with DEG showed significantly lower recovery, associated with the increased phase-mixing developed over the 12 weeks. The coating PH50-HDI-1,2-EG showed similar healing profile reaching up to 20% recovery.

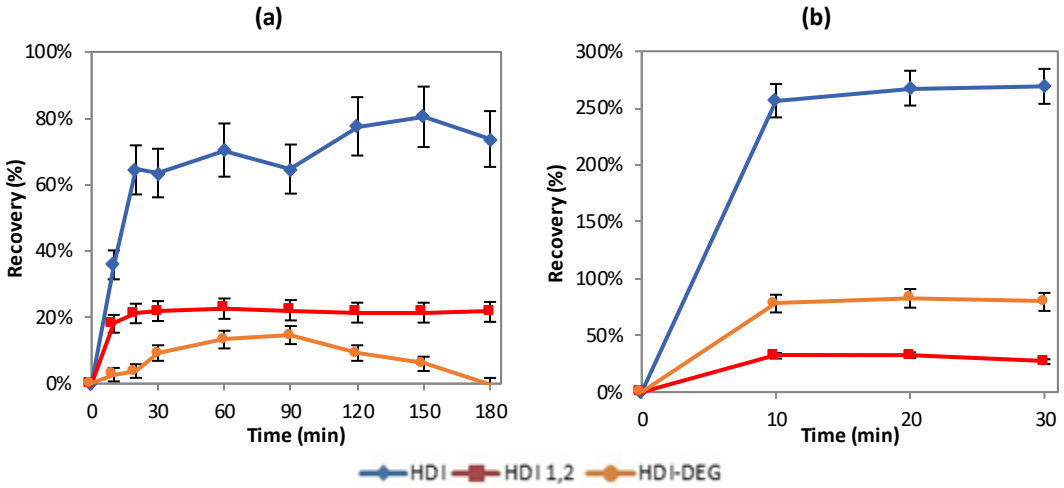

Figure 5-16. *Percentage recovery of HDI-based samples at (a) RT and (b) 60˚C after 12 weeks.*

Table 5-12. *Haze values of HDI-based coatings healed at room temperature after 12 weeks.*

Sample	Haze									
	Initial	Scratched	10 min	20 min	30 min	60 min	90 min	120 min	150 min	180 min
HDI	7.77	9.17	8.67	8.27	8.28	8.19	8.27	8.09	8.05	8.14
HDI-1,2-EG	1.57	2.96	2.71	2.67	2.66	2.65	2.65	2.66	2.66	2.66
HDI-DEG	1.51	2.74	2.70	2.69	2.62	2.57	2.56	2.62	2.66	2.74

At elevated temperatures the recovery of samples was found to be almost identical to the original recovery. However, the coating prepared without a CE showed higher percentage of recovery due to higher original haze value and decrease of the haze to values lower than original when heated (**Table 5-13**).

Table 5-13. *Haze values of HDI-based coatings healed at 60 ˚C after 12 weeks.*

Sample	Haze				
	Initial	Scratched	10 min	20 min	30 min
HDI	7.77	10.51	3.49	3.18	3.14
HDI-1,2-EG	1.57	3.89	3.15	3.14	3.27
HDI-DEG	1.51	3.11	1.86	1.79	1.84

The SH tests of IPDI-based samples repeated after 12 weeks (**Figure 5-17**) showed identical recovery efficiency at both RT (**Table 5-14**) and elevated temperatures (**Table 5-15**), proving that the ageing of IPDI-based polymers does not affect the healing properties of the coatings.

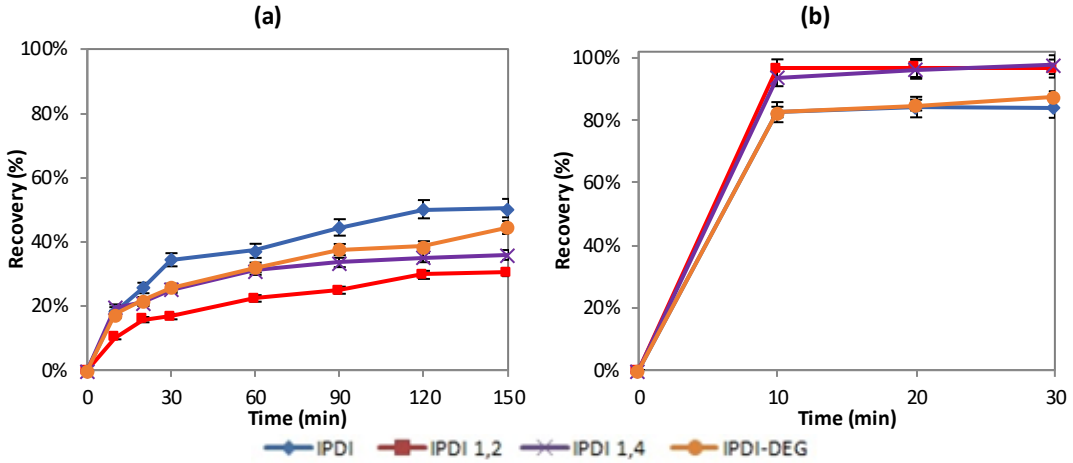

Figure 5-17. *Percentage recovery of IPDI-based samples at (a) RT and (b) 60˚C after 12 weeks.*

Table 5-14. *Haze values of IPDI-based coatings healed at room temperature after 12 weeks.*

Sample	Haze								
	Initial	Scratched	10 min	20 min	30 min	60 min	90 min	120 min	150 min
IPDI	1.16	4.04	3.51	3.30	3.05	2.97	2.76	2.60	2.59
IPDI-1,2-EG	0.94	5.12	4.69	4.47	4.43	4.19	4.08	3.88	3.85
IPDI-1,4-BD	1.34	5.33	4.55	4.49	4.33	4.09	3.99	3.93	3.90
IPDI-DEG	1.05	4.69	4.07	3.91	3.76	3.53	3.33	3.30	3.08

Table 5-15. *Haze values of IPDI-based coatings healed at 60 ˚C after 12 weeks.*

Sample	**Haze**				
	Initial	**Scratched**	**10 min**	**20 min**	**30 min**
IPDI	1.16	5.25	1.87	1.80	1.81
IPDI-1,2-EG	0.94	6.25	1.12	1.11	1.12
IPDI-1,4-BD	1.34	6.49	1.66	1.53	1.45
IPDI-DEG	1.05	8.85	2.40	2.23	2.02

The chemical stability of the coatings was examined by the weathering tests. Coatings prepared with HDI showed significant differences in the spectra in the amine stretch and carbonyl stretch regions, indicative of degradative chemistry occurring over 4 weeks of weathering, comparable to 30 weeks outdoor weathering (**Figure 5-18**).

The increase of absorbance of the peaks at 3600-2400 cm^{-1} and 1750-1700 cm^{-1} suggest an oxidative process leading to formation of new carbonyl groups. The new

peak appearing at 1600 cm^{-1} and decrease of the peak at 1540 cm^{-1} suggests another process, a homolytic bond scission of urethane groups leading to regeneration of isocyanate. A subsequent reaction with atmospheric water can lead to formation of carbamic acid and decomposition to amine and CO_2, as shown by Kim and Urban.[15]

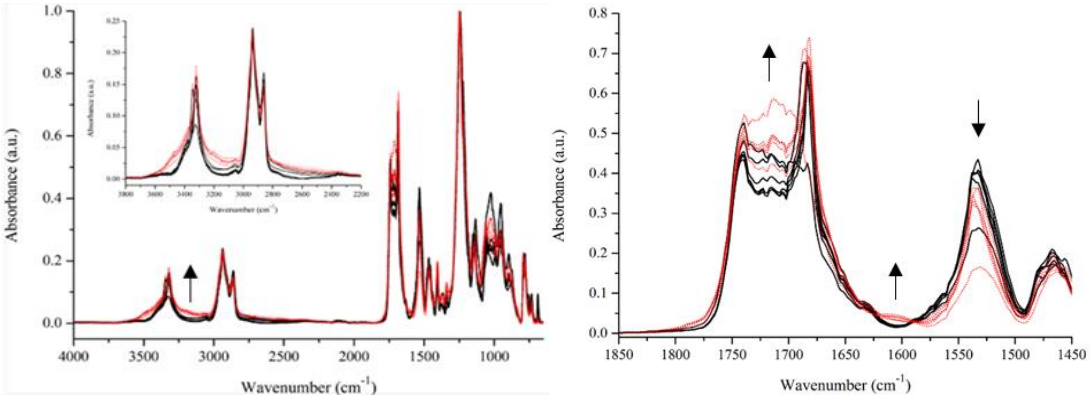

Figure 5-18. ATR FT-IR spectra of aged of HDI-based coatings, black solid line – unweathered, red dotted line – weathered.

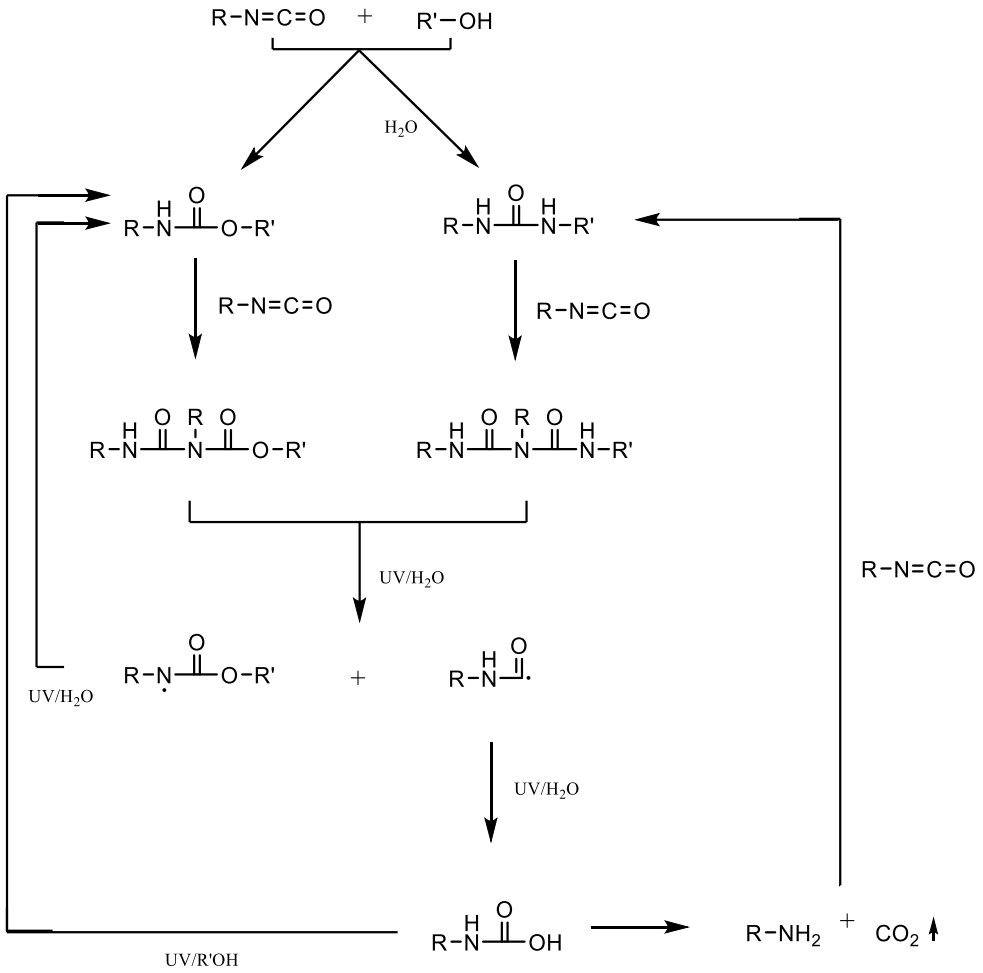

Figure 5-19. *The proposed molecular level chain scission mechanism of PU exposed to UV/H_2O.*[15]

The coatings prepared with IPDI showed higher chemical stability apparent by no changes in the ATR FT-IR spectra after 4 weeks of weathering (**Figure 5-20**). The weathering process is evident only in the HDI-based samples, partly due to the easier access of moisture in these low T_g coatings, and partly due to the slightly higher reactivity of HDI to water compared to IPDI.[16]

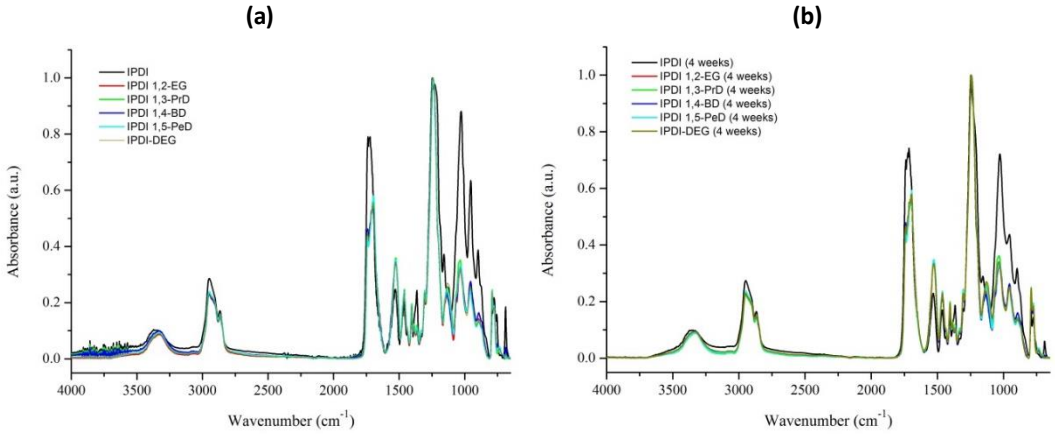

Figure 5-20. *ATR FT-IR spectra of IPDI-based coatings (a) before and (b) after weathering.*

5.7. SUMMARY AND DISCUSSION

As shown in the Chapter 4, the coatings prepared with IPDI were found to have a phase-mixed morphology linked to the unsymmetrical and non-planar structure of the isocyanate, apparent by the absence of crystallinity and higher T_g of the homogenous, phase-mixed phase composed of HS and SS. HDI-based coatings were found to be more phase-separated, influenced by the linear, symmetrical and planar structure of the isocyanate facilitating HS crystallisation and phase-separation, apparent by the presence of crystallinity and low T_g of the SS-rich phase. Phase-mixing of the segments was found to enable self-healing of damaged coatings.

The influence of the length and the chemistry of the diol chain extenders can be summarised as follows:

- **The absence of CE.** The lack of CE resulted in lowering of the hard segments content by approximately 6%. In the highly phase-separated HDI-based formulations the reduction of %HS resulted in a decrease of phase-separation and lower crystallinity, observed in the shift of peaks in the ATR FT-IR spectra and by

lower T_g and the lower enthalpy of melting in the DSC analysis. The increase of phase-mixing was reflected by an improved healing at both RT and elevated temperatures. Moreover, the sample showed a significant increase of the haze during ageing, associated with the low crystallinity of the SS-rich phase as well as the low T_g, enabling rearrangement of the polymer chains at RT and increase of phase-separation.

In the IPDI-based formulations the effect was less significant. The lower percentage of HS resulted in a lower T_g of the sample, improved healing at RT and higher stability of the system during ageing.

- **The length of diol CE in HDI-based formulations**. The increase of the length of CE in the HDI-based coatings was found to promote crystallinity, phase-separation and increase of haze caused by light scattering by the HS segments and crystallites including SS crystals. These changes can be related to a larger size of HS blocks (**Figure 5-21**). In the DSC analysis the glass transition temperatures were found mostly to decrease with the increase of the CE length, and the enthalpy of melting of the SS-rich phase was found to mostly increase. Multiple melting peaks of SS can be observed in the first heat cycle of all samples but PH50-HDI, while in the second heat cycle only the sample prepared with 1,4-BD shows cold crystallisation and melting. Formulation prepared with DEG initially showed higher level of phase-mixing but over time the phase-separation, crystallinity and haze were found to increase, confirmed by ATR FT-IR spectroscopy and DSC.

  The SH of HDI-based coating prepared with DEG was found to be superior to coatings prepared with other CE due to the increased phase-mixing of the system. However, due to the low T_g, as well as the haze and crystallinity developing with time, the coatings were found to be unsuitable for practical applications.

  The ageing process, indicated by the change in the haze value, was more significant for the sample prepared with DEG due to the initial higher extent of phase-mixing.

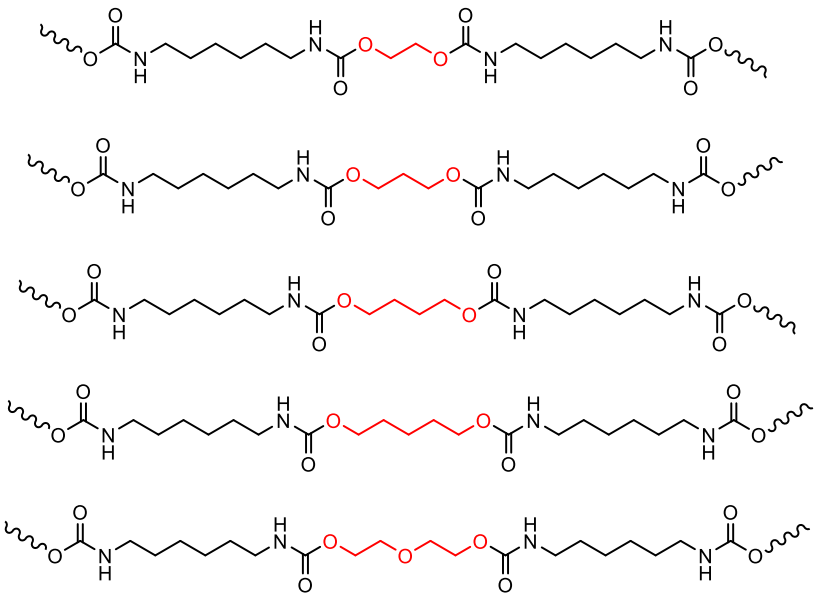

Figure 5-21. *The increase of the size of hard blocks with the increase of the length of CE.*

- **The length of diol CE in IPDI-based formulations.** In the IPDI-based coatings the effect of CE length was found to be less significant than in the HDI-based coatings. The formulations were found to be more phase-mixed and less crystalline due to the presence of bulky and non-symmetrical IPDI. The smaller effect of the length of the CE can be related to the variety of IPDI-CE-IPDI blocks that can be formed. For every CE there are three main structures of the smallest HS blocks that can be formed, depending on whether the CE's hydroxyl groups react with the isocyanato or isocyanatomethyl group (**Figure 5-22**). Therefore, the length of CE introduced less significant change to the overall morphology of the complex and varied PU matrix.

  The IPDI-based coatings showed a moderate recovery from damage at RT, and excellent recovery at elevated temperatures above their T_g, reaching 100% within the first 10 minutes of thermal treatment. The SH was not found to be dependent on the length of the CE.

  The samples did not show any significant changes in their ATR FT-IR spectra and DSC curves after 12 weeks, showing a low mobility of the chains at RT and high stability. The ageing of the samples was found to be not dependent on the length of the CE.

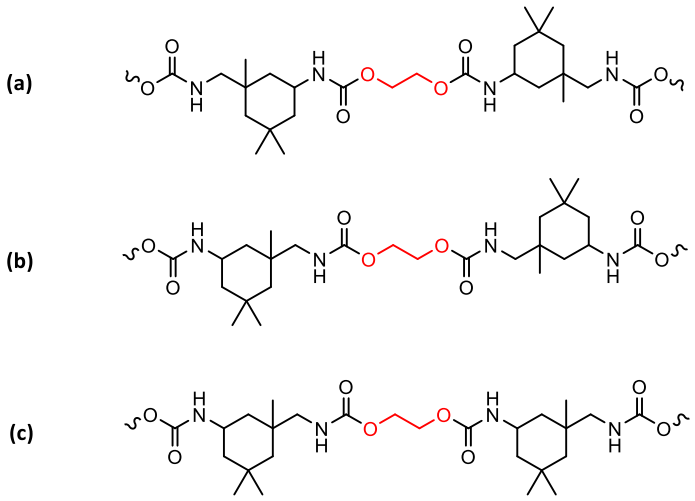

Figure 5-22. *Three structures of the HS, with the CE having reacted with (a) two isocyanato groups, (b) two isocyanatomethyl groups and (c) isocyanato and isocyanatomethyl groups.*

- **Weathering.** The effect of weathering of the samples was evident only in the HDI-based samples, due to the easier access of moisture in these low T_g coatings and the slightly higher reactivity of HDI to water compared to IPDI. The UV stability did not appear to be influenced by the length of the CE.

Therefore, coatings PH50-IPDI-1,2-EG and PH50-IPDI-1,4-BD were found to fulfil the four requirements of the research: exhibited haze below 2%, pencil hardness of B and above, suitable glass transition temperature and thermally-triggered SH properties reaching over 90% recovery from damage. The low cross-cut adhesion of coating PH50-IPDI-1,2-BD suggests incompatibility of the material with TAc. However, the coating may exhibit better adhesion properties when coated on other substrates.

5.8. REFERENCES

1 Z. Wirpsza, *Polyurethanes. Chemistry, Technology and Applications*, Ellis Hornwood Ltd, Midsomer Norton, 1st edn., 1993.
2 K. Gisselfält and B. Helgee, *Macromol. Mater. Eng.*, 2003, **288**, 265–271.
3 J. Blackwell, M. R. Nagarajan and T. B. Hoitink, *Polymer*, 1982, **23**, 950–956.
4 V. Kovačević, I. Šmit, D. Hace, M. Sućeska, I. Mudri and M. Bravar, *Int. J. Adhes. Adhes.*, 1993, **13**, 126–136.
5 R. K. Agrawal and L. T. Drzal, *J. Adhes.*, 1996, **55**, 221–243.
6 C. M. Gomez, D. Gutierrez, M. Asensio, V. Costa and A. Nohales, *J. Elastomers Plast.*, 2017, **49**, 77–95.
7 C. Prisacariu, in *Polyurethane Elastomers*, Springer-Verlag, Wien, 1st edn., 2011, pp. 23–60.
8 F. C. Stehling, C. S. Speed and L. Westerman, *Macromolecules*, 1981, **14**, 698–708.
9 E. Andreassen, A. Larsen, K. Nord-Varhaug, M. Skar and H. Emptysd, *Polym. Eng. Sci.*, 2002, **42**, 1082–1097.
10 F. S. Chuang, W. C. Tsen and Y. C. Shu, *Polym. Degrad. Stab.*, 2004, **84**, 69–77.
11 S. M. Cakić, M. Špírková, I. S. Ristić, J. K. B-Simendić, M. M-Cincović and R. Poręba, *Mater. Chem. Phys.*, 2013, **138**, 277–285.
12 I. Yilgör, E. Yilgör and G. L. Wilkes, *Polymer,* 2015, **58**, A1–A36.
13 C.-C. Chang, K.-S. Chen, T. L. Yu, Y.-S. Chen, C.-L. Tsai and Y.-H. Tseng, *Polym. J.*, 1999, 31, 1205–1210.
14 A. Eceiza, M. D. Martin, K. de la Caba, G. Kortaberria, N. Gabilondo, M. A. Corcuera and I. Mondragon, *Polym. Eng. Sci.*, 2008, **2**, 297–306.
15 H. Kim and M. W. Urban, *Langmuir*, 2000, **16**, 5382–5390.
16 F. Coutinho, *Eur. Polym. J.*, 1991, **27**, 213–216.

6. THE INFLUENCE OF AMINE CHAIN EXTENDER ON MORPHOLOGY AND SELF-HEALING PROPERTIES

Polyurethanes consist of soft segments composed of oligomer polyols and hard segments composed of isocyanate and chain extenders. The chemistry of both segments have a crucial influence on the morphology and the properties of PU.[1]

The influence of the chemistry and the length of polyols, the SS building blocks, on morphology and self-healing properties of protective polyurethane coatings was investigated in Chapter 3. Low-crystalline polycarbonate co-polymer of pentanediol and hexanediol with MW of 500 g mol^{-1} was chosen as the most suitable polyol.

Further, the relationship between the chemistry and morphology of HS was explored. In Chapter 4 the influence of two diisocyanates, HDI and IPDI, was evaluated. Linear, symmetrical HDI was found to promote separation of HS and SS, and facilitated development of crystallinity. Bulky and non-symmetrical IPDI was chosen as more suitable isocyanate due to its ability to disrupt crystallinity and promote formation of amorphous, homogenously mixed HS-SS phase. In the previous chapter, Chapter 5, the effect of diol chain extenders was investigated. The increase of the length of the CE in HDI-based coatings was found to promote crystallinity, phase-separation and haze. In IPDI-based coatings the influence of CE was found to be less significant. The IPDI-based samples showed excellent ageing, weathering and self-healing properties. Therefore, further investigation of IPDI-based coatings will be presented.

In this chapter the influence of chain extenders containing amine groups will be explored. Introduction of urea groups to PU often results in an improvement of mechanical and physical properties.[2] This is obtained by the presence of stronger H-bonds between the urea groups. However, in poly(urethane-urea) systems an increase of phase-separation is also commonly observed.[3] Therefore, in this chapter a number of IPDI-based formulations prepared with various amounts of urea groups will be investigated to establish the influence of urea groups on morphology and self-healing properties of transparent polyurethane coatings.

6.1. SYNTHESIS INFORMATION

The fourth set of formulations consists of seven materials prepared with various ratios of CE containing amine, leading to formation of urea groups. All materials were prepared using the polycarbonate polyol PH50 with MW of 500 g mol^{-1} and IPDI. The first formulation, reported in the previous chapters, contains 1,2-EG CE. In the following five formulations various ratios of 1,2-EG were replaced with ethanolamine (EA). The last formulation was prepared with a diamine CE, HDA (**Figure 6-1**).

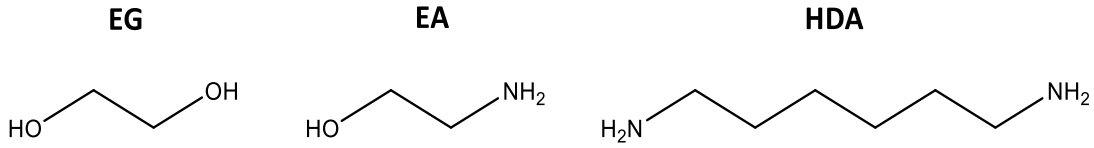

Figure 6-1. *Structure of CE used.*

All formulations were prepared using the acetone process, using DMPA (25mol% of the total number of moles of CE) and various CE (75mol% of the total number of moles of CE), as described in Section 2.2.5.

6.2. CHARACTERISATION OF DISPERSIONS

The experimental solid content of dispersions varied between 19.3% and 32.6% depending on the solubility of polymers in water and the viscosities of dispersions. The list of formulations, the ratio of CE used, and the percentage solid content of the dispersions are presented in **Table 6-1**.

Table 6-1. *Composition and solid content of the dispersions.*

Polyurethane	EG (%)	Amine CE (%)	Solid content (wt%)
PH50-IPDI-EG (0%)	100	0	23.1 ± 1.1
PH50-IPDI-EA/EG (5%)	95	5	33.4 ± 1.3
PH50-IPDI-EA/EG (10%)	90	10	22.4 ± 1.8
PH50-IPDI-EA/EG (25%)	75	25	30.1 ± 1.5
PH50-IPDI-EA/EG (50%)	50	50	32.6 ± 1.5
PH50-IPDI-EA (100%)	0	100	19.3 ± 2.0
PH50-IPDI-HDA	0	100	25.3 ± 3.4

6.3. CHARACTERISATION OF COATINGS

The percentage of hard segments of formulations varied insignificantly between 51.2% and 53.3% (**Table 6-2**). Coating prepared with IPDI and EG was found to be the hardest obtaining pencil hardness B. Increase of alkanolamine percentage led to creation of softer coatings, with a pencil hardness varying between 2B and 4B. The decrease of the hardness was related to increased brittleness of coatings and to the increased phase-mixing of the samples, known to reduce reinforcement from HS due to lower availability of groups able to form H-bonding.[4,5]. However, the coating prepared with diamine CE, HDA, showed pencil hardness B. The cross-cut adhesion was found to be 0 for all samples, indicating excellent adhesion properties.

All coatings exhibited low haze values. Sample prepared with 100% alkanolamine showed the highest haze, 4.8%, due to the increased amount of urea groups present, inducing phase-separation and promoting crystallinity. However, the coating prepared with HDA did not show such increase in haze, indicative of the length of CE having some influence on phase-mixing of the system.

Table 6-2. *Characterisation of coatings.*

Polyurethane	Hard segments (%)	Pencil Hardness	Cross-Cut Adhesion	Haze (%)
PH50-IPDI-EG (0%)	51.2	B	0	0.97
PH50-IPDI-EA/EG (5%)	51.2	4B	0	1.37
PH50-IPDI-EA/EG (10%)	51.2	3B	0	0.75
PH50-IPDI-EA/EG (25%)	51.2	3B	0	0.50
PH50-IPDI-EA/EG (50%)	51.2	3B	0	1.17
PH50-IPDI-EA (100%)	51.2	2B	0	4.80
PH50-IPDI-HDA	53.3	B	0	0.24

6.4. CHARACTERISATION OF COATINGS' MORPHOLOGIES

Figure 6-2 presents FT-IR spectra of the two sets of coatings. Among the important signals, a broad NH stretch can be observed between 3500 cm^{-1} and 3250 cm^{-1}, CH_2 stretches at 2935 cm^{-1} and 2860 cm^{-1}, and a broad peak between 3500 cm^{-1} and 2250 cm^{-1} assigned to carboxylic acid. Furthermore, multiple carbonyl stretches between 1740 cm^{-1} and 1650 cm^{-1}, C-N stretch and NH bend between 1600 cm^{-1}, and several CH signals below 1500 cm^{-1} can be observed.[6]

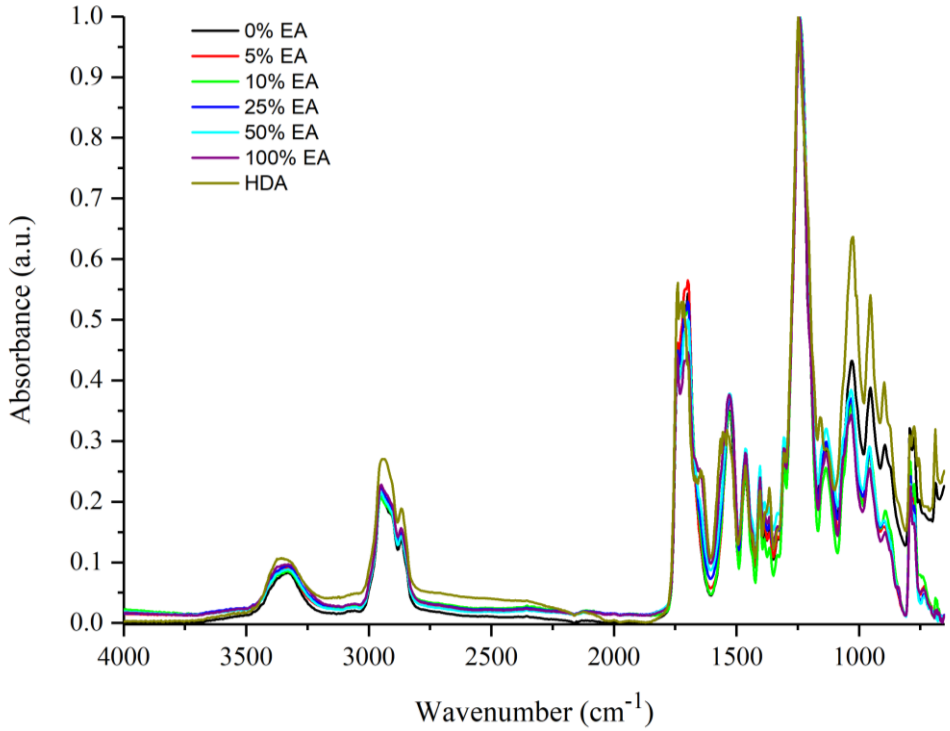

Figure 6-2. *ATR FT-IR spectra of the coatings.*

Figure 6-3a shows the NH region of spectra of the prepared coatings. Free N-H groups show stretching vibration at 3500-3400 cm^{-1}, while H-bonded N-H groups show stretch at lower wavenumbers, usually at 3350-3200 cm^{-1} (**Table 6-3**). The absence of peaks in 3500-3400 cm^{-1} region indicates that majority of NH groups are involved into H-bonding. The main NH peak shows between 3350 and 3300 cm^{-1} and is broad, indicating presence of HS-SS interactions and phase-mixing.[7] The coating prepared with HDA shows a small shift of the peak to the left, associated with the large amount of urea groups present.[8]

The analysis of the carbonyl region of ATR FT-IR spectrum of IPDI-based coatings shows the change of ratio of urethane and urea groups (**Figure 6-3b**). As the amount of urea groups increases, the absorbance of peaks at 1712 cm^{-1} and 1700 cm^{-1} associated with urethane groups decrease, and peaks at 1664 cm^{-1} and 1640 cm^{-1} associated with H-bonded monodentate urea groups increase.[9] The change can be also observed in the C-N stretch region, with the increase of the peak at 1560 cm^{-1} associated with urea groups and decrease of the peak at 1525 cm^{-1} associated with

urethane.[10] The changes in the absorbance of the peaks is most significant for the sample prepared with HDA.

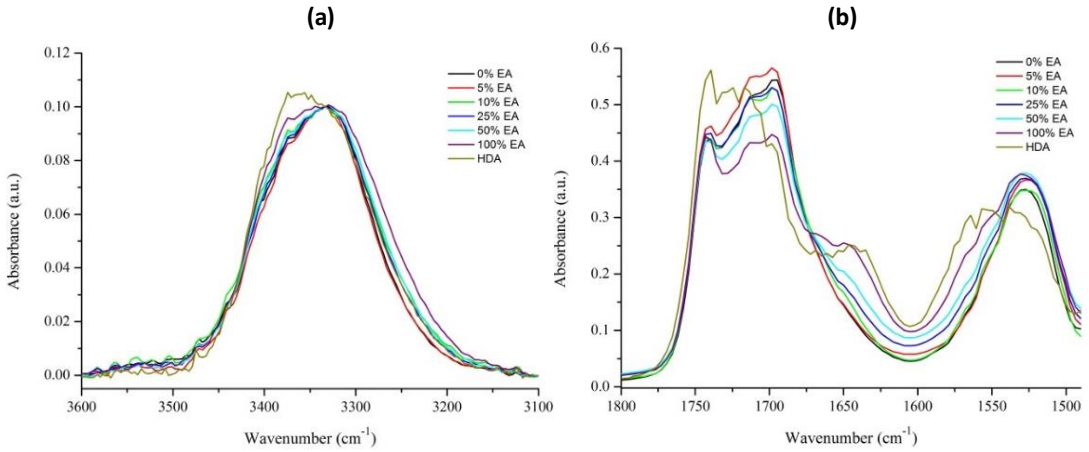

Figure 6-3. *ATR FT-IR spectra of samples: (a) the NH region and (b) the carbonyl region.*

Table 6-3. *Characteristic IR bands for phase-mixed and phase-separated systems.*[6-10]

Wavenumber (cm^{-1})	**Functional group ($\bar{\upsilon}$ – stretching, δ – bending)**	**Group assignment**	**Morphology**
3500-3400	$\bar{\upsilon}$(NH) free	Urethane	Free
3400-3350	$\bar{\upsilon}$(NH) bonded	Urethane	Phase-mixed
3350-3300	$\bar{\upsilon}$(NH) bonded	Urethane	Phase-separated
3340-3320	$\bar{\upsilon}$(NH) bonded, bidentate	Urea	Phase-separated
3240	$\bar{\upsilon}$(NH) bonded, monodentate	Urea	Phase-separated
1743	$\bar{\upsilon}$(C=O) free	Polyol	Free
1740-1730	$\bar{\upsilon}$(C=O) bonded	Polyol	Phase-mixed
1733-1730	$\bar{\upsilon}$(C=O) free	Urethane	Free
1723-1705	$\bar{\upsilon}$(C=O) bonded	Urethane	Phase-mixed
1700-1683	$\bar{\upsilon}$(C=O) bonded	Urethane	Phase-separated
1700-1680	$\bar{\upsilon}$(C=O) free	Urea	Free
1660-1635	$\bar{\upsilon}$(C=O) bonded, monodentate	Urea	Phase-mixed
1616-1627	$\bar{\upsilon}$(C=O) bonded, bidentate	Urea	Phase-separated
1580-1576	$\bar{\upsilon}$(CN) + δ(NH) bonded, bidentate	Urea	Phase-separated
1570-1554	$\bar{\upsilon}$(CN) + δ(NH) bonded, monodentate	Urea	Phase-mixed
1539-1530	$\bar{\upsilon}$(CN) + δ(NH) bonded	Urethane	Phase-separated
1526-1507	$\bar{\upsilon}$(CN) + δ(NH) bonded	Urethane	Phase-mixed

Figure 6-4 presents curves obtained from DSC. The broad T_g of the homogenous blend of HS and SS increases with the increase of percentage of EA, shifting from 16 ˚C for sample prepared with EG only to 44 ˚C for sample prepared with EA only in the first heating cycle, and from 32 ˚C to 46 ˚C in the second. The increase of the transition temperature reflects the presence of stronger H-bonding between urea groups within the phase-mixed blocks.[11] The variation is more significant while

comparing samples prepared with pure diol or pure alkanolamine CE, while samples prepared with blends of EG and EA showed a very small difference in their T_g. The formulation prepared with HDA shows the glass transition at higher temperature, at 58 °C in the first heat cycle and 68˚C in the second. Moreover, the transition present in the second cycle is very broad, occurring between 43 °C and 93 °C, indicating homogeneity of the HS-SS phase.[12] The increase of the T_g with the increase of urea content is not related here to increased phase-mixing of the system, but to stronger interactions between urethane groups within the homogenous HS-SS blocks.

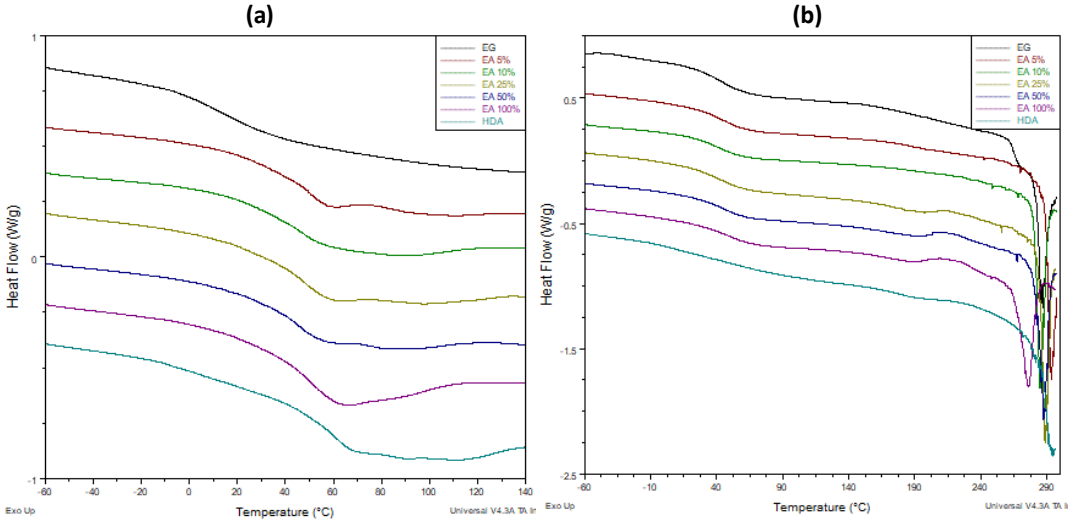

Figure 6-4. *DSC curves of coatings: (a) first heating cycle and (b) second heating cycle.*

The sample prepared with EG did not show any melting endotherms, indicating well phase-mixed, amorphous morphology induced by the presence of IPDI. Samples containing CE containing amine groups showed some melting endotherms in the 85 °C to 100 °C region, indicative of the development of crystallinity within the HS-SS blocks. The crystallinity increases with the increase of the content of strongly polar urea groups forming stronger interactions within the block, reflected by the raise of melting enthalpy from 2.9 J g^{-1} for the sample prepared with 5% EA to 4.0 J g^{-1} in the sample prepared with EA only and to 6.0 J g^{-1} in the sample prepared with diamine CE (**Table 6-4**). The increase of crystallinity confirms a mild increase of phase-separation within the systems.

As the crystallinity of SS is disturbed by the presence of IPDI and the development of crystallinity within the homogenously phase-mixed HS-SS blocks appears to be related to the presence of urea groups, the equivalent of the enthalpy in Joules per gram of polyol is not calculated.

The endotherms of HS-SS blocks are not present in the second heating cycle, indicating that the crystallinity develops slowly over time. Samples prepared with EG, 5% EA and 10% EA show a second glass transition between 181 °C and 185 °C, associated with amorphous HS. The remaining samples do not show this transition. However, development of small melting endotherms between 185 °C and 192 °C can be observed. This transition can be associated with a development of crystalline HS and a breakup of the short-range ordering, influenced by the presence of urea groups.[10] At higher temperatures, above 270 ˚C, melting peaks indicating breaking of long-range ordering of HS can be observed.[13]

The DSA characterisation data is summarised in **Table 6-4**.

Table 6-4. DSC characterisation data of samples prepared with various amounts of urea groups.

PU	Heat 1			Heat 2		
	T_g (°C)	T_m (°C)	ΔH_m (J/g)	T_g (°C)	T_m (°C)	ΔH_m (J/g)
PH50-IPDI-EG (0%)	16	-	-	32 181	- 287	-
PH50-IPDI-EA/EG (5%)	41	105	2.9	42 185	- 293	-
PH50-IPDI-EA/EG (10%)	38	90	2.7	40 182	- 285	-
PH50-IPDI-EA/EG (25%)	40	98	2.4	41 -	192 288	3.1 -
PH50-IPDI-EA/EG (50%)	41	95	2.2	42 -	191 288	4.7 -
PH50-IPDI-EA (100%)	44	87	4.0	46 -	185 276	5.2 -
PH50-IPDI-HDA	58	90	6.2	68 -	188 291	2.6 -

6.5. EVALUATION OF SELF-HEALING PROPERTIES

The SH efficiency tests of the samples prepared with various amount of urea groups introduced into their matrix are presented in **Figure 6-5**. The measured haze values during the SH evaluation are shown in **Table 6-5** and **Table 6-6.**

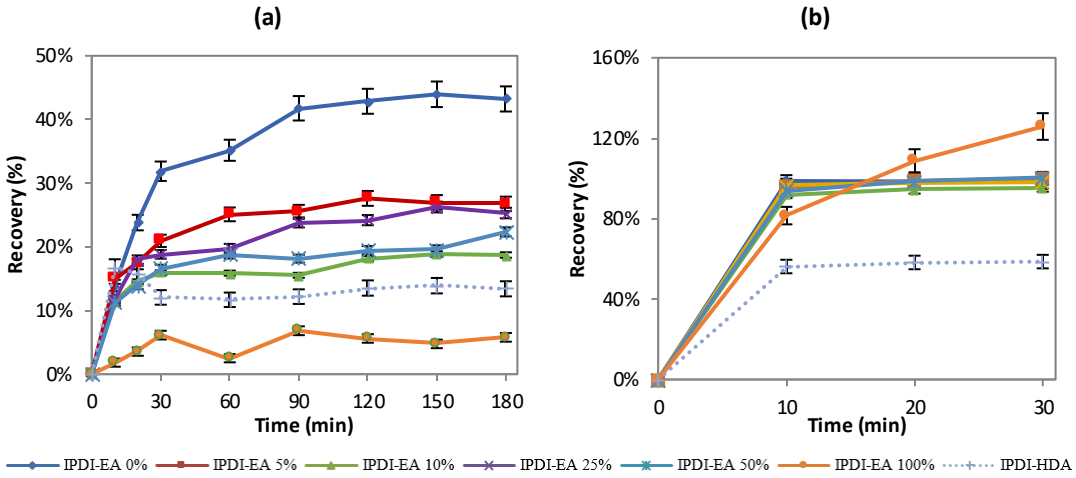

Figure 6-5. *Percentage recovery of samples prepared at RT (left) and 60˚C (right).*

Table 6-5. *Haze values of the coatings healed at room temperature.*

Sample	Haze									
	Initial	Scratched	10 min	20 min	30 min	60 min	90 min	120 min	150 min	180 min
EG	0.97	4.61	4.11	3.75	3.45	3.33	3.09	3.05	3.01	3.04
EA 5%	1.37	5.62	4.99	4.89	4.73	4.56	4.54	4.45	4.48	4.49
EA 10%	0.75	9.66	8.64	8.36	8.24	8.24	8.27	8.04	7.98	7.99
EA 25%	0.50	6.15	5.47	5.13	5.08	5.03	4.80	4.78	4.66	4.72
EA 50%	1.17	7.20	6.52	6.36	6.20	6.06	6.10	6.02	6.02	5.85
EA 100%	4.80	8.66	8.59	8.52	8.42	8.56	8.39	8.44	8.47	8.43
HDA	0.24	2.95	2.50	2.52	2.62	2.63	2.62	2.58	2.57	2.59

Table 6-6. *Haze values of the coatings healed at 60 ˚C.*

Sample	**Haze**				
	Initial	**Scratched**	**10 min**	**20 min**	**30 min**
PH50-IPDI-EG (0%)	0.24	4.88	0.32	0.31	0.31
PH50-IPDI-EA/EG (5%)	1.14	5.99	1.33	1.19	1.14
PH50-IPDI-EA/EG (10%)	0.76	8.96	1.42	1.23	1.15
PH50-IPDI-EA/EG (25%)	0.56	5.24	0.72	0.65	0.64
PH50-IPDI-EA/EG (50%)	1.19	7.11	1.53	1.27	1.16
PH50-IPDI-EA (100%)	4.51	7.50	5.06	4.25	3.74
PH50-IPDI-HDA	0.24	4.88	0.32	0.31	0.31

At RT the coating prepared with EG showed a moderate recovery of up to 45% (**Table 6-5**). This sample showed the T_g below RT, thus the phase-mixed, homogenous HS-SS block in the rubbery state was able to rearrange and partially heal the damage.

Coatings prepared with blends of EG and EA exhibited higher T_g and development of crystallinity. However, due to the onset of the glass transition being below RT the coatings showed minor healing at RT within 3 hours, recovering between 20 and 25% of the original haze.

The sample prepared with 100% EA showed the lowest recovery reaching only 6% at RT. The low recovery can be associated with the high crystallinity of the sample, higher T_g, as well as increased phase-separation of the system. The coating prepared with HDA also showed low recovery reaching 12%, also related to the high crystallinity of the sample, high T_g above RT, as well as increased phase-separation of the system, induced by the presence of urea groups.

While the increase of EA content, and thus the amount of urea groups, led to decreased healing of coatings at RT, such an effect was not observed during healing at elevated temperature. The coating prepared with EG, as well as coatings prepared with blends with EG and EA, showed a superb recovery of 100% at 60 °C, above the T_g of materials, allowing polymer chains to move, rearrange and restore broken H-bonds. The sample prepared with 100% EA showed recovery of over 100% caused by decrease of haze below the high initial haze value (**Table 6-6**).

The coating prepared with HDA showed recovery of up to 60%, showing an improvement comparing to the recovery at RT, although not reaching 100% due to more phase-separated structure, higher glass transition temperature and higher crystallinity.

6.6. *SUMMARY AND DISCUSSION*

The introduction of urea groups to the well phase-mixed IPDI-based polyurethane matrix was found to influence the polymer morphology and induce an increase of phase-separation. Moreover, an increase of the T_g was observed, enabling the self-healing process to be less efficient at RT and very efficient at elevated temperatures. Therefore, the adjustment of the chemistry of PU allows tailored design of self-healing coatings to the desired specification.

The influence of the introduction of urea groups by using alkanolamine and diamine chain extenders can be summarised as follows:

- **Hardness and haze.** The presence of chain extenders containing amine groups showed no improvement of the hardness of coatings and insignificantly affected the haze values and overall crystallinity. The decrease of the hardness was associated with increased brittleness of materials.
- **Phase-mixing.** The presence of urea groups did not significantly change the morphology of the samples; however, some increase of phase-separation and crystallinity was observed. The glass transition temperatures were affected moderately by the alkanolamine CE and increased significantly by 25 °C when a longer diamine CE was used. The increase of the T_g and crystallinity can be related to the increase of the urea groups known to form monodentate and bidentate interactions (**Figure 6-6**). The larger number of various interactions between urea groups requires higher energy to break these interactions and allow the material to undergo the glass transition. Simultaneously, the rearrangement of polymer chains after scratching is also hindered, even at elevated temperatures, due to the high T_g and high crystallinity of both HS-SS phase-mixed phase as well as pure HS phase.

  However, use of EA as the only CE increased the haze of the sample to level above 2%, indicating incompatibility between the amorphous and crystalline phase.

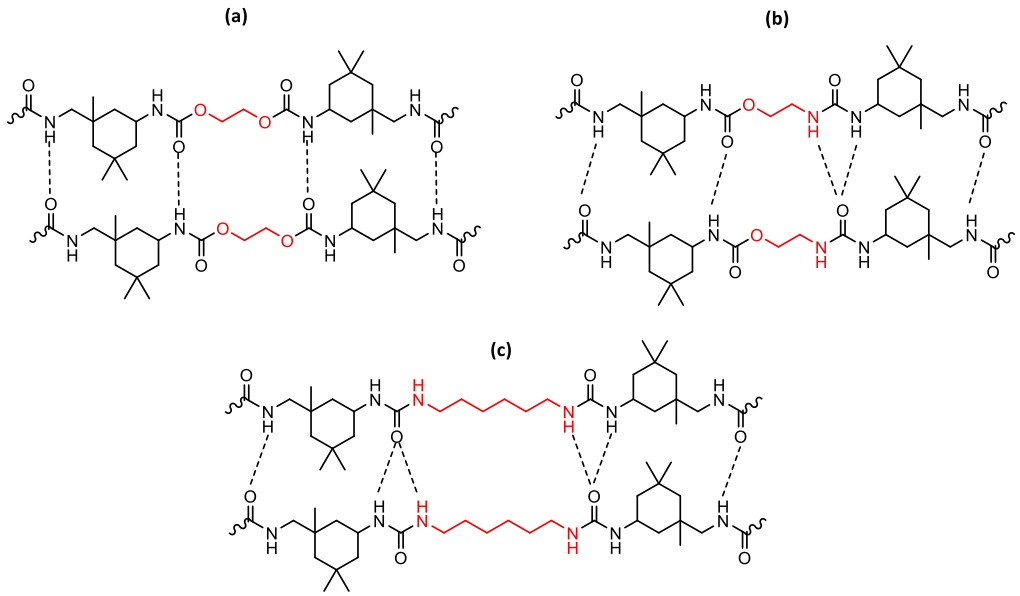

Figure 6-6. *Hydrogen bonding between (a) urethane groups, (b) urethane and urea groups and (c) urea groups – monodentate and bidentate.*

- **Self-healing**. The SH efficiency of the materials prepared with blends of EA and EG at 60˚C was unaffected by the presence of urea groups, showing 100% recovery of the damage within 10 minutes. However, the SH at RT was found to be reduced with the increase of the amount of alkoxyamine CE, allowing the process to be solely thermally-triggered. HDA, the long diamine CE, was found to significantly reduced the SH efficiency at elevated temperatures due to increased phase-mixing and crystallinity. Therefore, the presence of moderate amount of urea can allow tailoring the SH properties. However, the increase of T_g, crystallinity, haze and brittleness of the samples needs to be taken into consideration.

Therefore, only the coating PH50-IPDI-EG, also reported in the previous chapters, was found to fulfil the four requirements of the research: exhibited haze below 2%, pencil hardness of B and above, suitable glass transition temperature and thermally-triggered SH properties reaching over 90% recovery from damage.

Coating PH50-IPDI-HDA was found to fulfil three of the requirements. The SH efficiency at elevated temperature was found not to reach over 90% recovery due to high T_g and crystallinity of the sample. Nevertheless, the coating may exhibit more efficient healing at higher temperatures.

6.7. REFERENCES

1 Z. Wirpsza, *Polyurethanes. Chemistry, Technology and Applications*, Ellis Hornwood Ltd, Midsomer Norton, 1st edn., 1993.

2 A. Eyvazzadeh Kalajahi, M. Rezaei, F. Abbasi and G. Mir Mohamad Sadeghi, *Polym. Plast. Technol. Eng.*, 2017, **0**, 1–9.

3 R. A. Azzam, S. K. Mohamed, R. Tol, V. Everaert, H. Reynaers and B. Goderis, *Polym. Degrad. Stab.*, 2007, **92**, 1316–1325.

4 V. Kovačević, I. Šmit, D. Hace, M. Sućeska, I. Mudri and M. Bravar, *Int. J. Adhes. Adhes.*, 1993, **13**, 126–136.

5 R. K. Agrawal and L. T. Drzal, *J. Adhes.*, 1996, **55**, 221–243.

6 F. Sen Yen, L. L. Lin and J. L. Hong, *Macromolecules*, 1999, **32**, 3068–3079.

7 J. Mattia and P. Painter, *Macromolecules*, 2007, **40**, 1546–1554.

8 M. Shoaib and A. Bahadur, *E-Polymers*, 2016, **16**, 411–418.

9 E. Yilgor, I. Yilgor and E. Yurtsever, *Polymer*, 2002, **43**, 6551–6559.

10 E. Yilgor, E. Yurtsever and I. Yilgor, *Polymer*, 2002, **43**, 6561–6568.

11 G. J. E. Biemond, K. Brasspenning and R. J. Gaymans, *J. Appl. Polym. Sci.*, 2211, **124**, 1302–1315.

12 H. Jeong, J. Park, S. Kim, J. Lee, N. Ahn and H-g Roh, *Fibers Polym.*, 2013, **14**, 1082–1093.

13 A. Eceiza, M. D. Martin, K. de la Caba, G. Kortaberria, N. Gabilondo, M. A. Corcuera and I. Mondragon, *Polym. Eng. Sci.*, 2008, **2**, 297–306.

7. The influence of crosslinking on morphology and self-healing properties

In the previous chapters of this thesis the relationship between the chemistry of polyurethanes and their self-healing behaviour was presented. The investigation of the chemistry and the length of polyols, the SS building blocks, revealed that the low-crystalline polycarbonate PH50 was the most suitable polyol. Further studies showed that efficient self-healing of polyurethane coatings required a phase-mixed morphology of the polymers exhibiting low crystallinity.

During investigation of the chemistry of HS it was established that bulky and non-symmetrical IPDI disrupts crystallinity and promotes formation of amorphous, homogenously mixed HS-SS phase with glass transition temperatures above RT. The effect of the length of diol chain extenders on the healing properties was found to be minimal. However, the pencil hardness and cross-cut adhesion were found to decrease with an increase of the length of the diols. Introduction of urea groups to polymer matrices, obtained by use of alkanolamine and diamine chain extenders, was found to increase the undesirable phase-separation between the HS-SS and HS phases and crystallinity of both phases. The self-healing of coatings performed at RT decreased with an increase of urea group content. At 60 °C the healing was found to be unaffected at moderate concentrations of urea groups, and significantly reduced in formulation prepared with diamine chain extender.

In this chapter, the effect of increased crosslinking on self-healing behaviour will be presented. Chemical crosslinking was reported to improve mechanical and thermal stability of linear polyurethanes.[1] Rahman *et al.* reported that crosslinking improved adhesive strength, hardness and flexibility in waterborne polyurethane adhesives.[2] Petrovic *et al.* reported improvement of tear strength, hardness, solvent-resistance and SS glass transition of PU elastomers.[3,4] Therefore, the IPDI based coatings presented in this chapter are modified with various ratios of trimer isocyanate and trimer chain extenders, and the influence of crosslinking on the morphology of polymers and their SH behaviour is investigated.

7.1. SYNTHESIS INFORMATION

In this fifth set of formulations the effect of crosslinking on the morphology and self-healing properties of PU coatings is evaluated (**Table 7-1**). All materials were prepared using the polycarbonate polyol PH50 with MW of 500 g mol^{-1}. In the first subset various amounts of IPDI were replaced with *t*-IPDI. In the second subset, various amounts of EG were replaced with trimethylolpropane (TMP) (**Figure 7-1**).

All formulations were prepared using the acetone process, using DMPA (25mol% of the total number of moles of CE) and various CE (75mol% of the total number of moles of CE), as described in Section 2.2.5.

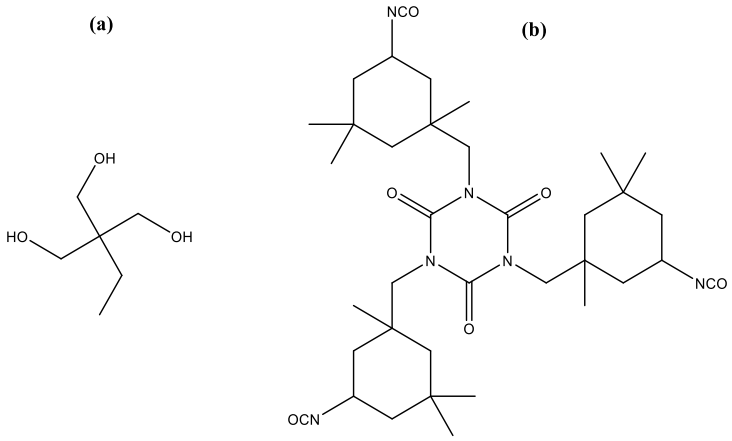

Figure 7-1. *Structure of trimers used: (a) TMP and (b) t-IPDI.*

Table 7-1. *Characterisation data of polyurethane coatings prepared.*

Polyurethane	Isocyanate – dimer (%)	Isocyanate – trimer (%)	Chain extender - dimer (%)	Chain extender - Trimer (%)
PH50-IPDI/t-IPDI-EG (0%)	100	0	100	0
PH50-IPDI/t-IPDI-EG (5%)	95	5	100	0
PH50-IPDI/t-IPDI-EG (10%)	90	10	100	0
PH50-IPDI/t-IPDI-EG (15%)	85	15	100	0
PH50-IPDI/t-IPDI-EG (20%)	80	20	100	0
PH50-IPDI/t-IPDI-EG (25%)	75	25	100	0
PH50-IPDI/t-IPDI-EG (50%)	50	50	100	0
PH50-IPDI-EG/TMP (0%)	100	0	100	0
PH50-IPDI-EG/TMP (5%)	100	0	95	5
PH50-IPDI-EG/TMP (10%)	100	0	90	10
PH50-IPDI-EG/TMP (20%)	100	0	80	20
PH50-IPDI-EG/TMP (50%)	100	0	50	50
PH50-IPDI-EG/TMP (100%)	100	0	0	100

7.2. CHARACTERISATION OF COATINGS

The percentage of hard segments within polyurethane matrices of formulations prepared with t-IPDI varied from 51.2% to 55.9%, depending on the amount of trimeric isocyanate used. Formulations prepared with over 25% of t-IPDI showed instant gelling and hardening, thus creation of waterborne dispersion and coating was impossible. The pencil hardness was found to decrease with increase of trimeric diisocyanate content, caused by an increase of coatings brittleness. The cross-cut adhesion was found to worsen for coatings with 5%, 10% and 15% of t-IPDI due to increase of phase-separation and crystallinity of coatings.[5,6] However, formulations prepared with larger amounts of t-IPDI were found to have an excellent adhesion. The haze of all coatings was found to be within the acceptable 0-2% level (**Table 7-2**).

The percentage of hard segments within polyurethane matrices of formulations prepared with trimeric chain extender TMP varied from 51.2% to 52.2%. The coating prepared with 5% of TMP was found to be the softest. However, further increase of the trimer content resulted in an improved coating hardness. The cross-cut adhesion was found to decrease with increased amount of crosslinking, linked to an increase of coatings brittleness and phase-separation.[5,6] The haze of all coatings but one was found to be within the acceptable 0-2% level (**Table 7-2**).

Table 7-2. *Characterisation data of polyurethane coatings prepared.*

Polyurethane	HS (%)	Pencil Hardness	Cross-Cut Adhesion	Haze (%)
PH50-IPDI-EG (0%)	51.2	B	0	0.97
PH50-IPDI/t-IPDI-EG (5%)	51.0	4B	5	1.47
PH50-IPDI/t-IPDI-EG (10%)	52.3	3B	5	0.48
PH50-IPDI/t-IPDI-EG (15%)	53.6	3B	5	0.31
PH50-IPDI/t-IPDI-EG (20%)	54.8	4B	0	0.54
PH50-IPDI/t-IPDI-EG (25%)	55.9	5B	0	0.35
PH50-IPDI/t-IPDI-EG (50%)	60.9	-	-	-
PH50-IPDI-EG (0%)	51.2	B	0	0.97
PH50-IPDI-EG/TMP (5%)	51.2	4B	4	0.59
PH50-IPDI-EG/TMP (10%)	51.3	3B	4	0.83
PH50-IPDI-EG/TMP (20%)	51.5	3B	5	2.31
PH50-IPDI-EG/TMP (50%)	51.7	2B	5	0.78
PH50-IPDI-EG/TMP (100%)	52.2	2B	5	1.83

The different gelling behaviour between materials prepared with t-IPDI and TMP materials can be explained by the difference in size of hard segments formed by the trimers.[7,8] **Figure 7-2** presents drawings of the smallest possible hard segments in both sets of samples, created from the chain extenders and isocyanates. Materials prepared with blends of a dimer and trimer CEs create more regular blocks with a predictable sequence. In the first step of reaction the polycarbonate diols are end-capped with diisocyanate. In the next step the chain extenders react with the remaining NCO groups creating hard segments with a central dimer or trimer CE. In these formulations smaller hard segments with a maximum molecular weight of 900 g mol^{-1} are formed, enabling better mixing of the polymer matrix and providing better solubility in water.

Materials prepared with t-IPDI form hard segments with a higher molecular weight of at least 1525 g mol^{-1}. The hard segments also possess a higher density of polar bonds, which results in gelling of materials prepared with more than 25% of t-IPDI. Due to the presence of di- and tri-isocyanates in the first step of the reaction, the structure of polymers and their sequence is also more random and unpredictable. Moreover, one of the remaining groups in the hard segment formed by t-IPDI, R', is likely to be another chain extender, creating even larger, more rigid hard segments.

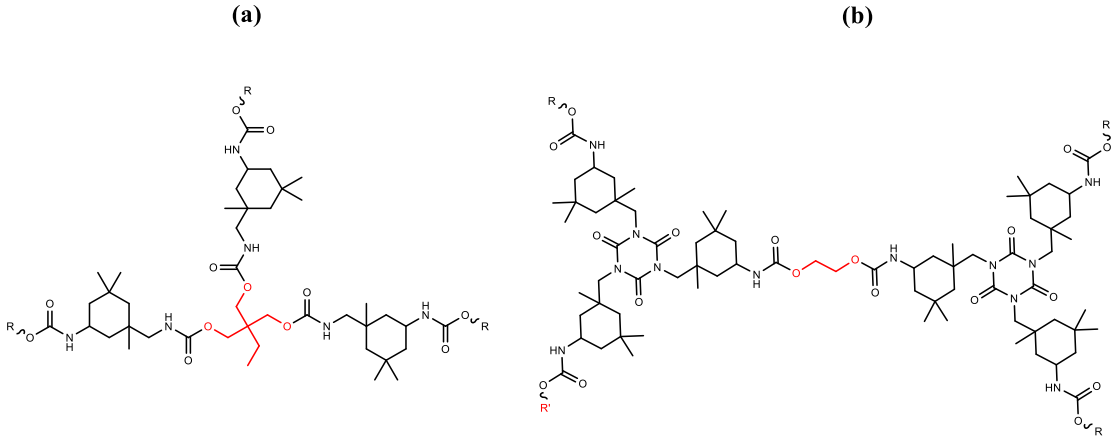

Figure 7-2. *The smallest possible hard segments of samples prepared with (a) TMP and (b) t-IPDI. R = polycarbonate polyol, R' = chain extender*

Solubility tests of the formulations showed a relationship between the crosslinking content and solvent resistance (**Table 7-3**). All samples showed an improvement of solvent resistance with an increase of the crosslinking and H-bond density. Coatings prepared with t-IPDI showed somewhat better solvent resistance, which may be linked to the larger size and marginally higher percentage of hard segments.

Table 7-3. *The results of solvent resistance tests of the coatings.*

Sample	Acetone	Ethanol	Toluene	Dichloromethane
PH50-IPDI/t-IPDI-EG (0%)	-	±	±	-
PH50-IPDI/t-IPDI-EG (5%)	±	±	±	±
PH50-IPDI/t-IPDI-EG (10%)	±	+	±	±
PH50-IPDI/t-IPDI-EG (15%)	±	+	±	±
PH50-IPDI/t-IPDI-EG (20%)	+	+	+	±
PH50-IPDI/t-IPDI-EG (25%)	+	+	+	±
PH50-IPDI/t-IPDI-EG (50%)	+	+	+	+
PH50-IPDI-EG/TMP (0%)	-	±	±	-
PH50-IPDI-EG/TMP (5%)	-	±	±	-
PH50-IPDI-EG/TMP (10%)	-	±	±	-
PH50-IPDI-EG/TMP (20%)	-	±	±	-
PH50-IPDI-EG/TMP (50%)	±	+	+	±
PH50-IPDI-EG/TMP (100%)	±	+	+	±

- dissolved, ± swelled, + solvent resistant

7.3. CHARACTERISATION OF COATINGS' MORPHOLOGIES

Figure 7-3 presents FT-IR spectra of the two sets of coatings. Among the important signals, a broad NH stretch can be observed between 3500 cm^{-1} and 3250 cm^{-1}, CH_2 stretches at 2935 cm^{-1} and 2860 cm^{-1}, and a broad peak between 3500 cm^{-1} and 2250 cm^{-1} assigned to carboxylic acid. Furthermore, multiple carbonyl stretches between

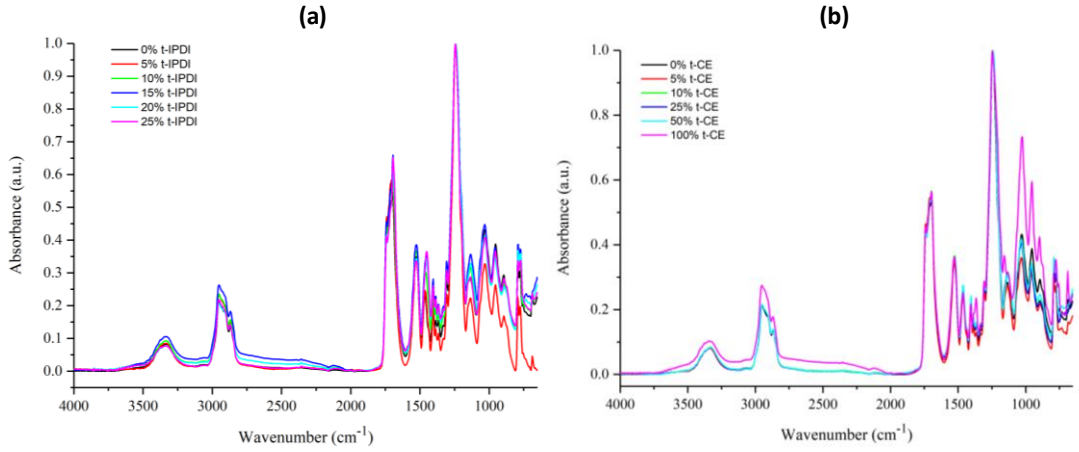

Figure 7-3. *ATR FT-IR spectra of the coatings prepared with (a) t-IPDI and (b) TMP.*

1740 cm^{-1} and 1650 cm^{-1}, C-N stretch and NH bend between 1600 cm^{-1}, and several CH signals below 1500 cm^{-1} can be observed.[9]

Figure 7-4 presents the NH region of ATR FT-IR spectra of samples prepared with various ratios of t-IPDI/IPDI and TMP/EG. For both sets of samples only a small amount of non H-bonded can be observed present as a shoulder peak at 3500-3400 cm^{-1}, suggesting that majority of NH groups are involved in H-bonding (**Table 7-4**).[10] All the samples show a broad NH peak at 3350 cm^{-1}, indicating the presence of mainly hard-soft segment interaction and phase-mixing.[11]

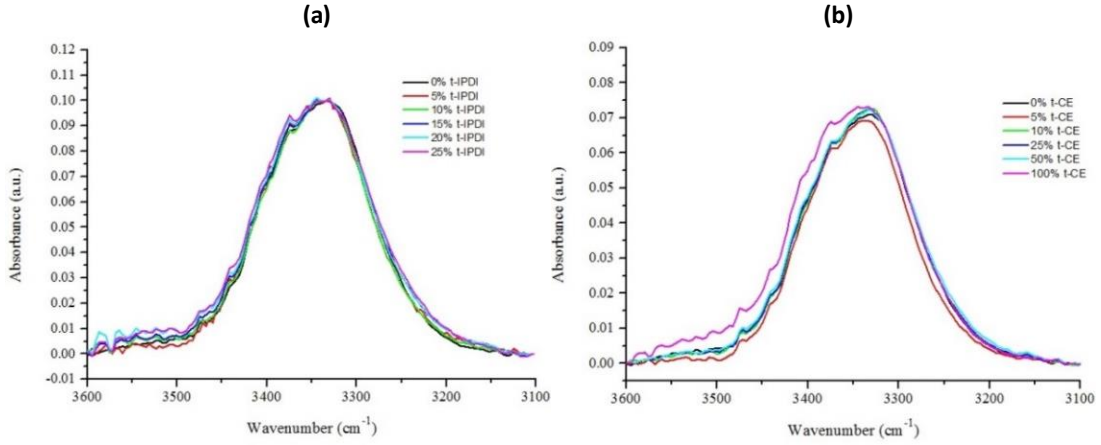

Figure 7-4. *The NH region of ATR FT-IR spectra of the coatings prepared with (a) t-IPDI and (b) TMP.*

Table 7-4. *Characteristic IR bands for phase-mixed and phase-separated systems.*[9-11]

Wavenumber (cm^{-1})	Functional group ($\bar{\upsilon}$ – stretching, δ – bending)	Group assignment	Morphology
3500-3400	$\bar{\upsilon}$(NH) free	Urethane	Free
3400-3350	$\bar{\upsilon}$(NH) bonded	Urethane	Phase-mixed
3350-3300	$\bar{\upsilon}$(NH) bonded	Urethane	Phase-separated
3340-3320	$\bar{\upsilon}$(NH) bonded, bidentate	Urea	Phase-separated
3240	$\bar{\upsilon}$(NH) bonded, monodentate	Urea	Phase-separated
1743	$\bar{\upsilon}$(C=O) free	Polyol	Free
1740-1730	$\bar{\upsilon}$(C=O) bonded	Polyol	Phase-mixed
1733-1730	$\bar{\upsilon}$(C=O) free	Urethane	Free
1723-1705	$\bar{\upsilon}$(C=O) bonded	Urethane	Phase-mixed
1700-1683	$\bar{\upsilon}$(C=O) bonded	Urethane	Phase-separated
1700-1680	$\bar{\upsilon}$(C=O) free	Urea	Free
1660-1635	$\bar{\upsilon}$(C=O) bonded, monodentate	Urea	Phase-mixed
1616-1627	$\bar{\upsilon}$(C=O) bonded, bidentate	Urea	Phase-separated
1580-1576	$\bar{\upsilon}$(CN) + δ(NH) bonded, bidentate	Urea	Phase-separated
1570-1554	$\bar{\upsilon}$(CN) + δ(NH) bonded, monodentate	Urea	Phase-mixed
1539-1530	$\bar{\upsilon}$(CN) + δ(NH) bonded	Urethane	Phase-separated
1526-1507	$\bar{\upsilon}$(CN) + δ(NH) bonded	Urethane	Phase-mixed

The analysis of the carbonyl region of ATR FT-IR spectra gives some additional insight into the morphology of the polymers (**Figure 7-5**). The peak at 1694 cm^{-1} can be assigned to phase-separated urethane groups, while the peak at 1710 cm^{-1} can be assigned to phase-mixed urethane groups.[12] In both sets of polymers an increase of the peak of phase-separated urethane groups at 1694 cm^{-1} with an increase of trimers content can be observed. The change is more prominent for the samples prepared with t-IPDI, due to the larger hard segment block showing higher density of polarity and leading to higher degree of phase-separation.

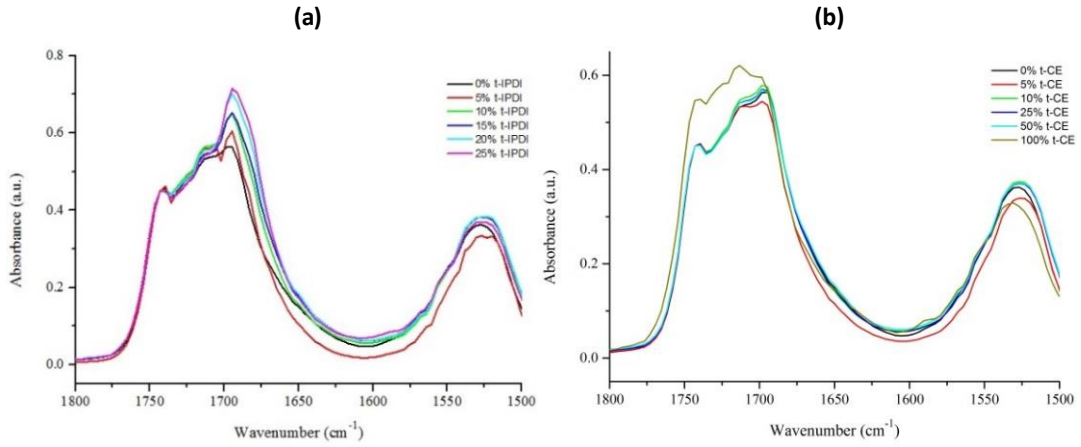

Figure 7-5. *The carbonyl region of FT-IR spectra of the coatings prepared with (a) t-IPDI and (b) TMP.*

Figure 7-6 presents DSC plots obtained for samples prepared with various ratios of IPDI and t-IPDI. In both cycles an increase of T_g with the increase of t-IPDI content can be observed. The broad transition can be associated with homogenously mixed amorphous HS-SS blocks, and shifts from 16 °C for the sample prepared without any t-IPDI to 46 °C for the sample prepared with 25% of t-IPDI in the first heat cycle, and from 32 °C to 56 °C in the second heat cycle, consistent with the increase of cross-linking and percentage of HS.[13] In the first heating cycle all samples also show melting endotherms present between 84 °C and 99 °C indicating presence of crystallinity within the HS-SS blocks. The enthalpies of melting values were found to be between 1.0 and 4.6 J g^{-1} (**Table 7-5**). As the crystallinity of SS is disturbed by the presence of IPDI and the development of crystallinity within the homogenously phase-mixed HS-SS blocks appears to be related to the presence of urea groups, the equivalent of the enthalpy in Joules per gram of polyol is not calculated.

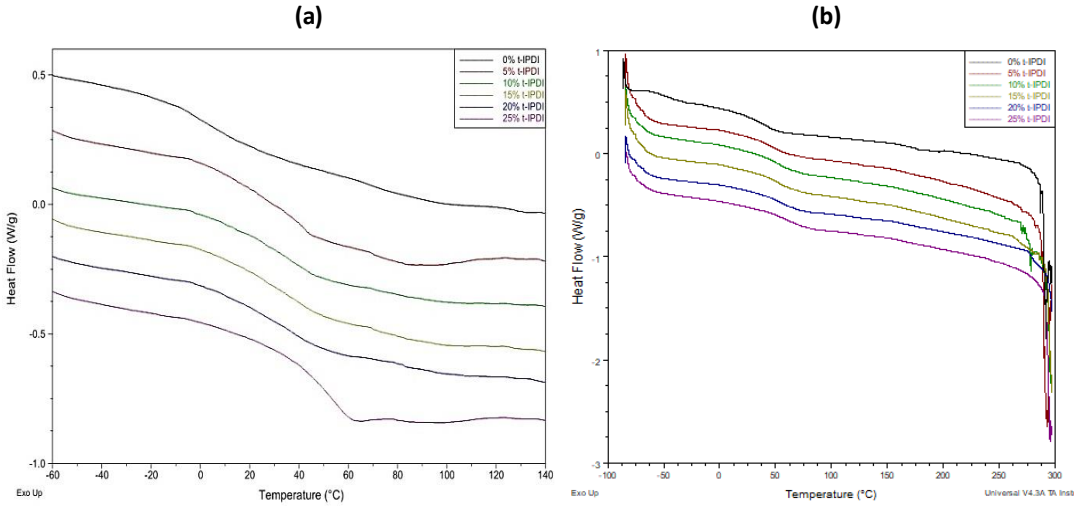

Figure 7-6. *DSC curves of coatings prepared with t-IPDI: (a) first and (b) second heating cycle.*

The endotherms of HS-SS blocks are not present in the second heating cycle, indicating that the crystallinity develops only slowly over time. Only the sample prepared with IPDI showed a second glass transition associated with the amorphous regions of HS, present at 181 °C. However, the transition is not well defined, suggesting a small amount of amorphous HS present in the PU. Materials prepared with various ratios of IPDI and t-IPDI did not show the second glass transition, reflective of the influence of crosslinking on restriction of mobility of polymer chains and development of crystallinity within the HS. The presence of crystalline regions of HS is apparent by the large melting endotherms at temperatures above 280 °C.[14]

Similar observations can be made for materials prepared with the trimeric CE, TMP (**Figure 7-7**). An increase of T_g with the increase of TMP content can be observed in both cycles, shifting from 16 °C to 42 °C in the first cycle, and from 32 °C to 45 °C in the second cycle, consistent with the increase of cross-linking and the percentage of HS. The broad transition can be associated with homogenously mixed amorphous HS-SS blocks. In the first heating cycle all samples showed melting endotherms, indicative of the presence of crystalline blocks within the HS-SS segment. The melting temperature was found to increase with the increase of TMP content, shifting from 83 °C in sample prepared with 5% TMP to 118 °C in a sample prepared with 100% TMP, reflecting the presence of crosslinking. Interestingly, the melting enthalpy was also found to somewhat increase with the increase of crosslinking (**Table 7-5**).

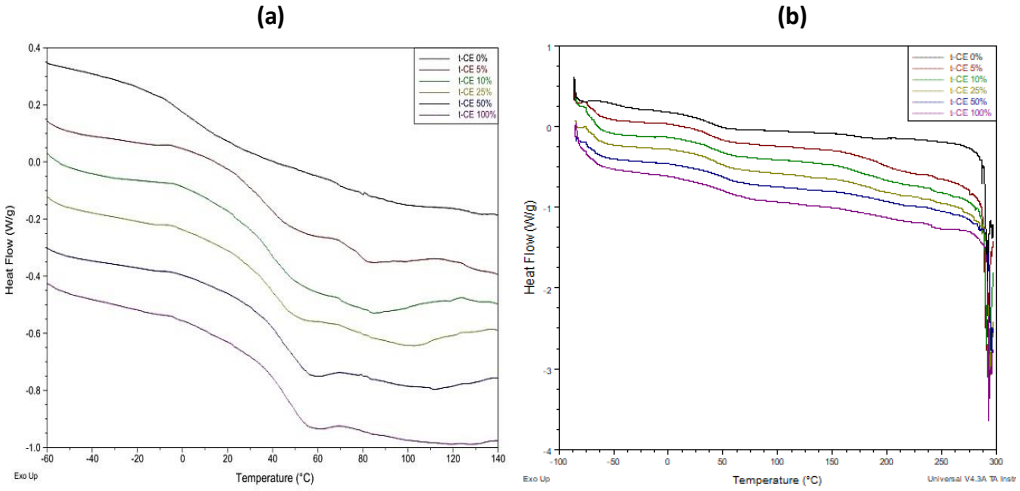

Figure 7-7. *DSC curves of coatings prepared with TMP: (a) first and (b) second heating cycle.*

Table 7-5. *DSC characterisation data of materials prepared with trimers.*

Polyurethane	Heat 1			Heat 2		
	T_g (°C)	T_m (°C)	ΔH_m (J/g)	T_g (°C)	T_m (°C)	ΔH_m (J/g)
IPDI	16	95	3.7	32 181	287	-
IPDI/t-IPDI (5%)	28	84	4.6	44 -	293	-
IPDI/t-IPDI (10%)	29	99	1.6	48 -	275	-
IPDI/t-IPDI (15%)	29	99	3.0	49 -	295	-
IPDI/t-IPDI (20%)	30	98	1.2	49 -	295	-
IPDI/t-IPDI (25%)	46	99	1.2	56 -	295	-
EG	16	95	3.7	32 181	287	-
EG/TMP (5%)	32	83	4.0	34 181	291	-
EG/TMP (10%)	34	85	4.6	36 183	293	-
EG/TMP (20%)	35	100	6.4	38 185	294	-
EG/TMP (50%)	41	112	5.8	42 189	295	-
EG/TMP (100%)	42	118	4.8	45 190	293	-

The endotherms of HS-SS blocks are not present in the second heating cycle, indicating that the crystallinity develops slowly over time. All samples showed a second glass transition associated with the amorphous regions of HS, increasing with the increase of TMP content from 180 °C to 191 °C. The transition appears to be less

defined with the increase of TMP, reflecting the influence of crosslinking on restriction of mobility of polymer chains. The restriction of mobility is smaller than in formulations prepared with t-IPDI due to the smaller size of HS. The presence of crystalline regions of HS is apparent by the large melting endotherms at temperatures above 285 °C.[14]

7.4. EVALUATION OF SELF-HEALING PROPERTIES

SH efficiency tests of coatings prepared with various ratios of t-IPDI (**Figure 7-6**) showed a small recovery at RT, which decreases with an increase of t-IPDI content (**Table 7-7** and **Table 7-8**). The highest SH efficiency was observed for the sample prepared without t-IPDI reaching 44% recovery, associated with the absence of trimers restricting molecular motion of SS, the lowest T_g and the highest extent of phase-mixing. Samples prepared with 5% and 15% of t-IPDI showed the lowest recovery of 5%, which may be related to the softness of the coatings and large amount of damage introduced during scratching. The remaining samples reached between 20% and 30% recovery. The presence of recovery can be associated with the onset of the glass transition below RT.

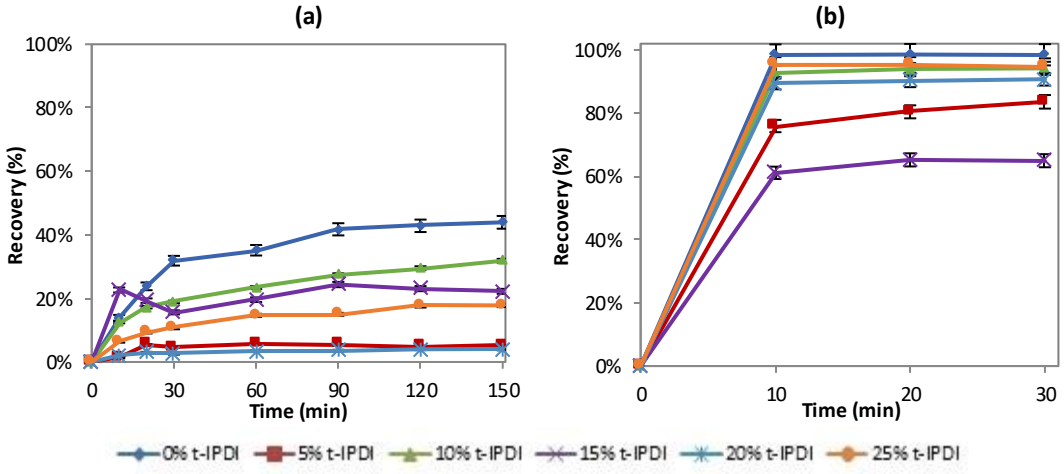

***Figure 7-8**. Percentage recovery of samples prepared with t-IPDI, SH at (a) RT and (b) 60 °C.*

At 60 °C most of the samples showed very efficient recovery of above 95% within the first 10 minutes. Samples prepared with 5% and 15% of t-IPDI showed lower recovery of 65 and 84% respectively. The decreased efficiency of SH might be caused by the

higher crystallinity of the HS-SS blocks of the two coatings, caused by unpredictable nature of the reaction due to different reactivities of IPDI and t-IPDI and the size of HS blocks containing t-IPDI.

Table 7-6. *Haze values of coatings prepared with t-IPDI healed at room temperature.*

Sample	Haze								
	Initial	Scratched	10 min	20 min	30 min	60 min	90 min	120 min	150 min
IPDI	0.97	4.61	4.11	3.75	3.45	3.33	3.09	3.05	3.01
IPDI/t-IPDI (5%)	1.47	14.37	14.20	13.67	13.77	13.63	13.67	13.73	13.70
IPDI/t-IPDI (10%)	0.48	9.79	8.63	8.19	8.03	7.61	7.24	7.04	6.83
IPDI/t-IPDI (15%)	0.31	5.75	4.52	4.70	4.90	4.69	4.43	4.50	4.54
IPDI/t-IPDI (20%)	0.54	9.79	9.62	9.52	9.55	9.48	9.46	9.42	9.43
IPDI/t-IPDI (25%)	0.35	7.32	6.87	6.66	6.57	6.29	6.27	6.09	6.08

Table 7-7. *Haze values of coatings prepared with t-IPDI healed at 60 °C.*

Sample	**Haze**				
	Initial	**Scratched**	**10 min**	**20 min**	**30 min**
PH50-IPDI-EG (0%)	0.24	4.88	0.32	0.31	0.31
PH50-IPDI/t-IPDI-EG (5%)	1.58	7.80	3.08	2.80	2.60
PH50-IPDI/t-IPDI-EG (10%)	0.45	7.62	0.95	0.90	0.87
PH50-IPDI/t-IPDI-EG (15%)	0.36	5.41	2.32	2.12	2.13
PH50-IPDI/t-IPDI-EG (20%)	0.60	7.78	1.35	1.30	1.27
PH50-IPDI/t-IPDI-EG (25%)	0.47	6.62	0.76	0.76	0.78

Formulations prepared with various ratios of dimer and trimer CE showed a clear relationship between the amount of crosslinking and SH efficiency (**Figure 7-9**, **Table 7-8** and **Table 7-9**). At RT the healing efficiency was found to decrease with the increase of TMP content, shifting from 45% of recovery for the sample prepared with EG only to 4% of recovery for the sample prepared with TMP only. The decrease of healing efficiency can be explained by the increasing amount of crosslinking leading to formation of a rigid, H-bonded matrix. This constrains polymer chain mobility and lowers the SH efficiency. The relationship is clearer than in the case of materials prepared with t-IPDI due to smaller size of HS and more predictable nature of the reaction. The recovery of materials below their T_g can be associated with the onset of the glass transition being below RT, thus enabling small amount of molecular mobility within the HS-SS blocks. Above the T_g of the coatings, at 60 °C, all the samples showed excellent recovery, reaching 100% within the first 10 minutes of healing.

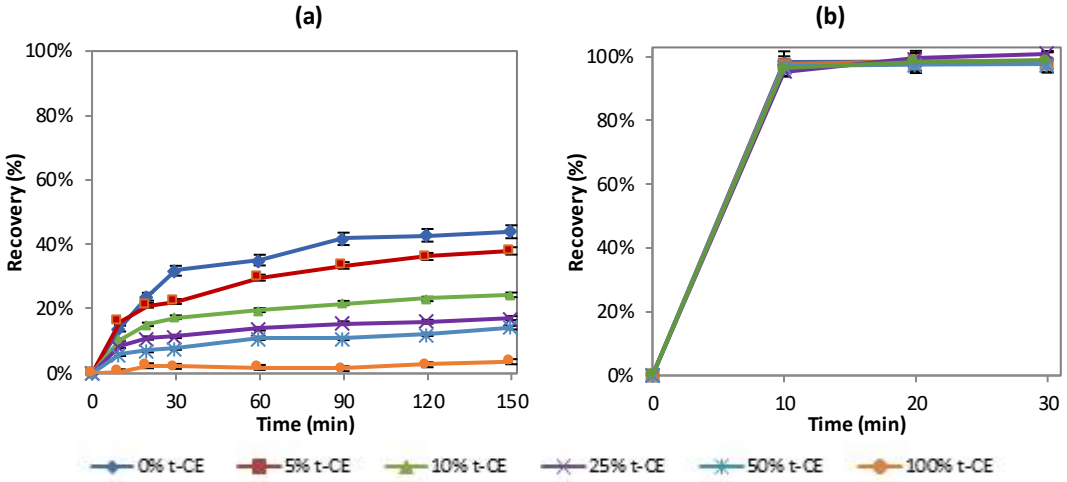

***Figure 7-9**. Percentage recovery of samples prepared with TMP, SH at (a) RT and (b) 60 ℃.*

***Table 7-8.** Haze values of coatings prepared with t-IPDI healed at room temperature.*

Sample	Haze									
	Initial	Scratched	10 min	20 min	30 min	60 min	90 min	120 min	150 min	180 min
EG	0.97	4.61	4.11	3.75	3.45	3.33	3.09	3.05	3.01	3.04
EG/TMP (5%)	0.59	6.22	5.32	5.03	4.97	4.55	4.34	4.18	4.08	3.86
EG/TMP (10%)	0.83	7.16	6.50	6.20	6.06	5.92	5.78	5.70	5.62	5.57
EG/TMP (25%)	2.31	8.20	7.71	7.55	7.52	7.38	7.28	7.25	7.19	7.19
EG/TMP (50%)	0.78	6.76	6.41	6.34	6.30	6.11	6.11	6.04	5.91	5.85
EG/TMP (100%)	1.83	5.03	5.01	4.95	4.96	4.97	4.98	4.94	4.91	4.93

***Table 7-9.** Haze values of coatings prepared with t-IPDI healed at 60 ℃.*

Sample	Haze				
	Initial	Scratched	10 min	20 min	30 min
PH50-IPDI-EG (0%)	0.24	4.88	0.32	0.31	0.31
PH50-IPDI-EG/TMP (5%)	0.74	5.99	0.86	0.81	0.83
PH50-IPDI-EG/TMP (10%)	0.56	5.56	0.70	0.66	0.64
PH50-IPDI-EG/TMP (25%)	1.81	8.15	2.09	1.84	1.75
PH50-IPDI-EG/TMP (50%)	0.86	6.45	1.03	1.00	1.00
PH50-IPDI-TMP/EG (100%)	1.08	6.72	1.27	1.17	1.13

7.5. SUMMARY AND DISCUSSION

The introduction of crosslinking to polyurethane SH materials resulted in a number of changes in the polymers' morphology.

- **Haze, hardness and cross-cut adhesion.** Crosslinking was not found to significantly change the haze values of the coatings. However, decrease of the coatings' hardness and cross-cut adhesion was observed in formulations

prepared with larger amount of trimers. The change can be associated with an increased brittleness of highly crosslinked polymers, as well as increased phase-separation of the systems, caused by the presence or mobility restricting crosslinks.

- **Solvent resistance.** Unsurprisingly, the introduction of trimers to the formulations resulted in creation of coatings with higher solvent resistance. The solvent resistance was found to increase with the amount of trimers within the polymer matrix.
- **Phase-mixing.** The increase of trimer content was found to result in an increased crosslinking and phase-separation of the systems. The effect was more significant for formulations prepared with t-IPDI, caused by the larger size of t-IPDI and formation of larger HS blocks, resulting in a higher restriction of mobility of polymer chains and entanglement of polymer chains. A visual representation in the different morphology of coatings prepared with TMP and t-IPDI is presented in **Figure 7-10**.

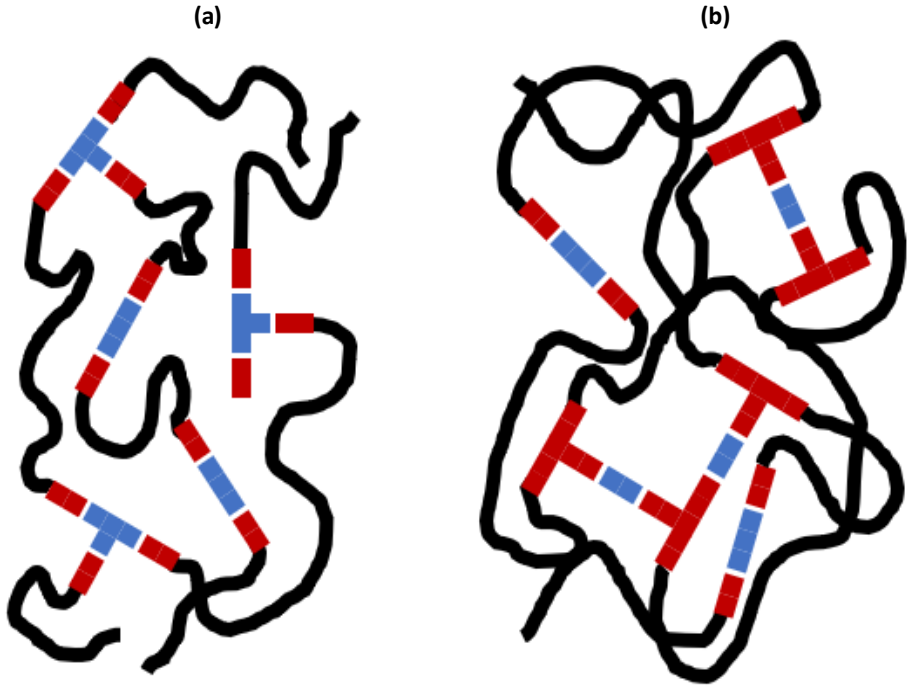

Figure 7-10. *The morphology of samples prepared with (a) TMP and (b) t-IPDI (blue – chain extenders, red – isocyanates). Samples prepared with t-IPDI create larger HS, resulting in a higher restriction of mobility and entanglement of polymer chains*

Formulations prepared with TMP showed a direct relationship between the increase of crosslinking and the change of morphology. The change was less obvious in materials prepared with t-IPDI due to the larger size of the HS blocks formed with the large isocyanate, as well as more unpredictable nature of the reaction. However, both sets of materials were found to develop crystallinity of HS-SS blocks apparent by the increase of melting temperatures and the enthalpy of endotherms with the increase of crosslinking. Moreover, an increase of T_g of both HS-SS blocks and pure HS blocks was observed, more apparent in formulations prepared with TMP. The ATR FT-IR analysis also indicated high degree of phase-mixing within the systems, indicated by a broad NH peak at high wavenumbers. However, small increase of phase-separation was observed with the increase of crosslinking.

- **Self-healing.** The use of trimers largely affected healing at room temperature, lowering the healing efficiency with the increase of the amount of trimers. The decrease of recovery from damage can be explained by the increasing amount of crosslinks restricting polymer chains mobility and lowering the SH efficiency. However, the majority of the coatings maintained the excellent healing properties at 60 °C, above the T_g of HS-SS blocks, reaching 100% recovery within the first 10 minutes of healing.

Therefore, only the coating PH50-IPDI-EG, also reported in the previous chapters, was found to fulfil the four requirements of the research: exhibited haze below 2%, pencil hardness of B and above, suitable glass transition temperature and thermally-triggered SH properties reaching over 90% recovery from damage.

Coatings prepared with high amounts of TMP showed an improved solvent resistance, as well as tailored SH properties allowing the healing to be reduced at RT and be very efficient at elevated temperatures. The low cross-cut adhesion of the coatings suggests incompatibility of the material with TAc. Nevertheless, the coating may exhibit better adhesion properties when coated on other substrates. The pencil hardness of the coatings does not fulfil the requirement of minimal hardness, but the materials might find use in other applications where the hardness is not crucial.

7.6. REFERENCES

1 M. Krumova, D. Lopez, R. Benavente, C. Mijangos and J. M. Perena, *Polymer*, 2000, **41**, 9265–9272.

2 M. M. Rahman, H. Do Kim and W. K. Lee, *Fibers Polym.*, 2009, **10**, 6–13.

3 Z. S. Petrovic, *Handbook of Polymer Synthesis*, Marcel Dekker, Inc., New York, 2nd edn., 2005.

4 Z. S. Petrović, M. Ilavský, K. Dusek, M. Vidaković, I. Javni and B. Banjanin, *J. Appl. Polym. Sci.*, 1991, **42**, 391–398.

5 V. Kovačević, I. Šmit, D. Hace, M. Sućeska, I. Mudri and M. Bravar, *Int. J. Adhes. Adhes.*, 1993, **13**, 126–136.

6 R. K. Agrawal and L. T. Drzal, *J. Adhes.*, 1996, **55**, 221–243.

7 S. A. Madbouly, J. U. Otaigbe, A. K. Nanda and D. A. Wicks, *Macromolecules*, 2005, **38**, 4014–4023.

8 S. A. Madbouly and J. U. Otaigbe, *Macromolecules*, 2005, **38**, 10178–10184.

9 F. Sen Yen, L. L. Lin and J. L. Hong, *Macromolecules*, 1999, **32**, 3068–3079.

10 J. Mattia and P. Painter, *Macromolecules*, 2007, **40**, 1546–1554.

11 C. M. Gomez, D. Gutierrez, M. Asensio, V. Costa and A. Nohales, *J. Elastomers Plast.*, 2017, **49**, 77–95.

12 E. Ylgor, I. Ylgor and E. Yurtsever, *Polymer*, 2002, **43**, 6551–6559.

13 H. Jeong, J. Park, S. Kim, J. Lee, N. Ahn and H. Roh, *Fibers Polym.*, 2013, **14**, 1082–1093.

8. THE INFLUENCE OF IONIC CONTENT ON MORPHOLOGY AND SELF-HEALING PROPERTIES

Polyurethanes, composed of soft segment and hard segments, exhibit a variety of properties related to the chemistry of these two phases.[1] In the previous chapters of this thesis the relationship between the chemistry of various SS and HS building blocks and self-healing behaviour was presented. Low-crystallinity polycarbonate PH50 was chosen as the most suitable polyol forming SS within PU, and the self-healing properties were related to a phase-mixed morphology and low crystallinity.

During the investigation of the chemistry of HS it was established that bulky and non-symmetrical IPDI disrupt crystallinity and promote formation of an amorphous, homogenously mixed HS-SS phase with glass transition temperatures above RT. The effect of the length of diol chain extenders on the healing properties was found to be minimal. The introduction of urea groups to polymer matrices was found to increase the undesirable phase-separation between the HS-SS and HS phases and crystallinity of both phases. The self-healing of coatings decreased with an increase of urea group content at RT, while at 60 °C remained unaffected with moderate concentrations of urea groups and significantly reduced with high amounts of urea. Increased crosslinking was found to increase phase-separation and solvent resistance, and reduce coatings hardness, cross-cut adhesion and healing at RT.

The last building block, the internal emulsifier DMPA used to provide dispersibility of the polyurethanes in water, will be studied in this chapter. There are only a few studies reporting the effect of DMPA on the morphology of PU. Lee *et al.* reported that increased amount of internal emulsifier decreased the particle size.[2] Cakic *et al.* found that increase of DMPA content resulted in lower thermal stability and gloss, while increased T_g, phase-separation, hardness and storage and loss modulus was observed.[3] Therefore, the IPDI based coatings presented in this chapter contain various amounts of DMPA, obtained by varying the DMPA/CE ratio previously set to be 3:1. The influence of the bulky internal emulsifier on the morphology of polymers and their SH behaviour is investigated.

8.1. SYNTHESIS INFORMATION

In the last set of formulations the amount of DMPA was varied. The materials were prepared using the polycarbonate polyol PH50 with MW of 500 g mol^{-1} and IPDI. Two subsets of formulations with different CE were prepared, one with EG and one with DEG. In each subset the amount of DMPA (**Figure 8-1**), the internal emulsifier, was varied between 15% and 100% (**Table 8-1**).

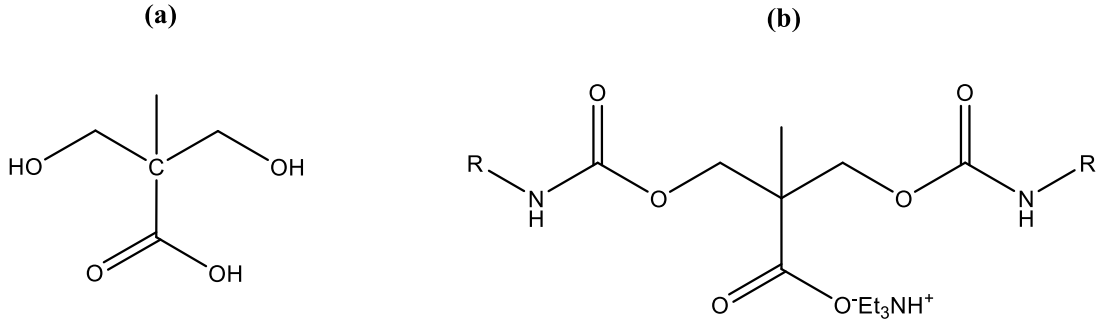

Figure 8-1. *The structure of (a) the internal emulsifier DMPA and (b) neutralised DMPA within PU.*

All formulations were prepared using the acetone process, as described in Section 2.2.5. The number of moles of CEs (EG/DEG and DMPA) remained unchanged. However, the ratio of the two CE varied - DMPA contributed to 15-100% of the total number of moles of CE, while EG or DEG to 0-85% of the total number of moles of CE.

Table 8-1. *List of formulations and their composition.*

Polyurethane	EG (mol%)	DMPA (mol%)	Total DMPA content (%)
PH50-IPDI-DMPA/EG (20%)	80	20	2.6
PH50-IPDI-DMPA/EG (25%)	75	25	3.3
PH50-IPDI-DMPA/EG (33%)	67	33	4.3
PH50-IPDI-DMPA/EG (50%)	50	50	6.4
PH50-IPDI-DMPA (100%)	0	100	12.4
PH50-IPDI-DMPA/DEG (15%)	85	15	1.9
PH50-IPDI-DMPA/DEG (20%)	80	20	2.5
PH50-IPDI-DMPA/DEG (25%)	75	25	3.2
PH50-IPDI-DMPA/DEG (33%)	67	33	4.2
PH50-IPDI-DMPA/DEG (50%)	50	50	6.3
PH50-IPDI-DMPA (100%)	0	100	12.4

8.2. *CHARACTERISATION OF DISPERSIONS*

Two subsets of materials were prepared, one with EG and DMPA and the other with DEG and DMPA. In each set the amount of internal emulsifier DMPA varied between 15% and 100%. The list of formulations, percentage solid content, as well as the appearance and viscosity of the dispersions are presented in **Table 8-2**.

The experimental solid content of dispersions prepared with the smallest amount of DMPA was approximately 7%. The low solid content, associated with the separation of the dispersion, was caused by a poor dispersibility of the polymer in the aqueous media due to reduced amount of the internal emulsifier DMPA. The remaining dispersions exhibited the solid content between 26% and 32%. It can be noticed that solid content increases with an increase of the amount of DMPA. Coatings prepared with smaller amounts of DMPA gelled during the reaction and did not disperse in the dispersion medium, thus they are not reported in the table below. The smallest amount of DMPA required to create a soluble and stable dispersion was found to be 25% of the total number of moles of CE for formulations prepared with EG and 20% of the total number of moles of CE for formulations prepared with DEG, accounting for approximately 3 wt% of the total polymer weight, consistent with the findings reported in the literature.[4,5]

Table 8-2. Characterisation data of the polyurethane dispersions.

Polyurethane	Solid content (%)	Appearance	Contact angle
PH50-IPDI-DMPA/EG (20%)	6.7 ± 1.0	Milky - separates	-
PH50-IPDI-DMPA/EG (25%)	31.9 ± 1.2	Milky	44.7 ± 1.8
PH50-IPDI-DMPA/EG (33%)	31.8 ± 1.1	Cloudy	41.4 ± 0.1
PH50-IPDI-DMPA/EG (50%)	29.7 ± 1.4	Clear	41.6 ± 2.1
PH50-IPDI-DMPA (100%)	30.7 ± 0.9	Clear	39.3 ± 1.9
PH50-IPDI-DMPA/DEG (15%)	7.2 ± 1.1	Milky – separates	-
PH50-IPDI-DMPA/DEG (20%)	25.9 ± 1.1	Milky	45.9 ± 1.7
PH50-IPDI-DMPA/DEG (25%)	27.9 ± 1.5	Milky	43.6 ± 0.4
PH50-IPDI-DMPA/DEG (33%)	27.3 ± 1.2	Cloudy	41.5 ± 1.1
PH50-IPDI-DMPA/DEG (50%)	31.3 ± 1.5	Clear	39.2 ± 1.1
PH50-IPDI-DMPA (100%)	30.7 ± 0.9	Clear	39.3 ± 1.9

Dispersions prepared with the smallest amount of DMPA were found to have a milky colour, and separation of phases was observed, indicative of a low solubility in water.

As the concentration of DMPA increased, the appearance of the dispersions shifted to completely transparent.

The contact angle of the dispersions measured on a glass surface was found to decrease with an increase of DMPA content. Lowering of the contact angle values reflects the increase of hydrophilicity of dispersions, caused by the larger amount of polar DMPA groups present.

8.3. CHARACTERISATION OF COATINGS

The variation of percentage of hard segments within sets was minimal, up to 3%, due to similar molecular weight of CEs and DMPA (**Table 8-3**). The pencil hardness was found to decrease with the increase of DMPA content, which might be explained by increase of phase-separation reported in the literature.[3]

The coatings prepared with the smallest amount of DMPA exhibited high haze values, above the acceptable 2% haze level, which may be linked to the poor solubility of the polymers in the dispersion and formation of coatings with a high surface roughness.[6,7] All the coatings with higher DMPA content showed lower haze values, below 1%.

The contact angle of water droplets on the surface of the coatings was found to decrease with the increase of DMPA in the coating, which is related to the increased content of carboxylic acid groups. The increase of the concentration of ionic groups leads to higher hydrophilicity of the surface, thus the droplets spread easier on the films, decreasing the contact angle.[8,9]

Table 8-3. *Characterisation data of the polyurethane coatings.*

Polyurethane	HS (%)	Pencil Hardness	Haze (%)	Contact angle
PH50-IPDI-DMPA/EG (20%)	51.0	3B	3.01	-
PH50-IPDI-DMPA/EG (25%)	51.2	B	0.22	71.4 ± 1.7
PH50-IPDI-DMPA/EG (33%)	51.5	2B	0.44	69.8 ± 3.0
PH50-IPDI-DMPA/EG (50%)	52.0	2B	0.31	68.2 ± 1.3
PH50-IPDI-DMPA (100%)	53.6	4B	0.23	65.3 ± 1.1
PH50-IPDI-DMPA/DEG (15%)	52.6	2B	17.70	-
PH50-IPDI-DMPA/DEG (20%)	52.7	3B	0.29	70.2 ± 1.3
PH50-IPDI-DMPA/DEG (25%)	52.7	2B	0.33	78.6 ± 1.3
PH50-IPDI-DMPA/DEG (33%)	52.8	4B	0.30	72.3 ± 1.4
PH50-IPDI-DMPA/DEG (50%)	53.0	4B	0.44	69.9 ± 0.7
PH50-IPDI-DMPA (100%)	53.6	4B	0.23	65.3 ± 1.1

The results of solubility tests are presented in **Table 8-4**. The materials were tested in four solvents: non-polar toluene, polar aprotic dichloromethane (DCM), polar aprotic acetone and polar and polar protic ethanol.

The materials were found to be resistant to non-polar toluene due to inability of formation of H-bonds or dipole-dipole interactions with the solvent. The polar aprotic DCM was found to dissolve the materials completely, due to its polarity. In the other two polar solvents, acetone and ethanol, the solvent resistance was found to somewhat decrease with an increase of the ionic groups content, due to the ability to form larger amount of H-bonds and dipole-dipole interactions with the solvents.

Table 8-4. The results of solvent resistance tests of the coatings.

Sample	Acetone	Ethanol	Toluene	Dichloromethane
PH50-IPDI-DMPA/EG (20%)	±	+	+	-
PH50-IPDI-DMPA/EG (25%)	±	+	+	-
PH50-IPDI-DMPA/EG (33%)	±	+	+	-
PH50-IPDI-DMPA/EG (50%)	±	±	+	-
PH50-IPDI-DMPA (100%)	-	±	+	-
PH50-IPDI-DMPA/DEG (15%)	±	+	+	-
PH50-IPDI-DMPA/DEG (20%)	±	+	+	-
PH50-IPDI-DMPA/DEG (25%)	±	+	+	-
PH50-IPDI-DMPA/DEG (33%)	±	+	+	-
PH50-IPDI-DMPA/DEG (50%)	±	+	+	-
PH50-IPDI-DMPA (100%)	-	±	+	-

- dissolved, ± swelled, + solvent resistant

8.4. CHARACTERISATION OF COATINGS' MORPHOLOGIES

Figure 8-2 presents FT-IR spectra of the two subsets of coatings. Among the important signals, a broad NH stretch can be observed between 3500 cm^{-1} and 3250 cm^{-1}, CH_2 stretches at 2935 cm^{-1} and 2860 cm^{-1}, and a broad peak between 3500 cm^{-1} and 2250 cm^{-1} assigned to carboxylic acid. Furthermore, multiple carbonyl stretches between 1740 cm^{-1} and 1650 cm^{-1}, C-N stretch and NH bend between 1600 cm^{-1}, and several CH signals below 1500 cm^{-1} can be observed.[10]

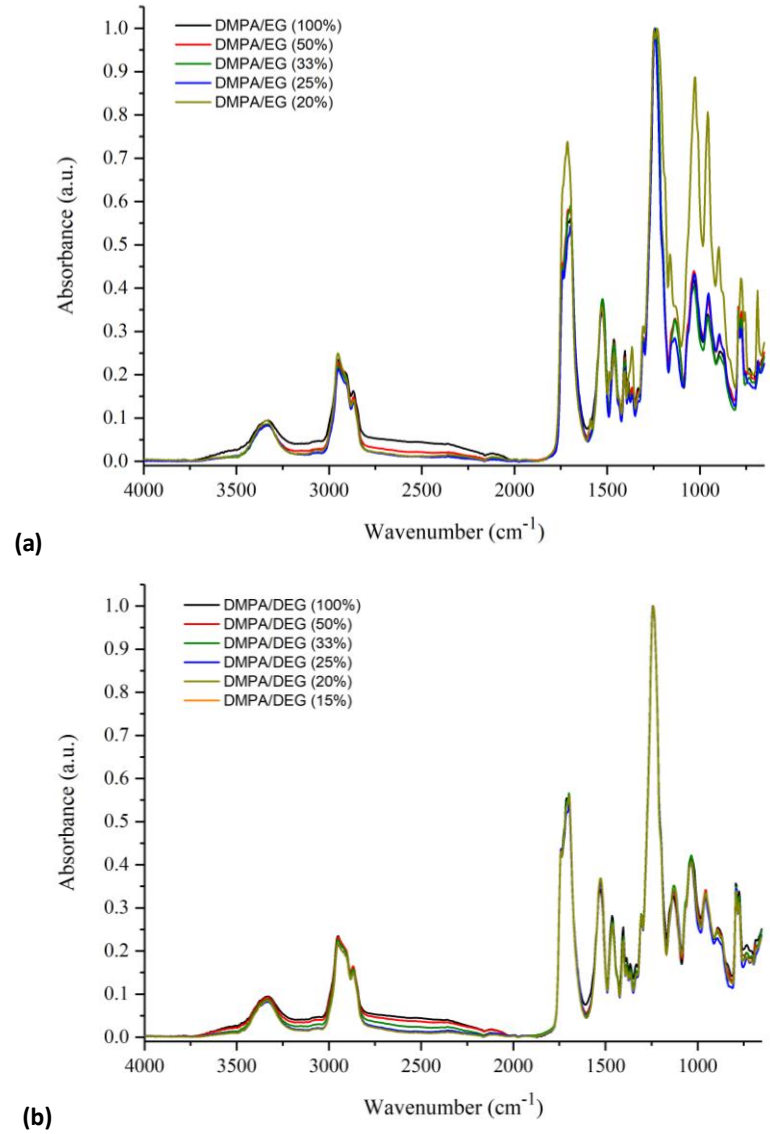

***Figure 8-2**. ATR FT-IR spectra of coatings prepared with (a) EG and (b) DEG.*

The most significant differences in the spectra of coatings can be observed in the 4000-2000 cm^{-1} region (**Figure 8-3**). A very broad band of carboxylic acid OH stretch can be observed between 3500 cm^{-1} and 2500 cm^{-1}. As expected, the absorbance of the band consequently increases with the amount of DMPA used. In the amine NH stretch region all three sets of samples show only a small amount of non H-bonded (3500-3400 cm^{-1} shoulder), suggesting that majority of NH groups are involved into H-bonding (**Table 8-5**).[11] The NH peaks is broad and not sharp, indicative of the presence of hard-soft segment interaction and mainly a phase-mixed morphology.[12,13] The phase-mixing is largely influenced by the presence of bulky,

non-symmetrical IPDI that promotes creation of multi-dimensional polymer chains, disrupting packing and crystallinity. However, as the carboxylic acid OH band overlays with the NH stretch band, the evaluation of the influence of DMPA on phase morphology of the coatings is limited.

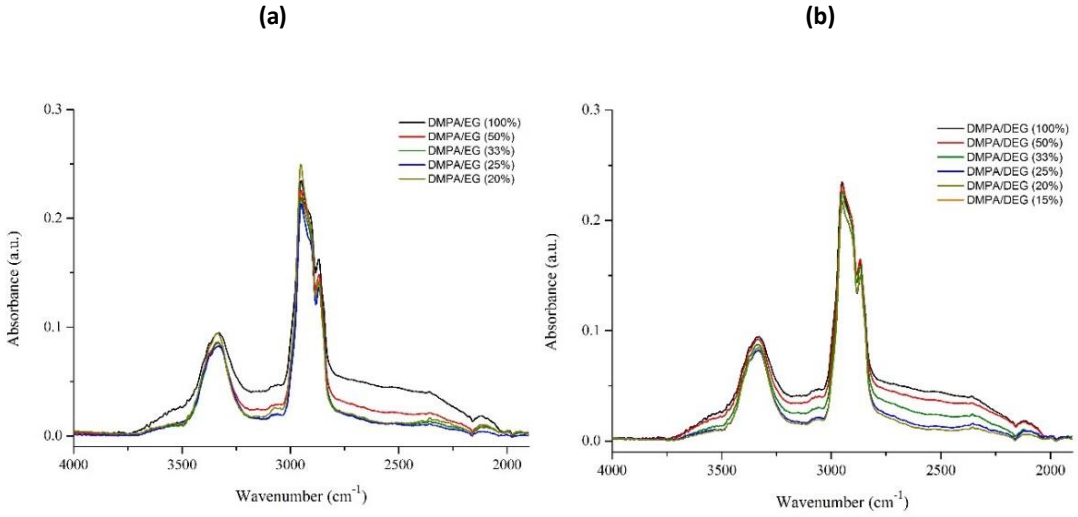

***Figure 8-3**. The NH region of ATR FT-IR spectra of coatings prepared with (a) EG and (b) DEG.*

***Table 8-5.** Characteristic IR bands for phase-mixed and phase-separated systems.[10-13]*

Wavenumber (cm^{-1})	Functional group ($\bar{\upsilon}$ – stretching, δ – bending)	Group assignment	Morphology
3500-3400	$\bar{\upsilon}$(NH) free	Urethane	Free
3400-3350	$\bar{\upsilon}$(NH) bonded	Urethane	Phase-mixed
3350-3300	$\bar{\upsilon}$(NH) bonded	Urethane	Phase-separated
1743	$\bar{\upsilon}$(C=O) free	Polyol	Free
1740-1730	$\bar{\upsilon}$(C=O) bonded	Polyol	Phase-mixed
1733-1730	$\bar{\upsilon}$(C=O) free	Urethane	Free
1723-1705	$\bar{\upsilon}$(C=O) bonded	Urethane	Phase-mixed
1700-1683	$\bar{\upsilon}$(C=O) bonded	Urethane	Phase-separated
1700-1680	$\bar{\upsilon}$(C=O) free	Urea	Free
1660-1635	$\bar{\upsilon}$(C=O) bonded, monodentate	Urea	Phase-mixed
1616-1627	$\bar{\upsilon}$(C=O) bonded, bidentate	Urea	Phase-separated
1580-1576	$\bar{\upsilon}$(CN) + δ(NH) bonded, bidentate	Urea	Phase-separated
1570-1554	$\bar{\upsilon}$(CN) + δ(NH) bonded, monodentate	Urea	Phase-mixed
1539-1530	$\bar{\upsilon}$(CN) + δ(NH) bonded	Urethane	Phase-separated
1526-1507	$\bar{\upsilon}$(CN) + δ(NH) bonded	Urethane	Phase-mixed

The analysis of the carbonyl region of the ATR FT-IR spectra (**Figure 8-4**) suggests a minimal amount of urea groups present in the polymers, formed during undesirable side reactions. The peak at 1745 cm^{-1} can be assigned to a polycarbonate carbonyl group. As expected, in all three sets of the spectra the absorbance of the peak at 1715 cm^{-1} associated with the carboxylic acid C=O stretch increases with the DMPA

content. The absorbance of the peak below 1700 cm^{-1} also increases with the amount of DMPA used due to a larger amount of polar carboxylic acid groups, thus confirming the increase of phase-separation.[14]

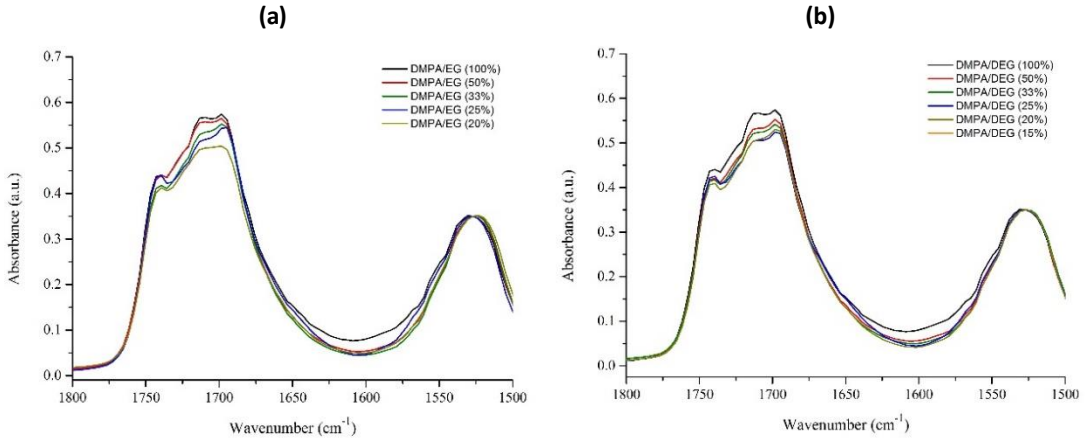

***Figure 8-4**. The carbonyl region of ATR FT-IR spectra of coatings prepared with (a) EG and (b) DEG.*

Figure 8-5 presents DSC plots obtained for samples prepared with the two CE. In the first healing cycle of the two sets of materials the T_g of the amorphous regions of the HS-SS blocks were found to very insignificantly, at approximately 35˚C for samples prepared with EG and 29˚C for samples prepared with DEG. However, a broadening of the transaction can be observed with the increased amount of DMPA, shifting the onset from approximately 20˚C for samples prepared with a minimal amount of DMPA to 10˚C for the sample prepared only with DMPA, indicating an increase of phase-separation of the systems. In the second heat cycle similar trend can be observed. Moreover, with the increase of DMPA content the T_g shifts to higher temperatures. The change is more significant for materials prepared with DEG, with the shift of T_g from 33˚C to 40˚C. Moreover, the glass transition occurs over a larger range of temperatures, with the onsets shifting to lower temperatures and the end of the transition shifting to higher temperatures.

The DSC curves of all the samples also show melting endotherms associated with the crystalline HS-SS blocks. The melting temperatures as well as the enthalpies of the transitions increase as the percentage of DMPA increases, shifting from temperatures below 100˚C to 125˚C (**Table 8-6**). The increase of crystallinity and phase-separation reflects the significant changes in the morphology of polyurethanes, influenced by

the increased amount of interactions between the polar DMPA, present in HS-SS regions.

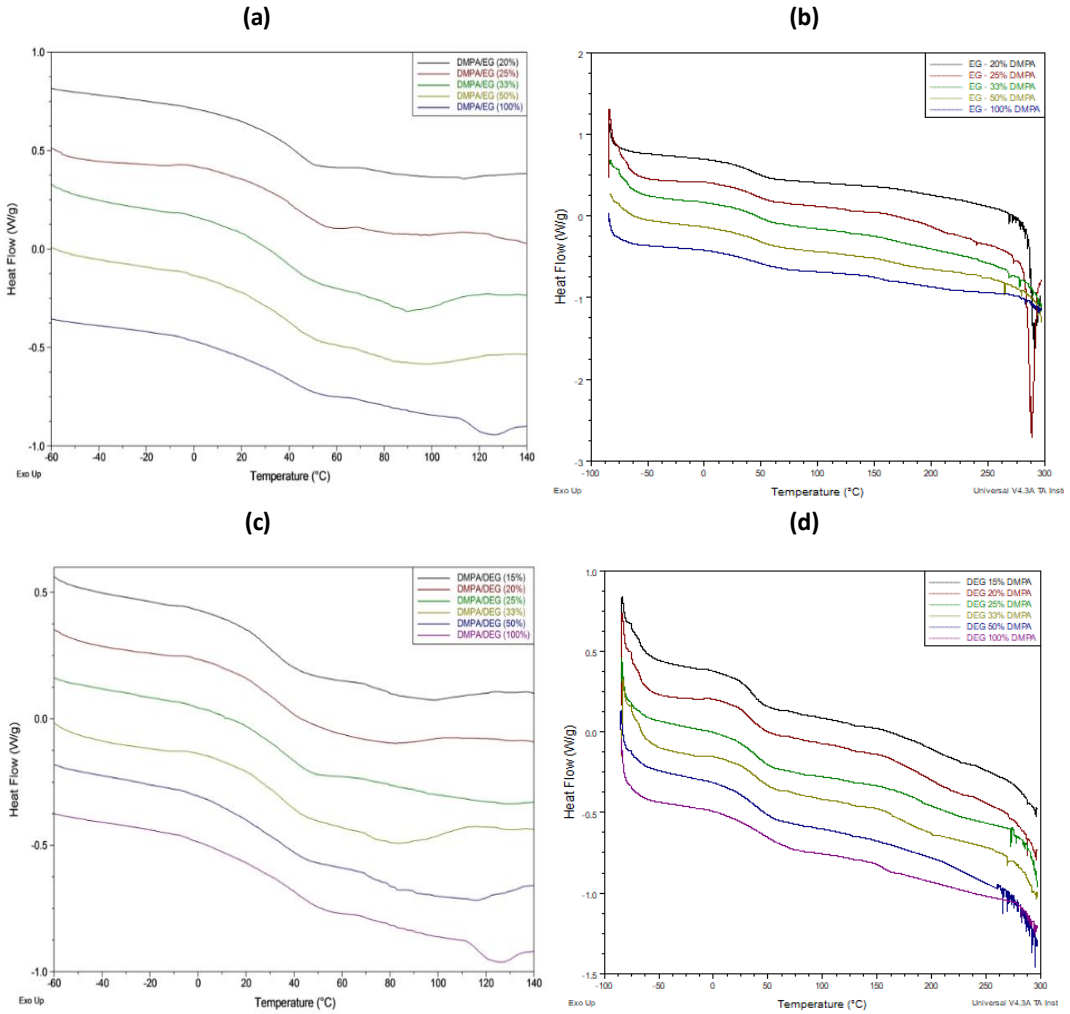

***Figure 8-5**. DSC curves of coatings prepared with a) EG, first heating cycle, b) EG, second heating cycle, c) DEG, first heating cycle and d) DEG, second heating cycle.*

In the second DSC cycles no melting endotherms of the crystalline HS-SS phase are present, indicating that crystallinity is being developed slowly over time. All samples showed a second glass transition associated with the amorphous regions of HS, decreasing with the increase of DMPA content from approximately 180 °C to 160 °C. the decrease of the T_g of the highly polar amorphous HS can be caused by the bulky structure of DMPA disturbing the interactions within the segment and reducing the amount of energy required by the polymer chains to gain mobility. The presence of crystalline regions within HS is apparent by the onset of melting endotherms at temperatures above 280 °C.[14]

Table 8-6. DSC characterisation data of HDI-based samples.

Polyurethane	Heat 1			Heat 2		
	T_g (°C)	T_m (°C)	ΔH (J/g)	T_g (°C)	T_m (°C)	ΔH (J/g)
DMPA/EG (20%)	37 (24 to 53)	113	4.2	39 (22 to 57) 178	291	-
DMPA/EG (25%)	38 (23 to 51)	85	2.1	40 (23 to 58) 180	288	-
DMPA/EG (33%)	36 (23 to 50)	90	6.6	42 (22 to 61) 156	295	-
DMPA/EG (50%)	33 (18 to 50)	96	7.4	42 (23 to 62) 161	295	-
DMPA (100%)	30 (11 to 50)	125	8.5	40 (15 to 66) 156	295	-
DMPA/DEG (15%)	29 (15 to 42)	98	4.7	33 (20 to 46) 195	-	-
DMPA/DEG (20%)	29 (14 to 44)	82	1.9	33 (17 to 49) 188	-	-
DMPA/DEG (25%)	31 (15 to 47)	118	3.4	36 (20 to 52) 183	-	-
DMPA/DEG (33%)	28 (14 to 43)	84	5.2	38 (23 to 53) 164	-	-
DMPA/DEG (50%)	26 (9 to 44)	115	10.6	35 (17 to 54) 160	-	-
DMPA (100%)	30 (11 to 50)	125	8.5	40 (18 to 66) 158	-	-

8.5. EVALUATION OF SELF-HEALING PROPERTIES

The results of self-healing efficiency tests of samples prepared with EG are presented in **Figure 8-6**. Dispersions that showed separation of phases and resulted in creation of coatings with high haze were not tested to evaluate their SH efficiency. The data obtained during tests performed at RT and at 60 °C are presented in **Table 8-7** and **Table 8-8**.

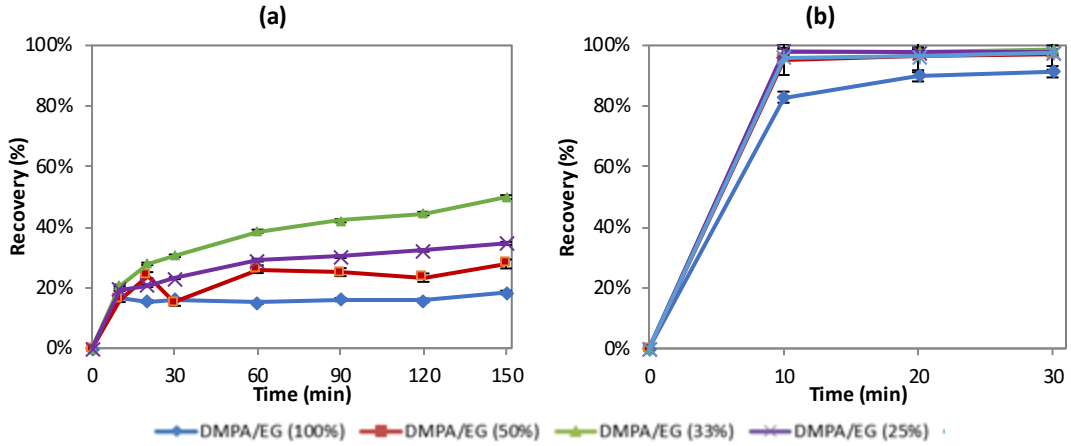

***Figure 8-6**. Percentage recovery of samples prepared with EG at (a) RT and (b) 60˚C.*

***Table 8-7.** Haze values of coatings prepared with EG healed at room temperature.*

Sample	Haze								
	Initial	Scratched	10 min	20 min	30 min	60 min	90 min	120 min	150 min
DMPA/EG (25%)	0.22	2.83	2.59	2.32	2.38	2.25	2.33	2.27	2.16
DMPA/EG (33%)	0.44	10.89	10.48	10.20	10.32	9.79	9.97	9.69	9.54
DMPA/EG (50%)	0.31	14.33	13.37	13.17	13.07	12.80	12.73	12.60	12.50
DMPA (100%)	0.23	5.36	4.49	4.56	4.53	4.58	4.53	4.55	4.41

***Table 8-8.** Haze values of coatings prepared with EG healed at 60 ˚C.*

Sample	**Haze**				
	Initial	**Scratched**	**10 min**	**20 min**	**30 min**
DMPA/EG (25%)	0.24	4.88	0.32	0.31	0.31
DMPA/EG (33%)	0.48	10.95	1.13	1.04	1.00
DMPA/EG (50%)	0.29	11.55	1.08	1.05	1.03
DMPA (100%)	0.63	4.85	1.35	1.05	1.00

At RT, below the glass transition of the coatings, the increase of DMPA content marginally lowers the SH efficiency. Samples prepared with 25% of DMPA and 75% of EG show the haze recovery of 26% within 150 minutes from scratching. As the DMPA content increases, the recovery of damaged coatings decreases, reaching only 13% for the sample prepared with DMPA only. The hindering of the healing can be explained by the increase of crystallinity of coatings as well as their phase-separation preventing the rearrangement of polymer chains and disappearance of scratches. The recovery of samples below their T_g can be associated with the onset of the transition below RT.

At 60 °C all coatings prepared with blends of EG and DMPA showed over 95% recovery from damage within the first 10 minutes. The sample prepared with DMPA only showed less efficient recovery, reaching 83% within the first 10 minutes and 90% after 30 minutes. As the healing process at 60 °C occurs above the glass transition of the coatings, the lower healing efficiency of the sample prepared with DMPA reflects the influence of phase-separation on the healing process, reducing the ability of polymer chains to move freely and rearrange.

Coatings prepared with DEG and DMPA showed somewhat better healing efficiency at RT, presented in **Figure 8-7**. The data obtained during tests performed at RT and at 60 °C are presented in **Table 8-9** and **Table 8-10**. At RT, which is below the glass transition of the coatings, all the samples showed the haze recovery of up to 50% within 150 minutes from scratching. The improved healing at RT can be related to the lower T_g of the HS-SS blocks. The recovery of samples below their T_g can be associated with the onset of the transition below RT.

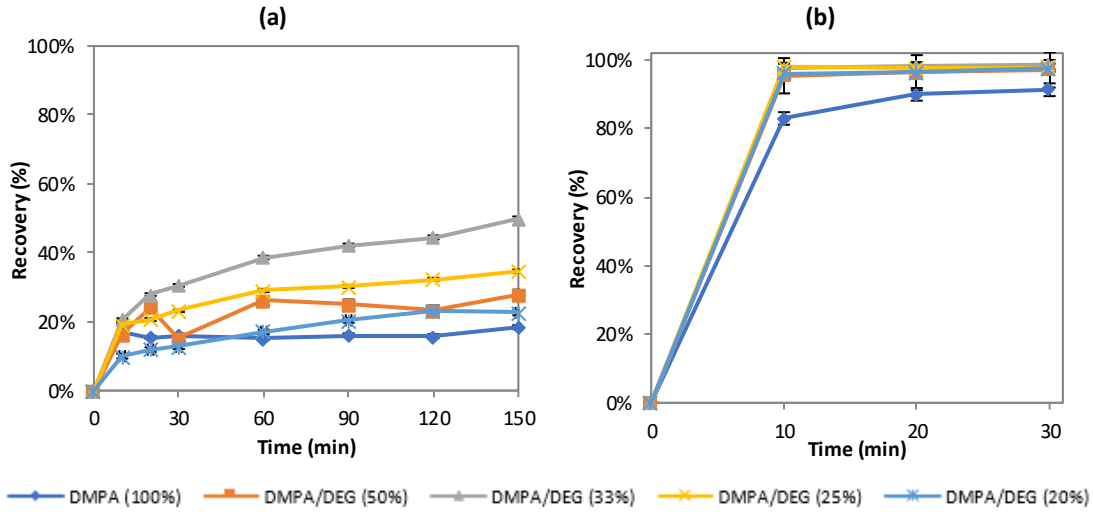

***Figure 8-7**. Percentage recovery of samples prepared with DEG at (a) RT and (b) 60°C.*

***Table 8-9.** Haze values of coatings prepared with DEG healed at room temperature.*

Sample	Haze								
	Initial	Scratched	10 min	20 min	30 min	60 min	90 min	120 min	150 min
DMPA/DEG (20%)	0.29	7.69	6.95	6.81	6.75	6.43	6.18	5.98	6.02
DMPA/DEG (25%)	0.33	4.36	3.58	3.53	3.43	3.19	3.14	3.06	2.96
DMPA/DEG (33%)	0.30	13.06	10.43	9.51	9.17	8.13	7.69	7.39	6.70
DMPA/DEG (50%)	0.44	10.68	9.02	8.21	9.13	8.01	8.11	8.29	7.83
DMPA (100%)	0.23	5.36	4.49	4.56	4.53	4.58	4.53	4.55	4.41

Table 8-10. *Haze values of coatings prepared with DEG healed at 60 °C.*

Sample	Haze				
	Initial	Scratched	10 min	20 min	30 min
DMPA/DEG (20%)	0.29	8.59	0.62	0.60	0.49
DMPA/DEG (25%)	0.33	3.35	0.39	0.40	0.40
DMPA/DEG (33%)	0.42	11.74	0.70	0.65	0.58
DMPA/DEG (50%)	0.30	13.44	0.90	0.79	0.68
DMPA (100%)	0.63	4.85	1.35	1.05	1.00

At 60 °C all coatings prepared with blends of CEs showed over 95% recovery from the damage within the first 10 minutes. The sample prepared with DMPA only shows lower recovery of 83% within the first 10 min, reaching 90% after 30 minutes. As previously mentioned, the healing process at 60 °C occurs above the glass transition of the coatings, thus the lower healing efficiency of the sample prepared with DMPA must reflect the influence of phase-separation on the healing process, reducing the ability of polymer chains to move freely and rearrange.

8.6. SUMMARY AND DISCUSSION

The minimal amount of DMPA required to create environment friendly, stable and well dispersed PUDs was determined to be between 20% and 25% of the chain extenders fraction, which accounts for approximately 3% of the complete polyurethane weight. With an increase of DMPA content the colour of the dispersions was observed to become less milky and more transparent. The viscosity and surface tension of dispersions, as well as contact angle and contact angle of coatings were found to increase due to the increase of the ionic content.

Moreover, the increase of DMPA content in polyurethane SH materials resulted in a number of changes in the polymers' morphology and their properties.

- **Haze and hardness.** The haze of coatings was found to be unaffected by the amount of DMPA, within the acceptable 0-2% haze levels. The hardness of coatings was found to decrease with the increase of the DMPA content, related to the increase of phase-separation.
- **Solvent resistance.** The solvent resistance of the materials was found to be decrease with an increase of the amount of the internal emulsifier. The change

was more significant in polar solvents, such as acetone or ethanol, due to the polar nature of DMPA and ability to form H-bonds and dipole-dipole interactions with the solvent.

- **Phase-mixing.** In the DSC analysis a broadening and a raise of glass transition temperatures and melting temperatures of HS-SS blocks was observed, as well as an increase of the melting enthalpy, indicative of an increase of phase-separation with the increase of the DMPA content. The observation was also confirmed by ATR FT-IR. The change in the morphology of the polymers can be explained by the polar nature of the internal emulsifier, allowing creation of stronger interactions within the HS within HS-SS blocks, as well as between the HS and SS, thus increasing the crystallinity and T_g of the homogenously mixed block. However, the bulky structure of DMPA also resulted in lowering of the T_g of amorphous HS by disruption of the interactions within the segment and reducing the amount of energy required by the polymer chains to gain mobility and undergo the glass transition (**Figure 8-8**).

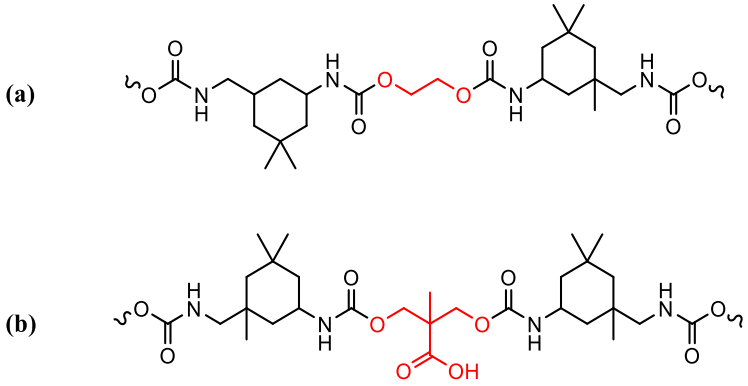

Figure 8-8. *The structures of HS prepared with (a) EG and (b) a bulky DMPA.*

- **Self-healing.** The self-healing behaviour was found to be influenced by phase-separation of the systems. The increase of DMPA content resulted in decreased healing at room temperature, caused by stronger interactions between the polar groups of the internal emulsifier within the HS-SS block. The effect was more significant in formulations prepared with blends of DEG and DMPA due to their lower T_g. However, the healing remained unchanged at 60 °C due to the polymer

chains gaining enough energy to become mobile and rearrange within the phase-mixed polymer matrix.

Therefore, only coating PH50-IPDI-DMPA/EG (25%), also reported in the previous chapters, was found to fulfil the four requirements of the research: exhibited haze below 2%, pencil hardness of B and above, suitable glass transition temperature and thermally-triggered SH properties reaching over 90% recovery from damage.

The other coatings prepared with larger amounts of DMPA showed an improved solvent resistance. The pencil hardness of the coatings does not fulfil the requirement of minimal hardness, but the materials might find use in other applications where the hardness is not crucial.

8.7. REFERENCES

1 Z. Wirpsza, *Polyurethanes. Chemistry, Technology and Applications*, Ellis Hornwood Ltd, Midsomer Norton, 1st edn., 1993.
2 D.-K. Lee, H.-B. Tsai and R.-S. Tsai, *J. Appl. Polym. Sci.*, 2006, **102**, 4419–4424.
3 S. M. Cakić, M. Špírková, I. S. Ristić, J. K. B-Simendić, M. M-Cincović and R. Poręba, *Mater. Chem. Phys.*, 2013, **138**, 277–285.
4 H. Sardon, L. Irusta, M. J. Fernandez-Berridi, J. Luna, M. Lansalot and E. Bourgeat-Lami, *J. Appl. Polym. Sci.*, 2011, **120**, 2054–2062.
5 G. N. Manvi and R. N. Jagtap, *J. Dispers. Sci. Technol.*, 2010, **31**, 1376–1382.
6 F. C. Stehling, C. S. Speed and L. Westerman, *Macromolecules*, 1981, **14**, 698–708.
7 E. Andreassen, A. Larsen, K. Nord-Varhaug, M. Skar and H. Emptysd, *Polym. Eng. Sci.*, 2002, **42**, 1082–1097.
8 M. Barikani, M. Valipour Ebrahimi and S. M. Seyed Mohaghegh, *J. Appl. Polym. Sci.*, 2007, **104**, 3931–3937.
9 S. Subramani, J. M. Lee, I. W. Cheong and J. H. Kim, *J. Appl. Polym. Sci.*, 2005, **98**, 620–631.
10 F. Sen Yen, L. L. Lin and J. L. Hong, *Macromolecules*, 1999, **32**, 3068–3079.
11 J. Mattia and P. Painter, *Macromolecules*, 2007, **40**, 1546–1554.
12 H. S. Lee, Y. K. Wang and S. L. Hsu, *Macromolecules*, 1987, **20**, 2089–2095.
13 C. M. Gomez, D. Gutierrez, M. Asensio, V. Costa and A. Nohales, *J. Elastomers Plast.*, 2017, **49**, 77–95.
14 E. Yilgör, E. Yurtsever and I. Yilgör, *Polymer.*, 2002, **43**, 6561–6568.

9. VARIOUS MODES OF EVALUATION OF SELF-HEALING PROPERTIES

In this last chapter of this thesis variation in the self-healing tests will be presented. Three coatings: PH50-IPDI-BD, PH50-IPDI-EG and PH50-IPDI-DEG were tested using various healing modes.

In the first one, the coatings underwent three subsequent damage-heal cycles. The scratching was performed as described in Section 2.3.10. Healing was performed at 60 °C. However, healing time was reduced to 10 minutes.

The second test involved scratching of the samples, followed by leaving them at room temperature for 1 week. Subsequently, the samples underwent thermally-triggered healing for 10 minutes at 60 °C.

In the third test the coatings were scratched and left at RT for 4 weeks. The haze was monitored at regular intervals during the test.

9.1. MORPHOLOGY OF THE COATINGS USED IN THE VARIOUS SH TESTS

The three coatings used in this chapter were prepared with the polycarbonate polyol PH50 and IPDI. The coatings were found to have a well-phase mixed morphology, allowing the HS and SS create a homogenous phase with T_g above RT and low crystallinity. However, not complete compatibility between the phases was observed. The presence of separate HS was indicated by the second glass transition at higher temperatures, as well as endotherms of crystalline HS.

The three coatings showed a broad glass transition of the amorphous HS-SS regions at 17 °C, 36 °C and 28 °C respectively in the first heat cycle and at 31 °C, 35 °C and 36 °C respectively in the second. The samples also showed small and broad melting peaks in the first heat cycle, between 98 °C and 123 °C, associated with the homogenous HS-SS phase. The enthalpy of melting was smaller than the one of pure polyol.

DEG was found to promote phase-mixing and lowering crystallinity in the HDI-based samples. The IPDI-based sample prepared with DEG also appears to be somewhat

more phase-mixed, indicated by the highest T_g and the lowest crystallinity among the studied samples .

All samples showed a second glass transition in the 172 °C to 182 °C region, associated with the amorphous regions of HS. However, the transition is not well defined, suggesting a small amount of amorphous HS present in the PU. The presence of crystalline regions of HS is apparent by the large melting endotherms at temperatures above 275 °C.

The recall summary of data obtained from DSC is presented below in **Figure 9-1** and **Table 9-1**.

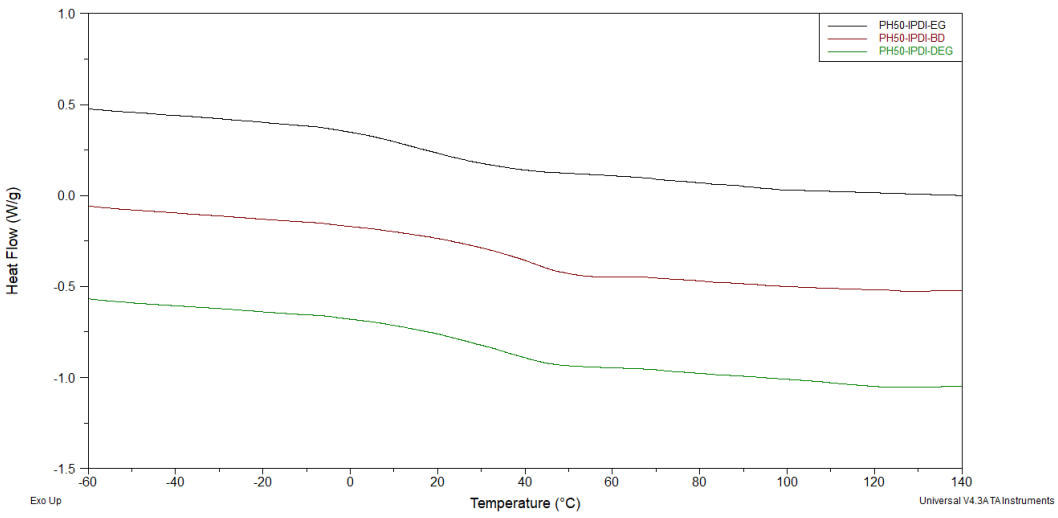

Figure 9-1. *The first heat DSC cycle of samples PH50-IPDI-BD, PH50-IPDI-EG and PH50-IPDI-DEG.*

Table 9-1. *The summary of DSC data of samples PH50-IPDI-BD, PH50-IPDI-EG and PH50-IPDI-DEG.*

PU	Heat 1			Heat 2		
	T_g (°C)	T_m (°C)	ΔH_m (J/g)	T_g (°C)	T_m (°C)	ΔH_m (J/g)
PH50	-69	74	7.5	-67	-	-
PH50-IPDI-EG	17	98	2.3 [4.7]	31 181	275	-
PH50-IPDI-BD	36	99	2.3 [4.8]	35 172	281	-
PH50-IPDI-DEG	28	123	1.0 [2.1]	36 172	279	-

The self-healing tests presented in Chapter 5 showed very low recovery of the samples at RT, reaching approximately 30% recovery after 180 minutes. The healing below T_g of the samples was associated with a well phase-mixed morphology of the

HS-SS phase, as well as the onset of the glass transition being below RT. The healing efficiency was significantly improved at 60 °C, reaching almost 100% within the first 10 minutes of the thermal treatment. The improvement of healing was associated with the process taking place at temperatures above the T_g of the samples.

The recall data is presented in **Figure 9-2**, **Table 9-2** and **Table 5-8**.

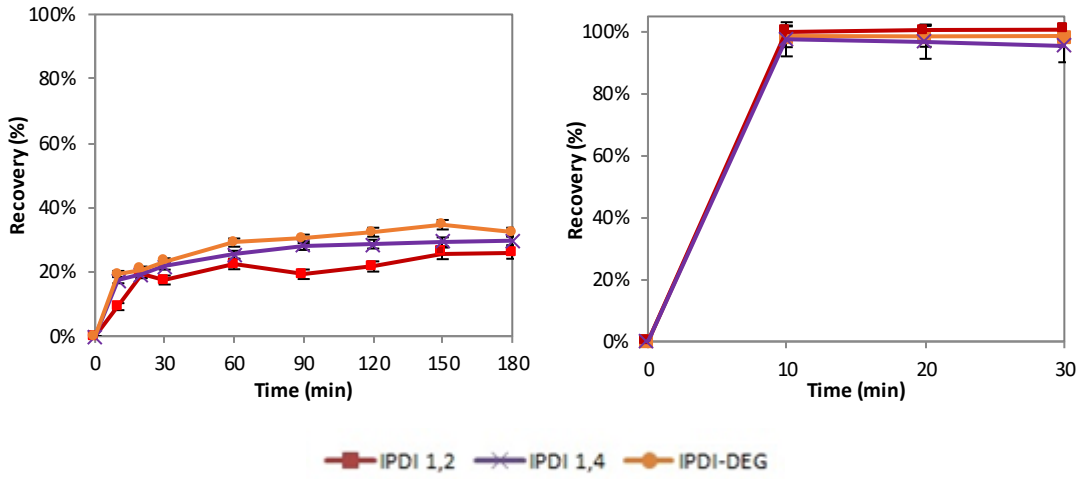

Figure 9-2. *Percentage recovery of the three coatings at (a) RT and (b) 60˚C.*

Table 9-2. *Haze values of the three coatings healed at room temperature.*

Sample	Haze									
	Initial	Scratched	10 min	20 min	30 min	60 min	90 min	120 min	150 min	180 min
IPDI-1,2-EG	0.22	2.83	2.59	2.32	2.38	2.25	2.33	2.27	2.16	2.16
IPDI-1,4-BD	0.44	4.17	3.52	3.46	3.36	3.23	3.12	3.11	3.08	3.07
IPDI-DEG	0.33	4.36	3.58	3.53	3.43	3.19	3.14	3.06	2.96	3.06

Table 9-3. *Haze values of the three coatings healed at 60 °C.*

Sample	Haze				
	Initial	Scratched	10 min	20 min	30 min
IPDI-1,2-EG	0.24	4.88	0.32	0.31	0.31
IPDI-1,4-BD	0.31	3.11	0.38	0.40	0.44
IPDI-DEG	0.33	3.35	0.39	0.40	0.40

9.2. MULTIPLE DAMAGE-HEAL CYCLES

The results of the first healing test, three subsequent damage-heal (60 °C) cycles, are presented below in **Figure 9-3**, **Table 9-4** and **Table 9-5**. All coatings showed excellent recovery from damage in the three damage-heal cycles. The coatings showed almost full recovery, reaching at least 90% after the first and second thermal treatment and 82% after the third. The second scratching of coating prepared with EG introduced significantly higher level of damage, increasing the haze of the sample to almost 20%. The difference might be associated with the softening of the coating after the thermal treatment due to the healing occurring above the T_g of the sample. Moreover, the second scratching cycle might have been performed too rapidly after the treatment, thus not allowing the sample to fully cool down. That might have also affected the recovery from damage after the third damage-heal cycle, due to introduction of a more permanent damage of the sample.

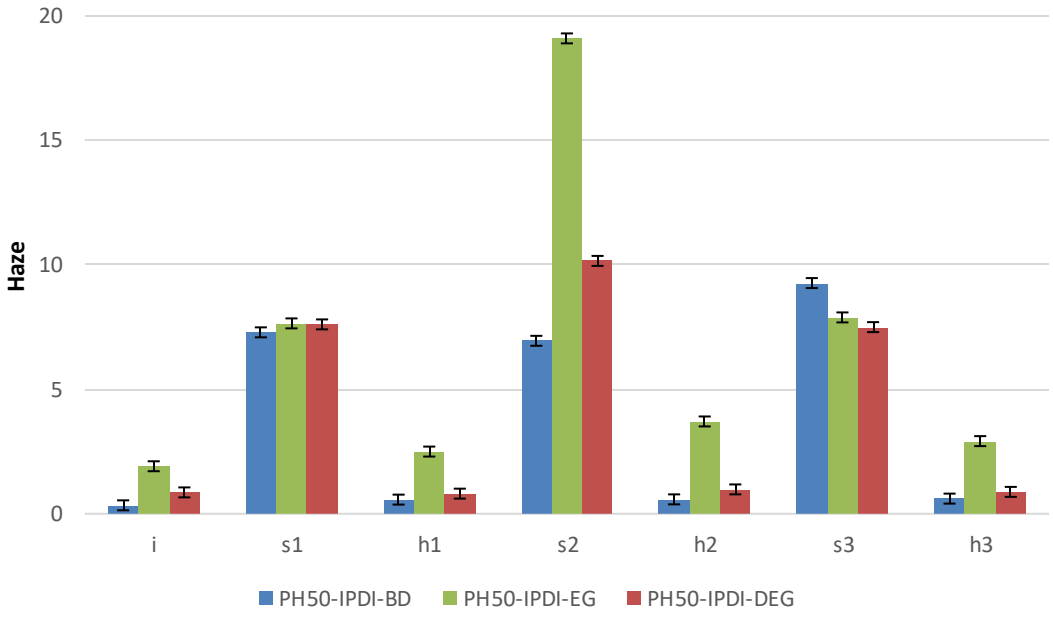

Figure 9-3. *Visual representation of haze values obtained during the first SH tests.*

Table 9-4. *The haze values measured during the first SH test (S-scratching, H- healing).*

Sample	Haze						
	Initial	1st S	1st H	2nd S	2nd H	3rd S	3rd H
PH50-IPDI-BD	0.34	7.29	0.57	6.95	0.58	9.27	0.61
PH50-IPDI-EG	1.91	7.65	2.50	19.10	3.71	7.89	2.92
PH50-IPDI-DEG	0.86	7.61	0.81	10.16	0.98	7.50	0.88

***Table 9-5**. The percentage recovery of haze obtained during the first SH test.*

Sample	Recovery		
	1st healing	2nd healing	3rd healing
PH50-IPDI-BD	97%	96%	97%
PH50-IPDI-EG	90%	90%	83%
PH50-IPDI-DEG	101%	99%	100%

9.3. *DELAYED HEALING OF THE COATINGS*

The results of the second healing test, in which the samples were scratched, left at RT for one week and subsequently treated for 10 minutes at 60 °C, are presented below in **Figure 9-4**, **Table 9-6** and **Table 9-7**. All coatings showed decreased haze values after one week at RT. The samples recovered 69%, 61% and 87% of their original haze respectively. The most efficient recovery was observed in the most phase-mixed sample prepared with DEG. The thermal treatment of the samples resulted in the haze values decreasing rapidly, reaching at least 90% recovery after 30 minutes at 60 °C.

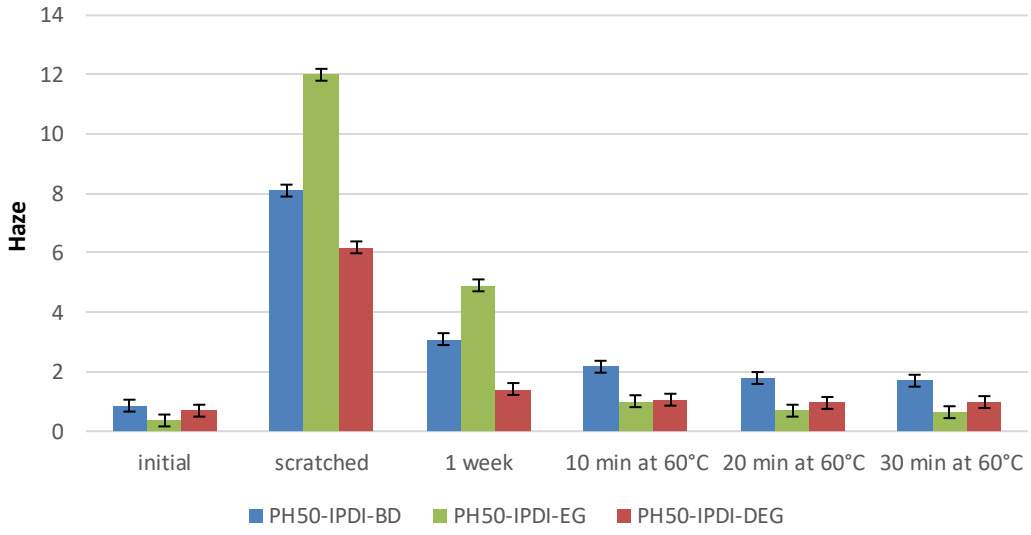

***Figure 9-4**. Visual representation of haze values obtained during the second SH tests.*

***Table 9-6.** The haze values measured during the second SH test.*

Sample	Haze					
	initial	scratched	1 week	10 min	20 min	30 min
PH50-IPDI-BD	0.86	8.10	3.10	2.17	1.79	1.60
PH50-IPDI-EG	0.36	12.00	4.91	1.01	0.69	0.64
PH50-IPDI-DEG	0.69	6.19	1.42	1.06	0.95	0.98

Table 9-7. *The percentage recovery of haze obtained during the second SH test.*

Sample	Recovery			
	1 week	10 min	20 min	30 min
PH50-IPDI-BD	69%	82%	87%	90%
PH50-IPDI-EG	61%	94%	97%	98%
PH50-IPDI-DEG	87%	93%	95%	95%

9.4. HEALING OF THE COATINGS WITHOUT A THERMAL TRIGGER

The results of the third healing test, in which the samples were scratched and left at RT for 4 weeks, are presented below in **Figure 9-5**, **Table 9-8** and **Table 9-9**. All coatings showed decreased haze values over the initial 4 weeks storage at RT period. The samples recovered between 70% and 86% of the original haze within the first week, 86-95% after 2 weeks, 88-95% after week 3, and 89-95% after 4 weeks. The most efficient recovery was observed in the most phase-mixed sample prepared with DEG, reaching 95% after 2 weeks.

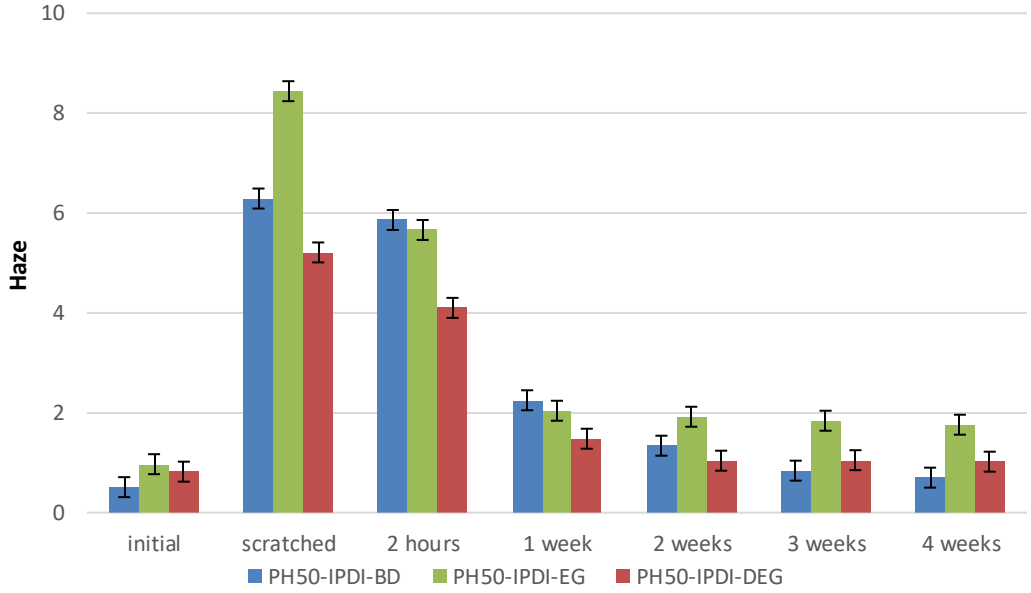

Figure 9-5. *Visual representation of haze values obtained during the third SH tests.*

Table 9-8. *The haze values measured during the third SH test.*

Sample	Haze						
	initial	scratched	2 hours	1 week	2 weeks	3 weeks	4 weeks
PH50-IPDI-BD	0.51	6.29	5.86	2.25	1.34	0.84	0.70
PH50-IPDI-EG	0.97	8.44	5.66	2.04	1.92	1.84	1.76
PH50-IPDI-DEG	0.82	5.21	4.10	1.48	1.04	1.05	1.02

Table 9-9. *The percentage recovery of haze obtained during the third SH test.*

Sample	Recovery				
	2 hours	**1 week**	**2 weeks**	**3 weeks**	**4 weeks**
PH50-IPDI-BD	7%	70%	86%	94%	97%
PH50-IPDI-EG	37%	86%	87%	88%	89%
PH50-IPDI-DEG	25%	85%	95%	95%	95%

9.5. SUMMARY AND DISCUSSION

The various self-healing tests indicated that:

- The self-healing of damaged coatings occurs slowly at RT and has a potential to reach full recovery over extended periods of time (more than 2 weeks).
- Thermal treatment of the samples results in accelerated healing, reaching almost full recovery from damage within the first 10 minutes at 60 °C, reaching at least 90% recovery.
- The thermally-triggered healing of the coatings is more efficient when performed immediately after scratching. However, the recovery from damage upon delayed thermal treatment reaches at least 80% after 10 minutes and 90% after 30 minutes. Therefore, delayed healing may require extended treatment time.
- The thermally-triggered healing of the samples is repeatable. The coatings obtained at least 90% of recovery of the original haze values after the first and second damage-heal cycle, and at least 80% after the second. However, the thermal treatment time during the multiple scratching tests was reduced to 10 minutes, thus extended treatment time may decrease to haze to even lower values.

10. Conclusions and further work

10.1. Recap of the project aims

The four main aims of the research identified at the beginning of this thesis were:

- Development of an optically clear, transparent coating with haze below 2%.
- Development of a coating with a pencil hardness of B or above.
- Development of a coating with the glass transition temperature above the room temperature and below 80 °C.
- Development of a coating exhibiting rapid, thermally-triggered self-healing properties, allowing above 90% recovery from damage within less than 10 min.

A number of polyurethane formulations was created from various starting materials, including seven polyols, two diisocyanates, one triisocyanate, diol, diamine, alkanolamine and triol chain extenders, as well as various amounts of the internal emulsifier, DMPA. The coatings were characterised using several techniques and tested to determine their self-healing properties.

This section will present the summary and overview of findings, as well as conclusions on each set of formulations, comments on their ability to fulfil the requirements presented above and future work suggestions

10.2. The influence of the chemistry of soft segments

The soft segment content in a typical PU varies between 40% and 80%.[1] The length and the chemistry of the oligomeric polyol, acting as the SS block within PU matrix, was found to play an important role and significantly influenced the morphology of coatings and their self-healing properties.

- **Haze**. The haze of coatings was found to relate to the crystallinity of SS and their compatibility with HS.

  Crystallinity of pure polyols was found to influence the crystallinity of SS and SS-rich segments within PU, apparent by the presence of melting peaks and their enthalpy values. Largely crystalline polyols such as PCL led to formation of highly

crystalline coatings. Crystalline polymers are known to be opaquer due to the large number of amorphous-crystalline interfaces, seen in the high haze values. Therefore, crystallinity of polyols was found to be unfavourable for creation of transparent, SH protective coatings. Moreover, crystallinity of polyols was found to be related to their symmetrical structure and short repeating unit.

Compatibility between the SS and HS was also found to significantly influence the haze of PU coatings. Compatible segments create phase-mixed matrix, exhibiting higher T_g and low haze. For example, polyol D1700, polydiethylene adipate glycol, showed very low compatibility with HDI-EG hard blocks, indicated by the low T_g and high haze of the phase-separated coating. Polyol D670, branched hydroxyl bearing polyester, showed high compatibility with HDI-EG hard blocks, indicated by the higher T_g and low haze of the phase-mixed coating. Therefore, the interactions between the HS and SS can be optimised by using shorter polyols forming smaller SS blocks and able to mix better with HS blocks.

- **Hardness.** The hardness of coatings was found to be related to the amount of HS within the PU matrix. Coatings prepared with polyols with high MW, and therefore having low percentage of HS, were found to be insufficiently hard. Coatings prepared with shorter polyols, thus exhibiting higher percentage of HS, showed better hardness.
- **Glass transition**. The glass transition of the SS-rich phase is related to the extent of mixing between HS and SS. Larger amount of HS 'dissolved' within the SS increases the number of interactions between the blocks and create a homogenously mixed HS-SS phase exhibiting higher T_g. Mixing of the phases is dependent on the compatibility between the segments, therefore low crystallinity polyols were found to improve phase-mixing, thus more significant increase of T_g was observed. Moreover, the shift of T_g is also related to the change of chemistry of the end groups of polyol during the reaction with isocyanate, and the effect was found to be more significant for low MW polyols.
- **Self-healing**. Efficient thermally-triggered self-healing of PU was found to be related to T_g of the materials and therefore the extent of phase-mixing.

Therefore, in order create self-healing polyurethane coatings well phase-mixed polyurethane matrix with a high compatibility between hard and soft segments is required. That can be obtained by using polyols with:

- low MW,
- low crystallinity, and
- short, unsymmetrical repeating units.

An example of a polyol fulfilling the requirements is the polycarbonate PH50, co-polymer of pentanediol and hexanediol with MW 500 g mol^{-1}.

10.3. THE INFLUENCE OF THE CHEMISTRY OF HARD SEGMENTS

The hard segment content in a typical PU varies between 20% and 60%.[1] HS are formed during the reaction of isocyanates with chain extenders and possess high density of polar urethane groups attracting each other and forming crystalline blocks.[2] The HS reinforce the structure of PU and have a large influence on the overall properties of the materials. Therefore, the choice of suitable building blocks of HS has a crucial influence on the self-healing behaviour of PU coatings.

3.1.1. Isocyanates

- **Haze.** The haze of coatings was largely influenced by the isocyanate. HDI, due to the linear, symmetrical and planar structure was found to allow easier alignment of HS, thus induced phase-separation, facilitate aggregation and crystallisation of the blocks, which resulted in coatings exhibiting high haze. Coatings prepared with IPDI showed increased phase-mixing, lower crystallinity and therefore lower haze. The unsymmetrical, nonplanar and bulky structure of the IPDI was found to hinder the alignment of the chains, prevent formation of large blocks of HS and avert crystallisation.
- **Hardness.** The hardness of coatings was minimally affected by the choice of isocyanate. Due to similar MW of HDI and IPDI, created materials exhibited similar HS content, thus the hardness.

- **Glass transition.** The T_g of SS-rich phase of PU coatings was found to be largely influenced by the isocyanate. As the research showed, an increase of the amount of the unsymmetrical, nonplanar and bulky IPDI resulted in increased phase-mixing and formation of SS-rich phase with a large amount of HS 'dissolved' in it. Therefore, the phase might be considered as a homogenous HS-SS phase, and therefore exhibited significantly higher T_g than materials prepared with HDI. Moreover, due to the increased extent of phase-mixing and higher T_g, IPDI-based coatings also showed better ageing and weathering behaviour, improving durability and weather resistance.
- **Self-healing.** The investigation of the relationship between the morphology of PU and their SH behaviour showed that mixing of HS and SS is crucial to enable the movement of polymer chains during healing from damage. Phase-mixing was found to be largely dependent on the choice of diisocyanate. Coatings prepared with the extent of a linear and symmetrical HDI exhibited a phase-separated morphology, apparent by the high crystallinity of SS and low T_g of the SS-rich phase. The amorphous SS-rich phase was found to have a limited mobility, thus full restoration of the damage was unattainable, even at temperatures above the T_g. That can be related to the restriction of movement induced by the crystalline regions of SS-rich phase, as well as the presence of dominantly crystalline HS separated from the SS. With the increase of IPDI content, an increase of phase-mixing was observed, apparent by the decrease of crystallinity levels and an increase of the T_g. In the almost fully phase-mixed system prepared with IPDI, the mixing of phases allowed an efficient and rapid rearrangement of damaged surfaces above the T_g and almost full recovery was observed. Coatings prepared with HDI also showed some self-healing behaviour at RT, related to their low T_g enabling limited rearrangement of the polymer chains. However, the healing was not improved at elevated temperatures.

Therefore, in order to create efficiently self-healing PU coatings, the use of bulky, non-symmetrical isocyanates is preferred over linear, symmetrical ones. The symmetrical HDI was found to promote phase-separation, crystallinity, high haze and

low T_g. Bulky IPDI was found to promote phase-mixing, low crystallinity, haze and higher T_g of the homogenous, phase-mixed phase composed of HS and SS.

Formulations prepared with PH50 and IPDI showed a well phase-mixed morphology. The coatings were found to exhibit self-healing reaching 100% recovery at temperatures above their lower T_g.

3.1.2. Chain extenders

- **Haze.** In phase-separated materials, prepared with HDI, the increase of the length of a diol CE was found to increase haze values of the coatings. The increase was related to formation of larger HS blocks, thus promoting phase-separation and crystallinity within the matrix. The higher crystallinity and phase-separation resulted in formation of high-haze coatings, caused by light scattering of the interfaces between HS and SS, as well as the presence of crystallites. In coatings prepared with IPDI the influence of the length of the CE was minimal and the haze values were found to be within the acceptable 0-2% level.

  Introduction of alkanolamine and diamine CE, thus the increase of the amount of urea groups, did not significantly influence the haze of coatings. The haze values of the coatings were found to be within the acceptable 0-2% level.
- **Hardness.** The hardness of coatings was minimally affected by the choice of diol CE. Due to similar MW of CE, created material exhibited similar HS content, thus the hardness of coatings remained unaffected.

  Introduction of alkanolamine CE resulted in decrease of the hardness of the coatings. The change was related to increased phase-separation of HS and SS, increased crystallinity and brittleness of materials with higher urea content, caused by the presence of stronger interactions between urea groups. However, the coating prepared with diamine CE showed an acceptable hardness. The improvement of the hardness of the coating prepared with diamine can be linked to the higher MW of the CE.
- **Glass transition.** The length of diol CE was found to increase phase-separation in HDI-based coatings, indicated by the decrease in T_g. The change was related to formation of larger HS promoting an increase of phase-separation. However, in

IPDI-based materials the effect was less significant and only a small increase of phase-mixing was observed, indicated by insignificantly higher T_g. Therefore, in the functional IPDI-based self-healing coatings, due to the bulky and unsymmetrical structure of the diisocyanate, the influence of the length of the diol chain extender on glass transition was minimal.

An introduction of chain extenders containing amine groups to IPDI-based coatings resulted in stronger interactions between HS and SS within the homogenous SS-rich phase. Therefore, an increase of T_g was observed.

- **Self-healing.** The length of diol CE was found to insignificantly change the self-healing behaviour of the coatings. The SH of HDI-based coating prepared with DEG was found to be superior to coatings prepared with other CE, and the change was related to the increased phase-mixing of the system. The absence of CE was found to improve phase-mixing of HDI-based materials, resulting in an improvement of the SH properties. In the IPDI-based formulations the absence of CE resulted in the lower percentage of HS and lower T_g of the coatings. The lower T_g was found to improve the healing efficiency at RT and did not affect the process at elevated temperatures.

  An introduction of urea groups to IPDI-based formulations was found to reduce the SH efficiency at RT. However, at elevated temperatures the SH was mainly unaffected. Therefore, the adjustment of the amount of urea groups was found to allow tailored design of the self-healing coatings, showing reduced healing at RT and efficient heat-triggered healing at elevated temperatures.

Therefore, in functional coatings prepared with PH50 and IPDI, the choice of diol CE did not significantly influence the desired properties of materials. However, the cross-cut adhesion between the coatings and TAc was significantly reduced in coatings prepared with long diol CE. Nevertheless, the self-healing properties of the materials, as well as their suitable haze, hardness and T_g allows them to be used as highly functional coatings.

The use of alkanolamine CE resulted in creation of softer coatings, not fulfilling the hardness requirements. However, the efficient healing of these coatings makes them suitable for applications where the hardness is not a crucial requirement.

3.1.3. Crosslinking

An increase of the amount of crosslinking within the HS is known to improve physical properties of PU materials. The crosslinking introduced to the coatings by using trimer CE and trifunctional IPDI resulted in a number of changes in the morphology and the properties of the polymers.

- **Haze.** Crosslinking was not found to significantly change the haze values of the coatings. The haze of highly crosslinked coatings was found to be within the acceptable 0-2% haze levels.
- **Hardness.** The hardness of coatings prepared with larger amount of trimers was found to decrease. The undesirable change can be associated with an increased brittleness and crystallinity of the highly crosslinked polymers.
- **Glass transition.** An introduction of crosslinking resulted in an increase of T_g of both HS-SS blocks and pure HS blocks. The change was related to the restricted mobility of the segments, limited by the presence of the trimers, thus an increase of T_g was observed.
- **Self-healing.** The use of trimers largely affected healing at room temperature, proportionally lowering the healing efficiency with the increase of the amount of trimers. The decrease of recovery from damage can be explained by the increasing amount of crosslinking creating rigid H-bonded matrix restraining mobility of polymer chains and lowering the SH efficiency. However, majority of the coatings maintained the excellent healing properties at elevated temperatures.

Additionally, the introduction of trimers to the formulations improved the solvent resistance of the coatings, apparent by the decrease of the materials' swelling and solubility in various solvents. The solvent resistance was found to increase with an increase of crosslinking, indicating higher amount of interactions and entanglement

of polymer chains, leading to reduced amount of interactions between the polymer chains and solvents, thus reducing the swelling and solubility of polymers.

Therefore, the introduction of trimers to the SH PU coatings did not affect the haze and improved the T_g and the self-healing properties. However, the decreased hardness of coatings made them unsuitable for the required application. Nevertheless, the coatings can be suitable for applications where the hardness is not a crucial requirement.

3.1.4. Internal emulsifier

The minimal amount of DMPA required to create environment friendly, stable and well dispersed PUDs was determined to be between 20% and 25% of the chain extenders fraction, which accounts for approximately 3% of the total polyurethane weight. The amount of DMPA also resulted in a number of changes in the morphology and the properties of the coatings.

- **Haze.** The haze of coatings was found to be unaffected by the amount of DMPA used. The haze of all coatings was found to be within the acceptable 0-2% level.
- **Hardness.** The hardness of coatings was found to decrease with the increase of the DMPA content, related to higher extent of phase-separation.
- **Glass transition.** In the DSC analysis a broadening and an increase of glass transition temperatures of the HS-SS blocks was observed, indicative of an increase of phase-separation with the higher amounts of DMPA. The change in the morphology of the polymers can be explained by the polar nature of the internal emulsifier, creating stronger interactions within the HS, as well as between the HS and SS, thus increasing the T_g of the homogenously mixed block.
- **Self-healing.** The self-healing behaviour was found to be influenced by phase-separation of the systems. The increase of DMPA content resulted in decreased healing efficiency at room temperature, related to the presence of stronger interactions between the polar groups of the internal emulsifier. The effect was more significant in formulations prepared with blends of DEG and DMPA due to

their lower T_g. However, the healing remained unchanged at 60 °C due to the healing process occurring above the T_g.

Therefore, the optimal amount of DMPA was found to be 25% of the chain extender fraction, which accounts for approximately 3% of the total polyurethane weight.

The summary of the influence of modification of various building blocks of the hard segments within formulations prepared with IPDI and PH50 is presented in **Table 10-1**.

Table 10-1. *The summary of the findings of modifications of HS within PH50-IPDI formulations*

Modification	Haze	Hardness	T_g	Healing		Phase-mixing	Crystallinity of HS	Cross-cut adhesion
				RT	60			
Length of **DIOL CE**	↔	↔	↑	↔	↔	↑	↔	↓
Amount of **AMINE CE**	↔	↓	↑	↓	↔	↓	↑	↔
Amount of **CROSSLINKING**	↔	↓	↑	↓	↔	↓	↑	↓
Amount of **DMPA**	↔	↓	↑	↓	↔	↓	↑	-

↑ - increase, ↓ - decrease, ↔ - no change

Two coatings reported in this thesis, PH50-IPDI-1,2-EG and PH50-IPDI-1,4-BD, were found to fulfil the four requirements of the research: exhibited haze below 2%, pencil hardness of B and above, suitable glass transition temperature and thermally-triggered SH properties reaching over 90% recovery from damage.

The low cross-cut adhesion of coating PH50-IPDI-1,4-BD suggests its incompatibility with TAc. However, the adhesion of the coating was not crucial for the chosen application. Moreover, the coating may exhibit better adhesion properties when coated on other substrates.

10.4. SELF-HEALING OF THE COATINGS

Majority of coatings prepared with PH50 and IPDI showed slow and limited self-healing at RT, and excellent self-healing behaviour at elevated temperatures. An example of the disappearance of scratches is presented in **Figure 10-1,** showing photographs of sample PH50-IPDI-1,2-EG before scratching, after scratching and after healing.

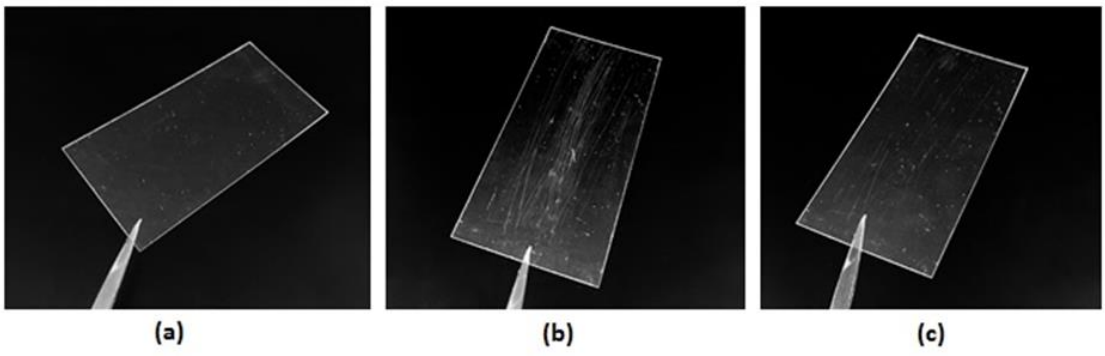

Figure 10-1. *Recovery of sample PH50/IPDI/1,2-EG at elevated temperature: a) before scratching, haze 0.94, b) after scratching, haze 6.25, c) after 10 min at 60˚C, haze 1.12*

Hydrogen bonded supramolecular polymers has been widely reported in the literature to exhibit self-healing characteristic.[3–7] Reversible physical bonds, such as H-bonds and ionic bonds were found to be suitable for coatings.[8] Such materials were reported to exhibit a thermally-triggered elastic response that leads to cracks closure, followed by breaking and reformation of H-bonds.[9] Moreover, H-bond disassembly and reassembly process was widely studied in systems reinforced by phase-segregation, use of supramolecular motifs and use of plasticisers.[7] In the case of biphasic systems, dynamic H-bonded supramolecular networks are imparted within soft segments reinforced through hard segments.[10] Recent efforts have been directed to creation of biphasic systems using block copolymers.[5,11] Highly functional coatings presented in this thesis showed excellent self-healing properties, obtaining the healing characteristics due to the presence of highly dynamic, reversible H-bonded networks.

The various self-healing tests of selected coatings reported in Chapter 9 showed that the self-healing process of damaged coatings occurs slowly at RT and has a potential

to reach full recovery over extended periods of time. The finding suggests that even limited molecular motion of the polymer chains within well phase-mixed SS-rich blocks allows an efficient rearrangement of the matrix and restoration of broken H-bonds. The mobility of chains is enabled by the onset of T_g being just below RT.

The thermal treatment of the samples resulted in accelerated healing, reaching almost full recovery from damage within the first 10 minutes at 60 °C, reaching at least 90% recovery. The increase of temperature leads to increased mobility of polymer chains. The acceleration of healing at elevated temperatures, above the T_g of the coatings, suggests that the healing is related to the increased mobility of polymer chains within the SS-rich phase, leading to a rearrangement of the matrix *via* reorganisation and re-mending of H-bonds. Moreover, the thermally induced mobility becomes sufficient to increase the rate of the diffusion of polymer chains, facilitating the closure of gaps created during the scratching process *via* bringing the H-bond donors and acceptors in close special proximity.[4]

The thermally-triggered healing of the coatings was found to be more efficient when performed immediately after scratching. However, the recovery from damage upon delayed thermal treatment reaches at least 80% after 10 minutes and 90% after 30 minutes. The lower recovery of samples healed not immediately after damage suggests a partial restoration of broken H-bonds occurring at RT. These bonds can therefore hinder the healing process at elevated temperatures, and longer heating time is required to break the newly formed bonds and rearrange them in order to restore the full functionality of the coatings.

Finally, the thermally-triggered healing of the samples was found to be repeatable. The coatings obtained at least 90% recovery of the original haze values after the first and second damage-heal cycle, and at least 80% after the third. The repeatability of the healing indicates that the recovery is related to the rearrangement of polymer matrix and restoration of H-bonds. Scratching of polymer matrix has been reported to induce covalent bond scission, leading to a decrease of polymer molecular mass in the vicinity of the damage. However, if the decrease of the polymer molecular mass was the fundamental trigger of healing, an improvement and acceleration of the

healing process would be observed during multiple healing tests. Moreover, in the case of relatively light scratching of protective coatings, the decrease of molecular mass would be localised on the surface of the polymer and only severely damaged samples would show a change in their overall molecular mass.

The fundamental mode of action of the self-healing process observed in the coatings presented in this thesis does not need to accommodate the re-formation of covalent bonds. Instead, the healing of the scratches is facilitated by molecular motion and driven by the formation of a highly directional and reversible hydrogen-bonded network in the phase-mixed region of the polymer.[3] When an external source of energy is used, the highly dynamic H-bonds can be disassembled, moving the equilibrium to the less H-bonded matrix, facilitating the healing process.[7] Moreover, these highly dynamic bonds are trapped within hard phase, which reinforce the polymer and maintain the mechanical properties of the materials.

Where HS-HS and SS-SS interactions dominate over HS-SS interactions, as in the chain-extended HDI formulations, extensive phase separation occurs, reducing the relative self-healing efficiency. Phase-separation also induces haze, and IPDI-based formulations, which show good phase-mixing are therefore favoured for high-clarity applications. The phase-mixed IPDI-based coatings were found to also had higher T_g. This creates a stable polymer morphology and thus a coating unable to heal at room temperature yet efficiently healing at elevated temperatures above T_g.

Small quantities of absorbed moisture, present in such PUs, may be expected to facilitate the healing process through plasticisation but is not a fundamental driver in itself.

10.5. FINAL REMARKS AND FURTHER WORK

The main goal of the project presented in this thesis was development of a highly functional, transparent self-healing material to be used as a protective coating. The literature review prepared at the beginning of the project allowed to evaluate and assess the current technologies and indicated that the use of copolymer-like systems such as polyurethanes would be the most promising route to successfully create the protective, self-healing coatings.

Two coatings reported in this thesis, PH50-IPDI-1,2-EG and PH50-IPDI-1,4-BD, were found to fulfil the requirements of a successful coatings, set up at the beginning of the project. Due to the low cross-cut adhesion of coating PH50-IPDI-1,4-BD to TAc, coating PH50-IPDI-1,2-EG was found to be the best performing material, showing unique mechanical properties and excellent self-healing behaviour.

Due to the industry-oriented nature of the project, the creation of a novel, highly functional coating to be used on customer goods was the main goal of the research. However, during development of the product, a number of features showing the relationship between the chemistry, functionality and properties of the prepared polyurethane coatings was discovered.

Nevertheless, in order to fully understand the relationship between the morphology and functionality of these self-healing smart materials, further studies of the micro- and macroorganisation of the phases, as well as better understanding of the healing process obtained *via* disassembly and reassembly of the dynamic H-bonded supramolecular networks is required. In particular, exploration of the molecular motion of the polymer chains, as well as the dynamics and kinetics of the H-bonds is necessary.

Techniques such as Small-Angle X-ray Scattering (SAXS) or Wide-Angle X-ray Scattering (WAXS) can be employed to study the morphology of polyurethane coatings, in particular to investigate the crystalline structures within the hard and soft segments. Various information obtained from these tests, such as changes in the crystallinity of samples or changes of the size of the segments during heating up can

provide insight into the morphology and self-healing behaviour. Electron Spin Resonance (ESR) can be employed in investigation of the amount and arrangement of hard segments and soft segments within polyurethane matrix. Moreover, detailed studies of the extent of H-bonding present within and between the segments can be performed with this technique.

Further investigation of the materials during their recovery would be of interest as it this would allow to understand the healing process better. The self-healing of damaged coatings could be monitored using various IR techniques, allowing to observe the changes in the amount and type of H-bonding. Various microscopic techniques can be also involved during the self-healing process of the samples. For example, AFM would allow investigation of the rearrangement of SS during heating and recovery of the surfaces.

It would be also of interest to study the morphology and phase-separation of the systems dielectric spectroscopy. Measurement of the dielectric properties of the coatings would allow identification of relaxation processes assigned to the different phases present within polyurethane. Some dielectric spectroscopy measurements have been already undertaken; however, the obtained data has not been fully analysed and interpreted yet.

Another area of interest would be a further investigation of physical and mechanical properties of the coatings. Techniques such as Dynamic Mechanical Thermal Analysis (DMTA) can be employed to perform creep measurements, stress-relaxation measurements or stress-strain tests. Rheometry could be used to measure storage and loss moduli of the materials, while temperature dependent rheology experiments of the melt can show formation of supramolecular clusters.

Determination of the molecular weight of the materials would provide additional insight into the relationship between the length of the polymer chains and their mechanical properties. Moreover, MW of the damaged samples could be measured to investigate the possibility of chain cleavage occurring during the scratching process and influencing the recovery of the coatings.

If more time was allowed, it would have been of a great interest to use the information gathered on the relationship between the chemistry and the performance of the PU coatings to develop other efficiently healing materials. Other non-crystalline polyols with low MW could be employed to synthesise coatings that might exhibit interesting self-healing properties. Moreover, other non-symmetrical diisocyanates, such as methylenedicyclohexyl diisocyanate (H_{12}MDI) or trimethylhexamethylene diisocyanate (TMDI), could be used in place of IPDI. The use of other starting materials could lead to creation of materials with even higher glass transition temperatures of the SS-rich phase, therefore completely hindering the healing process at RT and allowing the process to be fully thermally triggered.

Finally, coating of the actual customer goods would have been attempted. The large-scale coating process, as well as investigation of the customer goods coated with the self-healing PU materials would allow to investigate their actual utility and to evaluate the satisfaction of potential future customers. Only when successful large-scale coating has been performed and passed would the coatings be used in production.

10.6. *REFERENCES*

1 T. J. Touchet and E. M. Cosgriff-Hernandez, *Hierarchal Structure-Property Relationships of Segmented Polyurethanes*, Elsevier Ltd, 2016.

2 Merquinsa, *http://www.merquinsa.com/whats/whatsaPU.pdf*, (accessed August 2014).

3 S. J. Garcia, *Eur. Polym. J.*, 2014, **53**, 118–125.

4 P. Michael, D. Döhler and W. H. Binder, *Polymer*, 2015, **69**, 216–227.

5 S. Chen, N. Mahmood, M. Beiner and W. H. Binder, *Angew. Chemie - Int. Ed.*, 2015, **54**, 10188–10192.

6 F. Herbst, S. Seiffert and W. H. Binder, *Polym. Chem.*, 2012, **3**, 3084–3092.

7 L. M. De Espinosa, G. L. Fiore, C. Weder, E. Johan Foster and Y. C. Simon, *Prog. Polym. Sci.*, 2015, **49**–**50**, 60–78.

8 A. E. Hughes, *Self-healing coatings*, Elsevier Ltd., 2015.

9 S. J. Kalista, J. R. Pflug and R. J. Varley, *Polym. Chem.*, 2013, **4**, 4910–4926.

10 Y. Chen, A. M. Kushner, G. A. Williams and Z. Guan, *Nat. Chem.*, 2012, **4**, 467–472.

11 J. Hentschel, A. M. Kushner, J. Ziller and Z. Guan, *Angew. Chemie - Int. Ed.*, 2012, **51**, 10561–10565.